Università degli Studi di Pavia
Dottorato di Ricerca in Fisica - xxxiii Ciclo

Proton structure, an iridescent study:
from parton distributions to the emergence of the proton mass

Simone Rodini

2020

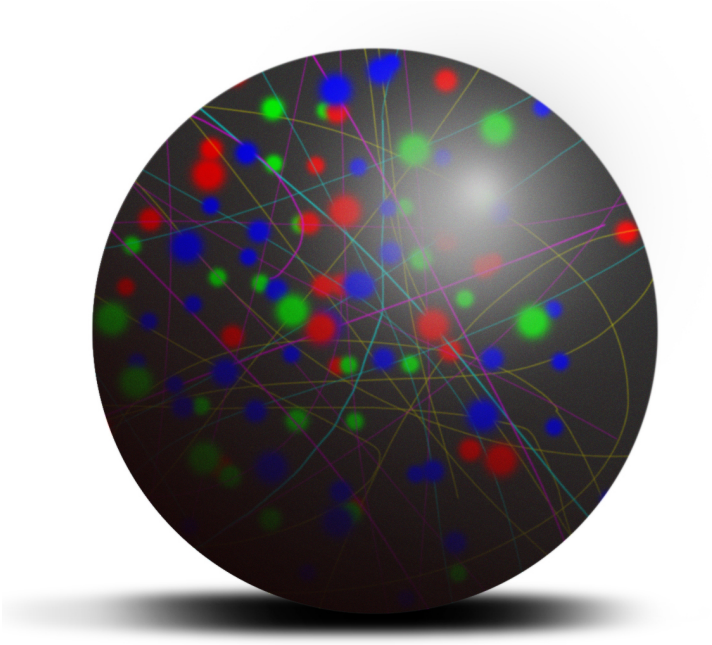

And lost he wandered under leaves,
And where the Elven-river rolled
He walked alone and sorrowing.
He peered between the hemlock-leaves
And saw in wonder flowers of gold
Upon her mantle and her sleeves,
And her hair like shadow following.

The Road goes ever on and on
Out from the door where it began.
Now far ahead the Road has gone,
Let others follow it who can!
Let them a journey new begin,
But I at last with weary feet
Will turn towards the lighted inn,
My evening-rest and sleep to meet.

J.R.R. Tolkien, *The lord of the Rings*

This thesis is partially based on the following works:

- **Published papers:**

A. Metz, B. Pasquini and S. Rodini, "Revisiting the proton mass decomposition", *Phys. Rev.* **D102** (2020) 114042 [2006.11171]

S. Rodini, A. Metz and B. Pasquini, "Mass sum rules of the electron in quantum electrodynamics", *J. High Energy Phys.* **9** (2020), 067 [2004.03704]

B. Pasquini, S. Rodini, A. Bacchetta, "Revisiting model relations between T-odd transverse-momentum dependent parton distributions and generalized parton distributions", *Phys. Rev.* **D100** (2019) 054039 [1907.06960]

B. Pasquini and S. Rodini, "The twist-three distribution $e^q(x, k_\perp)$ in a light-front model", *Phys. Lett.* **B788** (2019) 414 [1806.10932]

- **Conference proceedings:**

S. Rodini, B. Pasquini and A. Bacchetta, "Lensing function relation in hadrons", *PoS LC2019* (2020) 076; contribution to LC2019

S. Rodini, B. Pasquini and A. Bacchetta, "Lensing function relation in hadrons", *PoS DIS2019* (2019) 200; contribution to DIS 2019

S. Rodini and B. Pasquini, "Quark-gluon correlations in the twist-3 TMD using light-front wave functions", *PoS SPIN2018* (2019) 061; contribution to SPIN 2018

S. Rodini and B. Pasquini, "Twist-3 TMDs within a light-front model", *Nuovo Cim.* **C42** (2019) no.2-3-3, 112; contribution to EuNPC2018

Contents

Notations and conventions

We are going to use the following representation for the Dirac matrices:

$$\gamma^0 = \begin{pmatrix} \mathbb{I} & 0 \\ 0 & -\mathbb{I} \end{pmatrix}, \quad \gamma^i = \begin{pmatrix} 0 & \sigma^i \\ -\sigma^i & 0 \end{pmatrix}, \quad \gamma_5 = i\gamma^0\gamma^1\gamma^2\gamma^3 = \begin{pmatrix} 0 & \mathbb{I} \\ \mathbb{I} & 0 \end{pmatrix}, \tag{1}$$

where the 2-dimensional Pauli matrices are

$$\sigma^1 = \begin{pmatrix} 0 & 1 \\ 1 & 0 \end{pmatrix}, \quad \sigma^2 = \begin{pmatrix} 0 & -i \\ i & 0 \end{pmatrix}, \quad \sigma^3 = \begin{pmatrix} 1 & 0 \\ 0 & -1 \end{pmatrix}. \tag{2}$$

In light-front coordinates we have the definition of the $\gamma^\pm$ as:

$$\gamma^\pm = \frac{1}{\sqrt{2}}(\gamma^0 \pm \gamma^3) = \frac{1}{\sqrt{2}} \begin{pmatrix} \mathbb{I} & \pm\sigma^3 \\ \mp\sigma^3 & \mathbb{I} \end{pmatrix}, \tag{3}$$

and the light-cone projectors turns out to be:

$$\mathscr{P}^\pm = \frac{\gamma^\mp\gamma^\pm}{2} = \begin{pmatrix} \mathbb{I} & \pm\sigma^3 \\ \pm\sigma^3 & \mathbb{I} \end{pmatrix}. \tag{4}$$

We will adopt the standard convention for the Gell-Mann matrices (the $\hat{\cdot}$ indexes run in the adjoint representation):

$$T^{\hat{1}} = \frac{1}{2}\begin{pmatrix} 0 & 1 & 0 \\ 1 & 0 & 0 \\ 0 & 0 & 0 \end{pmatrix}, \quad T^{\hat{2}} = \frac{1}{2}\begin{pmatrix} 0 & -i & 0 \\ i & 0 & 0 \\ 0 & 0 & 0 \end{pmatrix}, \quad T^{\hat{3}} = \frac{1}{2}\begin{pmatrix} 1 & 0 & 0 \\ 0 & -1 & 0 \\ 0 & 0 & 0 \end{pmatrix}, \tag{5}$$

$$T^{\hat{4}} = \frac{1}{2}\begin{pmatrix} 0 & 0 & 1 \\ 0 & 0 & 0 \\ 1 & 0 & 0 \end{pmatrix}, \quad T^{\hat{5}} = \frac{1}{2}\begin{pmatrix} 0 & 0 & -i \\ 0 & 0 & 0 \\ i & 0 & 0 \end{pmatrix}, \quad T^{\hat{6}} = \frac{1}{2}\begin{pmatrix} 0 & 0 & 0 \\ 0 & 0 & 1 \\ 0 & 1 & 0 \end{pmatrix}, \tag{6}$$

$$T^{\hat{7}} = \frac{1}{2}\begin{pmatrix} 0 & 0 & 0 \\ 0 & 0 & -i \\ 0 & i & 0 \end{pmatrix}, \quad T^{\hat{8}} = \frac{1}{2\sqrt{3}}\begin{pmatrix} 1 & 0 & 0 \\ 0 & 1 & 0 \\ 0 & 0 & -2 \end{pmatrix}, \tag{7}$$

with the normalization

$$\mathrm{Tr}\left(T^{\hat{a}}T^{\hat{b}}\right) = \frac{1}{2}\delta^{\hat{a}\hat{b}} \tag{8}$$

and the commutation relations

$$\left[T^{\hat{a}}, T^{\hat{b}}\right] = i f^{\hat{a}\hat{b}}{}_{\hat{c}}\, T^{\hat{c}}, \tag{9}$$

where the structure constants are:

$$f^{\hat{1}\hat{2}}{}_{\hat{3}} = 1, \quad f^{\hat{4}\hat{5}}{}_{\hat{8}} = f^{\hat{6}\hat{7}}{}_{\hat{8}} = \frac{\sqrt{3}}{2},$$
$$f^{\hat{1}\hat{4}}{}_{\hat{7}} = -f^{\hat{1}\hat{5}}{}_{\hat{6}} = f^{\hat{2}\hat{4}}{}_{\hat{6}} = f^{\hat{2}\hat{5}}{}_{\hat{7}} = f^{\hat{3}\hat{4}}{}_{\hat{5}} = -f^{\hat{3}\hat{6}}{}_{\hat{7}} = \frac{1}{2}. \tag{10}$$

Chapter 1

Introduction

The current description of fundamental particle physics is performed in terms of Quantum Field Theories (QFTs). This class of theories combines the quantum description of the Nature with the Special Relativity, providing a tool to study microscopic and energetic phenomena. The Standard Model of particle physics is the current theory that describes the known fundamental particles and their interactions, using the language of the QFTs. We are interested in particular in the Quantum ChromoDynamics (QCD) sector of the Standard Model, which is the QFT of the strong force, i.e. the force acting between quarks and gluons. QCD is a non-abelian gauge theory, meaning that the force is mediated by gauge particles, i.e. the gluons, and that the gluons auto-interact. The auto-interaction of the gluons, combined with with the fact that they are massless, causes an increase of the strong coupling constant in the low-energy domain. This increase of the coupling constant prevents a perturbative approach to QCD at low-energy scales and leads to the phenomenon known as confinement: no free quarks or free gluons are observed in Nature, they only exist in bound, colorless states, which are known as hadrons. Quarks and gluons inside hadrons are collectively known as partons. Since a perturbative description of the partonic structure of the hadrons is not possible, one has to resort to other approaches. This motivates the thesis: using different tools of modern hadron physics, we try to improve the current understanding of the partonic structure of the proton, assumed as a prototype of hadron. To have a better description of the partonic structure of the proton has several consequences. First, we would have a much better interpretation of the experimental data, which in turns may open new possibility for searching evidences of physics beyond the Standard Model. Second, we would have a testing ground to validate theories that try to explain the emergence of the confinement from the internal parton dynamics.

The two main tools that we use in the thesis to investigate the partonic structure of the proton are the parton distribution functions and the Energy-Momentum Tensor (EMT). They offer different and, therefore, complementary descriptions of the partonic structure of the proton. The parton distribution functions encode information about the momentum distributions of the partons

inside the proton. A variety of parton distributions exists: the most general type encodes a six-dimensional momentum information (three-dimensional partonic momentum and three-dimensional proton-momentum transfer). From these mother distributions it is possible, via suitable limits and integrations, to access distributions that depend only on a sub-set of the six momentum variables. It is also possible to perform a Fourier transform from the proton-momentum transfer space to the impact-parameter space, in order to access the transverse position of the partons along with their three-dimensional momentum. The parton distributions enter in a variety of high-energy processes in which an hadron is involved, hence they are among the fundamental tools for precision experimental physics. The proton matrix elements of the QCD EMT carry information about global properties of the proton. A detailed study of the possible decompositions of the EMT in the separate contributions from quarks and gluons leads to important clues on how the global properties of the proton emerge from the properties of its elementary constituents.

1.1 Outline

In this thesis, we approach the study of the partonic structure of the proton from different perspectives. We propose a new model to describe the proton state in terms of its elementary constituents and discuss global properties of the proton, such as its mass, from the underlying dynamics of quarks and gluons.

Chapter 2 is devoted to a review of different ways to quantize a theory. For the most part, we are going to focus our attention on the light-front quantization, in which the (anti-)commutation relations among fields are imposed on a hyperplane tangent to the light-cone. Light-front quantization has many advantages compared to the standard, instant-form quantization, in the context of studying the proton structure. The most important one for our purposes is the possibility of having a well-defined Fock-space expansion of the proton state. This allows us to introduce the Light-Front Wave Functions (LFWFs). Moreover, it is the most natural language to formulate the theory of parton distributions.

In Chapter 3, we give an overview of the possible types of parton distributions, each of which provides complementary information on the parton composition of the proton. We also review the general link that exists between the LFWFs and the vacuum-to-proton matrix elements of quarks and gluons operators. Such transition matrix elements can be parametrized in terms of distributions amplitudes, and the connection between them and the LFWFs is at the core of our discussion on model calculations of parton distributions. In particular, we present how the QCD equations of motion can be used to obtain a link between sub-leading distribution amplitudes and LFWFs with non-vanishing parton orbital angular momentum for the three-quark state.

In Chapter 4, we lay out the foundations for a possible extraction of the Generalized Transverse Momentum Dependent parton distributions (GTMDs) from experiments. In particular, we study the cross-section for exclusive dijet

production in electron-proton collisions. We provide a parametrization of the full cross section in terms of form factors and angular modulations. The next step, which is left for future work, will be to link this parametrization to GTMDs and then to perform a sensitivity study to find the best kinematical conditions to extract the GTMDs from experimental measurements. This kind of study has been already performed in the contest of low-x physics to study the gluon contribution to GTMDs. Our aim is to go beyond the low-x approximation and to extend these works also to the intermediate x region, where one can probe other degrees of freedom than the gluons.

Chapter 5 is devoted to the study of model-induced relations between different types of parton distributions. In particular, we eviscerate the so-called lensing relation, that establishes a link between Transverse Momentum dependent parton Distributions (TMDs) and Impact Parameter Distributions. We show which are the conditions that must be fulfilled by models to obtain such a relation, and how, in the full QCD, it is unlikely to match these conditions.

Chapter 6 is devoted to the illustration of our model for the LFWFs, that is obtained exploiting the link between the LFWFs and the distribution amplitudes. In particular, our model includes a three-quark plus one gluon state in the proton Fock-space decomposition, which is fundamental to obtain a consistent model based on the distribution amplitudes for the LFWFs with non-vanishing orbital angular momentum for the three-quark state. With the explicit model, we show how it is possible to obtain leading-twist TMDs and generalized parton distributions as appropriate overlaps of LFWFs, showing the fundamental role played by the LFWFs in the study of parton distributions.

In Chapter 7, the attention is posed on the exploration, both theoretical and through our model, of one particular higher-twist TMD called $e^q(x, \boldsymbol{k}_\perp)$. Higher-twist TMDs are of particular interest, since they allow us to extract information of the quark-gluon correlations inside the proton. We review a general, model-independent, decomposition of $e^q(x, \boldsymbol{k}_\perp)$, addressing also some of the most recent works on it.

In Chapter 8, we deviate from the study of parton distributions to enter the realm of local operators and proton global properties. In particular, we study the EMT, both for an electron in Quantum ElectroDynamics (QED) and for a proton in QCD. The QED study allows us to explore the theoretical tools needed to approach the more complex QCD case. For the QED case, we explore the EMT electron matrix elements in both the off-forward and forward limit. The latter leads to the study of different electron mass decompositions in terms of electron and photon contributions. We then extend the discussion to study the proton mass decompositions. We explore the renormalization-scheme dependence of each decomposition and perform a study of the dependence of each term on the loop order.

Finally, in Chapter 9 we summarize our results and give some outlooks for future perspectives of this work.

Chapter 2

Foundations of Light-Cone Quantization

In this thesis, we will use both the standard formalism of instant-form quantization and light-front quantization. The latter has become more and more popular in the study of deeply inelastic processes, since it provides the most natural framework to investigate them. Since deeply inelastic processes are used, mainly, to study the internal structure of hadrons in Quantum ChromoDynamics (QCD), light-front quantization is also largely employed in the theoretical studies of hadron internal structure. It turns out that, in light-front quantization, theoretical calculations on the proton structure drastically simplify and the underlying physical picture emerges more clearly.

A general review of the basics of light-front quantization can be found in Ref. [1], from which this chapter is inspired.

2.1 Forms of quantization

We are interested in the study of field theories where the physical systems are described in terms of fields $\phi_i(\boldsymbol{x};t)$. The field theories can be either classical or quantum and either non-relativistic or relativistic. Since our main focus in the thesis will be the study of QED and QCD, we shall briefly review the basic concepts of all the four types of field theory, then focusing only on the relativistic quantum ones. In this brief illustration we shall consider a single field ϕ in order to keep the notation as simple as possible, also because the generalization to a collection of fields is relatively simple.

For a non-relativistic and classical field theory, once the density of Lagrangian $\mathscr{L}[\phi,\partial_t\phi]$ is assigned as a functional of the field, we can solve the equation of motions (EOM)[1]

$$\frac{\partial\mathscr{L}}{\partial\phi(\boldsymbol{x})}-\partial_t\frac{\partial\mathscr{L}}{\partial\left(\partial_t\phi(\boldsymbol{x})\right)}=0, \tag{2.1}$$

[1]We shall not distinguish the notation for the functional derivative and the standard partial derivative, since no confusion should arise.

to obtain the field configuration $\phi(\boldsymbol{x};t)$ at any given time t once the initial configuration $\phi_0(\boldsymbol{x}) = \phi(\boldsymbol{x}, t=0)$ is specified. This way to tackle the theory is usually called Lagrangian approach, but it is not the only one. In fact, in non-relativistic theories the Hamiltonian approach is often preferred. In order to obtain the Hamiltonian density from the Lagrangian, the canonical conjugate momentum $\pi[\phi]$ is introduced as:

$$\pi[\phi] = \frac{\partial \mathscr{L}}{\partial\left(\partial_t \phi(\boldsymbol{x})\right)}. \tag{2.2}$$

The Hamiltonian is then constructed as the Legendre transformation of the Lagrangian with respect to $\partial_t\phi$:

$$\mathscr{H}[\phi,\pi] = \pi[\phi]\partial_t\phi - \mathscr{L}[\phi, \partial_t\phi[\pi]]. \tag{2.3}$$

With the Hamiltonian one can compute the evolution equation for the field configuration via the Hamilton equations

$$\frac{\partial\phi}{\partial t} = \frac{\partial\mathscr{H}}{\partial\pi}, \quad \frac{\partial\pi}{\partial t} = -\frac{\partial\mathscr{H}}{\partial\phi}. \tag{2.4}$$

The interesting aspect of the Hamiltonian approach is that it gives a natural way to compute the time evolution of any functional of the fields in terms of the Poisson brackets of the functional of the fields and the Hamiltonian:

$$\frac{d\mathcal{A}[\phi,\pi]}{dt} = \frac{\partial\mathcal{A}}{\partial t} + [\mathcal{A},\mathscr{H}] = \frac{\partial\mathcal{A}}{\partial t} + \frac{\partial\mathcal{A}}{\partial\phi}\frac{\partial\mathscr{H}}{\partial\pi} - \frac{\partial\mathscr{H}}{\partial\phi}\frac{\partial\mathcal{A}}{\partial\pi}. \tag{2.5}$$

In a non-relativistic quantum theory the Poisson brackets are simply replaced with quantum commutators (or anti-commutators in case of fermionic degrees of freedom) and the time evolution is given by the Heisenberg equation. Gauge theories pose some issues when going from classical to quantum theories, because of the redundant gauge degrees of freedom and the fact that not all the fields have associated a canonical momentum, i.e. not all the fields are independent. We shall comment further on these issues in Sec. 2.2.1.

In a relativistic field theory (quantum or not) we cannot any longer treat the time as an independent parameter. In fact, the concepts of time and space are, to some extent, not uniquely defined in the context of a covariant theory: one can obtain a new parametrization of spacetime simply by transforming the coordinate from

$$x^\mu = (x^0, x^1, x^2, x^3) \tag{2.6}$$

to

$$\tilde{x}^\nu = \tilde{x}^\nu(x^\mu) \tag{2.7}$$

under the only condition that the transformation must possess an inverse. In the "tilde" coordinate system we have a different metric, given by:

$$\tilde{g}_{\mu\nu} = \frac{\partial x^\rho}{\partial\tilde{x}^\mu}\frac{\partial x^\sigma}{\partial\tilde{x}^\nu} g_{\rho\sigma}. \tag{2.8}$$

The Lagrangian must be invariant under the change in the spacetime parametrization described above in order to have a well-defined relativistic theory. The Hamiltonian, however, is not invariant under a change of parametrization, since it is constructed as the Legendre transform with respect to the time derivative of the field. This is the reason why, in most of the standard presentations of relativistic field theories, the Lagrangian approach is preferred in contrast to the Hamiltonian one. Moreover, in a relativistic theory, the concept of initial field configuration, i.e. the configuration of a field at fixed initial time, becomes somewhat problematic. First, for convenience, one defines the null hypersurface corresponding to the initial time to be the locus in Minkowski space with the same value of the "time-like" coordinate $\tilde{x}^0$. On the null hypersurface one imposes the initial conditions for the fields, or one imposes the commutation relations among fields in a quantum theory. The first subtlety is that $\tilde{x}_0 = \text{const}$ could identify a different hypersurface with respect to $\tilde{x}^0 = \text{const}$. This because the metric $\tilde{g}^{\mu\nu}$ can be non trivial and can change the interpretation of the coordinate when the index is lowered or raised. The second issue is that, in the standard instant-form approach where the initial conditions are fixed on the hyperplane $x^0 = 0$, as well as in any other spacetime parametrization that can be reached from the standard one via a Lorentz transformation, we have the conceptual problem of knowing precisely the state of the system on a spacetime surface simultaneously. The only spacetime parametrization that avoids these issues altogether is the light-front parametrization, as we shall see later.

There are, in principle, infinite possibilities for the choice of the parametrization. One must exclude, however, all those which are connected to each other through a Lorentz transformation, since they are equivalent in a covariant formalism. Only five independent parameterizations survive; each of them is in one-to-one correspondence with a unique null hypersurface. They are referred as forms of relativistic dynamics and correspond to the:

1. Instant Form. It is the textbook standard form in which we have $x^\mu = (x^0, x^1, x^2, x^3)$.

2. Light-Front Form. It replaces the time coordinate and one spatial coordinate (it is conventionally used x^3) with the combinations:

$$x^\pm = \frac{x^0 \pm x^3}{\sqrt{2}}. \tag{2.9}$$

It is custom to group the remaining spatial coordinates into a $\perp$ vector, leading to $\tilde{x}^\mu = (x^+, x^-, \boldsymbol{x}_\perp)$, $\boldsymbol{x}_\perp = (x^1, x^2)$. The metric in this new parametrization reads:

$$\tilde{g}^{\mu\nu} = \begin{pmatrix} 0 & 1 & 0 & 0 \\ 1 & 0 & 0 & 0 \\ 0 & 0 & -1 & 0 \\ 0 & 0 & 0 & -1 \end{pmatrix}. \tag{2.10}$$

The time variable is x^+ and the corresponding time variable in the covariant representation is x_- and not x_+, as it should be clear from the metric. This entails that the equal-time surfaces are identified by $x^+ = \text{const}$. This parametrization is well suited to study problems in which one can identify a preferential spatial direction. Moreover, since the null hypersurface is a plane tangent to the light cone, the state of the system for fixed x^+ can be in principle determined via the interaction with a massless field that has a negative momentum along the $\hat{x}^3$ axis. In this case, therefore, no conceptual problem is posed by the requirement of knowing the complete field configuration for fixed x^+. It will be the parametrization mainly used in this thesis.

3. Point Form. The spacetime parametrization is

$$x^\mu = \tau(\cosh(\omega), \sinh(\omega)\sin(\theta)\cos(\phi), \sinh(\omega)\sin(\theta)\sin(\phi), \sinh(\omega)\cos(\theta)), \tag{2.11}$$

with $\tilde{x}^\mu = (\tau, \omega, \theta, \phi)$ and

$$\tilde{g}^{\mu\nu} = \begin{pmatrix} 1 & 0 & 0 & 0 \\ 0 & -\tau^2 & 0 & 0 \\ 0 & 0 & -\tau^2\sinh^2(\omega) & 0 \\ 0 & 0 & 0 & -\tau^2\sinh^2(\omega)\sin^2(\omega) \end{pmatrix}. \tag{2.12}$$

The equal-time surface is the hyperboloid identified by $x^2 = \text{const}$, with $x^0 > 0$.

4. Point Form-2. It is similar to the point form, with the exception that the equal-time surface condition is $x^2 + (x^1)^2 = \text{const}$, with $x^0 > 0$.

5. Point Form-3. It is similar to the point form, with the exception that the equal-time surface condition is $x^2 + (x^1)^2 + (x^2)^2 = \text{const}$, with $x^0 > 0$.

The equal-time surfaces of each parametrization are shown in Fig. 2.1. Of course we cannot draw a three-dimensional hypersurface, hence all the plots are in $1 + 2$ dimensions, the time x^0 being the vertical axis in the pictures.

To gain a little more insight on the difference between the various parametrizations, we recall that the Poicaré group (semi-direct product of the proper and ortochronus Lorentz group and translations) has ten generators, each one characterizing a specific transformation that can be applied to the system: three boosts, three rotations, three space translations and one time translation. Lorentz transformations, i.e. rotations and boosts, are obtained from the Lorentz group generators $M^{\mu\nu} = -M^{\nu\mu}$, and the translation from the four-momentum[2] P^μ. They obey the following commutation relations:

$$[P^\mu, P^\nu] = 0, \quad \left[P^\mu, M^{\alpha,\beta}\right] = iP^\alpha g^{\mu\beta} - iP^\beta g^{\mu\alpha}, \tag{2.13}$$

[2]The identification between the translation generator and the four-momentum follows by the fact that $P^2 \equiv \left(P^0\right)^2 - \sum_{i=1}^3 \left(P^i\right)^2 = a\mathbb{1}$ is a Casimir operator, i.e. it commutes with all the generators of the group.

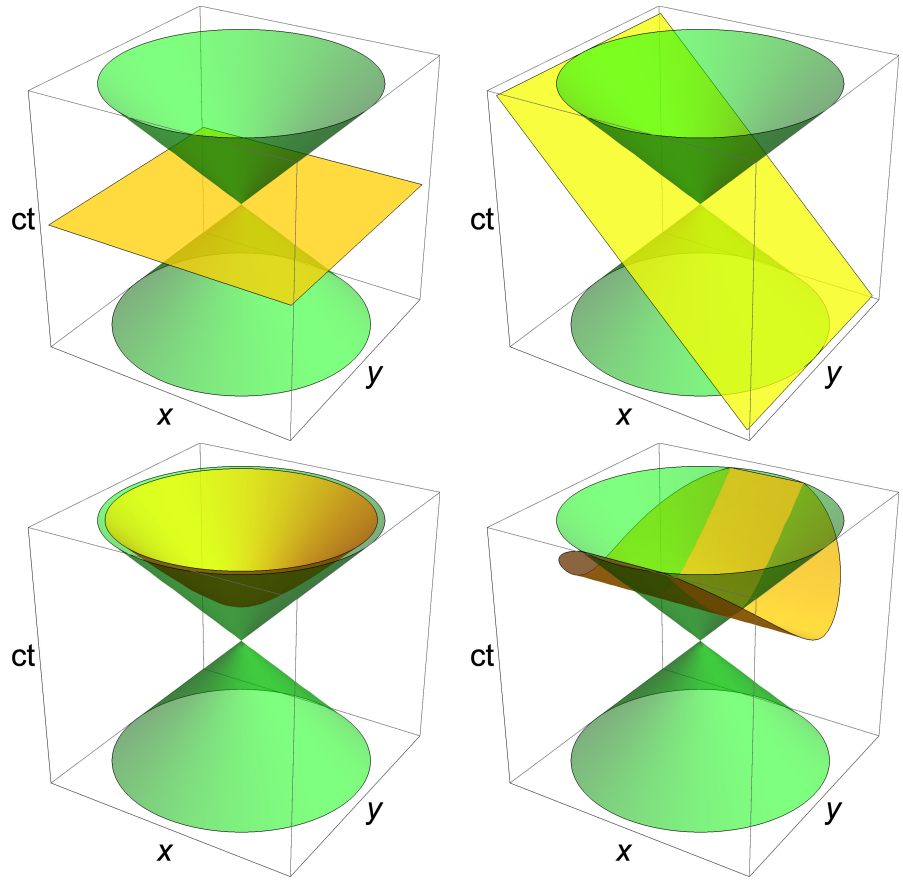

Figure 2.1: Equal-time surfaces (in yellow) for each spacetime parametrization presented in the text, in arbitrary units. In the top left: the instant-form; in the top right: the light-front form, in which we clearly see that the equal-time surface is tangent to the light cone. In the bottom left: the point form, in which the equal-time surface is an hyperboloid and finally in the bottom right we have the equal-time surface for the Point Form-2. The Point Form-3 in $1+2$ dimensions coincide with the instant-form parametrization.

$$\left[M^{\mu\nu}, M^{\alpha\beta}\right] = i\left(g^{\mu\alpha}M^{\nu\beta} + g^{\nu\beta}M^{\mu\alpha} - g^{\nu\alpha}M^{\mu\beta} - g^{\mu\beta}M^{\nu\alpha}\right). \tag{2.14}$$

The boost and the rotation operators are obtained from $M^{\mu\nu}$ as:

$$K^i = M^{0i}, \quad J^i = \varepsilon^{ijk}M^{jk}. \tag{2.15}$$

Different spacetime parametrizations mix the Poincaré generators in different combinations. In instant form, we have:

$K^1,\ K^2,\ K^3,$ generate boosts along the directions $\hat{x}^1, \hat{x}^2, \hat{x}^3$, respectively;
$J^1,\ J^2,\ J^3,$ generate rotations around the $\hat{x}^1, \hat{x}^2, \hat{x}^3$ axis, respectively;
$P^1,\ P^2,\ P^3,$ generate translations along $\hat{x}^1, \hat{x}^2, \hat{x}^3$ direction, respectively;
$P^0,$ generates a time translation.

In the instant form, the time is x^0, and the Hamiltonian of the system, i.e. the operator that generates time translations, is the zeroth component of $P^\mu = (P^0, P^1, P^2, P^3)$. From the definition of the finite translation operator

$$e^{-iP^\mu x_\mu}, \tag{2.16}$$

where x^μ is the parameter of the translation, one can infer which component of P^μ is the Hamiltonian. Since, by definition, the Hamiltonian is the generator of the time translation, and we have that $P^\mu x_\mu = x^0 P^0 - \boldsymbol{x}\cdot\boldsymbol{P}$, being x^0 the time in instant form, one concludes that P^0 is the Hamiltonian. Analogously, in the light-front form we have $P^\mu x_\mu = x^+P^- + x^-P^+ - \boldsymbol{x}_\perp\cdot\boldsymbol{P}_\perp$ and since x^+ is the time variable, we conclude that P^- is the Hamiltonian of the system. In coordinate representation for a free theory, we have $P^i = -i\partial^i$ and:

$$\partial^- = \frac{\partial}{\partial x_-} = \frac{\partial}{\partial x^+}, \tag{2.17}$$

i.e. P^- involves the time derivative. Conversely, P^+ is proportional to a derivative with respect to the variable x^-, that is a space variable.

One way to classify the Poincaré generators is to divide them in two classes, based on their action on the null hypersurface: the first class is formed by the so-called kinematic operators, which leave invariant the null hypersuperface. The remaining operators are called dynamical operators, and evolve equal-time hypersurfaces.

The different forms of dynamics have different classes of kinematic and dynamical operators. In the instant form, the kinematic operators are P^1, P^2, P^3 and J^1, J^2, J^3, i.e. the hyperplane $t = 0$ is left invariant under space translations and rotations.

In the light-front form, the kinematic operators are P^+, P^1, P^2, i.e. translations along $\hat{x}^+$, $\hat{x}^1, \hat{x}^2$, respectively, J^3, i.e. rotations around the $\hat{x}^3$ axis, K^3, i.e. boosts along the $\hat{x}^3$ direction, and B^1, B^2, defined as the following combinations of rotations and boosts:

$$B^1 = \frac{1}{\sqrt{2}}\left(K^1 + J^2\right), \quad B^2 = \frac{1}{\sqrt{2}}\left(K^2 - J^1\right). \tag{2.18}$$

For example, in the first case, we have a boost (K^1) along the $\hat{x}^1$ direction that mixes the x^0 and x^1 components, and a rotation (J^2) around the $\hat{x}^2$ axis that mixes the x^3 and x^1 components. The sum of the two operations leaves invariant $x^0 + x^3 = \sqrt{2}x^+$. The second generator B^2 corresponds to the same transformations with $1 \leftrightarrow 2$. It turns out, from a careful examination of the commutation relations among the Poincaré generators in light-front parametrization (see Tab. 2.1), that P^μ, $\boldsymbol{B}_\perp$ and J^3 form a sub-group of the Poincaré group that is isomorphic to the two-dimensional subgroup of non-relativistic Galilean transformations. This provides another explanation for the identification of P^- with the Hamiltonian in light-front parametrization. It also provides a more intuitive interpretation for the $\boldsymbol{B}_\perp$ operators: they are the two-dimensional Galilean transverse boosts.

The dynamical operators in the light-front parametrization are P^- and the following combinations of rotations and boosts:

$$S^1 = \frac{1}{\sqrt{2}}\left(K^1 - J^2\right), \quad S^2 = \frac{1}{\sqrt{2}}\left(K^2 + J^1\right). \tag{2.19}$$

In the point form, the kinematic generators are J^1, J^2, J^3 and K^1, K^2, K^3, and therefore all the four translational operators P^μ are dynamical operators. This form proves useful to connect the description of a system between a moving frame and its rest-frame. This because of the kinematical nature of boosts, that avoid the introduction of dynamical effects when changing frame via a Lorentz transformation.

In the case of the point form-2, the kinematic generators are J^3, K^2, K^3 and P^1.

In the case of the point form-3, the kinematic generators are K^3, J^3 and P^1, P^2.

In the following, we will work mainly with the light-front parametrization, and, to help the interested reader to reconstruct all the results that rely on the commutation relations among the operators in light-front parametrization, we summarized them in Tab. 2.1.

Before moving to the next section, which contains the basics of QCD on the light front, we would like to comment on the interesting feature of P^+ being a semi-positive definite operator. This can be seen by analyzing the Lorentz boost along the $\hat{x}^3$ axis in light-front parametrization. The boosted version of a generic operator $\mathcal{O}$ can be obtained as:

$$e^{i\omega K^3}\mathcal{O}e^{-i\omega K^3}, \tag{2.20}$$

where ω is the rapidity

$$\omega = \frac{1}{2}\log\left(\frac{1+\beta}{1-\beta}\right) = \frac{1}{2}\log\left(\frac{c+v}{c-v}\right), \quad \text{with } \beta = \frac{v}{c}. \tag{2.21}$$

In the case of P^+, the following commutation relation holds as can be verified using the commutation relations in Tab. 2.1:

$$\left[i\omega K^3, P^+\right] = \omega P^+. \tag{2.22}$$

	P^+	P^-	$P^i_\perp$	B^i	S^i	K^3	J^3
P^+	0	0	0	0	$iP^i_\perp$	iP^+	0
P^-	0	0	0	$iP^i_\perp$	0	$-iP^-$	0
$P^j_\perp$	0	0	0	$i\delta^{ji}P^+$	$i\delta^{ji}P^+$	0	$i\varepsilon^{jl}P^l_\perp$
B^j	0	$-iP^j_\perp$	$-i\delta^{ij}P^+$	0	$-i\delta^{ij}K^3$ $-i\varepsilon^{ij}J^3$	iB^j	$-i\varepsilon^{jl}B^l$
S^j	$-iP^j_\perp$	0	$-i\delta^{ij}P^+$	$-i\delta^{ji}K^3$ $-i\varepsilon^{ji}J^3$	0	$-iS^j$	$-i\varepsilon^{jl}S^l$
K^3	$-iP^+$	$-iP^-$	0	$-iB^i$	iS^i	0	0
J^3	0	0	$-i\varepsilon^{il}P^l_\perp$	$i\varepsilon^{il}B^l$	$i\varepsilon^{il}S^l$	0	0

Table 2.1: Summary of the light-front commutation relations. The table entries are intended as the result of $[\mathcal{O}_{\rm row}, \mathcal{O}_{\rm col}]$.

Hence, from the well known relation for two generic operators X, Y

$$e^X Y e^{-X} = Y + [X,Y] + \frac{1}{2!}[X,[X,Y]] + ..., \tag{2.23}$$

we obtain immediately that

$$e^{i\omega K^3} P^+ e^{-i\omega K^3} = e^{\omega} P^+. \tag{2.24}$$

Now, being $\omega > 0$ if the boost is performed along the positive direction of $\hat{x}^3$, we have that the eigenstate of P^+ with the lowest eigenvalue is associated with a particle at rest, for which $p^+ = m/\sqrt{2}$. For a massless particle we arrive at the same conclusion taking the four-momentum of the particle in the instant form as $p^\mu = (E, 0, 0, E)$ with the energy $E > 0$. Hence, the condition $k^+ = 0$ can be realized for a massive particle only in the limit of $\beta \to -1$, whereas we can have $k^+ = 0$ for a massless particle only for $\beta \neq 1$.

Because of the transformation (2.24), the light-front parametrization is usually adopted to study ultra-relativistic systems, in which one component of the three-momentum is dominant, that translates into a + component dominance in light-front parametrization.

2.2 Light-Front quantization

In the previous section, we did not distinguish between quantum or classical relativistic field theories. The main difference is that for a quantum theory we must impose (anti-)commutation relations between fields at fixed time, whereas in the classical case the initial conditions are sufficient for solving the dynamics. To quantizing a theory in a parametrization different from the instant-form one

means to impose the (anti-)commutation relations at equal $\tilde{x}^0$ instead of x^0. We will use only the instant-form and the light-front parametrizations, out of the five possible ones. Hence, we shall specify all the necessary details for the light-front form, keeping in mind that, *mutatis mutandis*, one could follow the exact same logic for all the other parametrizations. To quantize a theory on the light front we impose the (anti-)commutation relations between fields at equal x^+. Since we are mainly interested in the study of the electron in QED and quarks in QCD, i.e. spin-1/2 matter field, we restrict ourself to discuss Dirac fields and gauge fields only. In QCD the fermionic fields are known as quarks and the gauge fields as gluons, whereas in QED the fermionic fields are leptons and the gauge field is the photon. The light-front parametrization is rather special, since it allows us to separate, in a natural way, the two independent components out of the four possible ones for a spin-1/2 field. The independent components are known as the "good" components and the dependent components as "bad", where the naming would intend to express the fact that the bad components are completely determined by the good ones for fixed value of x^+. The projectors $\mathscr{P}^+$ and $\mathscr{P}^-$ that realize the separation between good and bad components are defined, respectively, as:

$$\mathscr{P}^{\pm} = \frac{1}{\sqrt{2}}\gamma^{\mp}\gamma^{\pm}, \tag{2.25}$$

and the good and bad components of a field ψ are:

$$\psi_{\pm} = \mathscr{P}^{\pm}\psi. \tag{2.26}$$

To explicitly see that the bad components are not independent, we need to exploit the Lagrangian EOM. First, the QCD is a quantum gauge-field theory with gauge symmetry $SU(3)$. The quarks belong to the fundamental representation of the symmetry group, whereas the gluons belong to the adjoint representation. The QCD Lagrangian reads:

$$\mathscr{L}_{\text{QCD}} = \sum_{a,b}\sum_{f} \bar{\psi}_a^{(f)} \left(i\not{D}_{ab} - m\delta_{ab}\right) \psi_b^{(f)} - \sum_{\hat{a}} \frac{1}{4} F^{\hat{a}}_{\mu\nu} F^{\mu\nu}_{\hat{a}}, \tag{2.27}$$

where the sum with respect to a, b is over the color index in the fundamental representation (i.e. the quarks form a color triplet), and the sum over $\hat{a}$ is instead performed in the adjoint representation (the gluons form a color octet), ψ is the fermionic field and D^{μ}_{ab} is the covariant derivative, defined as

$$D^{\mu}_{ab} = \partial^{\mu}\delta_{ab} - \sum_{\hat{c}} i g_s A^{\mu}_{\hat{c}} T^{\hat{c}}_{ab}, \tag{2.28}$$

with g_s the strong coupling constant. The superscript f upon the quark fields in the QCD Lagrangian labels the different possible flavors for the quarks: up, down, charm, strange, top, bottom. To distinguish between the fundamental and the adjoint representation we adopted, just for this section, the convention that the $\hat{\cdot}$ indexes run in the adjoint representation. $F^{\mu\nu}_{\hat{a}}$ is the gluon strength field tensor, defined as

$$F^{\mu\nu}_{\hat{a}} = \partial^{\mu} A^{\nu}_{\hat{a}} - \partial^{\nu} A^{\mu}_{\hat{a}} + g_s f_{\hat{a}}{}^{\hat{b}\hat{c}} A^{\mu}_{\hat{b}} A^{\nu}_{\hat{c}}, \tag{2.29}$$

where $f_{\hat{a}}{}^{\hat{b}\hat{c}}$ are the $SU(3)$ structure constants. We will suppress the color indexes in the following, unless they are necessary for the comprehension of the equations. Moreover, we will use the standard notation

$$A^\mu = \sum_{\hat{a}} A^\mu_{\hat{a}} T^{\hat{a}}. \tag{2.30}$$

The equation of motion for the quark fields reads:

$$\frac{\partial \mathcal{L}}{\partial \bar{\psi}} - \partial^\mu \frac{\partial \mathcal{L}}{\partial \left(\partial^\mu \bar{\psi}\right)} = 0. \tag{2.31}$$

After a little algebra and using the light-front parametrization, one obtains:

$$iD^+ \psi_-(z) = \frac{\gamma^+}{2} \left(i\boldsymbol{\gamma}_\perp \cdot \boldsymbol{D}_\perp + m\right) \psi_+(z). \tag{2.32}$$

The partial derivative ∂^+ that appears in Eq. (2.32) inside the covariant derivative D^+ is a spatial derivative:

$$\partial^+ = g^{+-}\partial_- = g^{+-}\frac{\partial}{\partial x^-}. \tag{2.33}$$

Since we established that the bad components are constrained fields, for the remaining of this chapter we assume to work only with good fermion fields.

2.2.1 Free fields: quarks and gluons

The essential ingredient to define a quantum field theory is having the (anti-) commutation relations for fields, i.e. quarks and gluons in the case of QCD. However, in order to properly write the anti-commutation relations for the quark fields, we need to establish the concept of helicity within the light-front quantization formalism, see Ref. [2]. Let $|p, \lambda\rangle$ be a generic eigenstate of the momentum operator P^μ

$$P^\mu |p, \lambda\rangle = p^\mu |p, \lambda\rangle . \tag{2.34}$$

The light-cone helicity λ is introduced as the eigenvalue of the operator

$$j_z = J^3 + \frac{\boldsymbol{B}_\perp \times \boldsymbol{P}_\perp}{P^+} \rightarrow j_z |p, \lambda\rangle = \lambda |p, \lambda\rangle , \tag{2.35}$$

where J^3 is the total angular momentum operator and $\boldsymbol{B}_\perp$ is the operator defined in Eq. (2.18). It can be shown (see Refs. [2, 3]) that, in the limit of large p^+, j_z reduces to the ordinary helicity operator $\boldsymbol{p} \cdot \boldsymbol{S}/p$. If the state is such as $p^\mu = (m/\sqrt{2}, m/\sqrt{2}, \boldsymbol{0}_\perp)$, then we have

$$\begin{aligned} j_z |(m/\sqrt{2}, m/\sqrt{2}, \boldsymbol{0}_\perp), \lambda\rangle &= J^3 |(m/\sqrt{2}, m/\sqrt{2}, \boldsymbol{0}_\perp), \lambda\rangle \\ &= \lambda |(m/\sqrt{2}, m/\sqrt{2}, \boldsymbol{0}_\perp), \lambda\rangle , \end{aligned} \tag{2.36}$$

from which we obtain, using the commutation relations in Tab. 2.1, that

$$j_z \left|p,\lambda\right\rangle = j_z e^{-i\boldsymbol{v}_\perp\cdot\boldsymbol{B}_\perp} e^{-i\omega K^3} \left|(m/\sqrt{2}, m/\sqrt{2}, \boldsymbol{0}_\perp),\lambda\right\rangle = \lambda \left|p,\lambda\right\rangle, \tag{2.37}$$

i.e. the light-cone helicity is invariant under light-front boosts.

This definition of light-cone helicity can be rewritten as the difference of total angular momentum minus the orbital part

$$j_z = J^3 - \boldsymbol{R}_\perp \times \boldsymbol{P}_\perp \tag{2.38}$$

by introducing the following operator

$$\boldsymbol{R}_\perp = -\frac{\boldsymbol{B}_\perp}{P^+}. \tag{2.39}$$

It turns out that this operator can be interpreted as the center of transverse momentum for a composite state and as the transverse position for a single-particle state. The operator (2.39) satisfy the following commutation relations:

$$[\boldsymbol{R}_\perp, \boldsymbol{B}_\perp] = \left[\boldsymbol{R}_\perp, K^3\right] = 0. \tag{2.40}$$

This ensures that j_z commutes both with $\boldsymbol{B}_\perp$ and $\boldsymbol{K}_\perp$, hence light-front boosts leave invariant the light-cone helicity.

Equipped with the above definition of light-cone helicity, the anti-commutation relations for the good component of the fermion fields in position space read:

$$\left\{\psi^{(f)}_{a,\lambda}(x), \left(\psi^{(q)}_{b,\sigma}(y)\right)^\dagger\right\}|_{x^+=y^+} = \delta_{ab}\delta^{fq}\delta_{\lambda\sigma}\delta(x^- - y^-)\delta(\boldsymbol{x}_\perp - \boldsymbol{y}_\perp). \tag{2.41}$$

We can transform the quark field in momentum representation, isolating the quark and antiquark component as:

$$\psi^{(f)}_{\downarrow/\uparrow}(x) = \int \frac{dk^+ d\boldsymbol{k}_\perp}{2k^+(2\pi)^3}\left[e^{-ik\cdot x} q_{\downarrow/\uparrow}(k) b^{(f)}_{\downarrow/\uparrow}(k) + e^{ik\cdot\xi} v_{\uparrow/\downarrow}(k) d^{(f)\dagger}_{\uparrow/\downarrow}(k)\right]_{k^2=m^2}, \tag{2.42}$$

where the light-cone spinors for quark and anti-quark states with light-cone helicity $\uparrow$ and $\downarrow$ are:

$$q_\uparrow(k) = \frac{1}{\sqrt{2\sqrt{2}k^+}}\begin{pmatrix}\sqrt{2}k^+ + m\\ \sqrt{2}k_R\\ \sqrt{2}k^+ - m\\ \sqrt{2}k_R\end{pmatrix}, \quad q_\downarrow(k) = \frac{1}{\sqrt{2\sqrt{2}k^+}}\begin{pmatrix}-\sqrt{2}k_L\\ \sqrt{2}k^+ + m\\ \sqrt{2}k_L\\ -\sqrt{2}k^+ + m\end{pmatrix},$$
$$v_\uparrow(k) = \frac{1}{\sqrt{2\sqrt{2}k^+}}\begin{pmatrix}\sqrt{2}k_L\\ -\sqrt{2}k^+ + m\\ -\sqrt{2}k_L\\ \sqrt{2}k^+ + m\end{pmatrix}, \quad v_\downarrow(k) = -\frac{1}{\sqrt{2\sqrt{2}k^+}}\begin{pmatrix}\sqrt{2}k^+ - m\\ \sqrt{2}k_R\\ \sqrt{2}k^+ + m\\ \sqrt{2}k_R\end{pmatrix}, \tag{2.43}$$

with

$$k_{R/L} = \frac{1}{\sqrt{2}} \left(k_x \pm i k_y \right), \tag{2.44}$$

and m the mass of the free quark. The light-cone spinors are equal to the Dirac spinors when $\boldsymbol{k} = 0$. In Eq. (2.42) the on-shell condition for the quark field reads:

$$k^- = \frac{m^2 + \boldsymbol{k}_\perp^2}{2k^+}. \tag{2.45}$$

The operators b, d in Eq. (2.42) are the annihilation operators of quark and antiquark states, respectively. These operators annihilate only good quark field. If the bad components are considered, the operators must be written using the equation of motion, see Sec. 3.4.3. The anti-commutation relations in Eq. (2.41) lead to the following relation in momentum space:

$$\begin{aligned} \left\{ b_e^{(f)}(k), b_{e'}^{(f')\dagger}(p) \right\} &= \left\{ d_e^{(f)}(k), d_{e'}^{(f')\dagger}(p) \right\} \\ &= 2k^+ (2\pi)^3 \delta_{e,e'} \delta_{f,f'} \delta \left(k^+ - p^+ \right) \delta \left(\boldsymbol{k}_\perp - \boldsymbol{p}_\perp \right), \end{aligned} \tag{2.46}$$

$$\begin{aligned} &\left\{ b_e^{(f)}(k), d_{e'}^{(f')\dagger}(p) \right\} = \left\{ b_e^{(f)}(k), b_{e'}^{(f')}(p) \right\} \\ &= \left\{ d_e^{(f)}(k), d_{e'}^{(f')}(p) \right\} = \left\{ b_e^{(f)}(k), d_{e'}^{(f')}(p) \right\} = 0. \end{aligned} \tag{2.47}$$

In the case of the gluon field the problem of gauge fixing arises. In fact, it is well known that in a gauge theory not all the four components of the gauge field A^μ are independent and one has to choose a gauge to remove the redundant components. For this section we shall assume the light-cone gauge [4, 5], i.e.

$$A^+ = 0. \tag{2.48}$$

The light-cone gauge is classified as an axial gauge. The above condition is not enough to completely fix the gauge. However, the residual gauge freedom is confined to the boundary conditions for $\boldsymbol{A}_\perp$ at light-cone infinity $\pm\infty^-$ (as we shall discuss in Sect. 2.4). Within the light-cone gauge, the A^- component is no longer independent, since it is fully determined by $\boldsymbol{A}_\perp$ at any given value of x^+. This can be seen via the EOM:

$$\partial^+ \partial^+ A^- - \partial^+ \partial^i A^i = -g_s J^+, \tag{2.49}$$

where the current J^+ is independent from the gluon field A^μ. The inversion of the EOM for both the quark and gluon fields is not a trivial task, because of the presence of the so-called zero modes, i.e. the fields at $k^+ = 0$. We will illustrate in detail the problem in Chapter 7. For this reason, we shall consider only the transverse components $A^i \equiv A^i_\perp$.

The commutation relations read:

$$\left[A^i_{\hat{a},\lambda}(x), -\partial^+ A^j_{\hat{b},\sigma}(y) \right] |_{x^+ = y^+} = i \delta^{ij} \delta^{\hat{a}\hat{b}} \delta_{\lambda\sigma} \delta(x^- - y^-) \delta(\boldsymbol{x}_\perp - \boldsymbol{y}_\perp), \tag{2.50}$$

where a, b are color indexes and λ, σ are the light-cone helicities.

The momentum-space representation is:

$$A^\mu(x) = \sum_{\lambda=\uparrow,\downarrow} \int \frac{dk^+ d\boldsymbol{k}_\perp}{2k^+(2\pi)^3} \left[e^{-ik\cdot\xi} \epsilon^\mu_\lambda(k) g_\lambda(k) + e^{ik\cdot\xi} \epsilon^{*\mu}_\lambda(k) g^\dagger_\lambda(k) \right], \tag{2.51}$$

with the gluon operator g_λ defined as:

$$g_\lambda = \sum_{\hat{a}} T^{\hat{a}} g^{\hat{a}}_\lambda. \tag{2.52}$$

The polarization vectors are:

$$\epsilon_\lambda(k) = \left(0, \frac{\boldsymbol{\epsilon}_{\perp\lambda}\cdot\boldsymbol{k}_\perp}{k^+}, \boldsymbol{\epsilon}_{\perp\lambda}\right), \quad \boldsymbol{\epsilon}_{\perp\uparrow} = \frac{-1}{\sqrt{2}}(1,i), \quad \boldsymbol{\epsilon}_{\perp\downarrow} = \frac{1}{\sqrt{2}}(1,-i). \tag{2.53}$$

In Eq. (2.51) the on-shell condition

$$k^- = \frac{\boldsymbol{k}^2_\perp}{2k^+} \tag{2.54}$$

is understood. The commutation relations in Eq. (2.50) translate into the following commutation relations in momentum space:

$$\left[g^{\hat{a}}_\lambda(k), \left(g^{\hat{b}}_\sigma\right)^\dagger(p) \right] = 2k^+(2\pi^3)\delta_{\hat{a}\hat{a}}\delta_{\lambda\sigma}\delta\left(k^+ - p^+\right)\delta\left(\boldsymbol{k}_\perp - \boldsymbol{k}_\perp\right), \tag{2.55}$$

$$\left[g^{\hat{a}}_\lambda(k), g^{\hat{b}}_\sigma(p) \right] = 0. \tag{2.56}$$

2.3 Fock-state decomposition

Equipped with the basic notions of light-front quantization, we can now start looking into eigenstates of QCD, namely hadrons. Hadrons are multi-particle states, i.e. they are composite systems constructed with the fundamental degrees of freedom of QCD: quarks and gluons. We will focus on the proton as a working example, but the concepts that we shall illustrate are, *mutatis mutandis*, applicable also to all the other types of hadrons[3]. A complete description of the proton starting from the QCD Lagrangian is still missing, since the perturbative methods fail at energies scales comparable with the proton mass due to the large strong coupling constant. The broad problem of solving QCD at low-energy scale is sometimes referred to as the confinement problem: we do not observe free fundamental QCD degrees of freedom.

The first historical attempt to organize the hadrons as multiplets of some sort led Gell-Mann to propose his famous "Eightfold way" [6], which allows one to classify all the hadrons on the basis of the quantum numbers of the quarks.

[3]We will not investigate states that are not stable in QCD, because this is beyond the scope of this thesis.

In this model, the proton is viewed as composite of two up quarks and one down quark. However, a number of problems emerges from this picture: an intrinsic gluon contribution to the proton was shown to be significant and not negligible; the helicity of quarks seems to add up to about one-third of the spin of the proton; other types of quarks are present, to different extent, inside the proton. An elegant way to encapsulate all these features in a theoretical description of the proton is to build the proton state as an element of the Fock space of QCD. The Fock space is constructed as the direct sum of the tensorial product of Hilbert spaces of free quarks (H_ψ), free gluons (H_A) and of the vacuum ($H_0 = \{|0\rangle\}$):

$$\mathcal{F} = H_0 + \bigoplus_{n=1}^{\infty} \left(\bigotimes_{i=1}^{n} H_\psi \right) + \bigoplus_{n=1}^{\infty} \left(\bigotimes_{i=1}^{n} H_A \right). \tag{2.57}$$

The individual Hilbert spaces are the ones associated with the momentum of the free particles $k^+, \boldsymbol{k}_\perp$ (k^- is fixed by the on-shell condition for the free particles), and with the light-cone helicity λ. We can introduce a basis for the Fock state as

$$\{|\sigma_n(k)\rangle\}_{n=0,1,\ldots} \tag{2.58}$$

Special attention deserves the vacuum state $n = 0$, upon which all the other states can be constructed via the creation operators of the free particles. One can indeed postulate the vacuum to be the lowest-energy state (assuming the vacuum energy to be zero) and to be invariant under Lorentz transformations [1]. This means, in particular, that the vacuum must be an eigenstate of the generators of space translations, namely[4]

$$P^+ |0\rangle = 0, \quad \boldsymbol{P}_\perp |0\rangle = \boldsymbol{0}_\perp. \tag{2.59}$$

If no gluons were present, these conditions, along with the fact that k^+ must be strictly positive for massive quarks, would have forced the vacuum to have a trivial structure. However, because the gluons can have $k^+ = 0$, the vacuum is populated by an infinite number of gluons, each of them having vanishing plus momentum [7, 8]. We shall not investigate further the vacuum structure, we only wish to remark that, although the light-front vacuum is simpler with respect to the instant-form vacuum, it is not trivial. We can now construct $|\sigma_n(k)\rangle$ for all n as:

$$|\sigma_n(p)\rangle = \prod_{i=1}^{n} a_i^\dagger(k_i^+, \boldsymbol{p}_{\perp,i}, \lambda_i) |0\rangle, \quad p^+ = \sum_{i=1}^{n} p_i^+, \ \boldsymbol{p}_\perp = \sum_{i=1}^{n} \boldsymbol{p}_{\perp,i}, \tag{2.60}$$

where $a_i^\dagger$ is a shorthand notation that includes gluon, quark, or antiquark creation operators in momentum space with light-cone helicity λ.

[4]For this Chapter only, we reserve P^μ as a notation to indicate the momentum operator and p^μ to indicate the momentum eigenvalue.

Since $\{|\sigma_n\rangle\}_n$ forms a basis for the Fock space, we have the completeness relation:

$$\sum_n \sum\!\!\!\!\!\!\int |\sigma_n\rangle \langle\sigma_n| = \mathbb{1}. \tag{2.61}$$

where the $\sum\!\!\!\!\!\!\int$ symbol is a shorthand notation to indicate the sum over all the discrete variables (like color, light-cone helicity, flavor) and the integration over all the continuous variables. For the momentum integral, the measure is the Lorentz invariant measure on the light cone, since we must have

$$\sum\!\!\!\!\!\!\int \langle\sigma_n(p)|\sigma_m(q)\rangle = \delta_{nm} 2p^+ \delta(p^+ - q^+)\delta(\boldsymbol{p}_\perp - \boldsymbol{q}_\perp). \tag{2.62}$$

A proton state is identified as the solution $|\Psi\rangle$ of the eigenvalue problem

$$P^- |\Psi\rangle = \frac{M^2 + \boldsymbol{P}_\perp^2}{2P^+} |\Psi\rangle = \frac{M^2 + \boldsymbol{p}_\perp^2}{2p^+} |\Psi\rangle \tag{2.63}$$

with mass M, momentum $P^+, \boldsymbol{P}_\perp$ and helicity Λ, and it can be decomposed in the Fock basis as:

$$|\Psi\rangle = \sum_n \sum\!\!\!\!\!\!\int \langle\sigma_n|\Psi\rangle |\sigma_n\rangle = \sum_n \sum\!\!\!\!\!\!\int \Psi_n |\sigma_n\rangle . \tag{2.64}$$

The coefficient in front of each basis state is called Light-Front Wave Function (LFWF). It depends upon the intrinsic variables of the partons inside the proton, i.e.

$$\Psi_n = \Psi_n \left(\{x_i, \boldsymbol{k}_{\perp,i}, \lambda_i\}, \Lambda\right), \tag{2.65}$$

where $x_i = k_i^+/p^+ i$ and

$$\sum_{i=1}^n \boldsymbol{k}_{\perp,i} = \boldsymbol{0}_\perp. \tag{2.66}$$

The fact that the LFWFs do not depend on the total momentum $\boldsymbol{p}_\perp$ is a consequence of the kinematical nature of transverse boosts in light-front parametrization, see Eq. (2.18). The dependence of the state $|\Psi\rangle$ on $\boldsymbol{p}_\perp$ is completely carried by the states $|\sigma_n\rangle$, where the individual parton states have transverse momentum

$$\boldsymbol{p}_{\perp,i} = \boldsymbol{k}_{\perp,i} + x_i \boldsymbol{p}_\perp. \tag{2.67}$$

In the following, the proton state $|\Psi\rangle$ will be indicated with $|p, \Lambda\rangle$, where p indicates the total proton momentum

$$p^\mu = \left(p^+, \frac{M^2 + \boldsymbol{p}_\perp^2}{2p^+}, \boldsymbol{p}_\perp\right), \tag{2.68}$$

and Λ its light-cone helicity. The normalization of the hadron state reads:

$$\langle p', \Lambda'|p, \Lambda\rangle = 2p^+ \delta(p^+ - p^{'+})\delta(\boldsymbol{p}_\perp - \boldsymbol{p}'_\perp)\delta_{\Lambda\Lambda'}, \tag{2.69}$$

with

$$\sum_n |\Psi_n|^2 = 1. \tag{2.70}$$

This leads to the interpretation of the LFWFs as the probability amplitudes of finding their corresponding Fock state in the proton state.

The light-cone helicity of the proton state Λ is the eigenvalue of the light-cone helicity operator introduced in Eq. (2.35). The operator $\boldsymbol{R}_\perp$ is determined by the transverse positions of the partons, weighted by their plus-momentum fractions with respect to the total plus-momentum of the hadron:

$$\boldsymbol{R}_\perp = \sum_{i=1}^{n} x_i \boldsymbol{b}_{\perp,i}. \tag{2.71}$$

The total transverse momentum is

$$\boldsymbol{p}_\perp = \sum_{i=1}^{n} \boldsymbol{p}_{\perp,i}. \tag{2.72}$$

Combining Eqs. (2.71)-(2.72), one is easily convinced that the sum of light-cone helicity of the individual partons is not enough to obtain the light-cone helicity of the proton in Eq. (2.38). Instead, the parton orbital angular momentum must be included.

2.4 Light-cone gauge

We devote this section to give a brief overview of the light-cone gauge [4, 5]. We will use light-cone gauge all throughout this thesis, with the only exception of Chapter 8 where we will use the Feynman gauge. In order to fix the gauge, we add an extra term to the Lagrangian in Eq. (2.27) as a Lagrangian multiplier. For the light-cone gauge this reads:

$$\mathcal{L}_{LC} = \lim_{\alpha\to\infty} -\frac{1}{2\alpha}(n_\mu A^\mu)^2, \tag{2.73}$$

where $n^\mu = (0, 1, \mathbf{0}_\perp)$ and α is a parameter necessary to obtain the correct dimension of the gauge-fixing term. For the Feynman gauge instead we have:

$$\mathcal{L}_F = -(\partial_\mu A^\mu)^2. \tag{2.74}$$

We can now derive the propagator in the light-cone gauge for a free gluon Refs. [9, 10]

$$-iq^2 D^{\mu\nu}(q) = -iq^2 \sum_{\lambda=1,2} (\varepsilon^\mu_\lambda)^*(q)\varepsilon^\nu_\lambda(q) = -g^{\mu\nu} + \frac{q^{\{\mu}n^{\nu\}}}{n\cdot q} - q^2\frac{n^\mu n^\nu}{(n\cdot q)^2}. \tag{2.75}$$

As previously noted, since the gluon is a massless particle, the "+" component of its momentum $q^+ = n \cdot q$ can vanish. Hence, Eq. (2.75) is intrinsically ill defined, and this is a direct consequence of the fact that $n \cdot A = 0$ does not fix completely the gauge. The residual gauge freedom can be fixed by

using additional boundary conditions on the gauge potential. There are three common choices:

$$\boldsymbol{A}_\perp(\infty^-) = 0, \qquad \boldsymbol{A}_\perp(-\infty^-) = 0, \qquad \boldsymbol{A}_\perp(\infty^-) + \boldsymbol{A}_\perp(-\infty^-) = 0, \tag{2.76}$$

known, respectively, as retarded, advanced and principal value prescription. These choices map directly to the following prescriptions [11]:

$$\text{Retarded:} \quad \frac{1}{n\cdot q} \longrightarrow \frac{1}{n\cdot q + i\varepsilon}, \tag{2.77}$$

$$\text{Advanced:} \quad \frac{1}{n\cdot q} \longrightarrow \frac{1}{n\cdot q - i\varepsilon}, \tag{2.78}$$

$$\text{Principal Value:} \quad \frac{1}{n\cdot q} \longrightarrow \frac{1}{2}\left(\frac{1}{n\cdot q + i\varepsilon} + \frac{1}{n\cdot q - i\varepsilon}\right), \tag{2.79}$$

with $\varepsilon > 0$.

For comparison, and for later convenience, the propagator in Feynman gauge reads:

$$-iq^2 D^{\mu\nu}(q) = -iq^2 \sum_{\lambda=0}^{4} (\varepsilon_\lambda^\mu)^*(q)\varepsilon_\lambda^\nu = -g^{\mu\nu} \tag{2.80}$$

and the gauge condition $\partial_\mu A^\mu$ is not imposed directly at the operator level but at the level of the physical states:

$$\partial_\mu A^\mu \,|\Psi\rangle = 0. \tag{2.81}$$

The choice of a particular gauge is mainly a matter of convenience, in order to simplify certain problems and/or calculations, since all the physical observables must be gauge independent.

Chapter 3

Parton Distributions Landscape

3.1 Introduction

In the previous chapter, we introduced the notion of light-front quantization and we used it to formally construct the proton state as a superposition of states of the QCD Fock space. The LFWFs are the coefficients of each state in the expansion. Direct access to the LFWFs is, however, not possible from an experimental point of view. Available information on the proton partonic structure relies largely on the possibility of extracting particular functions from experiments, called parton distributions functions, see Refs. [12–18] and the Habil. Thesis [19]. These distributions provide a multi-dimensional description of the proton in terms of its elementary constituents both in momentum and position space.

For illustration purposes, let us consider a process in which a proton of mass M, with initial momentum p and light-cone helicity Λ, interacts with a probe particle. After the interaction, the proton is in a state with momentum p' and light-cone helicity Λ'. Convenient variables for studying this type of processes are the unbalance in momentum between the final and initial proton and the average momentum of the two states (see Refs. [20, 21]):

$$\Delta = p' - p, \quad P = \frac{p + p'}{2}. \tag{3.1}$$

The on-shell condition for the initial and final proton states leads to

$$P^2 = M^2 - \frac{\Delta^2}{4}, \quad P \cdot \Delta = 0. \tag{3.2}$$

In order to obtain a physical picture of the scattering process, it is essential to identify all the energy scales at stake. Let us assume that μ is the largest energy scale of the process (typically, it can be identified as the four-momentum squared of a virtual photon exchanged between the probe and the proton target, but other cases are possible). If μ is "large" enough, i.e. if we have

$$\frac{\mu}{M^2} \gg 1, \tag{3.3}$$

the resolution power of the probe is enough to distinguish the individual partons inside the proton. In other words, we can reasonably assume that the interaction between the probe and the proton can be written as the convolution of a hard-scattering kernel between the probe and one parton inside the proton and a parton distribution function. This interpretation was proven true for some particular processes, like deeply virtual Compton scattering (DVCS) (see Ref. [22]), semi-inclusive deep inelastic scattering (SIDIS), Drell-Yan production (see Ref. [12]). In the other limit, in which the scale μ is small compared to the proton mass, the resolution power of the probe is not enough to access the parton distributions and the process can be described in terms of the resonant and non-resonant excitation spectrum of the proton. In the intermediate region a clear physical picture is still lacking.

We are going to focus only on the limit of large μ, and, generally, we are going to assume that the parton interacting with the probe is a quark and we will call it the "active parton".

3.1.1 Processes in the deep inelastic regime

SIDIS The semi-inclusive deep inelastic scattering is the process:

$$\ell(l) + P(p) \to \ell' + h(p_h) + X(P_X), \tag{3.4}$$

where ℓ is a lepton, typically an electron or a muon, P a proton, h a detected final hadron and X indicates an inclusive system of particles [23]. The four-momentum of each particle is indicated in brackets. The cross section in the one-photon exchange approximation is proportional to the product of a leptonic tensor, that encapsulates the information on the probe, and an hadronic tensor, that contains all the relevant information on the proton structure. In the SIDIS process the hard scale μ is provided by the four-momentum squared of the virtual photon.

DVCS The deeply virtual Compton scattering is an exclusive process:

$$\ell(l) + P(p) \to \ell' + \gamma(p_\gamma) + P(p'), \tag{3.5}$$

where ℓ is a lepton, typically an electron or a muon, P a proton with initial and final four-momentum p and p', respectively, and γ a detected real photon [23]. The four-momentum of each particle is indicated in brackets. Also in this case the cross section in the one-photon exchange approximation is proportional to the product of a leptonic tensor, that encapsulates the information on the probe, and an hadronic tensor, that contains all the relevant information on the proton structure. However, coherent interaction between the proton and the probe, i.e. the exchange of a single virtual photon and the emission of the final real photon via the Bremsstrahlung mechanism, exists alongside the partonic subprocess. In practice, the interference between the two processes is used to enhance the hadronic contribution and extract information on the proton structure. In DVCS the hard scale μ is provided by the four-momentum squared of the virtual photon.

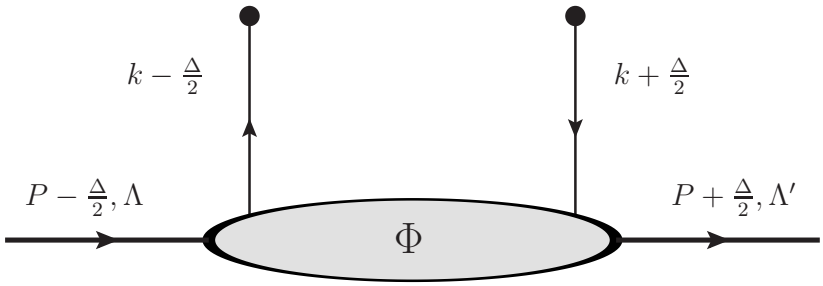

Figure 3.1: Diagram for the fully unintegrated parton correlator. The dots on top of the quark lines indicate that the quark line is attached to an hard-scattering kernel.

Drell-Yan Drell-Yan (DY) is hadronic lepton production, i.e.

$$A(p_a) + B(p_b) \to \ell(l)\bar{\ell}(l') + X(P_X), \tag{3.6}$$

where A and B indicate two initial-state hadrons (e.g. protons) and ℓ $\bar{\ell}$ a pair of lepton-antilepton detected in the final state. At variance with DVCS and SIDIS, the DY process does not require a leptonic probe, but rather an hadronic one, hence it is suitable for investigations at hadron-hadron colliders, such as LHC. In DY the hard scale μ is provided by the invariant mass squared of the final lepton sub-system.

3.2 Parton Correlator

The structure of the hadronic tensor for the above-mentioned processes can be exploited further to arrive at the fundamental object that describes the partonic structure of the proton: the parton correlator. All parton distributions are the fundamental building blocks of the parton correlator. The definition of the fully unintegrated quark-quark correlator reads [13]:

$$(\Phi_{\Lambda,\Lambda'})_{ij}(k, \Delta, P) = \int \frac{d^4\xi}{(2\pi)^4} \langle p', \Lambda' | \bar{\psi}_j(0)\psi_i(\xi) | p, \Lambda \rangle , \tag{3.7}$$

and it is diagrammatically represented in Fig. 3.1.

However, the simple picture of Fig. 3.1 is only an approximation, because it does neglect the interaction, mediated by the exchange of soft gluons, between the remnant and the active quark. A more realistic picture is shown in Fig. 3.2. For SIDIS, DVCS, DY processes, it was proven that the soft gluons can be factorized from the hard-scattering kernel, leading to the diagrammatic representation of the parton correlator given in Fig. 3.2. Therefore, appropriate definition of the parton distribution functions must be given in terms of the correlator of Fig. 3.2. Processes that break factorization cannot be described in terms of parton distribution functions, and we shall not consider them. The

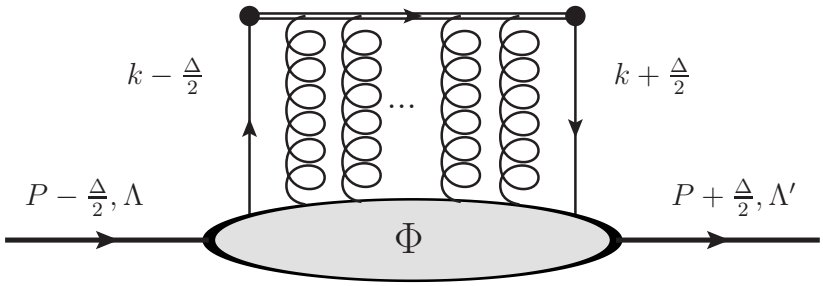

Figure 3.2: Diagram for the fully unintegrated parton correlator. The dots on top of the quark lines indicates that the quark line is attached to an hard-scattering kernel. The double line to which the gluon are attached represents the gauge-link insertion.

gluon contribution in Fig. 3.2 can be encapsulated in the so-called gauge link or Wilson line, as shown in Refs. [24–33]. The gauge link is defined as

$$\mathcal{W}(a,b) = \mathcal{P} e^{-ig\int_{\gamma(a,b)} d\zeta \cdot A(\zeta)}, \tag{3.8}$$

where $\gamma(a,b)$ is a path, connecting the four-dimensional spacetime points a and b, determined by the specific process under investigation, and $\mathcal{P}$ indicates the path-ordering of the exponential[1]:

$$\mathcal{W}(a,b) = 1 - ig_s \int_0^1 ds \gamma'(s)\cdot A(s) + (-ig_s)^2 \int_0^1 ds \int_0^s dt \gamma'(s)\cdot A(s)\gamma'(t)\cdot A(t) + ... \tag{3.9}$$

With the inclusion of the gauge link, Eq. (3.7) is modified into:

$$\left(\Phi_{\Lambda,\Lambda'}\right)_{ij}(k,\Delta,P,\gamma) = \int \frac{d^4z}{(2\pi)^4} e^{ik\cdot z} \left\langle p',\Lambda'\right| \bar{\psi}_j(0)\mathcal{W}(0,z)\psi_i(z)\left|p,\Lambda\right\rangle, \tag{3.10}$$

where we made explicit the dependence of the correlator on the path along which the gauge link runs. The Eq. (3.10) explicitly states that the quark correlator is defined in a process-dependent way, hence also the parton distributions are process-dependent quantities. This dependence is, however, under control, being related to the gauge-link path. The gauge link also ensures the gauge invariance of the quark correlator. In fact, the bi-local operator of the naïve version of the quark-quark correlator (Eq. (3.7))

$$\bar{\psi}(0)\psi(z) \tag{3.11}$$

is not invariant under local gauge transformation:

$$\bar{\psi}(0)\psi(z) \to \bar{\psi}'(0)\psi'(z) = \bar{\psi}(0)U^\dagger(0)U(z)\psi(z) \neq \bar{\psi}(0)\psi(z), \tag{3.12}$$

where U is the unitary matrix that implements the gauge transformation in the fundamental representation of the gauge group.

[1]The path ordering is inessential in the case of an abelian theory, such as QED.

It can be shown that under a gauge transformation the gauge link transforms as

$$\mathcal{W}'(a,b) = U(a)\mathcal{W}(a,b)U^\dagger(b). \tag{3.13}$$

In this case, the transformation is performed via unitary matrices in the fundamental representation, since the gauge link connects two quark fields. For gluon correlation functions the Wilson line transforms in the adjoint representation and it can be shown that two Wilson lines are necessary to ensure the gauge invariance of a gluon-gluon correlator. It is now immediate to see that the operator in Eq. (3.10) is gauge invariant.

3.2.1 The quark-quark correlator

The correlator in Eq. (3.10) has a Dirac structure that is inherited from the uncontracted Dirac indexes of the two quarks fields. The parton correlator can be parametrized in terms of parton distribution functions by taking the trace in Dirac space with appropriate Dirac matrices Γ:

$$\Phi^{[\Gamma]}_{\Lambda,\Lambda'}(k,\Delta,P,\gamma) = \int \frac{d^4z}{2(2\pi)^4} e^{ik\cdot z} \langle p',\Lambda'|\,\bar\psi(0)\mathcal{W}(0,z)\Gamma\psi(z)\,|p,\Lambda\rangle\,, \tag{3.14}$$

where we have that Γ belongs to the basis of Dirac structures, i.e.:

$$\Gamma \in \{\mathbb{1}, \gamma^\mu, \gamma_5, \gamma^\mu\gamma_5, i\sigma^{\mu\nu}\}. \tag{3.15}$$

Each Dirac matrix projects on different light-cone helicity configurations of both the proton and the active parton, encapsulating all the possible helicity changing combinations. If one or two bad components of the quark field are involved, they can be removed using the EOM. As a result, the parton distributions are expressed as the sum of different contributions given in terms of the good quark fields with different helicities. For each matrices in the set (3.15), Eq. (3.14) can be easily expressed in terms of parton distributions and momentum-dependent coefficients, as shown in Ref. [13].

Parton distributions cannot be calculated solely from the QCD Lagrangian with the current knowledge, since their nature is inherently non-perturbative. We can, however, extract a number of them from carefully designed experiments. However, to the present day, no process is yet being identified to gain access to the unintegrated correlator of Eq. (3.14). All the known processes give access only to the parton distributions that appear in the decomposition of the k^- integrated correlator:

$$\begin{aligned}\Phi^{[\Gamma]}_{\Lambda,\Lambda'}(\bar x,\boldsymbol{k}_\perp,\Delta,P,\gamma) &= \int dk^-\,\Phi^{[\Gamma]}_{\Lambda,\Lambda'}(k,\Delta,P,\gamma)\\ &= \int \frac{dz^-d\boldsymbol{z}_\perp}{2(2\pi)^3} e^{i\bar x P^+\cdot z^-} e^{-i\boldsymbol{k}_\perp\cdot\boldsymbol{z}_\perp} \langle p',\Lambda'|\,\bar\psi(0)\mathcal{W}(0,z)\Gamma\psi(z)\,|p,\Lambda\rangle\,\Big|_{z^+=0},\end{aligned} \tag{3.16}$$

where $\bar{x} = k^+/P^+$ is the average longitudinal-momentum fraction of the proton carried by the active parton. In the correlator of Eq. (3.16) is contained a six-dimensional information about the parton inside the proton. In fact the on-shell conditions for the initial and final proton reduce the number of independent component of Δ from four to three and the component that is eliminated is usually Δ^-. The other three-dimensional information is given in terms of the parton momentum.

From the six-dimensional momentum picture (three components of the parton momentum and the three components of Δ), we can extract a three dimensional map of the quark in the momentum space $(x, \boldsymbol{k}_\perp)$ plus a two-dimensional picture in transvserse-position space $(\boldsymbol{b}_\perp)$. This is done by taking the Fourier transform with respect to $\boldsymbol{\Delta}_\perp$ in the limit $\Delta^+ \to 0$, in order to ensure a proper partonic interpretation (see Refs. [34–37]):

$$\begin{aligned}
&\Phi^{[\Gamma]}_{\Lambda,\Lambda'}(\bar{x}, \boldsymbol{k}_\perp, \boldsymbol{b}_\perp, p, \gamma) = \int \frac{d\boldsymbol{\Delta}_\perp}{(2\pi)^2} e^{-i\boldsymbol{b}_\perp\cdot\boldsymbol{\Delta}_\perp} \Phi^{[\Gamma]}_{\Lambda,\Lambda'}(\bar{x}, \boldsymbol{k}_\perp, \Delta^+ = 0, \boldsymbol{\Delta}_\perp, p, \gamma) \\
&= \int \frac{dz^- d\boldsymbol{z}_\perp}{2(2\pi)^3} e^{i\bar{x}p^+\cdot z^-} e^{-i\boldsymbol{k}_\perp\cdot\boldsymbol{z}_\perp} \left\langle p^+, \boldsymbol{r}_\perp = \boldsymbol{0}_\perp, \Lambda' \right| \bar{\psi}(0^+, 0^-, \boldsymbol{b}_\perp) \\
&\times \mathcal{W}((0^+, 0^-, \boldsymbol{b}_\perp), (0^+, z^-, \boldsymbol{b}_\perp + \boldsymbol{z}_\perp)) \Gamma \psi(0^+, z^-, \boldsymbol{b}_\perp + \boldsymbol{z}_\perp) \left| p^+, \boldsymbol{r}_\perp = \boldsymbol{0}_\perp, \Lambda \right\rangle .
\end{aligned} \tag{3.17}$$

In Eq. (3.17), the proton is assumed to be in an eigenstate of the operator $\boldsymbol{R}_\perp$, see Eq. (2.39). This state can be obtained from the standard momentum eigenstate $|p^+, \boldsymbol{p}_\perp, \Lambda\rangle$ via the Fourier transform:

$$|p^+, \boldsymbol{r}_\perp, \Lambda\rangle = \mathcal{N} \int \frac{d^2\boldsymbol{p}_\perp}{(2\pi)^2} e^{-i\boldsymbol{r}_\perp\cdot\boldsymbol{p}_\perp} |p^+, \boldsymbol{p}_\perp, \Lambda\rangle , \tag{3.18}$$

where $\mathcal{N}$ is a normalization constant to ensure that:

$$\langle q^+, \boldsymbol{s}_\perp, \Lambda' | p^+, \boldsymbol{r}_\perp, \Lambda\rangle = \delta(\boldsymbol{s}_\perp - \boldsymbol{r}_\perp)\delta(q^+ - p^+)\delta_{\Lambda\Lambda'}. \tag{3.19}$$

The normalization constant in Eq. (3.18) turns out to be proportional to a Dirac delta function. To avoid an infinite normalization constant a momentum wave packet can be included in the Fourier transform. It is however shown in Ref. [38] that all the conclusions remain the same if the wave packet is ignored. Therefore, for simplicity, we shall never include it [37].

Finally, the state $|p^+, \boldsymbol{r}_\perp, \Lambda\rangle$ is a simultaneous eigenstate of the plus momentum and the transverse center of momentum because $\boldsymbol{B}_\perp$, and therefore $\boldsymbol{R}_\perp$, commute with P^+, as reported in Tab. 2.1.

Before moving on and classifying all various types of parton distributions, a final remark is in order. Depending on which Dirac matrix is chosen in Eq. (3.16) different powers of M/P^+ appears. If one identifies the hard scale μ with P^+, a natural ordering in the smallness parameter M/P^+ arises. We can classify all the objects in terms of the power in M/P^+ they carry in the parametrization of the correlator. This is called kinematical-twist expansion

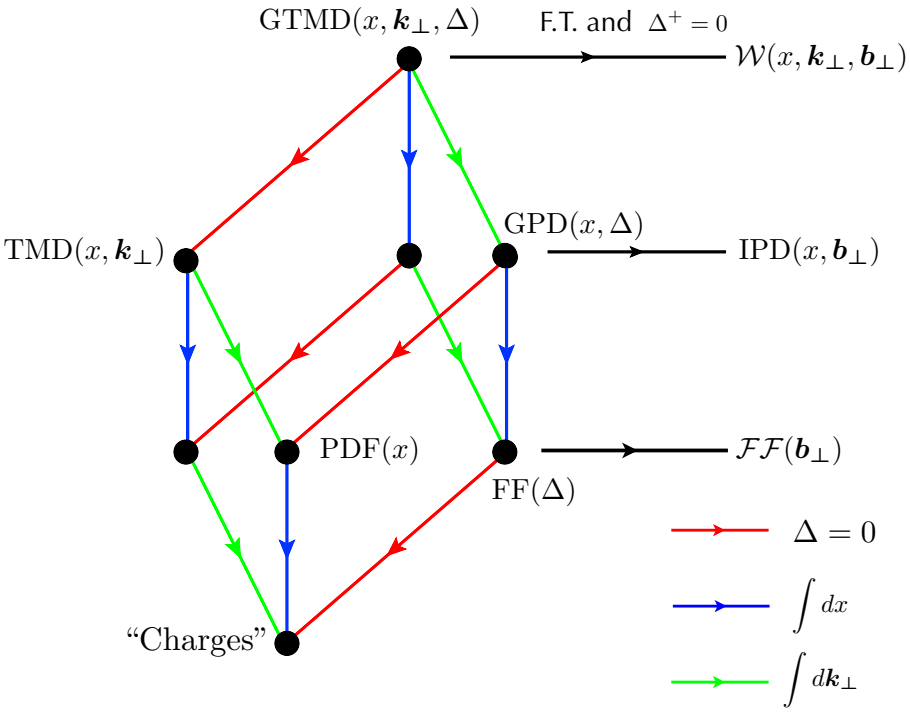

Figure 3.3: Links among different distribution functions at leading twist. The red, green, blu and black lines indicate the limits in which we take $\Delta = 0$, integrate over x, integrate over $\boldsymbol{k}_\perp$, take the Fourier transform at $\Delta^+ = 0$ with respect to $\boldsymbol{\Delta}_\perp$, respectively. The figure is inspired from Ref. [16].

[39], and for a given kinematical twist t the corresponding power of M/P^+ is:

$$\left(\frac{M}{P^+}\right)^{t-2}. \tag{3.20}$$

It happens that t can be $2, 3$ or 4 for the quark-quark correlator in Eq. (3.14). This classification is inherently different with respect to the geometric-twist expansion, that is related to the Lorentz-index structure of the operator [40].

3.3 Parton Distributions

In Fig. 3.3 is given a pictorial representation of all the possible (single) parton distributions at leading twist and form factors associated with the fully unintegrated parton correlator and its projections. It is clear from the figure that all the parton distributions can be obtained by performing suitable limits and/or integrations of the general k^--integrated correlator of Eq. (3.16). On the top of the figure there are the Generalized Transverse Momentum dependent parton Distributions (GTMDs), that are obtained directly from the correlator of Eq. (3.16) [13]. Via a Fourier transform of the GTMDs from $\boldsymbol{\Delta}_\perp$ to $\boldsymbol{b}_\perp$ and in the limit of vanishing Δ^+, we obtain the Wigner distributions, that are the QCD analogues of the classical phase-space distributions [34–36, 41].

From the GTMDs, in the limit of vanishing momentum transfer, one obtains the Transverse Momentum Dependent parton distributions (TMDs). The TMDs encode the three-dimensional momentum picture of the proton partonic structure. We will focus extensively on the TMDs in Chapters 5, 6 and 7. DY and SIDIS are the two most commonly known processes that allow one to extract information on TMDs. From the GTMDs, via integration over the parton transverse momentum, one obtains the Generalized Parton Distributions (GPDs) [19], that are related via a Fourier transform to the Impact Parameter Dependent parton distributions (IPDs) [37]. Special attention to these distributions and possible connections between IPDs and TMDs are posed in Chapter 5. Deeply Virtual Compton scattering as well as deeply virtual exclusive meson production represent the golden channels to access the GPDs. By integration over the parton transverse momentum[2], the TMDs reduce to the collinear Parton Distribution Functions (PDFs) that can be recovered also from the GPDs in the limit $\Delta \to 0$. Extensively studied are also the Form Factors (FFs), that can be obtained from the GPDs via the integration over the light-cone fraction of momentum x, as shown in Fig. 3.3. By taking the Fourier transform of the FFs, one obtains the charge and magnetization densities in impact-parameter space. Fully integrated quantities (at the bottom of the figure) are called charges, and encode global properties of the proton. Trying to access the global properties of the proton via parton distributions can be challenging, especially from the experimental point of view, since the reconstruction of the full range in the integration variables is necessary. An alternative way to obtain the charges is to look at local operators, like the Energy Momentum Tensor, to which the Chapter 8 is entirely devoted.

We notice here that, if one cuts the diagram in Fig. 3.3 perpendicularly to the red line ($\Delta \to 0$ line), the remaining top right portion is entirely populated of parton distributions that can be accessed only in exclusive experiments, since the reconstruction of the final proton is necessary. These distributions show up at the amplitude level. On the contrary, the remaining bottom left portion of the diagram contains only parton distributions that can be accessed in (semi-)inclusive processes and which are defined at the cross section level.

3.3.1 GTMDs and Wigner distributions

In order to properly decompose Eq. (3.16) in terms of GTMDs, we need to fix the gauge-link path upon which the correlator depends. We choose to work with the most common paths shown in Fig. 3.5.

They are composed of three different pieces: two straight lines that run along the minus direction from either 0 or z to $\pm\infty^-$ and a straight line that runs along the transverse direction at $\pm\infty^-$. The two gauge links associated to ∞^- and $-\infty^-$ are characteristic of SIDIS and DY, respectively. We will give a brief

[2]The integral over the transverse momentum requires a suitable regularization of the ultraviolet region, which leads to modifications of this simple picture. More details can be found in the literature, see, e.g., Ref. [15].

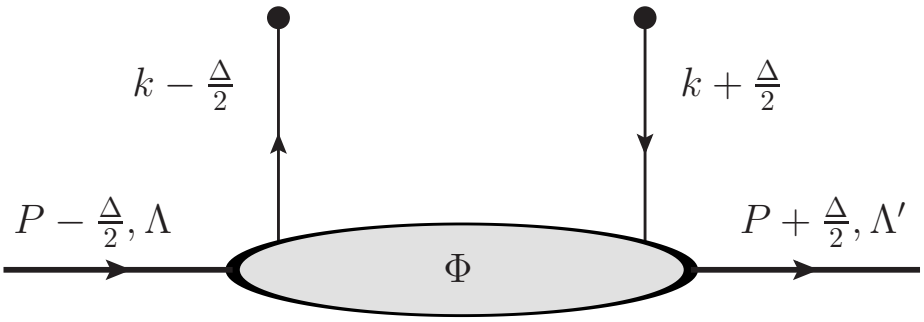

Figure 3.4: Diagrammatic representation of the GTMDs correlator Φ. The full dots on the quark lines indicate that the quark is extracted from the proton and enters the hard-scattering part (left dot), or it exits the hard-scattering part and is re-inserted in the proton (right dot). The diagram enters at the amplitude level.

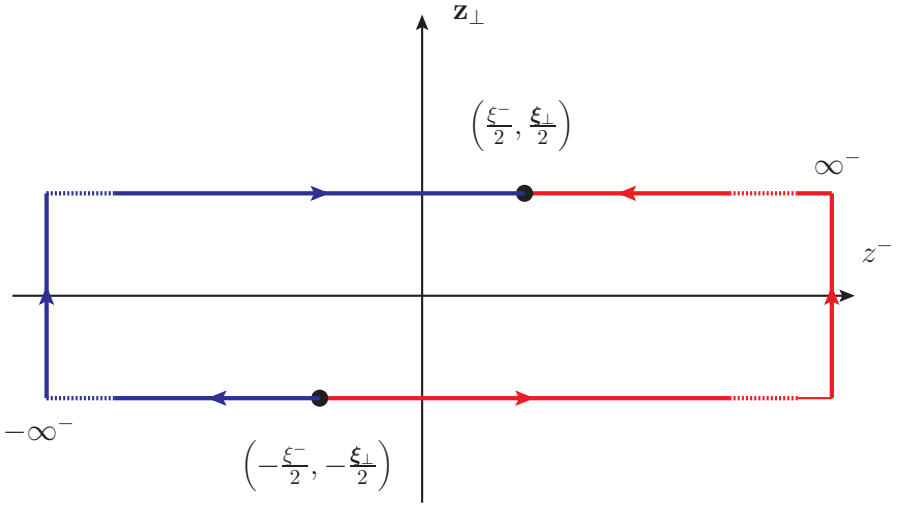

Figure 3.5: Schematic representation of two possible gauge links. The red one runs from the starting point $(-\frac{\xi^-}{2}, -\frac{\boldsymbol{\xi}_\perp}{2})$ to $+\infty^-$ along the light-cone direction, then it has a transverse piece at light-cone infinity, and it runs to the end point $\left(\frac{\xi^-}{2}, \frac{\boldsymbol{\xi}_\perp}{2}\right)$ along the light-cone direction. The blue path is very similar, the only difference being that it runs to $-\infty^-$ instead of $+\infty^-$. The red path is characteristic of SIDIS processes and it encodes the final-state interactions. The blue one is proper of Drell-Yan-like events and encodes the initial-state interactions.

description of these processes in Sec. 3.3.2. Following Ref. [13], we parametrize the choice with $\eta\infty^-$, where $\eta = \pm 1$. Here we note that the gauge link encodes the initial-state interactions ($\eta = -1$) or the final-state interactions ($\eta = +1$), see Sec. 3.3.2. The leading-twist sector (twist-2) is obtained with

$$\Gamma = \gamma^+, \gamma^+\gamma_5, i\sigma^{+i}\gamma_5, \tag{3.21}$$

and corresponds to

$$\begin{aligned}
\Phi^{[\gamma^+]}_{\Lambda,\Lambda'}(\bar{x}, \boldsymbol{k}_\perp, \Delta, P, \eta) &= \frac{1}{2M}\bar{u}(p', \Lambda')\Bigg[F_{1,1} + \frac{i\sigma^{i+}k^i_\perp}{P^+}F_{1,2} \\
&\quad + \frac{i\sigma^{i+}\Delta^i_\perp}{P^+}F_{1,3} + \frac{i\sigma^{ij}k^i_\perp\Delta^j_\perp}{M^2}F_{1,4}\Bigg]u(p, \Lambda), \qquad (3.22)\\
\Phi^{[\gamma^+\gamma_5]}_{\Lambda,\Lambda'}(\bar{x}, \boldsymbol{k}_\perp, \Delta, P, \eta) &= \frac{1}{2M}\bar{u}(p', \Lambda')\Bigg[\frac{-i\varepsilon^{ij}_\perp k^i_\perp\Delta^j_\perp}{M^2}G_{1,1} + \frac{i\sigma^{i+}\gamma_5 k^i_\perp}{P^+}G_{1,2} \\
&\quad + \frac{i\sigma^{i+}\gamma_5\Delta^i_\perp}{P^+}G_{1,3} + i\sigma^{+-}\gamma_5 G_{1,4}\Bigg]u(p, \Lambda), \qquad (3.23)\\
\Phi^{[i\sigma^{j+}\gamma_5]}_{\Lambda,\Lambda'}(\bar{x}, \boldsymbol{k}_\perp, \Delta, P, \eta) &= \frac{1}{2M}\bar{u}(p', \Lambda')\Bigg[\frac{-i\varepsilon^{ij}_\perp k^i_\perp}{M}H_{1,1} - \frac{i\varepsilon^{ij}_\perp\Delta^i_\perp}{M}H_{1,2} \\
&\quad + \frac{M}{P^+}i\sigma^{j+}\gamma_5 H_{1,3} + \frac{k^j_\perp i\sigma^{i+}\gamma_5 k^i_\perp}{MP^+}H_{1,4} \\
&\quad + \frac{\Delta^j_\perp i\sigma^{i+}\gamma_5 k^i_\perp}{MP^+}H_{1,5} + \frac{\Delta^j_\perp i\sigma^{i+}\gamma_5\Delta^i_\perp}{MP^+}H_{1,6} \\
&\quad + \frac{k^j_\perp i\sigma^{+-}\gamma_5}{M}H_{1,7} + \frac{\Delta^j_\perp i\sigma^{+-}\gamma_5}{M}H_{1,8}\Bigg]u(p, \Lambda), \qquad (3.24)
\end{aligned}$$

where $\varepsilon^{ij}_\perp = \varepsilon^{+-ij}$. The letter and subscript convention is as follows: F, G, H indicate, respectively, an unpolarized, longitudinally- or transversely-polarized proton target, the first subscript indicates the twist minus 1, the second subscript serves the only purpose of enumerating the different functions. The twist-3 GTMDs are obtained with the matrices $\Gamma = \mathbb{1}, \gamma_5, \gamma^j, \gamma^j\gamma_5, i\sigma^{ij}\gamma_5, i\sigma^{+-}\gamma_5$. We will not list all the twist-3 GTMDs, since it is beyond the scope of this work, and the interested reader can find all of them in Ref. [13]. We shall, however, give the explicit expressions for $\Gamma = \mathbb{1}$, since we are going to study one of the corresponding TMDs in Chapter 7:

$$\begin{aligned}
\Phi^{\mathbb{1}}_{\Lambda,\Lambda'}(\bar{x}, \boldsymbol{k}_\perp, \Delta, P, \eta) &= \frac{1}{2P^+}\bar{u}(p', \Lambda')\Bigg[E_{2,1} + \frac{i\sigma^{i+}k^i_\perp}{P^+}E_{2,2} \\
&\quad + \frac{i\sigma^{i+}\Delta^i_\perp}{P^+}E_{2,3} + \frac{i\sigma^{ij}k^i_\perp\Delta^j_\perp}{M^2}E_{2,4}\Bigg]u(p, \Lambda). \qquad (3.25)
\end{aligned}$$

The twist-4 GTMDs are obtained with $\Gamma = \gamma^-, \gamma^-\gamma_5, i\sigma^{j-}\gamma_5$. Each GTMD depends on the set of variables $(x, \xi, \boldsymbol{k}_\perp^2, \boldsymbol{\Delta}_\perp^2, \boldsymbol{k}_\perp \cdot \boldsymbol{\Delta}_\perp; \eta)$, where ξ is called skewness and measures the relative size of the transferred plus-momentum with respect to the average plus-momentum:

$$\xi = -\frac{\Delta^+}{2P^+}. \tag{3.26}$$

All the GTMDs are complex-valued functions and they must satisfy constraints imposed by hermiticity and time reversal (parity is ensured since it is implemented at the level of the Lorentz structures). With X denoting a generic GTMD, the hermiticity constraint imposes that:

$$X(\bar{x}, \xi, \boldsymbol{k}_\perp^2, \boldsymbol{\Delta}_\perp^2, \boldsymbol{k}_\perp \cdot \boldsymbol{\Delta}_\perp; \eta) = \pm X^*(\bar{x}, -\xi, \boldsymbol{k}_\perp^2, \boldsymbol{\Delta}_\perp^2, -\boldsymbol{k}_\perp \cdot \boldsymbol{\Delta}_\perp; \eta), \tag{3.27}$$

where the + sign holds for $F_{1,1/3/4}$ $G_{1,1/2/4}$ $H_{1,2/3/4/6/7}$ and $E_{2,1/3/4}$, and the minus sign for all the others. Time-reversal invariance imposes that:

$$X^*(\bar{x}, \xi, \boldsymbol{k}_\perp^2, \boldsymbol{\Delta}_\perp^2, \boldsymbol{k}_\perp \cdot \boldsymbol{\Delta}_\perp; \eta) = X(\bar{x}, \xi, \boldsymbol{k}_\perp^2, \boldsymbol{\Delta}_\perp^2, \boldsymbol{k}_\perp \cdot \boldsymbol{\Delta}_\perp; -\eta). \tag{3.28}$$

To gain more insights into the constraint imposed by the time-reversal invariance, we can express all the GTMDs as a sum of a real and an imaginary part:

$$X = X^e(\bar{x}, \xi, \boldsymbol{k}_\perp^2, \boldsymbol{\Delta}_\perp^2, \boldsymbol{k}_\perp \cdot \boldsymbol{\Delta}_\perp) + iX^o(\bar{x}, \xi, \boldsymbol{k}_\perp^2, \boldsymbol{\Delta}_\perp^2, \boldsymbol{k}_\perp \cdot \boldsymbol{\Delta}_\perp; \eta). \tag{3.29}$$

In Eq. (3.29) only the imaginary part depends on the direction of the gauge link, as can be deduced from Eq. (3.28):

$$X^o(\bar{x}, \xi, \boldsymbol{k}_\perp^2, \boldsymbol{\Delta}_\perp^2, \boldsymbol{k}_\perp \cdot \boldsymbol{\Delta}_\perp; \eta) = -X^o(\bar{x}, \xi, \boldsymbol{k}_\perp^2, \boldsymbol{\Delta}_\perp^2, \boldsymbol{k}_\perp \cdot \boldsymbol{\Delta}_\perp; -\eta), \tag{3.30}$$

$$X^e(\bar{x}, \xi, \boldsymbol{k}_\perp^2, \boldsymbol{\Delta}_\perp^2, \boldsymbol{k}_\perp \cdot \boldsymbol{\Delta}_\perp; \eta) = X^e(\bar{x}, \xi, \boldsymbol{k}_\perp^2, \boldsymbol{\Delta}_\perp^2, \boldsymbol{k}_\perp \cdot \boldsymbol{\Delta}_\perp; -\eta). \tag{3.31}$$

The real and imaginary part $X^{e,o}$ are known, respectively, as naïve T-even and naïve T-odd, because of their behavior under time reversal. The sign change in Eq. (3.30) was the reason why some of the TMDs, originally defined without the inclusion of the gauge link, were believed to vanish due to time-reversal invariance. This also warns us that the GTMDs are, in fact, process-dependent distributions, since they depend on the gauge-link path in a non-trivial way. We are able, however, to predict such dependence to some extent, and this can be used as a powerful testing tool for the theory when compared to the experiments.

The Wigner distributions can be calculated as Fourier transforms of the GTMDs at $\xi = 0$:

$$\mathcal{X}(\bar{x}, \xi, \boldsymbol{k}_\perp^2, \boldsymbol{b}_\perp^2, \boldsymbol{k}_\perp \cdot \boldsymbol{b}_\perp; \eta) = \int \frac{d\boldsymbol{\Delta}_\perp}{(2\pi)^2} e^{-i\boldsymbol{b}_\perp \cdot \boldsymbol{\Delta}_\perp} X(\bar{x}, \xi, \boldsymbol{k}_\perp^2, \boldsymbol{\Delta}_\perp^2, \boldsymbol{k}_\perp \cdot \boldsymbol{\Delta}_\perp; \eta). \tag{3.32}$$

One of the main interesting points about Wigner distributions is the possibility to gain direct access to information about the parton OAM. As shown

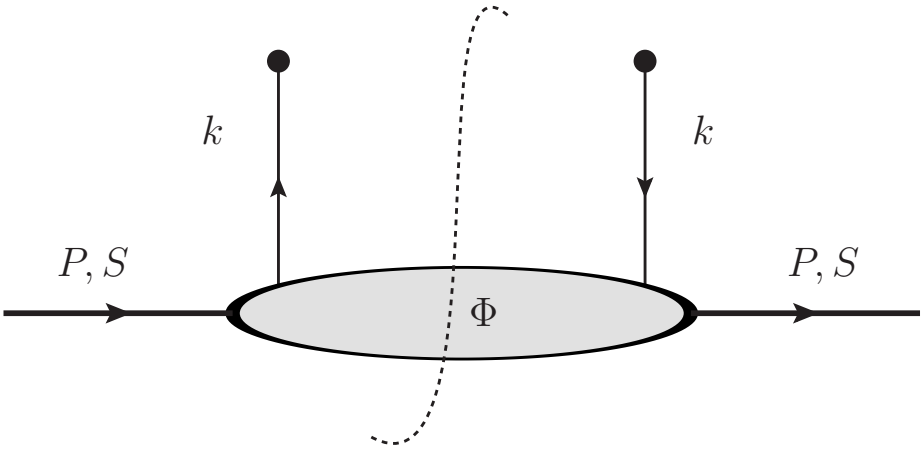

Figure 3.6: Diagrammatic representation of the TMDs correlator. The dashed line that cuts the diagrams, not present in the case of the GTMDs, indicates that the diagram is representing a cross section, not an amplitude. TMDs exist only at the cross-section level.

in Refs. [34–36, 41, 42], we can express the $\hat{z}$ component of the quark angular momentum as:

$$\begin{aligned} L_z^q(\gamma) &= \int d\bar{x} d\boldsymbol{k}_\perp d\boldsymbol{b}_\perp \varepsilon_\perp^{ij} k_{j\perp} b_{i\perp} \Phi_{++}^{\gamma^+}(\bar{x}, \boldsymbol{k}_\perp, \boldsymbol{b}_\perp, p, \gamma) \\ &= -\int d\bar{x} d\boldsymbol{k}_\perp \frac{\boldsymbol{k}_\perp^2}{M^2} F_{1,4}(\bar{x}, 0, \boldsymbol{k}_\perp^2, 0, 0, \gamma). \end{aligned} \tag{3.33}$$

Interestingly, the differences between all the possible definitions of the OAM are encoded in the dependence on the gauge-link path γ of Eq. (3.33), see Ref. [43] for the analysis of two of the most popular definitions of OAM.

3.3.2 Transverse-Momentum dependent parton Distributions

From the general expression of the GTMD correlator, by setting $\Delta = 0$, we recover the general TMD correlator [24, 44–48]:

$$\Phi_{\Lambda,\Lambda'}^{[\Gamma]}(x, \boldsymbol{k}_\perp, p^+, \boldsymbol{p}_\perp = \boldsymbol{0}_\perp, \eta) = \Phi_{\Lambda,\Lambda'}^{[\Gamma]}(\bar{x}, \boldsymbol{k}_\perp, \Delta = 0, P^+, \boldsymbol{P}_\perp = \boldsymbol{0}_\perp, \eta), \tag{3.34}$$

where $x = k^+/p^+ = \bar{x}$ since $\Delta = 0$. TMDs are given as real-value functions, therefore they correspond to either the real or to the imaginary part of appropriate GTMDs. Moreover, the TMDs are usually defined from the quark-quark correlator given in the proton spin basis, rather than in the light-cone helicity base. To connect the two expressions for the correlator, we need the proton-spin vector, defined as:

$$S = \left(\Lambda \frac{p^+}{M}, -\Lambda \frac{M}{2p^+}, \boldsymbol{S}_\perp \right). \tag{3.35}$$

The correlator in the spin basis then reads (see Refs. [49, 50]):

$$\Phi^{[\Gamma]}(x, \boldsymbol{k}_\perp, p, S, \eta) = \frac{1+\Lambda}{2} \Phi_{++}^{[\Gamma]}(x, \boldsymbol{k}_\perp, p, \eta) + \frac{1-\Lambda}{2} \Phi_{--}^{[\Gamma]}(x, \boldsymbol{k}_\perp, p, \eta)$$

$$+\frac{S_L}{2}\Phi^{[\Gamma]}_{+-}(x,\boldsymbol{k}_\perp,p,\eta)+\frac{S_R}{2}\Phi^{[\Gamma]}_{-+}(x,\boldsymbol{k}_\perp,p,\eta). \tag{3.36}$$

From the comparison with Eqs. (3.22)-(3.25) we have:

$$\Phi^{[\gamma^+]}(x,\boldsymbol{k}_\perp,p,S,\eta)=f_1(x,\boldsymbol{k}_\perp^2)-\frac{k_\perp^i S_\perp^j\varepsilon_\perp^{ij}}{M}f_{1T}^\perp(x,\boldsymbol{k}_\perp^2), \tag{3.37}$$

$$\Phi^{[\gamma^+\gamma_5]}(x,\boldsymbol{k}_\perp,p,S,\eta)=\Lambda g_1(x,\boldsymbol{k}_\perp^2)-\frac{\boldsymbol{k}_\perp\cdot\boldsymbol{S}_\perp}{M}g_{1T}(x,\boldsymbol{k}_\perp^2), \tag{3.38}$$

$$\begin{aligned}\Phi^{[i\sigma^{j+}\gamma_5]}(x,\boldsymbol{k}_\perp,p,S,\eta)&=S_\perp^j h_1(x,\boldsymbol{k}_\perp^2)+\Lambda\frac{k_\perp^i}{M}h_{1L}^\perp(x,\boldsymbol{k}_\perp^2)\\&\quad-\frac{k_\perp^i\boldsymbol{k}_\perp\cdot\boldsymbol{S}_\perp+\frac{1}{2}\boldsymbol{k}_\perp^2 S_\perp^j}{M}h_{1T}^\perp(x,\boldsymbol{k}_\perp^2)+\frac{\varepsilon^{ji}k_\perp^i}{M}h_1^\perp(x,\boldsymbol{k}_\perp^2),\end{aligned} \tag{3.39}$$

$$\Phi^{[\mathbb{1}]}(x,\boldsymbol{k}_\perp,p,S,\eta)=\frac{M}{p^+}\left(e(x,\boldsymbol{k}_\perp^2)-\frac{k_\perp^i S_\perp^j\varepsilon_\perp^{ij}}{M}e_T^\perp(x,\boldsymbol{k}_\perp^2)\right). \tag{3.40}$$

With these expressions, the connection between GTMDs and TMDs is easily obtained:

$$f_1(x,\boldsymbol{k}_\perp^2)=F^e_{1,1}(x,0,\boldsymbol{k}_\perp^2,0,0), \tag{3.41}$$

$$f_{1T}^\perp(x,\boldsymbol{k}_\perp^2)=-F^0_{1,2}(x,0,\boldsymbol{k}_\perp^2,0,0,\eta), \tag{3.42}$$

$$g_1(x,\boldsymbol{k}_\perp^2)=G^e_{1,4}(x,0,\boldsymbol{k}_\perp^2,0,0), \tag{3.43}$$

$$g_{1T}(x,\boldsymbol{k}_\perp^2)=G^e_{1,2}(x,0,\boldsymbol{k}_\perp^2,0,0), \tag{3.44}$$

$$h_1^\perp(x,\boldsymbol{k}_\perp^2)=-H^o_{1,1}(x,0,\boldsymbol{k}_\perp^2,0,0,\eta), \tag{3.45}$$

$$h_{1L}^\perp(x,\boldsymbol{k}_\perp^2)=H^e_{1,7}(x,0,\boldsymbol{k}_\perp^2,0,0), \tag{3.46}$$

$$h_{1T}^\perp(x,\boldsymbol{k}_\perp^2)=H^e_{1,4}(x,0,\boldsymbol{k}_\perp^2,0,0), \tag{3.47}$$

$$e(x,\boldsymbol{k}_\perp^2)=E^e_{2,1}(x,0,\boldsymbol{k}_\perp^2,0,0), \tag{3.48}$$

$$e_T^\perp(x,\boldsymbol{k}_\perp^2)=-E^o_{2,2}(x,0,\boldsymbol{k}_\perp^2,0,0,\eta). \tag{3.49}$$

The notation used for labelling the TMDs is related to the polarizations of the parent hadron and the active quark. Here we adopt the convention proposed in Ref. [47]: the letters L and T refer to the situation where the spin of the hadron is along the longitudinal direction and in the transverse plane, respectively. Similarly, the letters f, g and h refer to unpolarized, longitudinally-polarized and transversely-polarized active quark, respectively. The $\perp$ symbol indicates that the TMD enters the decomposition of the correlator with a weighting factor that depends on $\boldsymbol{k}_\perp$ with an open index. The classification of the TMDs in terms of the proton and active-quark polarization is correct only for the leading-twist TMDs. For the twist-3 and twist-4 TMDs, the interpretation in terms of states with well defined polarization of the good quark-field components is lost. A schematic summary of the twist-2 TMDs is given in Tab. 3.1.

It is also interesting to note that the naïve T-odd TMDs (at twist-2 the Sivers function $f_{1T}^\perp$ and the Boer-Mulders function $h_1^\perp$) are not directly related

quark pol.

nucleon pol.	U	L	T
U	f_1		$h_1^\perp$
L		g_1	$h_{1L}^\perp$
T	$f_{1T}^\perp$	g_{1T}	h_1, $h_{1T}^\perp$

Twist-2 TMDs

Table 3.1: Tables of the leading-twist TMDs with their relation to nucleon and quark polarization states.

to the quark OAM, as it is evident from Eq. (3.33). In fact, the OAM is expressed in terms of $F_{1,4}$ that does not appear in the TMD limit.

3.3.3 Generalized Parton Distributions and Impact Parameter Distributions

Generalized Parton Distributions can be obtained from the GTMDs by integrating over the parton transverse momentum:

$$\begin{aligned}\Phi^{[\Gamma]}_{\Lambda\Lambda'}(x,\Delta,P) &= \int d\boldsymbol{k}_\perp \Phi^{[\Gamma]}_{\Lambda\Lambda'}(x,\boldsymbol{k}_\perp,\Delta,P) \\ &= \int \frac{d\zeta^-}{4\pi} e^{ixP^+\zeta^-} \langle p',\Lambda'|\,\bar\psi(0)\mathcal{W}(0,\zeta)\psi(\zeta)\,|p,\Lambda\rangle\,\Big|_{\zeta^+=0,\boldsymbol{\zeta}_\perp=\mathbf{0}_\perp}.\end{aligned} \tag{3.50}$$

We note that the gauge-link path for a GPD runs along the light-cone direction ζ^-, without any contribution from the transverse direction. This entails that all the dependence on η that could derive from the GTMDs disappears. This immediately leads to the conclusion that all the GPDs are T-even distributions. We also note that, with a clever choice of the gauge, the gauge link in the definition of the GPDs can be reduced to unity. In light-cone gauge (see Sec. 2.4) we immediately have

$$\mathcal{W}(0,\zeta^-) = \mathcal{P}e^{-ig_S\int_0^{\zeta^-} dz^- A^+} = 1. \tag{3.51}$$

This argument strongly favors to using the light-cone gauge when dealing with the GPDs.

As we have done for the TMDs, we are going to give here the explicit expression for the traced GPDs correlator. We restrict ourself to the twist-2 GPDs, since our interest will never go beyond the leading twist:

$$\Phi^{[\gamma^+]}_{\Lambda\Lambda'}(x,\Delta,P) = \frac{1}{2P^+}\bar u(p',\Lambda')\Big(\gamma^+ H(x,\xi,t) + \frac{i\sigma^{+\mu}\Delta_\mu}{2M}E(x,\xi,t)\Big)u(p,\Lambda), \tag{3.52}$$

$$\Phi^{[\gamma^+\gamma_5]}_{\Lambda\Lambda'}(x,\Delta,P) = \frac{1}{2P^+}\bar{u}(p',\Lambda')\Big(\gamma^+\gamma_5\tilde{H}(x,\xi,t) - \frac{\xi\gamma_5 P^+}{M}\tilde{E}(x,\xi,t)\Big)u(p,\Lambda), \tag{3.53}$$

$$\begin{aligned}\Phi^{[i\sigma^{j+}\gamma_5]}_{\Lambda\Lambda'}(x,\Delta,P) = -\frac{\varepsilon^{ij}_\perp}{2P^+}\bar{u}(p',\Lambda')\Big(&i\sigma^{+i}H_T(x,\xi,t) + \frac{\gamma^{[+}\Delta^{i]}}{2M}E_T(x,\xi,t)\\ &+ \frac{P^{[+}\Delta^{i]}}{2M}\tilde{H}_T(x,\xi,t) + \frac{\gamma^{[+}P^{i]}}{2M}\tilde{E}_T(x,\xi,t)\Big)u(p,\Lambda),\end{aligned} \tag{3.54}$$

where we introduced the shorthand notation $a^{[\mu}b^{\nu]} := a^\mu b^\nu - a^\nu b^\mu$. The GPDs depend on the average momentum fraction x, the skewness ξ (introduced in the GTMD section) and the Mandelstam variable $t = -\Delta^2$.

The connection between GPDs and GTMDs is a little more involved compared to the TMD case. Since we will never make use of these relations in the present work, we refer the interested reader to Ref. [13].

The GPDs allow us to access the quark contribution to the total proton angular momentum via the relation (see Ref. [51]):

$$\langle J^z_q\rangle = \frac{1}{2}\int_0^1 dx x\left(H_q(x,\xi,0) + E_q(x,\xi,0)\right). \tag{3.55}$$

A similar relation holds for the gluon contribution to the total proton angular momentum. These relations require to integrate the GPDs over the full range in x to access the total proton angular momentum. Another way to obtain the same information is to use an appropriate local operator evaluated between proton states. We will analyze this topic in greater detail in Chapter 8. The integral in Eq. (3.55) are independent on the skewness ξ. This is a consequence of Lorentz invariance: the integration over x removes all reference to the particular light-cone direction with respect to which ξ is defined, so that the result must be ξ-independent.

From the GPDs, via Fourier transform, we can obtain the IPDs. At first, one could think of considering the three-dimensional Fourier transform

$$\int \frac{d\Delta^+ d\boldsymbol{\Delta}_\perp}{(2\pi)^3} e^{ib^-\Delta^+ - i\boldsymbol{b}_\perp\cdot\boldsymbol{\Delta}_\perp}\Phi^{[\Gamma]}_{\Lambda\Lambda'}(x,\Delta,P) \tag{3.56}$$

that would encapsulate three-dimensional space information on the distribution of the partons. However, as shown in Ref. [52], this definition is plagued with relativistic corrections, that spoil any probabilistic interpretation. Since the relativistic corrections are proportional to the energy transferred between the initial and final state, i.e. Δ^+ in light-front coordinates, one way to avoid this problem is to replace Eq. (3.56) with the following

$$\int \frac{d\Delta^+ d\boldsymbol{\Delta}_\perp}{(2\pi)^3} 2\pi\delta(\Delta^+) e^{-i\boldsymbol{b}_\perp\cdot\boldsymbol{\Delta}_\perp}\Phi^{[\Gamma]}_{\Lambda\Lambda'}(x,\Delta,P). \tag{3.57}$$

Hence, we obtain the following definition for the one plus two-dimensional IPD correlator

$$\Phi^{[\Gamma]}_{\Lambda\Lambda'}(x,\boldsymbol{b}_\perp,P) = \int \frac{d\boldsymbol{\Delta}_\perp}{(2\pi)^2} e^{-i\boldsymbol{b}_\perp\cdot\boldsymbol{\Delta}_\perp}\Phi^{[\Gamma]}_{\Lambda\Lambda'}(x,\xi=0,\boldsymbol{\Delta}_\perp,P). \tag{3.58}$$

Formally, the correlator on the left-hand side of Eq. (3.58) has the same structure as the TMDs correlator, with the role of $\boldsymbol{k}_\perp$ taken by $\boldsymbol{b}_\perp$. For this reason, there have been attempts to connect IPDs and TMDs, at least in model calculations. In particular naïve T-odd TMDs were found to be connected to some IPDs in simple models for the proton, see Refs. [37, 52–59]. The connection between the naïve T-odd TMDs and the T-even IPDs was established via a naïve T-odd function, known as 'lensing function', see Chapter 5. In Chapter 5 we are going to present an argument, that we consider both strong and convincing, to show that model-independent relations between TMDs and IPDs can not in general hold.

3.4 Light-Front Wave Functions and Distribution Amplitudes

In view of the variety of parton distributions that give access to different pictures of the parton content of the proton, a unified framework to describe the proton structure is desirable. To this aim, the LFWFs introduced in Sec. 2.3 are good candidates, both because of their interpretation and their versatility in model calculations. A complete description of the proton in terms of LFWFs is right now unrealistic, mainly because the Fock expansion is an infinite series. Even if we were able to exactly solve the QCD hamiltonian, that would reasonably happen only for the first few Fock states. Despite these limitations, we believe that the LFWFs offer the best tool at our disposal to describe the parton distributions, since each parton distribution can be seen as a particular combination of overlaps of LFWFs. We can exploit the LFWF framework to connect fits of (the valence part of) different types of parton distributions. This will eventually lead to a unified description of the parton distributions of the proton, that incorporates all available experimental measurements. If a model is being used, in which the Fock-state expansion is truncated up to some number of partons n, we can parametrize the error associated with this assumption by computing the norm deficiency in the proton state. For illustration purposes, let us assume that we truncate the Fock decomposition at the state with n partons:

$$|p,\Lambda\rangle_n = \sum_{i=1}^{n} \sum\!\!\!\!\!\!\int \Psi_i \, |\sigma_i\rangle \, . \tag{3.59}$$

Then we have:

$$_n\langle p',\Lambda'|p,\Lambda\rangle_n = 2p^+\delta(p'^+ - p^+)\delta(\boldsymbol{p}'_\perp - \boldsymbol{p}_\perp)\delta_{\Lambda',\Lambda}\sum_{i=1}^{n}\mathbb{P}_i, \tag{3.60}$$

where $\{\mathbb{P}_i\}_{i=1}^n$ are the probabilities associated with the Fock state with i partons, and can be expressed as the squared module of LFWFs for the corresponding

state. They satisfy:

$$\sum_{i=1}^{n} \mathbb{P}_i < 1 \quad \forall n, \quad \sum_{i=1}^{\infty} \mathbb{P}_i = 1. \tag{3.61}$$

Therefore, since each Fock state ultimately contributes to any parton distribution proportionally to its probability $\mathbb{P}_i$, we have an indication of how close is the approximation to the full result. From a practical point of view, besides the truncation of the Fock-space expansion, we need to introduce a model for the LFWFs. We are going to choose a specific model, outlined in Chapter 6. We shall fit the model parameters to available phenomenological extractions of the PDFs and then use these fit results to give predictions for the TMDs and GPDs. We believe that this approach provides a useful and practical tool for the extraction of the parton distribution functions in a unified framework: instead of creating an *ad hoc* model for each distribution, we rely on the substrate of LFWFs to provide the general model for all of them, and use the information extracted from one fit to obtain predictions for different distributions.

3.4.1 Distribution Amplitudes

A complementary information on the proton structure with respect to the parton distributions is given by the Distribution Amplitudes (DAs). These are proton-to-vacuum matrix elements of non-local gauge-invariant operators built of quark and gluon fields at light-like separations. The DAs can be directly linked to the LFWFs, unlike parton distributions that are given in terms of overlaps of the LFWFs. The DAs therefore provide a window to look directly into the physics of the LFWFs. In this section, we shall illustrate how such a connection is carried out. For illustration purposes, and to establish the basis for future chapters, we are going to truncate the Fock-space expansion of the proton state to the three-quark plus one-gluon state. All the arguments that we are going to present can be applied also to higher-Fock components, with the obvious increase in complexity due to the increasing number of partons. For our discussion we need the proton-to-vacuum matrix element of three-quark field operators:

$$\langle 0| \, \varepsilon^{ijk} u_{\lambda_1,i'}(a_1) \mathcal{W}_{i',i}(a_1,a_0) u_{\lambda_2,j'}(a_2) \mathcal{W}_{j',j}(a_2,a_0) d_{\lambda_3,k'}(a_3) \mathcal{W}_{k',k}(a_3,a_0) \, |p,\Lambda\rangle \, , \tag{3.62}$$

and the proton-to-vacuum matrix element of three-quark and one gluon operators:

$$\begin{aligned} &\langle 0| \, i g_s \varepsilon^{ijk} u_{\downarrow,i'}(a_1) \mathcal{W}_{i',i}(a_1,a_0) u_{\uparrow,j'}(a_2) \mathcal{W}_{j',j}(a_2,a_0) \\ &\times \left[\partial^+ \bar{A}^a_L(a_4) T^a_{k'l'} \mathcal{W}_{l',l}(a_4,a_0) d_{\downarrow l}(a_3)\right] \mathcal{W}_{k',k}(a_3,a_0) \, |p,\Lambda\rangle \, , \end{aligned} \tag{3.63}$$

$$\begin{aligned} &\langle 0| \, i g_s \varepsilon^{ijk} u_{\uparrow,i'}(a_1) \mathcal{W}_{i',i}(a_1,a_0) \left[\partial^+ \bar{A}^a_L(a_4) T^a_{j'l'} \mathcal{W}_{l',l}(a_4,a_0) u_{\downarrow,l}(a_2)\right] \\ &\times \mathcal{W}_{j',j}(a_2,a_0) d_{\downarrow k'}(a_3) \mathcal{W}_{k',k}(a_3,a_0) \, |p,\Lambda\rangle \, , \end{aligned} \tag{3.64}$$

$$\langle 0|\, ig_s\varepsilon^{ijk}\left[\partial^+\bar{A}^a_L(a_4)T^a_{i'l'}\mathcal{W}_{l',l}(a_4,a_0)u_{\downarrow,l}(a_1)\right]\mathcal{W}_{i',i}(a_1,a_0)u_{\downarrow,j'}(a_2)$$
$$\times\,\mathcal{W}_{j',j}(a_2,a_0)d_{\downarrow k'}(a_3)\mathcal{W}_{k',k}(a_3,a_0)\,|p,\Lambda\rangle\,. \tag{3.65}$$

All the points a_i are of the form

$$a_i^\mu = (0, a_i^-, \mathbf{0}_\perp), \tag{3.66}$$

hence, all the gauge links run along the minus light-cone direction. We are going to adopt the light-cone gauge, therefore all the gauge links in Eqs. (3.62)-(3.65) reduce to unity.

We also need the truncated Fock expansion for the proton state:

$$|p,\Lambda\rangle = \sum_{\{\beta_3\}}\int[d\sigma_3]\Psi^\Lambda_{\{\beta_3\}}(\sigma_3)\,|\sigma_3,\{\beta_3\}\rangle + \sum_{\{\beta_4\}}\int[d\sigma_4]\Psi^\Lambda_{\{\beta_4\}}(\sigma_4)\,|\sigma_4,\{\beta_4\}\rangle\,, \tag{3.67}$$

where we explicitly have indicated the sum over the discrete quantum numbers (light-cone helicities and color indexes) and the integral over the momenta, i.e. we used the definition of the symbol $\not\int$ in Eq. (2.64). The three-quark Fock state basis, by explicitly writing Eq. (2.60), reads:

$$|\sigma_3,\{\beta_3\}\rangle = \frac{\varepsilon^{c_1c_2c_3}}{\sqrt{6}}\sum_{\{q_i\}=\{u,u,d\}}\prod_{i=1}^3|\lambda_i,q_i,c_i,x_i,\boldsymbol{p}_{\perp,i}\rangle\,, \tag{3.68}$$

with:

$$|\lambda_i,q_i,c_i,x_i,\boldsymbol{p}_{\perp,i}\rangle = \left(q^{c_i}_{i,\lambda}(x_i,\boldsymbol{p}_{\perp,i})\right)^\dagger|0\rangle\,, \tag{3.69}$$

where c_i are the color indices, λ_i denote the quark light-cone helicities and

$$\boldsymbol{p}_{\perp,i} = \boldsymbol{k}_{\perp,i} + x_i\boldsymbol{p}_\perp \tag{3.70}$$

are the total transverse momenta[3]. The next-to-leading Fock state has a similar expression:

$$|\sigma_4,\{\beta_4\}\rangle = \sum_{\{q_i\}=\{u,u,d\}}\varepsilon^{dc_2c_3}T^a_{d,c_1}\left(\prod_{i=1}^3|\lambda_i,q_i,c_i,x_i,\boldsymbol{p}_{\perp,i}\rangle\right)|\lambda_4,g,a,x_4,\boldsymbol{p}_{\perp,4}\rangle\,. \tag{3.71}$$

In Eq. (3.71), via the following identity:

$$\sum_{l=1}^3\epsilon^{ijl}\left(T^a\right)_{lk} + \epsilon^{ilk}\left(T^a\right)_{lj} + \epsilon^{ljk}\left(T^a\right)_{li} = 0, \tag{3.72}$$

we can shift the coupling of the gluon from the down quark to the up quarks.

As we already noticed, since the transverse light-cone boosts are kinematic, the LFWFs do not depend on $\boldsymbol{p}_\perp$, i.e. the transverse motion of the transverse

[3]As already outlined in Sec. 2.3, the dependence of the state on the total transverse momentum is completely contained in the single-parton states.

center of momentum decouples from the intrinsic transverse motion of the partons inside the proton. For this reason, we can assume $\boldsymbol{p}_\perp = \boldsymbol{0}_\perp$, without affecting any of the following considerations. For the proton state we therefore have from Eq. (2.38) that

$$j_z = J^3 = \sum_{i=1}^{n} J_i^3 = \sum_{i=1}^{n} j_{z,i} + \sum_{i=1}^{n} l_{z,i} = \sum_{i=1}^{n} j_{z,i} + L_z, \tag{3.73}$$

where j_z, J^3, and L_z are, respectively, the light-cone helicity, the total angular momentum and the total OAM of the proton, while $j_{z,i}$, J_i^3 and $l_{z,i}$ are the corresponding contributions from the individual i-th parton. The total angular momentum and the OAM are intended as the components along the $\hat{z}$ direction. For the general Fock state the integration measure can be written in terms of the intrinsic coordinates (i.e. the integration variables are changed from $\{\boldsymbol{p}_{\perp,i}\}$ to $\{\boldsymbol{k}_{\perp,i}\}$) as:

$$[d\sigma_n] \longrightarrow [Dx]_n = \frac{[dx]_n [dk_\perp]_n}{\sqrt{\prod_{i=1}^{n} x_i}}, \tag{3.74}$$

$$[dx]_n = \prod_{i=1}^{n} dx_i \delta\left(1 - \sum_{i=1}^{n} x_i\right), \tag{3.75}$$

$$[dk_\perp]_n = \left(\frac{1}{2(2\pi)^3}\right)^{n-1} \prod_{i=1}^{n} d\boldsymbol{k}_{i,\perp} \delta\left(\sum_{i=1}^{n} \boldsymbol{k}_{i,\perp}\right). \tag{3.76}$$

For all the Fock states we can make explicit the sum over the light-cone helicity and the parton OAM. This allows us to isolate the so-called Light-Front Wave Amplitudes (LFWAs). They depend only on the parton momentum and are eigenstate of the parton OAM operator. Following Ref. [60], one can classify the number of independent LFWAs in a model-independent way. First, we make explicitly the sum over the parton light-cone helicities and OAM, noticing that each unit of OAM for the i-th parton contributes with a factor $k_{R/L,i}$, where R/L are for the case $l_{z,i} > 0$ or $l_{z,i} < 0$, respectively and

$$k_{R/L} = k_{x,\perp} \pm i k_{y,\perp}. \tag{3.77}$$

We have:

$$\sum\!\!\!\!\!\!\int \Psi_n |\sigma_n\rangle = \int [d\sigma_n] \sum_{\{l_{z,i}\},\{\lambda_i\}} \prod_{i=1}^{n-1} k_{R/L,i}^{|l_{z,i}|} \psi_n(\{x_i, \boldsymbol{k}_{\perp,i}\}) |\sigma_n, \{\lambda_i\}, \{c_i\}\rangle. \tag{3.78}$$

Second, assuming that $L_z \geq 0$ (the argument is very similar for the case $L_z \leq 0$), we isolate all the pairs $k_{R,i}^{l_{z,i}} k_{L,j}^{-l_{z,j}}$ for which $l_{z,j} < 0$ and $l_{z,i} > |l_{z,j}|$. Note that, being $L_z > 0$, it is always possible to pair the parton momenta in this way. Then we make use of the identity:

$$k_{R,i}^{l_{z,i}} k_{L,j}^{-l_{z,j}} = k_{R,i}^{l_{z,i}+l_{z_j}} \left(\boldsymbol{k}_{\perp,i} \cdot \boldsymbol{k}_{\perp,j} + i\varepsilon^{mn} k_{m,i} k_{n,j}\right)^{-l_{z,j}}$$

$$= k_{R,i}^{l_{z,i}+l_{z,j}} \left(\phi_0 + \phi_1 i\varepsilon^{mn} k_{m,i} k_{n,j}\right),$$

where, from the first to the second line, we used

$$\varepsilon^{ij}\varepsilon^{mn} = \delta^{im}\delta^{jn} - \delta^{in}\delta^{jm}, \quad i\varepsilon^{mn} k_{m,i} k_{n,j} k_{R,i} = \boldsymbol{k}_{\perp,i}\cdot\boldsymbol{k}_{\perp,i} k_{R,j} - \boldsymbol{k}_{\perp,i}\cdot\boldsymbol{k}_{\perp,j} k_{R,i} \tag{3.79}$$

to recast Eq. (3.78) into

$$\begin{aligned}\cancel{\Psi}\,|\sigma_n\rangle = \int [d\sigma_n] \sum_{\{m_{z,i}\},\{\lambda_i\}} \prod_{i=1}^{n-1} k_{R/L,i}^{m_{z,i}} \Bigg(& \psi_n(\{x_i, \boldsymbol{k}_{\perp,i}\}) \\ & + \sum_{i<j|l_{z,i}+l_{z,j}=0} i\varepsilon^{mn} k_{m,i} k_{n,j} \psi_{n,(ij)}(\{x_i, \boldsymbol{k}_{\perp,i}\}) \Bigg) |\sigma_n, \{\lambda_i\}\rangle\,,\end{aligned} \tag{3.80}$$

with $m_{z,i} = l_{z,i} + l_{z,j} \geq 0$.

This expression can be made explicit for each parton number n. We therefore need the explicit expressions for the three-quark state and the three-quark plus one-gluon state. The first one reads:

$$\begin{aligned}|p,+\rangle_{3q} = \int [d\sigma_3] \Big\{ & \psi^{L_z=0}(\{x_i, \boldsymbol{k}_{\perp,i}\})\,|\sigma_3, \{\uparrow\uparrow\downarrow\}\rangle + \psi^{L_z=1}(\{x_i, \boldsymbol{k}_{\perp,i}\})\,|\sigma_3, \{\uparrow\downarrow\downarrow\}\rangle \\ & + \psi^{L_z=2}(\{x_i, \boldsymbol{k}_{\perp,i}\})\,|\sigma_3, \{\downarrow\downarrow\downarrow\}\rangle + \psi^{L_z=-1}(\{x_i, \boldsymbol{k}_{\perp,i}\})\,|\sigma_3, \{\uparrow\uparrow\downarrow\}\rangle \Big\},\end{aligned} \tag{3.81}$$

where we labelled the coefficient of each state with the corresponding value for L_z. More explicitly, from Eq. (3.80), the component $L_z = 0$ reads:

$$\begin{aligned}|p,+\rangle_{3q}^{L_z=0} = & \frac{-\epsilon^{ijk}}{\sqrt{6}} \int [Dx]_{123} \left(\psi_{123}^{(0)} - i\varepsilon^{lm} k_{1,l} k_{2,m} \psi_{123}^{(2)}\right) \\ & \times \left(u_{\uparrow,i}^\dagger(1) u_{\downarrow,j}^\dagger(2) d_{\uparrow,k}^\dagger(3) - u_{\uparrow,i}^\dagger(1) d_{\downarrow,i}^\dagger(2) u_{\uparrow,k}^\dagger(3)\right)|0\rangle\,,\end{aligned} \tag{3.82}$$

where we used the shorthand notations

$$u(i) = u(x_i, \boldsymbol{p}_{\perp,i}), \quad \psi_{123} = \psi(x_1, \boldsymbol{k}_{\perp,1}, x_2, \boldsymbol{k}_{\perp,2}, x_3, \boldsymbol{k}_{\perp,3}). \tag{3.83}$$

We notice here that $\psi^{(2)}$, corresponding to $\psi_{n,(ij)}$ of Eq. (3.80), encapsulates the information on the state with two quarks having the same absolute value of OAM along the $\hat{z}$ axis, but with opposite sign. Hence, the total L_z for $\psi^{(2)}$ is zero, while the OAM of the individual quarks is not vanishing. The other eigenstates of the total OAM along z read:

$$\begin{aligned}|p,+\rangle_{3q}^{L_z=1} = & \frac{\epsilon^{ijk}}{\sqrt{6}} \int [Dx]_{123} \left[k_{R,1}\psi^{(3)}(123) + k_{R,2}\psi^{(4)}(123)\right] \\ & \times \left(u_{\uparrow,i}^\dagger(1) u_{\downarrow,j}^\dagger(2) d_{\uparrow,k}^\dagger(3) - u_{\uparrow,i}^\dagger(1) d_{\downarrow,i}^\dagger(2) u_{\uparrow,k}^\dagger(3)\right)|0\rangle\,,\end{aligned} \tag{3.84}$$

$$|p,+\rangle_{3q}^{L_z=-1} = \frac{\epsilon^{ijk}}{\sqrt{6}} \int [Dx]_{123} \left[-k_{L,2}\psi^{(5)}(123)\right] \times \left(u^\dagger_{\uparrow,i}(1)u^\dagger_{\uparrow,j}(2)d^\dagger_{\uparrow,k}(3)\right)|0\rangle\,, \tag{3.85}$$

$$|p,+\rangle_{3q}^{L_z=2} = -\frac{\epsilon^{ijk}}{\sqrt{6}} \int [Dx]_{123} \left[k_{R,1}k_{R,3}\psi^{(6)}(123)\right] \times u^\dagger_{\downarrow,i}(1)u^\dagger_{\downarrow,j}(2)d^\dagger_{\downarrow,k}(3)\,|0\rangle\,. \tag{3.86}$$

The functions $\psi^{(i)}$ in Eqs. (3.82)-(3.86) are the LFWAs. We can clearly see that they depend only on the parton momenta, and, since we have factored out the $k_{R/L,i}$ associated with the OAM, the LFWAs can only depend on the products $\boldsymbol{k}_{\perp,i}\cdot\boldsymbol{k}_{\perp,i}$, see Eq. (3.80).

From Ref. [61], one can read also the full expressions for the three-quarks plus one gluon state. However, due to the very large number (126) of LFWAs, we are going to explicitly report only the case $L_z = 0$, that is the only one of interest for our purposes:

$$|p,+\rangle_{3qg\downarrow}^{L_z=0} = \epsilon^{ijk} \int [Dx]_{1234} \Psi^{\downarrow}(1234)\; T^a_{\sigma i} g^{a\dagger}_{\downarrow}(4) u^\dagger_{\uparrow,\sigma}(1) u^\dagger_{\uparrow,j}(2) d^\dagger_{\uparrow,k}(3)\,|0\rangle\,, \tag{3.87}$$

$$\begin{aligned}|p,+\rangle_{3qg\uparrow}^{L_z=0} = \epsilon^{ijk} \int [Dx]_{1234} \Bigg[& \Psi^{1\uparrow}(1234) T^a_{\sigma i} g^{a\dagger}_{\uparrow}(4) u^\dagger_{\downarrow,\sigma}(1) \\ & \times \left(u^\dagger_{\uparrow,j}(2) d^\dagger_{\downarrow,k}(3) - d^\dagger_{\uparrow,j}(2) u^\dagger_{\downarrow,k}(3)\right) \\ & + \Psi^{2\uparrow}(1234) T^a_{\sigma j} g^{a\dagger}_{\uparrow}(4) u^\dagger_{\downarrow,i}(1) \left(u^\dagger_{\downarrow,\sigma}(2) d^\dagger_{\uparrow,k}(3) - d^\dagger_{\downarrow,\sigma}(2) u^\dagger_{\uparrow,k}(3)\right) \Bigg] |0\rangle\,.\end{aligned} \tag{3.88}$$

It can be noticed that all the expressions for the proton state given so far refer to the state with positive light-cone helicity. The corresponding expressions for a state with negative light-cone helicity can be obtained via the application of the light-cone parity operator $\hat{Y}$ (see Refs. [61, 62]), i.e.

$$|p,\lambda\rangle \longrightarrow \widehat{Y}\,|p,\lambda\rangle = (-1)^{s+\lambda}\eta\,|p,-\lambda\rangle\,, \tag{3.89}$$

where s is the total angular momentum of the hadron (i.e. $s = \frac{1}{2}$ for the proton), λ is the light-cone helicity of the state and η is the intrinsic parity of the hadron. For a quark, the intrinsic parity is $\eta = +1$, and for a gluon is $\eta = -1$.

Before discussing the connection between the LFWAs and the DAs, we must point out the difference in our Eqs. (3.85) and (3.87), and the corresponding expressions in Ref. [61]. A careful examination of the symmetry relations of the LFWAs will bring clarity in the problem. As an example, we are going to work with the case of $\Psi^{\downarrow}$, but the same reasoning applies, *mutatis mutandis*, to the case of $\psi^{(5,6)}$. In Ref. [61] the state is given as

$$u^\dagger_{\uparrow,\sigma}(1)\left(u^\dagger_{\uparrow,j}(2)d^\dagger_{\uparrow,k}(3) - d^\dagger_{\uparrow,j}(2)u^\dagger_{\uparrow,k}(3)\right)|0\rangle\,, \tag{3.90}$$

instead of

$$u^\dagger_{\uparrow,\sigma}(1)u^\dagger_{\uparrow,j}(2)d^\dagger_{\uparrow,k}(3)\left|0\right\rangle . \tag{3.91}$$

The underlying assumption of Eq. (3.90) is the anti-symmetric behavior of $\Psi^\downarrow(1234)$ under the exchange $2 \leftrightarrow 3$. The key point, even if trivial, is that the proton as well as the up and down quarks have isospin one-half. Since we are not interested in any other type of quarks, we restrict our argument to state of isospin 1/2. The inclusion of different types of quarks would put the quarks in an higher isospin state, leaving nevertheless the proton in an isospin 1/2 state. The isospin-1/2 operators share the same algebra as the spin-1/2, i.e. $SU(2)$. In the isospin notation, the generators of the group, i.e. the basis of the algebra, can be called I_i with $i = 1, 2, 3$:

$$I_1 = \frac{1}{2}\begin{pmatrix} 0 & 1 \\ 1 & 0 \end{pmatrix}, \quad I_2 = \frac{1}{2}\begin{pmatrix} 0 & -i \\ i & 0 \end{pmatrix}, \quad I_3 = \frac{1}{2}\begin{pmatrix} 1 & 0 \\ 0 & -1 \end{pmatrix}, \tag{3.92}$$

with the commutation relations:

$$[I_i, I_j] = i\epsilon_{ijk}I_k. \tag{3.93}$$

The up quark is defined as the isospin eigenstate with eigenvalue $I_3 = +\frac{1}{2}$ and the down quark as the state with $I_3 = -\frac{1}{2}$:

$$I_3\left|u\right\rangle = \frac{1}{2}\left|u\right\rangle , \qquad I_3\left|d\right\rangle = -\frac{1}{2}\left|d\right\rangle . \tag{3.94}$$

We can also introduce the ladder operators:

$$I_\pm = I_1 \pm iI_2, \tag{3.95}$$

which act on the up- and down-quark state state as:

$$I_+\left|u\right\rangle = 0, \qquad I_-\left|u\right\rangle = \left|d\right\rangle , \qquad I_+\left|d\right\rangle = \left|u\right\rangle , \qquad I_-\left|d\right\rangle = 0. \tag{3.96}$$

The action of I_+ is to "replace" the down quark with an up quark, and *viceversa* for I_-. Now we are ready to come back to the flavor symmetry of $\Psi^\downarrow$. The third component of the isospin of the proton state, i.e. I_3, is given by the sum of the I_3-components of the quarks and gluon, which has $I_3 = 0$:

$$I_3\left|p,+\right\rangle_{3qg\downarrow} = \frac{1}{2}\left|p,+\right\rangle_{3qg\downarrow} . \tag{3.97}$$

If we impose $I_+\left|P,+\right\rangle_{3qg\downarrow} = 0$, we are able to find a constraint on the LFWA. We have:

$$I_+\left|p,+\right\rangle_{3qg\downarrow} = \epsilon^{ijk}\int [Dx]_{1234}\Psi^\downarrow(1234)\ T^a_{\sigma i}g^{a\dagger}_\downarrow(4)u^\dagger_{\uparrow,\sigma}(1)u^\dagger_{\uparrow,j}(2)u^\dagger_{\uparrow,k}(3)\left|0\right\rangle , \tag{3.98}$$

and after projecting into the following state of three-quarks and a gluon:

$$\langle 0|\, g^b_{\downarrow}(8) u_{\uparrow,n}(7) u_{\uparrow,m}(6) u_{\uparrow,l}(5), \tag{3.99}$$

we obtain the equation:

$$\Psi^{\downarrow}(1234) + \Psi^{\downarrow}(1324) - \Psi^{\downarrow}(3124) - \Psi^{\downarrow}(3214) = 0. \tag{3.100}$$

Of course, if $\Psi^{\downarrow}$ is anti-symmetric in the third and the fourth arguments, the condition is fulfilled. However, the most general solution to this equation can be written as a sum of three terms:

$$\Psi^{\downarrow}(1234) = \Psi^{\downarrow(+)}(1234) - \Psi^{\downarrow(+)}(1324) + \Psi^{\downarrow(0)}(1234), \tag{3.101}$$

where the superscripts indicate a well-defined behavior under a cyclic permutation of the quark arguments:

$$\Psi^{\downarrow(0)}(1234) = \Psi^{\downarrow(0)}(2314), \qquad \Psi^{\downarrow(+)}(1234) = e^{\frac{2\pi}{3} i} \Psi^{\downarrow(+)}(2314). \tag{3.102}$$

The Eq. (3.102) implies that the function $\Psi^{\downarrow}$ does not have a definite behavior under the exchange of two quarks. This entails that the state in Eq. (3.90) is not correct, since it relies on the assumption of the anti-symmetric behavior under the exchange of the second and third argument of $\Psi^{\downarrow}$.

3.4.2 Link with the Light-Front Wave Amplitudes

The DAs introduced in Eqs. (3.62)-(3.65) will be now studied in more detail. Most of our knowledge of the DAs relies on model calculations (see Ref. [63]) and few information from lattice QCD (see Refs. [64–66]. Since, as we are going to show, DAs and LFWAs are deeply connected, a good understanding of the proton DAs has repercussions on the understanding of the various parton distributions that, we recall, can be written as overlapping integrals of LFWAs.

We shall start the discussion about the link between DAs and LFWAs with the simplest case: the three-quark state with $L_z = 0$. To isolate this contribution, Eq. (3.62) must be projected in the Dirac space with the appropriate Dirac structures. We refer to Ref. [67] for the general decomposition of Eq. (3.62). It happens that the three-quark $L_z = 0$ state is also the leading-twist contribution in Eq. (3.62), and reads[4]:

$$\begin{aligned} &\langle 0|\varepsilon^{ijk} \left(u^T_{i\uparrow}(z_1) C\gamma^+ u_{j\downarrow}(z_2)\right) \gamma^+ d_{k\uparrow}|p,\uparrow\rangle \\ &= -\frac{1}{2} p^+ \gamma^+ N_{\uparrow}(p) \int [dx]_3 e^{-ip^+ \sum x_i z_i} \Phi_3(x_1, x_2, x_3), \end{aligned} \tag{3.103}$$

where $N(p)$ represents the proton spinor in momentum space, Φ_3 is the leading-twist three-quark distribution amplitude and $C = i\gamma^2\gamma^0$ is the charge conjugation matrix, essential to give rise to the correct quark annihilation operator.

[4]No gauge links appear, since we are working in the light-cone gauge.

In this case, the leading twist is twist-3, from which the subscript of Φ_3 comes. By the insertion of Eq. (3.82) into Eq. (3.103) we obtain:

$$\Phi_3(x_1, x_2, x_3) = 4\sqrt{6} \int [d\boldsymbol{k}_\perp]_3 \; \psi^{(0)}_{123}. \tag{3.104}$$

As it should be clear by its definition, the DA cannot provide information on the actual $\boldsymbol{k}_\perp$ shape of the LFWAs, but only on the dependence on the fractions of longitudinal quark momentum.

For the four-parton DA we limit ourself to the leading-twist components, which correspond to twist-4:

$$\begin{aligned}
&\langle 0|ig_s\epsilon^{ijk}u^+_{i\downarrow}(z_1)u^+_{j\uparrow}(z_2)\left(\partial_4^+ A_L^{a\dagger}(z_4)T^a_{k\sigma}\right)d^+_{\sigma\downarrow}(z_3)|P,\uparrow\rangle \\
&= \frac{-(P^+)^{5/2}m}{4}\int [dx]_3 e^{-iP^+\sum x_i z_i}\Phi_4^g(x_1,x_2,x_3,x_4), \qquad (3.105)\\
&\langle 0|ig_s\epsilon^{ijk}u^+_{i\uparrow}(z_1)\left(\partial_4^+ A_L^{a\dagger}(z_4)T^a_{j\sigma}\right)u^+_{\sigma\downarrow}(z_2)d^+_{k\downarrow}(z_3)|P,\uparrow\rangle \\
&= \frac{-(P^+)^{5/2}m}{4}\int [dx]_3 e^{-iP^+\sum x_i z_i}\Psi_4^g(x_1,x_2,x_3,x_4), \qquad (3.106)\\
&\langle 0|ig_s\epsilon^{ijk}\left(\partial_4^+ A_L^{a\dagger}(z_4)T^a_{i\sigma}\right)u^+_{\sigma\downarrow}(z_1)u^+_{j\downarrow}(z_2)d^+_{k\downarrow}(z_3)|P,\downarrow\rangle \\
&= \frac{-(P^+)^{5/2}m}{4}\int [dx]_3 e^{-iP^+\sum x_i z_i}\Xi_4^g(x_1,x_2,x_3,x_4), \qquad (3.107)
\end{aligned}$$

where the + on the spinors identifies the good components.

The same approach used for the three-quark state can be applied here to compute the connection between the DAs and the LFWFs for the three-quark and one gluon ($3qg$) Fock state:

$$2\sqrt{x_4}\int [d\boldsymbol{k}_\perp]_4 \; \Psi^{\downarrow}_{1234} = \frac{M}{96 g_s}\left(2\Xi_4^g(x_1,x_2,x_3,x_4) + \Xi_4^g(x_2,x_1,x_3,x_4)\right), \tag{3.108}$$

$$2\sqrt{x_4}\int [d\boldsymbol{k}_\perp]_4 \; \Psi^{1,\uparrow}_{1234} = -\frac{M}{96 g_s}\left(2\Psi_4^g(x_2,x_1,x_3,x_4) + \Phi_4^g(x_1,x_2,x_3,x_4)\right), \tag{3.109}$$

$$2\sqrt{x_4}\int [d\boldsymbol{k}_\perp]_4 \; \Psi^{2,\uparrow}_{1234} = \frac{M}{96 g_s}\left(2\Phi_4^g(x_1,x_2,x_3,x_4) + \Psi_4^g(x_2,x_1,x_3,x_4)\right). \tag{3.110}$$

The Eq. (3.110) differs by a sign from the corresponding relation in Ref. [68]. The opposite sign comes from correctly implementing the light-front parity transformation to change the light-cone helicity of the proton, see Eq. (3.89).

In the case of vanishing parton OAM, we showed that the connection between DAs and LFWFs is very simple. This is because in the definition of the DAs only the good components of the quark fields and the transverse components of the gluon field appear. The sub-leading twist DAs, i.e. twist-4 for the three-quark state and twist-5 for the three-quark plus one-gluon state, involve bad components of the quark fields. Although the calculation becomes more cumbersome,

in this case one can access the LFWAs with $L_z \neq 0$. The bad components in the DA operators cannot be straightforwardly annihilated with the quark operators in the Fock state, since the Fock state is constructed only using the good components. Therefore, our general strategy is to use the quark EOM given in Eq. (2.32) to rewrite the bad components in terms of the good ones.

3.4.3 Inversion of the Equations of Motion

The differential form of the EOM given in Eq. (2.32) must be cast into an integral form in order to remove the bad quark-field components from the definition of the DAs. The first step is to remove the covariant + derivative in Eq. (2.32) in favor of the partial + derivative. To achieve this, we can make use of the following property

$$\mathcal{W}\left((z^+,\zeta^-,\boldsymbol{z}_\perp),z\right) iD^+_{z^-} = i\partial^+_{z^-}\mathcal{W}\left((z^+,\zeta^-,\boldsymbol{z}_\perp),z\right). \tag{3.111}$$

Hence, Eq. (2.32) takes the form:

$$i\partial^+_{z^-}\mathcal{W}\left((z^+,\zeta^-,\boldsymbol{z}_\perp),z\right)\psi_-(z) = \frac{\gamma^+}{2}\mathcal{W}\left((z^+,\zeta^-,\boldsymbol{z}_\perp),z\right)(i\boldsymbol{\gamma}_\perp\cdot\boldsymbol{D}_\perp + m)\,\psi_+(z). \tag{3.112}$$

Note that this expression for the EOM can be trivially deduced in light-cone gauge $A^+ = 0$ since the Wilson line runs along the light-cone direction. The general solution in position space for Eq. (2.32) can be obtained using the Green function that satisfies

$$\partial^+_{z^-}G(\xi^- - z^-) = \delta(\xi^- - z^-), \tag{3.113}$$

and using the relation between gauge links

$$\mathcal{W}^\dagger(a^-,b^-) = \mathcal{W}(b^-,a^-). \tag{3.114}$$

From Ref. [69] we have:

$$\begin{aligned}\psi_-(z^-) = &\int d\xi^-\mathcal{W}(z^-,\xi^-)\psi_-(\xi^-)\\ &+\int d\xi^-\frac{\gamma^+}{2i}G(\xi^- - z^-)\mathcal{W}(z^-,\xi^-)(i\boldsymbol{D}_\perp\cdot\boldsymbol{\gamma}_\perp + m)\psi_+(\xi^-).\end{aligned} \tag{3.115}$$

In the first term of the equation we recognize the zero-modes for the bad quark field. The boundary conditions for the bad quark field are reflected in the explicit structure for the Green function. As in the case of the boundary conditions for the transverse gluon field in light-cone gauge, three common choices exist:

$$\psi_-(\infty^-) = 0, \quad \psi_-(-\infty^-) = 0, \quad \psi_-(\infty^-) + \psi_-(-\infty^-) = 0, \tag{3.116}$$

known as retarded, advanced and principal-value boundary conditions, respectively. Each choice determines the explicit structure for the Green function. They are, respectively:

$$G(x) = \theta(x), \quad G(x) = -\theta(-x), \quad G(x) = \frac{1}{2}\left(\theta(x) - \theta(-x)\right), \tag{3.117}$$

where we shortened the notation using $x = \xi^- - z^-$. Note that, trivially, we cannot have a Green function that ensures the boundary conditions

$$\psi_-(\infty^-) - \psi_-(-\infty^-) = 0, \tag{3.118}$$

since it should be proportional to

$$G(x) \propto \theta(x) + \theta(-x) = 1. \tag{3.119}$$

Specifying Eq. (3.115) for the light-cone gauge, that essentially allows us to neglect the gauge links, we have in momentum space:

$$\begin{aligned}\psi_-(k) = &\int d\xi^- \psi_-(\xi^-, k^-, \boldsymbol{k}_\perp)\delta(k^+) + \frac{\gamma^+}{2k^+}(m + \boldsymbol{\gamma}_\perp \cdot \boldsymbol{k}_\perp)\psi_+(k) \\ &+ g_s \frac{\gamma^+}{2k^+}\boldsymbol{\gamma}_\perp \cdot [\boldsymbol{A}_\perp \psi_+](k) + \text{B.C.},\end{aligned} \tag{3.120}$$

where we defined

$$\psi_\pm(k) = \int d^4z \; e^{ik\cdot z}\psi_\pm(z), \tag{3.121}$$

$$[\boldsymbol{A}_\perp \psi_+](z) = \boldsymbol{A}_\perp(z)\psi_+(z), \tag{3.122}$$

$$[\boldsymbol{A}_\perp \psi_+](k) = \int d^4z \; e^{ik\cdot z}[\boldsymbol{A}_\perp \psi_+](z). \tag{3.123}$$

The boundary-condition (B.C.) term in Eq. (3.120) depends on the specific choice of the Green function :

$$\begin{aligned}\text{B.C.} = \pm\pi\delta(k^+) \int d\xi^- \Big(&(m + \boldsymbol{\gamma}_\perp \cdot \boldsymbol{k}_\perp)\psi_+(\xi^-, k^-, \boldsymbol{k}_\perp) \\ &+ g_s \boldsymbol{\gamma}_\perp \cdot [\boldsymbol{A}_\perp \psi_+](\xi^-, k^-, \boldsymbol{k}_\perp)\Big),\end{aligned}$$

where the plus sign refers to the retarded boundary conditions and the minus sign to the advanced boundary conditions. In the principal-value prescription we have instead

$$\text{B.C.} = 0. \tag{3.124}$$

Note that all the boundary-conditions terms are proportional to $\delta(k^+)$. We shall come back to the boundary conditions of the EOM in Chapter 7, when we are going to investigate the higher-twist TMDs. For the remaining of this Chapter, we are going to ignore the boundary-condition terms, and this allows us to express Eq. (3.120) as follows:

$$\begin{aligned}k^+ \left(\psi_-^q(k) + \psi_-^{\bar{q}}(-k)\right) &= \frac{\gamma^+}{2}\left(m + \boldsymbol{k}_\perp \cdot \boldsymbol{\gamma}_\perp\right)\left(\psi_+^q(k) + \psi_+^{\bar{q}}(-k)\right) \\ &+ g_s \frac{\gamma^+}{2} \int \frac{dp^+ d\boldsymbol{p}_\perp}{2p^+(2\pi)^3} \frac{k^+ p^+}{\left(\frac{k^+}{2} - p^+\right)\left(\frac{k^+}{2} + p^+\right)}\end{aligned}$$

$$\times \left[\boldsymbol{\gamma}_\perp \cdot \boldsymbol{A}_\perp \left(\frac{k}{2} + p \right) \left(\psi_+^q \left(\frac{k}{2} - p \right) + \psi_+^{\bar{q}} \left(-\frac{k}{2} + p \right) \right) \right.$$
$$\left. + \boldsymbol{\gamma}_\perp \cdot \boldsymbol{A}_\perp^\dagger \left(-\frac{k}{2} - p \right) \left(\psi_+^q \left(\frac{k}{2} - p \right) + \psi_+^{\bar{q}} \left(-\frac{k}{2} + p \right) \right) \right], \tag{3.125}$$

where we separated the quark and antiquark components, labelled with q and $\bar{q}$ respectively. For the good components of the quark field, we have the explicit representation

$$\psi^q(k) = u(k)b(k), \quad \psi^{\bar{q}}(k) = v(k)d^\dagger(k), \tag{3.126}$$

where the light-cone helicity and color indexes are understood. Using Eq. (2.51) in Eq. (3.125) we have that

$$A_\perp^{i(\dagger)}(k) = \sum_{\lambda=\uparrow/\downarrow} \epsilon_\lambda^{i(*)}(k) g_\lambda^{(\dagger)}(k). \tag{3.127}$$

In the first line of Eq. (3.125), the on-shell condition

$$k^- = \frac{m^2 + \boldsymbol{k}_\perp^2}{2k^+} \tag{3.128}$$

is understood, whereas, in the second line, the on-shell conditions read (from a careful evaluation of the on-shell deltas in the field expansion):

$$p^- = \frac{-k^+ m^2 - \boldsymbol{k}_\perp^2 p^+ - 2m^2 p^+ + 2k^+ \boldsymbol{k}_\perp \cdot \boldsymbol{p}_\perp - 4p^+ \boldsymbol{p}_\perp^2}{2(k^+ - 2p^+)(k^+ + 2p^+)}, \tag{3.129}$$

$$k^- = \frac{4p^+(m^2 - 2\boldsymbol{k}_\perp \cdot \boldsymbol{p}_\perp) + k^+(\boldsymbol{k}_\perp^2 + 2m^2 + 4\boldsymbol{p}_\perp^2)}{4(k^+ - 2p^+)(k^+ + 2p^+)}. \tag{3.130}$$

For future use, we now specify Eq. (3.125) in the case of a quark, ignoring the antiquark part, and ignoring the gluon creation operator $\boldsymbol{A}_\perp^\dagger$. Moreover, we project Eq. (3.125) into states of definite chirality via the projectors

$$\mathcal{C}_\pm = \frac{1}{2}\left(\mathbb{1} \pm \gamma_5\right), \quad \mathcal{C}_\pm \psi_{\xi=\pm} = \pm \psi_{\xi=\pm}, \tag{3.131}$$

where ξ is the field chirality. We then obtain:

$$k^+ \gamma^- \psi_{-,\xi}(k) = \boldsymbol{k}_\perp \cdot \boldsymbol{\gamma}_\perp \psi_{+,\xi}(k) + m\psi_{+,-\xi}(k)$$
$$+ g_s \int \frac{dp^+ d\boldsymbol{p}_\perp}{2p^+(2\pi)^3} \boldsymbol{A}_\perp \left(\frac{k}{2} + p \right) \cdot \boldsymbol{\gamma}_\perp \psi_{+,\xi} \left(\frac{k}{2} - p \right) \frac{k^+ p^+}{\left(\frac{k^+}{2} - p^+\right)\left(\frac{k^+}{2} + p^+\right)}. \tag{3.132}$$

Since we are assuming vanishing zero modes, this entails that $k^+ > 0$, and inverting the previous equation is straightforward. Note that all the results of the following section are still valid if the zero modes would have been present, with the caveat of redefining the generic DA $\mathcal{D}$ as:

$$\mathcal{D} = \mathcal{D}_{\text{full}} - \mathcal{D}_{\text{zero modes}}. \tag{3.133}$$

As we are going to show in Chapter 6, our model for the DAs will have vanishing values for $k^+ = 0$, hence we are, for all practical purposes, using $\mathcal{D}$ as a DA instead of $\mathcal{D}_{\text{full}}$.

3.4.4 Higher-twist Distribution Amplitudes and Light-Front Wave Amplitudes

In this section, we are going to use Eq. (3.132) to construct a system of equations that will allow us to express the twist-4 DAs in terms of the LFWAs. The general definition of twist-4 three-quark DAs in light-cone gauge is as follows:

$$\begin{aligned}
&\langle 0|\, \varepsilon^{lmn} \left(u^T_{l,\uparrow}(z_1) C\gamma^+ u_{m,\downarrow}(z_2)\right) \gamma^- d_{n,\uparrow}\, |p\rangle \\
&= -\frac{\gamma^+}{2} N_\uparrow \int [dx]_3 e^{-ip^+ \sum x_i z_i} \Phi_4(x_1, x_2, x_3), \qquad (3.134)\\
&\langle 0|\, \varepsilon^{lmn} \left(u^T_{l,\uparrow}(z_1) C\gamma^+ \gamma_j \gamma^- u_{m,\downarrow}(z_2)\right) \gamma^j \gamma^+ d_{n,\downarrow}\, |p\rangle \\
&= -M\gamma^+ N_\uparrow \int [dx]_3 e^{-ip^+ \sum x_i z_i} \Psi_4(x_1, x_2, x_3), \qquad (3.135)\\
&\langle 0|\, \varepsilon^{lmn} \left(u^T_{l,\uparrow}(z_1) C\gamma^- \gamma^+ u_{m,\uparrow}(z_2)\right) \gamma^+ d_{n,\uparrow}\, |p\rangle \\
&= \frac{M\gamma^+}{2} N_\uparrow \int [dx]_3 e^{-ip^+ \sum x_i z_i} \Xi_4(x_1, x_2, x_3). \qquad (3.136)
\end{aligned}$$

By direct inspection of these equations, one can see that they involve one bad component and two good ones: in Eq. (3.134) the bad component is from the down quark, in Eqs. (3.135) and (3.136) the bad component is from $u(z_2)$ and $u(z_1)$, respectively. Equipped with Eqs. (3.134)-(3.136), we can clearly see that each twist-4 DA can be written in terms of LFWAs as a sum of three distinct pieces: a mass term connected to the three-quark $L_z = 0$ LFWA, a gluon term, connected with the three-quark plus one-gluon $L_z = 0$ LFWA, and a $\boldsymbol{k}_\perp$ term, connected to the $L_z = \pm 1$ LFWAs for the three-quark state. We can invert these relations to express the $L_z = \pm 1$ LFWAs in terms of twist-4 DAs and the $L_z = 0$ LFWA. Twist-5 and twist-6 DAs, defined in Ref. [68], involve two and three quark bad components, respectively:

$$\begin{aligned}
&\langle 0|\, \varepsilon^{lmn} \left(u^T_{l,\uparrow}(z_1) C\gamma^- u_{m,\downarrow}(z_2)\right) \gamma^+ d_{n,\uparrow}\, |p\rangle \\
&= -\frac{M^2\gamma^+}{4p^+} N_\uparrow \int [dx]_3 e^{-iP^+ \sum x_i z_i} \Phi_5(x_1, x_2, x_3), \qquad (3.137)\\
&\langle 0|\, \varepsilon^{lmn} \left(u^T_{l,\uparrow}(z_1) C\gamma^- \gamma_j \gamma^+ u_{m,\downarrow}(z_2)\right) \gamma^j \gamma^- d_{n,\downarrow}\, |p\rangle \\
&= -M\gamma^- N_\uparrow \int [dx]_3 e^{-ip^+ \sum x_i z_i} \Psi_5(x_1, x_2, x_3), \qquad (3.138)\\
&\langle 0|\, \varepsilon^{lmn} \left(u^T_{l,\uparrow}(z_1) C\gamma^+ \gamma^- u_{m,\uparrow}(z_2)\right) \gamma^- d_{n,\uparrow}\, |p\rangle \\
&= \frac{M\gamma^-}{2} N_\uparrow \int [dx]_3 e^{-ip^+ \sum x_i z_i} \Xi_5(x_1, x_2, x_3), \qquad (3.139)\\
&\langle 0|\, \varepsilon^{lmn} \left(u^T_{l,\uparrow}(z_1) C\gamma^- u_{m,\downarrow}(z_2)\right) \gamma^- d_{n,\uparrow}\, |p\rangle \\
&= -\frac{M^2\gamma^-}{4P^+} N_\uparrow \int [dx]_3 e^{-ip^+ \sum x_i z_i} \Phi_6(x_1, x_2, x_3). \qquad (3.140)
\end{aligned}$$

Therefore, from the inversion of the EOM in Eq. (3.132), they can be written as combinations of a mass term, an OAM term and a gluon term. However, the

gluon term involves both the $L_z \neq 0$ LFWAs for the three-quark plus one-gluon state as well as the LFWAs for the two- and three-gluon state with $L_z = 0$. For these reasons, the complexity associated with the inversion of the LFWA-DA system increases rapidly. We notice that the LFWA $\psi^{(2)}$ is linked to the twist-5 DAs even if it has $L_z = 0$ because the OAM of the individual quarks is not vanishing for $\psi^{(2)}$. We shall illustrate in this section only the case of twist-4 DAs, because we will restrict our model to include only the $L_z = \pm 1$ LFWAs (see Chapter 6). We stress that the techniques that we are going to show can be generalized to incorporate any N parton Fock state, meaning that a complete knowledge of the proton DAs generates a complete knowledge of the ($\boldsymbol{k}_\perp$ integrated) LFWAs and vice versa. We think that this construction gives also a really clear indication of how to build a consistent model for the Fock expansion of the proton state: when considering contribution of states with $L_z \neq 0$, one should take into account also the contribution from the higher-order Fock states which come into play from the relation between DAs and LFWAs.

In the last part of this section, we are going to explore in detail the connection between the three twist-4 DAs and the LFWAs $\psi^{(3,4,5)}$. Let us start with defining the decomposition:

$$\Phi_4 = \Phi_4^{(m)} + \Phi_4^{(\boldsymbol{k}_\perp)} + \Phi_4^{(g)}, \tag{3.141}$$

$$\Psi_4 = \Psi_4^{(m)} + \Psi_4^{(\boldsymbol{k}_\perp)} + \Psi_4^{(g)}, \tag{3.142}$$

$$\Xi_4 = \Xi_4^{(m)} + \Xi_4^{(\boldsymbol{k}_\perp)} + \Xi_4^{(g)}. \tag{3.143}$$

The mass terms is the simplest term to compute for all the DAs, and the results are:

$$\Phi_4^{(m)}(x_1, x_2, x_3) = -\frac{m}{M x_3}\Phi_3(x_2, x_1, x_3), \tag{3.144}$$

$$\Psi_4^{(m)}(x_1, x_2, x_3) = \frac{m}{M x_2}\left(\Phi_3(x_2, x_3, x_1) + \Phi_3(x_1, x_3, x_2)\right), \tag{3.145}$$

$$\Xi_4^{(m)}(x_1, x_2, x_3) = \frac{m}{M x_1}\Phi_3(x_2, x_1, x_3), \tag{3.146}$$

where the leading-twist DA can be expressed in terms of $\psi^{(0)}$ by means of Eq. (3.104).

The $\boldsymbol{k}_\perp$ terms are the one of interest for us, since they connect the twist-4 DAs to the $L_z = \pm 1$ LFWAs through the following relations

$$\Phi_4^{(\boldsymbol{k}_\perp)}(x_1, x_2, x_3) = -\frac{4\sqrt{6}}{M x_3}\int [d\boldsymbol{k}_\perp]_3 \left(k_{3,R} k_{2,L}\psi^{(3)}(2,1,3) + k_{3,R} k_{1,L}\psi^{(4)}(2,1,3)\right), \tag{3.147}$$

$$\Psi_4^{(\boldsymbol{k}_\perp)}(x_1, x_2, x_3) = -\frac{4\sqrt{6}}{M x_2}\int [d\boldsymbol{k}_\perp]_3 \left(k_{1,R} k_{2,L}\psi^{(3)}(1,2,3) + k_{2,R} k_{2,L}\psi^{(4)}(1,2,3)\right), \tag{3.148}$$

$$\Xi_4^{(\boldsymbol{k}_\perp)}(x_1,x_2,x_3)=\frac{4\sqrt{6}}{Mx_1}\int[d\boldsymbol{k}_\perp]_3\left(k_{1,R}k_{1,L}\psi^{(5)}(2,1,3)+k_{1,R}k_{2,L}\psi^{(5)}(1,2,3)\right). \tag{3.149}$$

Last, the gluon contributions read:

$$\Phi_4^{(g)}(x_1,x_2,x_3)=-\frac{1}{2}\int_0^{x_3}dy\frac{1}{x_3(x_3-y)}\Phi_4^g(x_1,x_2,y,x_3-y), \tag{3.150}$$

$$\Psi_4^{(g)}(x_1,x_2,x_3)=-\frac{1}{2}\int_0^{x_2}dy\frac{1}{x_2(x_2-y)}\Psi_4^g(x_1,y,x_3,x_2-y), \tag{3.151}$$

$$\Xi_4^{(g)}(x_1,x_2,x_3)=-\frac{1}{2}\int_0^{x_1}dy\frac{1}{x_1(x_1-y)}\Xi_4^g(y,x_2,x_3,x_1-y). \tag{3.152}$$

These results and the link between the gluon DAs and the three-quark plus one-gluon $L_z=0$ LFWAs in Eqs. (3.108)-(3.110) highlight the connection between the three-quark LFWAs with $L_z\neq 0$ and the LFWAs for a state with an extra gluon. To make this connection explicit, we invert the systems of equations (3.141)-(3.143), with the result:

$$\begin{aligned}\Phi_4^{(\boldsymbol{k}_\perp)}&=-\frac{4\sqrt{6}}{Mx_3}\int[d\boldsymbol{k}_\perp]_3\left(k_{3,R}k_{2,L}\psi^{(3)}(2,1,3)+k_{3,R}k_{1,L}\psi^{(4)}(2,1,3)\right)\\&\equiv -A(213)=\Phi_4(x_1,x_2,x_3)-\Phi_4^{(m)}(x_1,x_2,x_3)-\Phi_4^{(g)}(x_1,x_2,x_3)\\&=\Phi_4(x_1,x_2,x_3)+\frac{m}{Mx_3}\Phi_3(x_2,x_1,x_3)\\&+\frac{1}{2}\int_0^{x_3}dy\frac{1}{x_3(x_3-y)}\Phi_4^g(x_1,x_2,y,x_3-y),\end{aligned} \tag{3.153}$$

$$\begin{aligned}\Psi_4^{(\boldsymbol{k}_\perp)}&=-\frac{4\sqrt{6}}{Mx_2}\int[d\boldsymbol{k}_\perp]_3\left(k_{1,R}k_{2,L}\psi^{(3)}(1,2,3)+k_{2,R}k_{2,L}\psi^{(4)}(1,2,3)\right)\\&\equiv -B(123)=\Psi_4(x_1,x_2,x_3)-\Psi_4^{(m)}(x_1,x_2,x_3)-\Psi_4^{(g)}(x_1,x_2,x_3)\\&=\Psi_4(x_1,x_2,x_3)-\frac{m}{Mx_2}\left(\Phi_3(x_2,x_3,x_1)+\Phi_3(x_1,x_3,x_2)\right)\\&+\frac{1}{2}\int_0^{x_2}dy\frac{1}{x_2(x_2-y)}\Psi_4^g(x_1,y,x_3,x_2-y),\end{aligned} \tag{3.154}$$

$$\begin{aligned}\Xi_4^{(\boldsymbol{k}_\perp)}&=\frac{4\sqrt{6}}{Mx_1}\int[d\boldsymbol{k}_\perp]_3\left(k_{1,R}k_{1,L}\psi^{(5)}(2,1,3)+k_{1,R}k_{2,L}\psi^{(5)}(1,2,3)\right)\\&\equiv C(123)=\Xi_4(x_1,x_2,x_3)-\Xi_4^{(m)}(x_1,x_2,x_3)-\Xi_4^{(g)}(x_1,x_2,x_3)\\&=\Xi_4(x_1,x_2,x_3)-\frac{m}{Mx_1}\Phi_3(x_2,x_1,x_3)\\&+\frac{1}{2}\int_0^{x_1}dy\frac{1}{x_1(x_1-y)}\Xi_4^g(y,x_2,x_3,x_1-y).\end{aligned} \tag{3.155}$$

To proceed further, we need to perform the integrals over the transverse momenta. We can compute these integrals only in a particular model for the LFWAs, as it will be described in Chapter 6.

To conclude this chapter, we notice that one could generalize the matrix elements defining the DAs by assuming a dependence of the fields on the transverse position, along with the light-cone minus position. However, in this case, it would appear a transverse gauge-link that does not reduce to unity in the light-cone gauge. Therefore the connection with the LFWAs would become more involved and less transparent.

Chapter 4

A study of the exclusive dijet cross section

4.1 Introduction

In recent years, an increasing amount of effort and resources were devoted to investigate different approaches that could allow us to access information on the quark and gluon OAM inside the proton. As we introduced in Chapter 3, a clear and direct information on the OAM can only be obtained via the Wigner distributions (or their momentum-space counterpart, the GTMDs). For this reason, every process that allows one to gain insight on GTMDs is of great interest. Unfortunately, at present, only very few processes are known to give access to GTMDs, at least in principle [70–80]. Practical difficulties make the candidate processes very hard to analyze with a precision sufficient to extract information on the GTMDs. A promising example among the possible processes is given by the diffractive dijet production in the quasi-real photon limit [72–79]. The process can be described in the partonic picture by a gluon exchange between a pair created by the photon and the proton. The final-jet invariant mass provides the hard scale necessary for the partonic interpretation of the process. The characteristics of the process make it suitable to study the gluon Wigner distributions in the small-x approximation [80–82]. Extensive work was done in this direction, with particular focus on specific cross-section angular modulations, which allow one to specifically access the gluon OAM contribution in the small-x region [79]. However, at the best of our knowledge, no explicit and complete cross-section decomposition was presented in literature so far. We aim to provide such a decomposition in this chapter. We believe that this will open the possibility for future works to explore the structure functions associated with different angular modulations. Moreover, with the fully differential cross section at our disposal, it might be possible to extend the study of this process beyond the small-x approximation, eventually leading to a full description in terms of Wigner functions for moderate values of x.

P	target initial momentum
P'	target final momentum
S	target spin vector
q	quasi-real photon momentum
j	momentum of the first jet
l	momentum of the second jet
k	momentum of the incoming lepton
k'	momentum of the scattered lepton

Table 4.1: Summary of the momenta of the particles/jets involved in the dijet diffractive production process.

4.1.1 Conventions

Since we aim to study diffractive dijet production in the quasi-real photon limit, we assume that the photon is generated by a leptonic probe. This is inessential, since the photon source can also be of different nature, like an heavy ion in ion-proton collisions at large impact parameters (in this case we refer to the process as ultra-peripheral pA collisions). The last ones can be explored at the Large Hadron Collider (LHC) at CERN (Geneva, Switzerland), whereas the lepton-proton version of the process is useful in perspective of studies at the future Electron-Ion Collider (EIC) at the Brookahven National Lab (BNL) in the US. We also assume the one-photon exchange approximation. We then focus on the process:

$$\ell(k) + p(P) \to p(P') + J(j) + J(l) + \ell(k'), \tag{4.1}$$

where e, p, J stand, respectively, for an electron, a proton and a jet with the momentum of each particle/jet in brackets. To help the reader, a summary of the notation for the momenta is shown in Tab. 4.1.

We will adopt the following shorthand notations

$$a^{[\mu}b^{\nu]} := \frac{1}{2}\left(a^\mu b^\nu - a^\nu b^\mu\right), \tag{4.2}$$

$$a^{\{\mu}b^{\nu\}} := \frac{1}{2}\left(a^\mu b^\nu + a^\nu b^\mu\right), \tag{4.3}$$

$$\varepsilon^{\cdots q\cdots} := \varepsilon^{\cdots\alpha\cdots} q_\alpha. \tag{4.4}$$

For a partonic description of the process, we need to identify a hard scale. Since we are working under the assumption of quasi-real photon, the hard scale is provided by the invariant mass of one of the two jets: $\mu = \sqrt{j^2}$ or $\mu = \sqrt{l^2}$ or $\mu = \sqrt{j^2} \simeq \sqrt{l^2}$.

4.2 Reference frame

It is useful to introduce the following Lorentz scalars to parametrize the process:

$$x = \frac{Q^2}{2P\cdot q},\ y = \frac{P\cdot q}{P\cdot k},\ z_j = \frac{P\cdot j}{P\cdot q},\ z_l = \frac{P\cdot l}{P\cdot q}.$$

The cross section will be differential in the above variables. Having in mind to utilize the cross section to extract information on the partonic structure, and in particular on the Wigner functions, we need to make the cross section differential in more variables. In particular, we would like to introduce as variables the azimuthal angles of the produced jets and the polarization angle of the target proton. To specify such angles, it is useful to choose a reference frame, although it is possible to define the angles in a frame-invariant way as shown in Ref. [83]. For simplicity, we choose to work in the Target Rest Frame (TRF) with the photon three-momentum defining the $\hat{x}^3$ axis. Hence, the additional variables that we choose to describe the process are:

$$\phi_S,\ j_\perp^2,\ l_\perp^2,\ \phi_j,\ \phi_l,$$

where the $\perp$ stands for the components of the vector orthogonal to the direction of motion of the photon. The angle ϕ_S is the proton polarization angle, $\phi_{j,l}$ are the angles of the $\perp$ components of the jets with respect to the plane identified by the lepton and photon momentum. A representation of the reference frame is shown in Fig. 4.1. It is also useful to introduce a parameter that controls the size of the target-mass correction as:

$$\gamma =: \frac{2Mx}{Q}. \tag{4.5}$$

Finally, the invariant masses of the two jets, i.e.

$$j^2 = W_j^2,\ l^2 = W_l^2, \tag{4.6}$$

are considered fixed quantities, in analogy to the mass of an hadron. To simplify the calculations, we shall assume massless electrons, i.e.:

$$k^2 = (k')^2 = 0. \tag{4.7}$$

In this frame and with these assumptions, we have the explicit expression in instant-form representation for the relevant four-vectors:

$$P^\mu = \begin{pmatrix} M \\ 0 \\ 0 \\ 0 \end{pmatrix},\ S^\mu = \begin{pmatrix} 0 \\ S_\perp \cos\phi_S \\ S_\perp \sin\phi_S \\ -S_L \end{pmatrix},\ q^\mu = \begin{pmatrix} q^0 \\ 0 \\ 0 \\ q^3 \end{pmatrix},$$

$$k^\mu = \begin{pmatrix} k^0 \\ \tilde{k}\sin\theta_e \\ 0 \\ \tilde{k}\cos\theta_e \end{pmatrix},\ j^\mu = \begin{pmatrix} j^0 \\ j_\perp\cos\phi_j \\ j_\perp\sin\phi_j \\ j^3 \end{pmatrix},\ l^\mu = \begin{pmatrix} l^0 \\ l_\perp\cos\phi_l \\ l_\perp\sin\phi_l \\ l^3 \end{pmatrix},$$

where $a_\perp = |\boldsymbol{a}_\perp|$ for any transverse vector $\boldsymbol{a}_\perp$ and $\tilde{k}$ is the magnitude of the three-momentum of the electron. We can express all the components in terms of the invariants of the process (for the expression of the angle of the lepton see Ref. [23]):

$$\begin{aligned}
q^\mu &= \frac{Q}{\gamma}(1,0,0,\sqrt{1+\gamma^2}),\\
k^\mu &= \frac{Q}{y\gamma}(1,\sin\theta_e,0,\cos\theta_e) \ \text{ with}\\
\cos\theta_e &= \frac{1+\frac{y\gamma^2}{2}}{\sqrt{1+\gamma^2}},\ \sin\theta_e = \frac{\gamma}{\sqrt{1+\gamma^2}}\sqrt{1-y-\frac{y^2\gamma^2}{4}},\\
j^\mu &= z_j\frac{Q}{\gamma}\left(1,\frac{j_\perp\gamma}{Qz_j}\cos\phi_j,\frac{j_\perp\gamma}{Qz_j}\sin\phi_j,\sqrt{1-\frac{\gamma^2}{Q^2z_j^2}\left(j_\perp^2+W_j^2\right)}\right),\\
l^\mu &= z_l\frac{Q}{\gamma}\left(1,\frac{l_\perp\gamma}{Qz_l}\cos\phi_l,\frac{l_\perp\gamma}{Qz_l}\sin\phi_l,\sqrt{1-\frac{\gamma^2}{Q^2z_l^2}\left(l_\perp^2+W_l^2\right)}\right).
\end{aligned}$$

For any four-vector v it is useful to introduce the auxiliary vector

$$v_q^\mu =: v^\mu - q^\mu\frac{v\cdot q}{q^2} \tag{4.8}$$

that satisfies the property:

$$v_q\cdot q = 0. \tag{4.9}$$

The general expression for the cross section is

$$d\sigma = \frac{|\mathcal{M}|^2 d\omega}{\mathcal{F}}, \tag{4.10}$$

where $\mathcal{F}$ is the flux factor, $d\omega$ is the differential phase space of the final particles and $|\mathcal{M}|^2$ is the amplitude square of the process. The phase space is simply:

$$d\omega = (2\pi)^4\delta(P'+k'+j+l-k-P)\frac{d^3k'}{2k'^0(2\pi)^3}\frac{d^3P'}{2P'^0(2\pi)^3}\frac{d^3j}{2j^0(2\pi)^3}\frac{d^3l}{2l^0(2\pi)^3}. \tag{4.11}$$

In the following, we eliminate the delta function for the overall momentum conservation by simply integrating over P'. We can manipulate the remaining phase-space factors to express all the differentials in terms of the chosen variables and invariants:

$$\frac{d^3j}{2j^0} = \frac{j_\perp Q^2 z_j}{\gamma^2 j^3}dj_\perp d\phi_j dz_j = \frac{Q^2 z_j}{2\gamma^2 j^3}dj_\perp^2 d\phi_j dz_j, \tag{4.12}$$

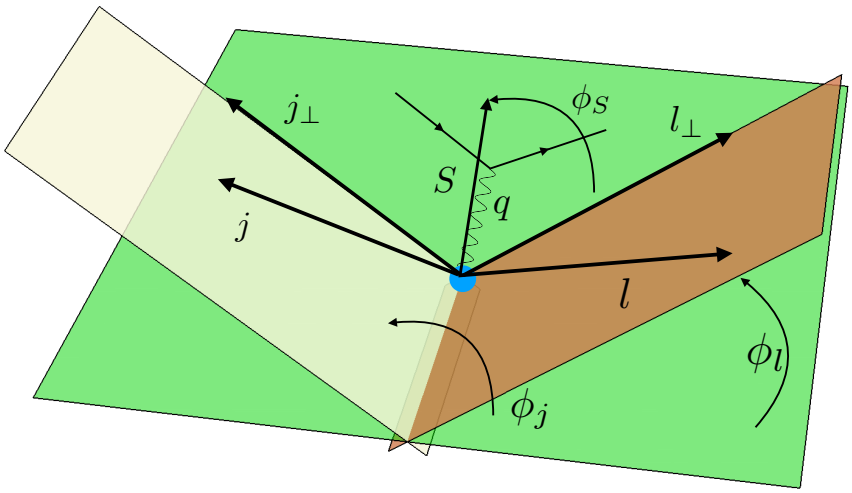

Figure 4.1: Pictorial representation of the reference frame for the diffractive dijet production in the one-photon exchange approximation. For a summary of the momenta involved see Tab. 4.1.

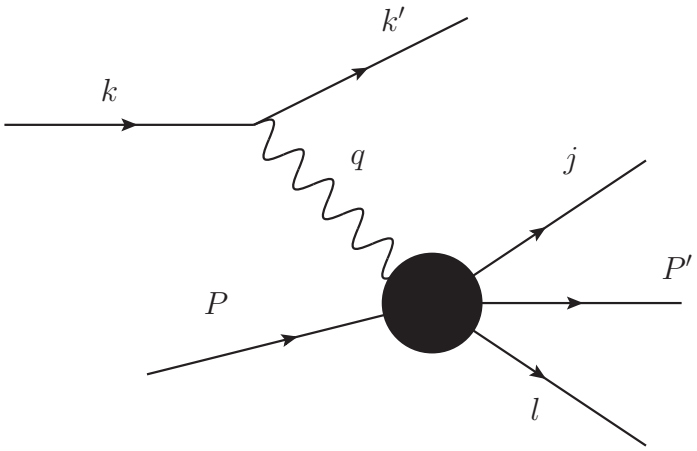

Figure 4.2: Schematic representation of the dijet process.

$$\frac{d^3l}{2l^0} = \frac{l_\perp Q^2 z_l}{\gamma^2 l^3} dl_\perp d\phi_l dz_l = \frac{Q^2 z_l}{2\gamma^2 l^3} dl_\perp^2 d\phi_l dz_l, \tag{4.13}$$

$$\frac{d^3k'}{2k'^0} = \frac{y}{4x} dx dQ^2 d\psi = \frac{Q^2}{4x} dx dy d\psi = \frac{Q^2}{4x} dx dy d\phi_S \frac{\cos(\theta_e)}{1 - \sin^2(\theta_e)\sin^2(\phi_S)}. \tag{4.14}$$

The flux factor can be computed as:

$$\mathcal{F} = 4\sqrt{(P \cdot k)^2 - P^2 k^2} = \frac{4MQ}{\gamma y}. \tag{4.15}$$

Finally, the amplitude square for the process can be written as the product of the leptonic-probe tensor and an (unknown) hadronic tensor

$$|\mathcal{M}|^2 = L_{\mu\nu} W^{\mu\nu} \frac{e^4}{Q^4} = L_{\mu\nu} W^{\mu\nu} \frac{16\pi^2\alpha^2}{Q^4}, \tag{4.16}$$

where α is the electromagnetic coupling constant and $1/Q^2$ comes from the photon propagator. The leptonic tensor is summed over the final lepton polarization, but we keep the possibility to have a polarized incoming lepton beam with polarization λ_e:

$$\begin{aligned} L_{\mu\nu} &= \sum_\sigma \bar{u}_\sigma(k')\gamma_\nu u_\lambda(k)\bar{u}_\lambda(k)\gamma_\mu u_\sigma(k') \\ &= 4k_{\{\mu}k'_{\nu\}} - 2(k\cdot k')g_{\mu\nu} + 2i\lambda_e\varepsilon_{\mu\nu kk'} = 4k_{\{\mu}k'_{\nu\}} + 2(k\cdot q)g_{\mu\nu} + 2i\lambda_e\varepsilon_{\mu\nu kq}. \end{aligned} \tag{4.17}$$

Combining all together, we can express Eq. (4.10) as:

$$\begin{aligned} d\sigma &= \frac{\alpha^2 16\pi^2}{\mathcal{F}Q^4} W_{\mu\nu} L^{\mu\nu} 2\pi \frac{d^3l}{2l^0(2\pi)^3} \frac{d^3j}{2j^0(2\pi)^3} \frac{d^3k'}{2k'^0(2\pi)^3} \\ &= W_{\mu\nu} L^{\mu\nu} \frac{\gamma y}{4MQ} \frac{Q^2}{4x} \frac{Q^2 z_j}{2\gamma^2 j^3} \frac{Q^2 z_l}{2\gamma^2 l^3} \frac{\alpha^2 16\pi^2}{Q^4} \frac{1}{(2\pi)^8} dj_\perp^2 d\phi_j dz_j dl_\perp^2 d\phi_l dz_l dx dy d\psi. \end{aligned} \tag{4.18}$$

4.3 Hadronic tensor

All the proton-structure information is encoded in the hadronic tensor of Eq. (4.18). The standard approach in this kind of problems is to decompose the hadronic tensor on a basis of independent Lorentz tensors. Each Lorentz structure appears with an unknown coefficient, called structure function, that depends on the whole set of possible Lorentz scalars. In a partonic picture of the process, each structure function could then be written in terms of appropriate combinations of parton correlators, Dirac matrixes and particle propagators. We shall analyze the process only at the level of structure functions. The main goal of the decomposition of the hadronic tensor in a Lorentz basis is to factorize all the angular dependences, in such a way that each structure function can be extracted as the amplitude of a given angular modulation of the cross section

(or a given combination of them). Therefore, by construction, the structure functions can depend only on scalar products that are independent from the azimuthal angles $\phi_{S,j,l}$. Such products are:

$$q \cdot j, \quad q \cdot l, \quad P \cdot j, \quad P \cdot l, \quad q \cdot P. \tag{4.19}$$

The only scalar product of momenta that brings a dependence on the angles is:

$$j \cdot l = \frac{Q^2 z_j z_l - j^3 l^3}{\gamma^2} - j_\perp l_\perp \cos\left(\phi_j - \phi_l\right). \tag{4.20}$$

In general, we obtain:

$$(j \cdot l)^n = F_0^{(n)} + \sum_{k=1}^{n} F_k^{(n)} \cos\left(k(\phi_j - \phi_l)\right), \tag{4.21}$$

where

$$F_k^{(n)} = F_k^{(n)}\left(j_\perp, l_\perp, z_j, z_l, \gamma^2, Q^2\right), \quad \forall n, k \in \mathbb{N},\ k \leq n \tag{4.22}$$

can be computed from Eq. (4.20).

We would like to stress the difference between our approach and the one presented in Ref. [84] for SIDIS di-hadron production. The conceptual basis is very similar, since the structure of the cross section is the same and only the description at the partonic level changes. However, we chose to decompose the cross section using different variables, in particular we are working with the individual azimuthal angles of the two jets instead of the average angle or the difference. This choice was made because it is a more straightforward generalization of single-hadron SIDIS process.

We impose constraints on the hadronic tensor that derive from parity, hermiticity and gauge invariance [85, 86]:

$$\text{parity: } W^{\mu\nu}(P,q,j,l,S) = \Lambda^\mu{}_\alpha \Lambda^\nu{}_\beta W^{\alpha\beta}\left(\tilde{P},\tilde{q},\tilde{j},\tilde{l},-\tilde{S}\right), \tag{4.23}$$

$$\text{hermiticity: } W^{\mu\nu}(P,q,j,l,S) = \left[W^{\nu\mu}(P,q,j,l,S)\right]^*, \tag{4.24}$$

$$\text{gauge invariance: } q_\mu W^{\mu\nu}(P,q,j,l,S) = q_\nu W^{\mu\nu}(P,q,j,l,S) = 0. \tag{4.25}$$

The parity matrix Λ and the "tilde" vectors are defined as follow:

$$\Lambda^\mu{}_\nu = \begin{pmatrix} 1 & 0 & 0 & 0 \\ 0 & -1 & 0 & 0 \\ 0 & 0 & -1 & 0 \\ 0 & 0 & 0 & -1 \end{pmatrix}, \quad \tilde{v}^\mu = \Lambda^\mu{}_\nu v^\nu. \tag{4.26}$$

A direct consequence of the parity invariance is the fact that S can appear only linearly in the hadronic tensor and only in combination with the antisymmetric symbol $\varepsilon^{\mu\nu\alpha\beta}$. The hermiticity constraint imposes the symmetric part of the

hadronic tensor to be real and the antisymmetric part to be imaginary. The gauge invariance gives constraints on the possible Lorentz structures, in particular, if an open index is carried by a vector, then the vector must be in the form of Eq. (4.8). In the following we shall analyze all the terms in the hadronic tensor, organizing the discussion in sections. Each section treats either the unpolarized or the polarized hadronic tensor and either the symmetric or antisymmetric part.

4.3.1 Unpolarized symmetric part

The, by far, most intuitive and simple part of the hadronic tensor is the symmetric and unpolarized one. We will analyze this part with care, because it introduces us to the techniques and the caveats that must be carefully considered also when dealing with the other parts of the hadronic tensor. In the unpolarized and symmetric sector of the hadronic tensor, the following independent and gauge invariant Lorentz structures are present:

$$\begin{aligned}&\mathcal{U}_1^{\mu\nu} = g^{\mu\nu} - \frac{q^\mu q^\nu}{q^2},\ \mathcal{U}_2^{\mu\nu} = P_q^{\{\mu} P_q^{\nu\}},\ \mathcal{U}_3^{\mu\nu} = P_q^{\{\mu} j_q^{\nu\}},\\ &\mathcal{U}_4^{\mu\nu} = P_q^{\{\mu} l_q^{\nu\}},\ \mathcal{U}_5^{\mu\nu} = j_q^{\{\mu} j_q^{\nu\}},\ \mathcal{U}_6^{\mu\nu} = j_q^{\{\mu} l_q^{\nu\}},\ \mathcal{U}_7^{\mu\nu} = l_q^{\{\mu} l_q^{\nu\}}.\end{aligned} \tag{4.27}$$

The structures with two antisymmetric symbols that involve a single-jet momentum like

$$\varepsilon^{qPj\{\mu}\varepsilon^{\nu\}qPj} \tag{4.28}$$

can be written in terms of the scalar products in Eq. (4.19) and the existing structures in Eq. (4.27) by means of Eq. (A.4). Instead, the structures that involve the momenta of both jets, like the following one

$$\varepsilon^{qPj\{\mu}\varepsilon^{\nu\}qPl} \tag{4.29}$$

can be written in terms of the product $j \cdot l$ and the existing structures in Eq. (4.27). Finally, the fully-contracted term

$$\left(\varepsilon^{qPjl}\right)^{2n} \tag{4.30}$$

involves the product $j \cdot l$ and the scalar products Eq. (4.19). These considerations imply that, using Eq. (4.21) to write the scalar product $(j \cdot l)^n$ in terms of $\cos\left(k(\phi_j - \phi_l)\right)$, we have for an arbitrary $k \in \mathbb{N}$:

$$\left(\mathcal{U}_1^{\mu\nu}\right)^{(k)} = \cos\left(k(\phi_j - \phi_l)\right)\left(g^{\mu\nu} - \frac{q^\mu q^\nu}{q^2}\right), \tag{4.31}$$

$$\left(\mathcal{U}_2^{\mu\nu}\right)^{(k)} = \cos\left(k(\phi_j - \phi_l)\right) P_q^{\{\mu} P_q^{\nu\}}, \tag{4.32}$$

$$\left(\mathcal{U}_3^{\mu\nu}\right)^{(k)} = \cos\left(k(\phi_j - \phi_l)\right) P_q^{\{\mu} j_q^{\nu\}}, \tag{4.33}$$

$$\left(\mathcal{U}_4^{\mu\nu}\right)^{(k)} = \cos\left(k(\phi_j - \phi_l)\right) P_q^{\{\mu} l_q^{\nu\}}, \tag{4.34}$$

$$\left(\mathcal{U}_5^{\mu\nu}\right)^{(k)} = \cos\left(k(\phi_j - \phi_l)\right) j_q^{\{\mu} j_q^{\nu\}}, \tag{4.35}$$

$$(\mathcal{U}_6^{\mu\nu})^{(k)} = \cos\left(k(\phi_j - \phi_l)\right) j_q^{\{\mu} l_q^{\nu\}}, \tag{4.36}$$

$$(\mathcal{U}_7^{\mu\nu})^{(k)} = \cos\left(k(\phi_j - \phi_l)\right) l_q^{\{\mu} l_q^{\nu\}}. \tag{4.37}$$

Therefore, we arrived at the following decomposition for the unpolarized and symmetric hadronic tensor:

$$W^{\mu\nu} = \sum_{k=0}^{\infty} \sum_{i=1}^{7} (\mathcal{U}_i^{\mu\nu})^{(k)} B_i^{(k)}, \tag{4.38}$$

where $B_i^{(k)}$ are unknown coefficients that depend on all the invariants of the process but not on $j \cdot l$.

To match the standard convention adopted in the description of the SIDIS and DVCS processes, we introduce the auxiliary variables:

$$\varkappa = \frac{1}{y}\sqrt{1 - y - \frac{y^2\gamma^2}{4}}, \quad \ell = \sqrt{2}\left(\frac{1}{2} - \frac{1}{y}\right), \tag{4.39}$$

that can be expressed in terms of ratio between longitudinal and transverse photon flux ϵ, defined as (see Ref. [83])[1]:

$$\epsilon = \frac{1 - y - \frac{y^2\gamma^2}{4}}{1 - y + \frac{y^2}{4}(2 + \gamma^2)}, \tag{4.40}$$

$$\epsilon = \frac{\varkappa^2}{\ell^2 - \varkappa^2}, \quad \ell^2 - \varkappa^2 = \frac{1 + \gamma^2}{2(1 - \epsilon)}. \tag{4.41}$$

By inverting the above relations, we obtain:

$$\varkappa = \frac{\sqrt{1 + \gamma^2}}{\sqrt{2(1 - \epsilon)}}\sqrt{\epsilon}, \ \ell = \frac{\sqrt{1 + \gamma^2}}{\sqrt{2(1 - \epsilon)}}\sqrt{1 + \epsilon}, \ \varkappa\ell = \frac{1 + \gamma^2}{2(1 - \epsilon)}\sqrt{\epsilon(1 + \epsilon)}. \tag{4.42}$$

As noticed above, the symmetric part of the hadronic tensor must be real due to the hermiticity constraint in Eq. (4.24). Therefore, the contraction with the imaginary part of the leptonic tensor must vanish (the check of this property is straightforward). Explicit results can be found in the App. A and, since they are quite lenghty, they are given for the unpolarized and symmetric case only. Here we isolate only the relevant polarization coefficients of Eqs. (4.42), leaving all the invariants inside the coefficients A_i. For the basic structures of Eq. (4.27) we have:

$$\left(g^{\mu\nu} - \frac{q^\mu q^\nu}{q^2}\right) \mathcal{R}e\left(L_{\mu\nu}\right) = A_1, \tag{4.43}$$

$$P_q^{\{\mu} P_q^{\nu\}} \mathcal{R}e\left(L_{\mu\nu}\right) = A_2 \frac{\epsilon}{1 - \epsilon}, \tag{4.44}$$

[1]The symbol ε is reserved for the antisymmetric symbol and ϵ for the photon polarization factor. Confusion should not arise.

$$P_q^{\{\mu} j_q^{\nu\}} \mathcal{R}e\left(L_{\mu\nu}\right) = A_3 \frac{\epsilon}{1-\epsilon} + A_4 \sqrt{\frac{\epsilon(1+\epsilon)}{1-\epsilon}} \cos\left(\phi_j\right), \tag{4.45}$$

$$P_q^{\{\mu} l_q^{\nu\}} \mathcal{R}e\left(L_{\mu\nu}\right) = A_5 \frac{\epsilon}{1-\epsilon} + A_6 \sqrt{\frac{\epsilon(1+\epsilon)}{1-\epsilon}} \cos\left(\phi_l\right), \tag{4.46}$$

$$\begin{aligned} j_q^{\{\mu} j_q^{\nu\}} \mathcal{R}e\left(L_{\mu\nu}\right) = {} & A_7 \frac{1}{1-\epsilon} + A_8 \frac{\epsilon}{1-\epsilon} + A_9 \sqrt{\frac{\epsilon(1+\epsilon)}{1-\epsilon}} \cos\left(\phi_j\right) \\ & + A_{10} \frac{\epsilon}{1-\epsilon} \cos\left(2\phi_j\right), \end{aligned} \tag{4.47}$$

$$\begin{aligned} l_q^{\{\mu} l_q^{\nu\}} \mathcal{R}e\left(L_{\mu\nu}\right) = {} & A_{11} \frac{1}{1-\epsilon} + A_{12} \frac{\epsilon}{1-\epsilon} + A_{13} \sqrt{\frac{\epsilon(1+\epsilon)}{1-\epsilon}} \cos\left(\phi_l\right) \\ & + A_{14} \frac{\epsilon}{1-\epsilon} \cos\left(2\phi_l\right), \end{aligned} \tag{4.48}$$

$$\begin{aligned} j_q^{\{\mu} l_q^{\nu\}} \mathcal{R}e\left(L_{\mu\nu}\right) = {} & A_{15} \frac{\epsilon}{1-\epsilon} + A_{16} \sqrt{\frac{\epsilon(1+\epsilon)}{1-\epsilon}} \cos\left(\phi_j\right) \\ & + A_{17} \sqrt{\frac{\epsilon(1+\epsilon)}{1-\epsilon}} \cos\left(\phi_l\right) + A_{18} \frac{1}{1-\epsilon} \cos\left(\phi_j - \phi_l\right) \\ & + A_{19} \frac{\epsilon}{1-\epsilon} \cos\left(\phi_j + \phi_l\right). \end{aligned} \tag{4.49}$$

The contraction between the unpolarized hadronic tensor in Eq. (4.38) and the leptonic tensor in Eq. (4.17), using Eqs. (4.43)-(4.49), leads to:

$$\begin{aligned} \mathcal{R}e\left(W^{\mu\nu}\right) \mathcal{R}e\left(L_{\mu\nu}\right) = \frac{1}{1-\epsilon} \sum_{k=0}^{\infty} \cos\left(k\phi_j - k\phi_l\right) \Bigg\{ & G_1^{(k)} + G_2^{(k)} \epsilon \\ & + G_3^{(k)} \sqrt{\epsilon(1+\epsilon)} \cos\left(\phi_j\right) + G_4^{(k)} \sqrt{\epsilon(1+\epsilon)} \cos\left(\phi_l\right) \\ & + G_5^{(k)} \epsilon \cos\left(2\phi_j\right) + G_6^{(k)} \epsilon \cos\left(2\phi_l\right) + G_7^{(k)} \epsilon \cos\left(\phi_j + \phi_l\right) \Bigg\}. \end{aligned} \tag{4.50}$$

4.3.2 Antisymmetric unpolarized part

The antisymmetric and unpolarized part of the hadronic tensor gives non vanishing contribution only when contracted with the imaginary part of the leptonic tensor (we recall that the antisymmetric part of the hadronic tensor must be purely imaginary from the hermiticity constraint). We have only three independent structures:

$$\begin{aligned} \left(\mathcal{P}_1^{\mu\nu}\right)^{(k)} &= \cos\left(k(\phi_j - \phi_l)\right) P_q^{[\mu} j_q^{\nu]}, \\ \left(\mathcal{P}_2^{\mu\nu}\right)^{(k)} &= \cos\left(k(\phi_j - \phi_l)\right) P_q^{[\mu} l_q^{\nu]}, \\ \left(\mathcal{P}_3^{\mu\nu}\right)^{(k)} &= \cos\left(k(\phi_j - \phi_l)\right) j_q^{[\mu} l_q^{\nu]}. \end{aligned}$$

Therefore, the unpolarized and antisymmetric part of the hadronic tensor reads:

$$W^{\mu\nu} = \sum_{k=0}^{\infty} \sum_{i=1}^{3} \left(\mathcal{P}_i^{\mu\nu}\right)^{(k)} C_i^{(k)}, \tag{4.51}$$

where $C_i^{(k)}$ are unknown coefficients that depend on all the invariant of the process, but not on $j \cdot l$.

Using the definitions (4.40)-(4.41), we have:

$$\begin{aligned}
\mathcal{P}_1^{\mu\nu}\mathfrak{Im}\left(L_{\mu\nu}\right) &= B_1\sqrt{\frac{\epsilon}{1-\epsilon}}\sin\left(\phi_j\right), \\
\mathcal{P}_2^{\mu\nu}\mathfrak{Im}\left(L_{\mu\nu}\right) &= B_2\sqrt{\frac{\epsilon}{1-\epsilon}}\sin\left(\phi_l\right), \\
\mathcal{P}_3^{\mu\nu}\mathfrak{Im}\left(L_{\mu\nu}\right) &= B_3\sqrt{\frac{\epsilon}{1-\epsilon}}\sin\left(\phi_j\right) \\
&\quad + B_4\sqrt{\frac{\epsilon}{1-\epsilon}}\sin\left(\phi_l\right) + B_5\sqrt{1+\epsilon}\sin\left(\phi_j-\phi_l\right).
\end{aligned} \tag{4.52}$$

Combining these results, we finally obtain the contraction between the leptonic part and the hadronic part as:

$$\begin{aligned}
\mathfrak{Im}\left(W^{\mu\nu}\right)\mathfrak{Im}\left(L_{\mu\nu}\right) = \lambda_e\frac{1}{1-\epsilon}\sum_{k=0}^{\infty}\cos\left(k(\phi_j-\phi_l)\right)\Bigg\{ & H_1^{(k)}\sqrt{\epsilon(1-\epsilon)}\sin\left(\phi_j\right) \\
& + H_2^{(k)}\sqrt{\epsilon(1-\epsilon)}\sin\left(\phi_l\right) + H_3^{(k)}\sqrt{1-\epsilon^2}\sin\left(\phi_j-\phi_l\right).
\end{aligned} \tag{4.53}$$

4.3.3 Polarized symmetric part

We can now start the study of the hadronic tensor for a polarized target. The complexity increases due to the larger number of possible combinations of vectors that lead to allowed Lorentz structures. For simplicity and to keep the notation clear, here we confine ourself to $(j \cdot l)^0$, and the generalization to $(j \cdot l)^n$ for all n is straightforward (see Sec. 4.3.1). In this section, we also include the results of Sec. 4.3.1 for the unpolarized case, to obtain the final result for the contraction between the real parts of the hadronic and leptonic tensor. The hadronic tensor reads:

$$\begin{aligned}
\mathcal{R}e\left(W^{\mu\nu}\right) =& \mathcal{U}_1^{\mu\nu} + \left(g^{\mu\nu} + \frac{q^\mu q^\nu}{Q^2}\right)\left(\varepsilon^{SqPj}\Phi_1 + \varepsilon^{SqPl}\Phi_2 + \varepsilon^{Sqjl}\Phi_3\right) \\
&+\mathcal{U}_2^{\mu\nu} + P_q^{\{\mu}P_q^{\nu\}}\left(\varepsilon^{SqPj}\Phi_4 + \varepsilon^{SqPl}\Phi_5 + \varepsilon^{Sqjl}\Phi_6\right) \\
&+\mathcal{U}_3^{\mu\nu} + P_q^{\{\mu}j_q^{\nu\}}\left(\varepsilon^{SqPj}\Phi_7 + \varepsilon^{SqPl}\Phi_8 + \varepsilon^{Sqjl}\Phi_9\right) \\
&+\mathcal{U}_4^{\mu\nu} + P_q^{\{\mu}l_q^{\nu\}}\left(\varepsilon^{SqPj}\Phi_{10} + \varepsilon^{SqPl}\Phi_{11} + \varepsilon^{Sqjl}\Phi_{12}\right) \\
&+\mathcal{U}_5^{\mu\nu} + j_q^{\{\mu}j_q^{\nu\}}\left(\varepsilon^{SqPj}\Phi_{13} + \varepsilon^{SqPl}\Phi_{14} + \varepsilon^{Sqjl}\Phi_{15}\right)
\end{aligned}$$

$$
\begin{aligned}
&+\mathcal{U}_6^{\mu\nu} + j_q^{\{\mu} l_q^{\nu\}} \left(\varepsilon^{SqPj}\Phi_{16} + \varepsilon^{SqPl}\Phi_{17} + \varepsilon^{Sqjl}\Phi_{18}\right)\\
&+\mathcal{U}_7^{\mu\nu} + l_q^{\{\mu} l_q^{\nu\}} \left(\varepsilon^{SqPj}\Phi_{19} + \varepsilon^{SqPl}\Phi_{20} + \varepsilon^{Sqjl}\Phi_{21}\right)\\
&+\varepsilon^{qPjl} S_q^{\{\mu} \left(P_q^{\nu\}}\Phi_{22} + j_q^{\nu\}}\Phi_{23} + l_q^{\nu\}}\Phi_{24}\right)\\
&+P_q^{\{\mu} \left(\varepsilon^{\nu\}SqP}\Phi_{25} + \varepsilon^{\nu\}Sqj}\Phi_{26} + \varepsilon^{\nu\}Sql}\Phi_{27}\right)\\
&+j_q^{\{\mu} \left(\varepsilon^{\nu\}SqP}\Phi_{28} + \varepsilon^{\nu\}Sqj}\Phi_{29} + \varepsilon^{\nu\}Sql}\Phi_{30}\right)\\
&+l_q^{\{\mu} \left(\varepsilon^{\nu\}SqP}\Phi_{31} + \varepsilon^{\nu\}Sqj}\Phi_{32} + \varepsilon^{\nu\}Sql}\Phi_{33}\right). \qquad (4.54)
\end{aligned}
$$

However, not all the 40 Lorentz structures lead to independent contributions when contracted with the leptonic tensor. This is a direct consequence of the following relation:

$$
\det \begin{pmatrix}
\mathcal{R}e\left(L_{\mu\nu}\right) P_q^{\{\mu}\varepsilon^{\nu\}SqP} & \mathcal{R}e\left(L_{\mu\nu}\right) P_q^{\{\mu}\varepsilon^{\nu\}Sqj} & \mathcal{R}e\left(L_{\mu\nu}\right) P_q^{\{\mu}\varepsilon^{\nu\}Sql}\\
\mathcal{R}e\left(L_{\mu\nu}\right) j_q^{\{\mu}\varepsilon^{\nu\}SqP} & \mathcal{R}e\left(L_{\mu\nu}\right) j_q^{\{\mu}\varepsilon^{\nu\}Sqj} & \mathcal{R}e\left(L_{\mu\nu}\right) j_q^{\{\mu}\varepsilon^{\nu\}Sql}\\
\mathcal{R}e\left(L_{\mu\nu}\right) l_q^{\{\mu}\varepsilon^{\nu\}SqP} & \mathcal{R}e\left(L_{\mu\nu}\right) l_q^{\{\mu}\varepsilon^{\nu\}Sqj} & \mathcal{R}e\left(L_{\mu\nu}\right) l_q^{\{\mu}\varepsilon^{\nu\}Sql}
\end{pmatrix} = 0. \qquad (4.55)
$$

This implies that we have 30 independent polarized structures (at order $(j\cdot l)^0$) when we contract the hadronic tensor in Eq. (4.54) and the leptonic tensor. From this observation we conclude that the lepton-hadron scattering in the one photon-exchange approximation is not able to distinguish all the, in principle, independent Lorentz structures present in the hadronic tensor. Different processes, that can be described via the same hadronic tensor, are, in general, necessary to fully reconstruct it. The discussion of such processes is beyond the scope of this work.

The contraction between the leptonic and the hadronic tensors leads to the following result at order $(j\cdot l)^0$:

$$
\begin{aligned}
&\mathcal{R}e\left(W^{\mu\nu}\right)\mathcal{R}e\left(L_{\mu\nu}\right)\\
&= \imath\ell S_\perp \sin\left(\phi_S\right) G_1 \;+\imath\ell S_\perp \sin\left(\phi_S - 2\phi_j\right) G_2\\
&+\imath\ell S_\perp \sin\left(\phi_S - 2\phi_l\right) G_3 \;+\left(\ell^2 - \imath^2\right) S_\perp \sin\left(\phi_S - 2\phi_j + \phi_l\right) G_4\\
&+\left(\ell^2 - \imath^2\right) S_\perp \sin\left(\phi_S - 2\phi_l + \phi_j\right) G_5 \;+\imath^2 S_\perp \sin\left(\phi_S + 2\phi_j - \phi_l\right) G_6\\
&+\imath^2 S_\perp \sin\left(\phi_S + 2\phi_l - \phi_j\right) G_7 \;+\imath^2 S_\perp \sin\left(\phi_S - 2\phi_j - \phi_l\right) G_8\\
&+\imath^2 S_\perp \sin\left(\phi_S - 2\phi_l - \phi_j\right) G_9 \;+\left(A_1\imath^2 + B_1\left(\ell^2 - \imath^2\right) + C_1\right) S_\perp \sin\left(\phi_S - \phi_j\right) G_{10}\\
&+\left(A_2\imath^2 + B_2\left(\ell^2 - \imath^2\right) + C_2\right) S_\perp \sin\left(\phi_S - \phi_l\right) G_{11} \;+\imath^2 S_\perp \sin\left(\phi_S + \phi_j\right) G_{12}\\
&+\imath^2 S_\perp \sin\left(\phi_S + \phi_l\right) G_{13} \;+\imath^2 S_\perp \sin\left(\phi_S - 3\phi_j\right) G_{14}\\
&+\imath^2 S_\perp \sin\left(\phi_S - 3\phi_l\right) G_{15} \;+\imath\ell S_\perp \sin\left(\phi_S - \phi_l\right) \cos\left(\phi_j\right) G_{16}\\
&+\imath\ell S_\perp \sin\left(\phi_S - \phi_j\right) \cos\left(\phi_l\right) G_{17} \;+\imath\ell S_L \sin\left(\phi_j\right) G_{18}\\
&+\imath\ell S_L \sin\left(\phi_l\right) G_{19} \;+\imath^2 S_L \sin\left(2\phi_j\right) G_{20}\\
&+\imath^2 S_L \sin\left(2\phi_l\right) G_{21} \;+\left(A_3\imath^2 + B_3\left(\ell^2 - \imath^2\right) + C_3\right) S_L \sin\left(\phi_j - \phi_l\right) G_{22}\\
&+\imath^2 S_L \sin\left(\phi_j + \phi_l\right) G_{23} \;+\imath\ell S_L \sin\left(\phi_j - 2\phi_l\right) G_{24} \;+\imath\ell S_L \sin\left(\phi_l - 2\phi_j\right) G_{25}\\
&+\left(\ell^2 - \imath^2\right) S_L \sin\left(2\phi_j - 2\phi_l\right) G_{26} \;+\imath^2 S_L \sin\left(\phi_j - 3\phi_l\right) G_{27}
\end{aligned}
$$

$$
\begin{aligned}
&+ \mathfrak{r}^2 S_L \sin(\phi_l - 3\phi_j)\, G_{28} \;+ \mathfrak{r}\ell \cos(\phi_j)\, G_{29} \\
&+ \mathfrak{r}\ell \cos(\phi_l)\, G_{30} \;+ \mathfrak{r}^2 \cos(2\phi_j)\, G_{31} \\
&+ \mathfrak{r}^2 \cos(2\phi_l)\, G_{32} \;+ \left(\ell^2 - \mathfrak{r}^2\right) \cos(\phi_j - \phi_l)\, G_{33} \\
&+ \mathfrak{r}^2 \cos(\phi_j + \phi_l)\, G_{34} \;+ \left(A_4 \mathfrak{r}^2 + B_4\left(\ell^2 - \mathfrak{r}^2\right) + C_4\right).
\end{aligned}
$$

We note that some spurious angular structures appear, like $\sin(2\phi_j - 2\phi_l)$, since it can be written as:

$$
\sin(2\phi_j - 2\phi_l) = 2\sin(\phi_j - \phi_l)\cos(\phi_j - \phi_l), \tag{4.56}
$$

meaning that it belongs to $(j \cdot l)^1$ order, or like $\cos(\phi_j - \phi_l)$ that appears in front of G_{33} and is clearly a constant contribution at order $(j \cdot l)^1$.

Using the definitions in Eq. (4.42) and eliminating all the spurious contributions, we obtain the following result:

$$
\begin{aligned}
&\mathcal{R}e\left(W^{\mu\nu}\right)\mathcal{R}e\left(L_{\mu\nu}\right) = \frac{1}{1-\epsilon}\sum_{k=0}^{\infty}\cos(k\phi_j - k\phi_l) \\
&\times \Bigg\{ G_1^{(k)} + G_2^{(k)}\epsilon + G_3^{(k)}\sqrt{\epsilon(1+\epsilon)}\cos(\phi_j) + G_4^{(k)}\sqrt{\epsilon(1+\epsilon)}\cos(\phi_l) \\
&+ G_5^{(k)}\epsilon\cos(2\phi_j) + G_6^{(k)}\epsilon\cos(2\phi_l) + G_7^{(k)}\epsilon\cos(\phi_j + \phi_l) \\
&+ \sqrt{\epsilon(1+\epsilon)}S_\perp \sin(\phi_S)\, G_8^{(k)} + \sqrt{\epsilon(1+\epsilon)}S_\perp \sin(\phi_S - 2\phi_j)\, G_9^{(k)} \\
&+ \sqrt{\epsilon(1+\epsilon)}S_\perp \sin(\phi_S - 2\phi_l)\, G_{10}^{(k)} + S_\perp \sin(\phi_S - 2\phi_j + \phi_l)\, G_{11}^{(k)} \\
&+ S_\perp \sin(\phi_S - 2\phi_l + \phi_j)\, G_{12}^{(k)} + \epsilon S_\perp \sin(\phi_S + 2\phi_j - \phi_l)\, G_{13}^{(k)} \\
&+ \epsilon S_\perp \sin(\phi_S + 2\phi_l - \phi_j)\, G_{14}^{(k)} + \epsilon S_\perp \sin(\phi_S - 2\phi_j - \phi_l)\, G_{15}^{(k)} \\
&+ \epsilon S_\perp \sin(\phi_S - 2\phi_l - \phi_j)\, G_{16}^{(k)} + \left(G_{17}^{(k)} + G_{18}^{(k)}\epsilon\right) S_\perp \sin(\phi_S - \phi_j) \\
&+ \left(G_{19}^{(k)} + G_{20}^{(k)}\epsilon\right) S_\perp \sin(\phi_S - \phi_l) + \epsilon S_\perp \sin(\phi_S + \phi_j)\, G_{21}^{(k)} \\
&+ \epsilon S_\perp \sin(\phi_S + \phi_l)\, G_{22}^{(k)} + \epsilon S_\perp \sin(\phi_S - 3\phi_j)\, G_{23}^{(k)} \\
&+ \epsilon S_\perp \sin(\phi_S - 3\phi_l)\, G_{24}^{(k)} + \sqrt{\epsilon(1+\epsilon)}S_\perp \sin(\phi_S - \phi_l)\cos(\phi_j)\, G_{25}^{(k)} \\
&+ \sqrt{\epsilon(1+\epsilon)}S_\perp \sin(\phi_S - \phi_j)\cos(\phi_l)\, G_{26}^{(k)} + \sqrt{\epsilon(1+\epsilon)}S_L \sin(\phi_j)\, G_{27}^{(k)} \\
&+ \sqrt{\epsilon(1+\epsilon)}S_L \sin(\phi_l)\, G_{28}^{(k)} + \epsilon S_L \sin(2\phi_j)\, G_{29}^{(k)} \\
&+ \epsilon S_L \sin(2\phi_l)\, G_{30}^{(k)} + \left(G_{31}^{(k)} + G_{32}^{(k)}\epsilon\right) S_L \sin(\phi_j - \phi_l) \\
&+ \epsilon S_L \sin(\phi_j + \phi_l)\, G_{33}^{(k)} + \sqrt{\epsilon(1+\epsilon)}S_L \sin(\phi_j - 2\phi_l)\, G_{34}^{(k)} \\
&+ \sqrt{\epsilon(1+\epsilon)}S_L \sin(\phi_l - 2\phi_j)\, G_{35}^{(k)} + \epsilon S_L \sin(\phi_j - 3\phi_l)\, G_{36}^{(k)} \\
&+ \epsilon S_L \sin(\phi_l - 3\phi_j)\, G_{37}^{(k)} \Bigg\}.
\end{aligned} \tag{4.57}
$$

We note that 37 independent structures appear in Eq. (4.57), consistently with what one would expects from the hadronic tensor in Eq. (4.54) taking into account the three constraints from Eq. (4.55).

4.4 Polarized antisymmetric part

Following the same procedure of the previous section, we have in total 24 independent structures at order $(j\cdot l)^0$ when including the polarization of the target, i.e.

$$\begin{aligned}\mathfrak{Im}\left(W^{\mu\nu}\right) =&\mathscr{P}_1^{\mu\nu} + P_q^{[\mu} j_q^{\nu]}\left(\varepsilon^{SqPj}\Gamma_1 + \varepsilon^{SqPl}\Gamma_2 + \varepsilon^{Sqjl}\Gamma_3\right)\\ &+\mathscr{P}_2^{\mu\nu} + P_q^{[\mu} l_q^{\nu]}\left(\varepsilon^{SqPj}\Gamma_4 + \varepsilon^{SqPl}\Gamma_5 + \varepsilon^{Sqjl}\Gamma_6\right)\\ &+\mathscr{P}_3^{\mu\nu} + j_q^{[\mu} l_q^{\nu]}\left(\varepsilon^{SqPj}\Gamma_7 + \varepsilon^{SqPl}\Gamma_8 + \varepsilon^{Sqjl}\Gamma_9\right)\\ &+P_q^{[\mu}\left(\varepsilon^{\nu]SqP}\Gamma_{10} + \varepsilon^{\nu]Sqj}\Gamma_{11} + \varepsilon^{\nu]Sql}\Gamma_{12}\right)\\ &+j_q^{[\mu}\left(\varepsilon^{\nu]SqP}\Gamma_{13} + \varepsilon^{\nu]Sqj}\Gamma_{14} + \varepsilon^{\nu]Sql}\Gamma_{15}\right)\\ &+l_q^{[\mu}\left(\varepsilon^{\nu]SqP}\Gamma_{16} + \varepsilon^{\nu]Sqj}\Gamma_{17} + \varepsilon^{\nu]Sql}\Gamma_{18}\right)\\ &+\varepsilon^{qPjl}S_q^{[\mu}\left(P_q^{\nu]}\Gamma_{19} + j_q^{\nu]}\Gamma_{20} + l_q^{\nu]}\Gamma_{21}\right).\end{aligned} \tag{4.58}$$

Also in this case, not all the polarized structures lead to independent structure functions once contracted with the leptonic tensor. This is due to the following identities:

$$\det\begin{pmatrix}\varepsilon_{\nu Pkq}\varepsilon^{\nu SqP} & \varepsilon_{\nu Pkq}\varepsilon^{\nu Sqj} & \varepsilon_{\nu Pkq}\varepsilon^{\nu Sql}\\ \varepsilon_{\nu jkq}\varepsilon^{\nu SqP} & \varepsilon_{\nu jkq}\varepsilon^{\nu Sqj} & \varepsilon_{\nu jkq}\varepsilon^{\nu Sql}\\ \varepsilon_{\nu lkq}\varepsilon^{\nu SqP} & \varepsilon_{\nu lkq}\varepsilon^{\nu Sqj} & \varepsilon_{\nu lkq}\varepsilon^{\nu Sql}\end{pmatrix} = 0, \tag{4.59}$$

$$\det\begin{pmatrix}\varepsilon_{Pjkq}\varepsilon^{SqPj} & \varepsilon_{Pjkq}\varepsilon^{SqPl} & \varepsilon_{Pjkq}\varepsilon^{Sqjl}\\ \varepsilon_{Plkq}\varepsilon^{SqPj} & \varepsilon_{Plkq}\varepsilon^{SqPl} & \varepsilon_{Plkq}\varepsilon^{Sqjl}\\ \varepsilon_{jlkq}\varepsilon^{SqPj} & \varepsilon_{jlkq}\varepsilon^{SqPl} & \varepsilon_{jlkq}\varepsilon^{Sqjl}\end{pmatrix} = 0. \tag{4.60}$$

Moreover, after contraction with the leptonic tensor, the structures in front of $\Gamma_{9,20,21}$ become no longer independent (see Eq. (A.5)). We hence have just 17 independent angular structures at order $(j\cdot l)^0$.

$$\begin{aligned}&\mathfrak{Im}\left(W^{\mu\nu}\right)\mathfrak{Im}\left(L_{\mu\nu}\right)\\ &= \lambda_e \text{ɤ} S_\perp \cos\left(\phi_S\right) F_1\\ &+ \lambda_e \ell S_\perp \cos\left(\phi_S - \phi_j\right) F_2 \;+ \lambda_e \ell S_\perp \cos\left(\phi_S - \phi_l\right) F_3\\ &+ \lambda_e \text{ɤ} S_\perp \cos\left(\phi_S - 2\phi_j\right) F_4 \;+ \lambda_e \text{ɤ} S_\perp \cos\left(\phi_S - 2\phi_l\right) F_5\\ &+ \lambda_e \text{ɤ} S_\perp \sin\left(\phi_j\right)\sin\left(\phi_S - \phi_l\right) F_6 \;+ \lambda_e \text{ɤ} S_\perp \sin\left(\phi_l\right)\sin\left(\phi_S - \phi_j\right) F_7\\ &+ \lambda_e \ell S_\perp \cos\left(\phi_S - 2\phi_j + \phi_l\right) F_8 \;+ \lambda_e \ell S_\perp \cos\left(\phi_S - 2\phi_l + \phi_j\right) F_9\\ &+ \lambda_e \text{ɤ} S_L \cos\left(\phi_j\right) F_{10} \;+ \lambda_e \text{ɤ} S_L \cos\left(\phi_l\right) F_{11}\\ &+ \lambda_e \text{ɤ} S_L \cos\left(\phi_j - 2\phi_l\right) F_{12} \;+ \lambda_e \text{ɤ} S_L \cos\left(\phi_l - 2\phi_j\right) F_{13}\\ &+ \lambda_e \ell S_L \cos\left(\phi_j - \phi_l\right) F_{14} \;+ \lambda_e \ell S_L \cos\left(2\phi_j + 2\phi_l\right) F_{15}\\ &+ \lambda_e \ell S_L F_{16} \;+ \lambda_e \text{ɤ} \sin\left(\phi_j\right) F_{17}\end{aligned}$$

$$+ \lambda_e \tau \sin(\phi_l)\, F_{18} \; + \lambda_e \ell' \sin(\phi_j - \phi_l)\, F_{19}.$$

The angular structures associated with $F_{14,15}$ are actually spurious, corresponding to the contributions at order $(j \cdot l)^1$ and $(j \cdot l)^2$ to the "constant" term $F_{16}^{(1)}$ and $F_{16}^{(2)}$, respectively.

We then have, to all orders in $(j \cdot l)$:

$$\begin{aligned}
\mathfrak{Im}\,(W^{\mu\nu})\,\mathfrak{Im}\,(L)_{\mu\nu} = \lambda_e \frac{1}{1-\epsilon} \sum_{k=0}^{\infty} \cos(k\phi_j - k\phi_l) \Bigg\{ & \sqrt{\epsilon(1-\epsilon)} \sin(\phi_j)\, H_1^{(k)} \\
& + \sqrt{\epsilon(1-\epsilon)} \sin(\phi_l)\, H_2^{(k)} + \sqrt{1-\epsilon^2} \sin(\phi_j - \phi_l)\, H_3^{(k)} \\
& + \sqrt{\epsilon(1-\epsilon)} S_\perp \cos(\phi_S)\, H_4^{(k)} + \sqrt{1-\epsilon^2} S_\perp \cos(\phi_S - \phi_j)\, H_5^{(k)} \\
& + \sqrt{1-\epsilon^2} S_\perp \cos(\phi_S - \phi_l)\, H_6^{(k)} + \sqrt{\epsilon(1-\epsilon)} S_\perp \cos(\phi_S - 2\phi_j)\, H_7^{(k)} \\
& + \sqrt{\epsilon(1-\epsilon)} S_\perp \cos(\phi_S - 2\phi_l)\, H_8^{(k)} + \sqrt{\epsilon(1-\epsilon)} S_\perp \sin(\phi_j) \sin(\phi_S - \phi_l)\, H_9^{(k)} \\
& + \sqrt{\epsilon(1-\epsilon)} S_\perp \sin(\phi_l) \sin(\phi_S - \phi_j)\, H_{10}^{(k)} + \sqrt{1-\epsilon^2} S_\perp \cos(\phi_S - 2\phi_j + \phi_l)\, H_{11}^{(k)} \\
& + \sqrt{1-\epsilon^2} S_\perp \cos(\phi_S - 2\phi_l + \phi_j)\, H_{12}^{(k)} + \sqrt{\epsilon(1-\epsilon)} S_L \cos(\phi_j)\, H_{13}^{(k)} \\
& + \sqrt{\epsilon(1-\epsilon)} S_L \cos(\phi_l)\, H_{14}^{(k)} + \sqrt{\epsilon(1-\epsilon)} S_L \cos(\phi_j - 2\phi_l)\, H_{15}^{(k)} \\
& + \sqrt{\epsilon(1-\epsilon)} S_L \cos(\phi_l - 2\phi_j)\, H_{16}^{(k)} + \sqrt{1-\epsilon^2} S_L H_{17}^{(k)} \Bigg\}.
\end{aligned}$$

4.5 Conclusions

The derivation of the general expression for the cross section of the exclusive dijet process is the necessary first step to set the basis for future works. The ultimate goal is to derive the explicit expression of the structure functions in terms of Wigner distributions and to identify a set of promising observables that eventually will allow one to extract information on these functions. A diagrammatic representation for the dijet amplitude in the partonic picture is shown in Fig. 4.3. The explicit link between the structure functions and the Wigner functions is far from being trivial, since we have an infinite number of structure functions associated with all the possible values for the total angular momentum of the two jets. This is a demanding task and is left for future work. However, the dijet process holds the promise of being a key measurement to access information on the Wigner distributions and therefore to give new insights into our understanding of the partonic structure of the proton.

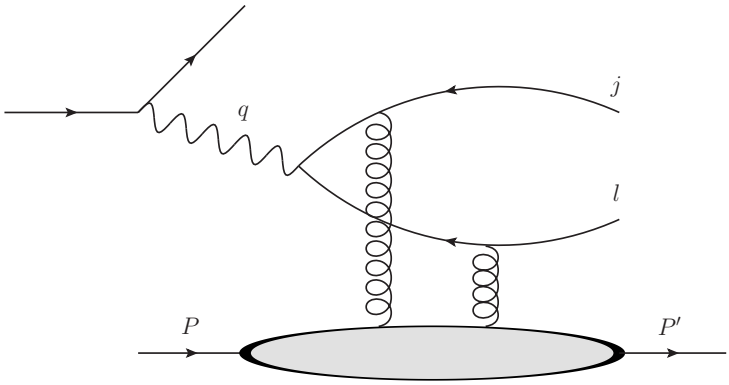

Figure 4.3: Diagrammatic representation of the amplitude for the dijet process in the partonic picture. The two jets are originated from the fragmentation of the two quark lines labelled with j and l in the diagram.

Chapter 5

Lensing relation

5.1 Introduction

Model-induced relations among different TMDs or among TMDs and GPDs have been studied for a long time, since they can provide intuition about the complex QCD phenomena. Some example of such model-induced relations and corresponding studies can be found in Refs. [53, 56, 87–91].

We reviewed in Chapter 3 that two different ways to access a "three - dimensional" parton picture of the proton are possible. The first one is given by the GPDs from which one can define IPDs as the Fourier transforms from the momentum space to the impact-parameter space at zero longitudinal momentum transfer, see Sec. 3.3.3. The IPDs give access to a $2 + 1$ picture of the proton, meaning that they contain a bi-dimensional spatial information (the distance in transverse space of the active parton from the center of transverse momentum) and a mono-dimensional momentum information (the parton fraction of longitudinal momentum with respect to the parent proton). An independent way to access a three-dimensional picture of the proton is given by the TMDs. In this case the description of the proton is given in terms of the parton transverse-momentum and longitudinal fraction of momentum with respect to the parent proton. In Secs. 3.3.2-3.3.3 we briefly summarized the basics of TMDs and GPDs classification at leading twist when the active parton is a quark. We recall that eight TMDs and eight GPDs exist at leading twist, each one being related to a specific proton and quark polarization state, see Eqs. (3.52)-(3.54) and Eqs. (3.37)-(3.39). In Secs. 3.3.2 and 3.3.3 we showed how the GPDs and TMDs can be derived from a more general type of distributions, known as Generalized Transverse Momentum Parton Distributions, see Refs. [13, 14, 16, 35, 59] and Sec. 3.3.1. In a variety of different model calculations, relations between distinct parton distributions were found. Inspecting the models' details to understand which specific features allow the emerging of such relations was the main focus of a part of the literature of the past few years, see, e.g., Refs. [49, 89, 90]. One of the non-trivial relation between parton distributions establishes a connection between TMDs and IPDs. The

formal similarities between the structure of the TMD correlator and the IPD correlator, when the role of the transverse momentum $\boldsymbol{k}_\perp$ is taken by the impact parameter $\boldsymbol{b}_\perp$, offer a justification for the emerging of the relation. This expectation was indeed realized by a non-trivial lensing relation proven in a particular model calculation, see Refs. [53, 56]. This relation describes how the naïve T-odd effects in single spin asymmetries (SSAs) can be factorized in a so-called "chromodynamics lensing function", that encapsulates the effects of final state interactions (FSIs), and the spatial distortion described by the IPDs, see Refs. [53, 56] and Ref. [87] for a review. Being the SSAs described in terms of TMDs, the lensing relation automatically implies a well-defined connection between TMDs and IPDs. The first TMD, in historical order, for which the relation was established is the Sivers function $f_{1T}^{\perp}$. This is connected to the IPD for unpolarized partons in a transversely polarized nucleon target. The relation was verified using spectator models [55, 92] and a quark target model [49], and was also used in a phenomenological extraction of the Sivers function [93]. Later, the lensing relation has been discussed for the Boer-Mulders effect and a certain combination of chiral-odd IPDs describing transversely polarized quark in an unpolarized target, such as the nucleon [57] or the pion [14, 58, 94]. However, both these relations have been found to be violated within three-quark model calculations for the nucleon [95–99]. More in general, it has been argued that even in the context of spectator models these relations are far from being obvious if one considers Fock-state contributions beyond the leading terms [49].

In this Chapter, we discuss in detail the lensing relation, with particular emphasis on the specific conditions that have to be imposed on the FSIs in order to express T-odd TMDs in terms of an impact-parameter distortion and a lensing function. These conditions are typically fulfilled only in models where the target is described as two-body bound system and the FSI modifies only the spectator transverse momentum, leaving unchanged any of the other spectator quantum numbers, see Ref. [87].

In Sec. 5.2, after a brief recall of the expressions for the relevant TMDs and IPDs, we discuss how a link between them can be realized. We put particular emphasis on the assumptions behind the derivation, clarifying were these assumptions begin to be crucial for the derivation. After discussed the generally theory, we proceed in Sec. 5.3 to derive the lensing relation for the Boer-Mulders effect in the case of the pion target, described in terms of the lowest $q\bar{q}$ Fock-state component. We stress how the two-body nature of the system is an essential ingredient for the validity of the lensing relation. Beside that, we clarify how the assumption of a perturbative coupling between the spectator parton and the Wilson gluon, responsible for the FSIs in a SIDIS process, is another key assumption for the lensing relation. We briefly discuss how an effective interaction vertex between the Wilson gluon and the spectator may spoil the lensing relation, and we find that an helicity-conserving vertex that depends only on the transverse momentum of the exchanged gluon is the only coupling that allows the lensing relation. We then proceed to study the possible factorization of the FSIs in a proton target. First, in Sec. 5.4 the proton

is modeled as a three-quark bound state and we provide a general argument for the non-validity of the lensing relation, assuming a perturbative coupling for the Wilson gluon, a general argument for the non-validity of the lensing relation. Since a three-body model for the proton fails in reproducing the lensing relation, in Sec. 5.4.1 we study models that describe the nucleon as a two-body system. In particular great attention is paid to models in which the spectator system is assumed to be a diquark. We then elucidate under which conditions one can restore the lensing relations within this class of models.

5.2 The lensing-function relation

In this section, we summarize the arguments that lead to infer a possible non-trivial relation between naïve T-odd TMDs and IPDs. We recall that the TMD definition is given in terms of the following correlator (see Eq. (5.1))

$$\Phi^{[\Gamma]}(x,\boldsymbol{k}_\perp,S)=\int\frac{dz^-d\boldsymbol{z}_\perp}{2(2\pi)^3}e^{ik\cdot z}\,\langle p,S|\overline{\psi}\left(-\frac{z}{2}\right)\Gamma\mathcal{W}\left(-\frac{z}{2},\frac{z}{2}\right)\psi\left(\frac{z}{2}\right)|p,S\rangle\,\Big|_{z^+=0}. \tag{5.1}$$

The Wilson line $\mathcal{W}$ is of fundamental importance to ensure the color gauge invariance of the correlator and is defined in Eq. (3.8) and it will play the central role in deriving the lensing relation. We are going to work with the Wilson line shown in Fig. 3.5 (i.e., we are assuming a SIDIS-like process described in terms of TMDs) and, if necessary, we will show also the results by assuming a future pointing Wilson line (i.e., by considering a Drell-Yan-like process described in terms of TMDs). As we already discussed in Chapter 3, the Wilson line in Eq. (5.1) breaks the naïve time-reversal invariance of the correlator and, as a consequence, naïve T-odd TMDs do not vanish. In Chapter 3 we discussed how this gives rise to the naïve T-odd TMDs for a spin-1/2 hadron: the Sivers function $f_{1T}^{\perp}(x,\boldsymbol{k}_\perp^2)$ [45, 100] and the Boer-Mulders function $h_1^{\perp}(x,\boldsymbol{k}_\perp^2)$ [48]. In the case of spin-0 hadron, only the contribution of the Boer-Mulders function is non-vanishing.

The IPDs were briefly introduced in Sec. 3.3.3. Integrating Eq. (3.17) over $\boldsymbol{k}_\perp$, we obtain from Eq. (3.58) the following expression for the IPDs correlator:

$$\begin{aligned}&\mathcal{F}^{[\Gamma]}(x,\boldsymbol{b}_\perp,S)\\&=\frac{1}{2}\int\frac{dz^-}{2\pi}e^{ixp^+z^-}\,\langle p^+,\boldsymbol{r}_\perp=\boldsymbol{0}_\perp,S|\overline{\psi}(z_1)\Gamma\mathcal{W}\,(z_1,z_2)\,\psi\,(z_2)\,|p^+,\boldsymbol{r}_\perp=\boldsymbol{0}_\perp,S\rangle\,,\end{aligned} \tag{5.2}$$

where the quark fields are evaluated at $z_{1,2}=(0^+,\mp\frac{z^-}{2},\boldsymbol{b}_\perp)$ and the hadron state is expressed as an eigenstate of the plus-momentum operator P^+ and the center of transverse momentum operator $\boldsymbol{R}_\perp$ (see Eq. (2.39)) with eigenvalues p^+ and $\boldsymbol{r}_\perp=\boldsymbol{0}_\perp$, respectively, see Refs. [37, 52, 101] and Sec. 3.2.1

In the following we will also need the GPD definition given in Eqs. (3.52)-(3.54). For $\xi=0$, the GPD correlator (3.50) is related to the IPD correlator by a Fourier transform from the coordinates $\boldsymbol{\Delta}_\perp$ to $\boldsymbol{b}_\perp$, see Eq. (3.58).

quark pol.

nucleon pol.	U	L	T
U	$\mathcal{H}$		$\mathcal{E}_T + 2\widetilde{\mathcal{H}}_T$
L		$\widetilde{\mathcal{H}}$	
T	$\mathcal{E}$		$\mathcal{H}_T$,$\widetilde{\mathcal{H}}_T$

Twist-2 IPDs

Table 5.1: Impact-parameter distributions (IPDs) with their relation to nucleon and quark polarization states. For the complete definition, we refer to Refs. [49, 50].

The full list of leading-twist IPDs is shown in a schematic way in Tab. 5.1. At leading twist and for spin-1/2 targets, the correlator (3.58) with $\Gamma = \gamma^+$ and transversely polarized targets can be parametrized in terms of the derivative of the IPD $\mathcal{E}$, while with $\Gamma = i\sigma^{j+}\gamma_5$ and unpolarized target we access the derivative of the combination $\mathcal{E}_T + 2\widetilde{\mathcal{H}}_T$ of chiral-odd IPDs. In the case of spin-zero targets, the contributions from the IPDs $\mathcal{E}$ and $\mathcal{E}_T$ are absent. Because the GPDs and, as a consequence, the IPDs, are defined in terms of a Wilson line that runs only along the light cone, no naïve T-odd GPDs or IPDs can exist.

The analogy between the tensor structure of the parametrizations of the quark TMD and IPD correlators suggests the following correspondences for the distributions of spin-1/2 targets [49, 50]

$$f_{1T}^{\perp}\left(x, \boldsymbol{k}_{\perp}^2\right) \leftrightarrow -\mathcal{E}'\left(x, \boldsymbol{b}_{\perp}^2\right), \quad h_1^{\perp}\left(x, \boldsymbol{k}_{\perp}^2\right) \leftrightarrow -\mathcal{E}_T'\left(x, \boldsymbol{b}_{\perp}^2\right) - 2\widetilde{\mathcal{H}}_T'\left(x, \boldsymbol{b}_{\perp}^2\right), \tag{5.3}$$

where we used the following notation for the derivative of a generic IPD $\mathcal{X}$

$$\mathcal{X}'\left(x, \boldsymbol{b}_{\perp}^2\right) = \frac{\partial}{\partial \boldsymbol{b}_{\perp}^2}\mathcal{X}\left(x, \boldsymbol{b}_{\perp}^2\right). \tag{5.4}$$

Similarly, the correspondence for spin-zero targets reads

$$h_1^{\perp}\left(x, \boldsymbol{k}_{\perp}^2\right) \leftrightarrow -\widetilde{\mathcal{H}}_T'\left(x, \boldsymbol{b}_{\perp}^2\right). \tag{5.5}$$

In order to exemplify the derivation of the explicit form of the link in Eqs. (5.3) and (5.5), we take the average quark transverse momentum of an unpolarized quark in a transversely polarized target given by

$$\langle k_{\perp}^i(x)\rangle_{UT} = \int d\boldsymbol{k}_{\perp} k_{\perp}^i \Phi^{[\gamma^+]}(x, \boldsymbol{k}_{\perp}, \boldsymbol{S}_{\perp}), \tag{5.6}$$

where the first subscript outside the bra-ket refers to the polarization of the quark and the second one to the polarization of the hadron.

Following the derivation in Ref. [49], Eq. (5.6) can be rewritten as

$$\langle k_{\perp}^i(x)\rangle_{UT} = \frac{1}{2}\int \frac{dz^-}{2\pi} e^{ixp^+z^-}$$

$$\times \langle p, \boldsymbol{S}_\perp | \overline{\psi}\left(-\frac{z}{2}\right) \mathcal{W}\left(-\frac{z}{2}, \frac{z}{2}\right) \mathcal{G}^i\left(\frac{z}{2}\right) \gamma^+ \psi\left(\frac{z}{2}\right) | p, \boldsymbol{S}_\perp \rangle \big|_{z^+=\boldsymbol{z}_\perp=0}$$
$$= \frac{1}{2} \int d\boldsymbol{b}_\perp \int \frac{dz^-}{2\pi} e^{ixp^+z^-}$$
$$\times \langle p^+, \boldsymbol{r}_\perp = \boldsymbol{0}_\perp, \boldsymbol{S}_\perp | \bar{\psi}(z_1) \mathcal{W}(z_1, z_2) \mathcal{G}^i(z_2) \gamma^+ \psi(z_2) | p^+, \boldsymbol{r}_\perp = \boldsymbol{0}_\perp, \boldsymbol{S}_\perp \rangle \,. \quad (5.7)$$

In Eq. (5.7), the operator $\mathcal{G}^i(z)$ encodes the contribution of the FSIs, and is defined as

$$\mathcal{G}^i(z) = \frac{g_s}{2} \int dy^- \mathcal{W}\left((z^-, z^+, \boldsymbol{z}_\perp), (y^-, z^+, \boldsymbol{z}_\perp)\right)$$
$$\times G^{+i}\left(y^-, z^+, \boldsymbol{z}_\perp\right) \mathcal{W}\left((y^-, z^+, \boldsymbol{z}_\perp), (z^-, z^+, \boldsymbol{z}_\perp)\right), \quad (5.8)$$

with G^{+i} the gluon-field strength tensor.

Eq. (5.8) has a more intuitive interpretation in the light-cone gauge, introduced and discussed in Sec. 2.4. In this case, the Wilson lines in the definition of $\mathcal{G}^i(z)$ run along the light cone, and reduce to unity. As a result, one has

$$\mathcal{G}^i(z) = \frac{g_s}{2}\Big(A^i_\perp\left(\infty^-, z^+, \boldsymbol{z}_\perp\right) - A^i_\perp\left(-\infty^-, z^+, \boldsymbol{z}_\perp\right)\Big). \quad (5.9)$$

In a similar fashion as in the derivation of the quark EOM given in Sec. 3.4.3, it does not exist a choice of boundary conditions that allow ones to set to zero the difference in Eq. (5.9). This ensures that we always obtain a non-vanishing $\mathcal{G}^i(z)$ no matter the choice of boundary conditions for the $\boldsymbol{A}_\perp$ field at light-cone infinity.

We choose to work with the advanced boundary condition $\boldsymbol{A}_\perp(-\infty^-) = 0$, but analogous results hold for the other two prescriptions (as it should be, since all the results must be gauge invariant). Our choice leads to the following results

$$\langle k^i_\perp(x) \rangle_{UT} = \frac{g_s}{2} \int \frac{dz^-}{2\pi} e^{ixp^+z^-} \langle p, \boldsymbol{S}_\perp | \overline{\psi}\left(-\frac{z^-}{2}\right) A^i_\perp\left(\infty^-\right) \gamma^+ \psi\left(\frac{z^-}{2}\right) | p, \boldsymbol{S}_\perp \rangle \,, \quad (5.10)$$

$$\langle k^i_\perp(x) \rangle^j_{TU} = \frac{g_s}{2} \int \frac{dz^-}{2\pi} e^{ixp^+z^-} \langle p | \overline{\psi}\left(-\frac{z^-}{2}\right) A^i_\perp\left(\infty^-\right) i\sigma^{j+}\gamma_5 \psi\left(\frac{z^-}{2}\right) | p \rangle \,. \quad (5.11)$$

One notices from Eq. (5.11) that the FSIs in the light-cone gauge with advanced boundary conditions (and, similarly, with the retarded or principal value prescriptions) reduce to the exchange of a transverse gluon at light-cone infinity between the active quark and the spectator partons.

Up to this point no-limiting assumptions were made (the light-cone gauge has been assumed just to obtain the clean physical picture in Eq. (5.9), but it is unessential since all the results are gauge independent). To further proceed towards an expression that involves the IPDs we must impose some very specific conditions on the operator $\mathcal{G}^i(z)$, see Ref. [87]. Using the completeness relation,

we can rewrite the first line of Eq. (5.7) as

$$\langle k_\perp^i(x)\rangle_{UT} = \frac{1}{2}\int d\boldsymbol{b}_\perp \int \frac{dz^-}{2\pi} e^{ixp^+z^-} \sum\!\!\!\!\!\!\int_{X,X'} \langle X|\mathcal{J}^i(z_2)|X'\rangle \\ \times \langle p^+, \boldsymbol{r}_\perp = \boldsymbol{0}_\perp, \boldsymbol{S}_\perp|\bar{\psi}(z_1)\mathcal{W}(z_1,z_2)|X\rangle\, \gamma^+ \,\langle X'|\psi(z_2)|p^+, \boldsymbol{r}_\perp = \boldsymbol{0}_\perp, \boldsymbol{S}_\perp\rangle\,. \tag{5.12}$$

Since we are working with leading-twist distributions, only the good components of the quark fields are involved. Therefore, we can Fourier transform the quark operators $\psi(z/2)$ and $\phi\left(\frac{z}{2}\right) = \bar{\psi}\left(-\frac{z}{2}\right)\mathcal{W}\left(-\frac{z}{2};\frac{z}{2}\right)$ using Eq. (2.42), and use the light-front Fock expansion for the intermediate states. As a result, Eq. (5.12) becomes [87]

$$\langle k_\perp^i(x)\rangle_{UT} = \frac{1}{2}\int \{dk_1\}\{dk_2\}\{dl\} \int \frac{dz^-}{2\pi} e^{ixp^+z^-} e^{-i\frac{z^-}{2}(k_1^+ + k_2^+ + l^+)} \\ \times \sum_{n,m}\sum_{\beta,\beta'} \int \prod_{i=1}^{n} \frac{dq_i^+ d\boldsymbol{q}_{\perp,i}}{(2\pi)^3 2q_i^+} \prod_{i=1}^{m} \frac{dw_i^+ d\boldsymbol{w}_{\perp,i}}{(2\pi)^3 2w_i^+} \\ \times \langle p^+, \boldsymbol{p}_\perp = \boldsymbol{0}_\perp, \boldsymbol{S}_\perp|\phi(k_1)\gamma^+|\{q_i^+, \boldsymbol{q}_{\perp,i}\}_n\rangle \,\langle\{q_i^+, \boldsymbol{q}_{\perp,i}\}_n, \beta'|I^i(l)|\{w_i^+, \boldsymbol{w}_{\perp,i}\}_m\rangle \\ \times \langle\{w_i^+, \boldsymbol{w}_{\perp,i}\}_m, \beta'|\psi(k_2)|p^+, \boldsymbol{p}_\perp = \boldsymbol{0}_\perp, \boldsymbol{S}_\perp\rangle\,, \tag{5.13}$$

where $\{dk\}$ is a shorthand notation to indicate the Lorentz invariant integration measure. In Eq. (5.13), the index β and β' are collective indexes to label the flavor, the color and the helicity of the intermediate states. As we are going to show, the factorization of the lensing function and the IPD in Eq. (5.13) can be achieved by requiring that the matrix element of the operator $I^i(l)$ satisfies the following relation

$$\langle\{q_i^+, \boldsymbol{q}_{\perp,i}\}_n|I^i(l)|\{w_i^+, \boldsymbol{w}_{\perp,i}\}_m\rangle = 2\pi L^i\left(\frac{\boldsymbol{l}_\perp}{1-x}\right)\delta_{n,m}\delta_{\beta\beta'}\delta(l^+) \\ \times \prod_{i=1}^{n}(2\pi)^3 2q_i^+\delta(q_i^+ - w_i^+)\delta\left(\boldsymbol{q}_{\perp,i} - \boldsymbol{w}_{\perp,i} - x_i\frac{\boldsymbol{l}_\perp}{1-x}\right), \tag{5.14}$$

where x_i is the light-cone momentum fraction of the i-th constituent with respect to the hadron target light-cone momentum, i.e. $x_i = w_i^+/p^+$, with the constraint $\sum_i x_i = 1 - x$. In the matrix element of the operator $I^i(l)$ in Eq. (5.14) are encoded all the interactions between the active parton and the spectator system that result in the FSIs of a SIDIS process (similar conclusion can be reached for a Drell-Yan process, with the caveat of a different explicit expression for the operator $I^i(l)$, in which the initial-state interactions must be considered). The relation (5.14) imposes several different conditions, some of them more stringent than others, that can be summarized as follows [87]:

1) the FSIs should connect Fock states with the same number of constituents and the same parton, helicity and color content;

2) the FSIs should transfer the total transverse momentum $\boldsymbol{l}_\perp/(1-x)$ to the whole spectator system;

3) the FSIs can not transfer momentum in the light-cone direction to the spectator system;

4) the FSIs should transfer a fraction of the total transverse momentum, corresponding to $x_i = w_i^+/p^+$, to each constituent of the spectator system.

The last condition is the most stringent. It is crucial to obtain the correct transverse light-front boost that gives the off-diagonal matrix element defining the GPD and, as a direct consequence, the transverse distortion in impact-parameter space that is proper of the IPD.

Before discussing the implication of condition 4), we are going to derive the four conditions in Eq. (5.14). Condition 1) follows from the requirement that the IPD we want to factorize in Eq. (5.13) is diagonal in the parton Fock space. Analogously, condition 2) is necessary to recover the correct Fourier transform of the quark fields that enters the definition of the IPD correlator. Conditions 3) and 4) are consequences of momentum conservation. The matrix element of the function $I^i(l)$ in Eq. (5.14) connects states with total momenta given by

$$\begin{aligned} \boldsymbol{W}_\perp &= \sum_{i=1}^n \boldsymbol{w}_{\perp,i}, \quad W^+ = \sum_{i=1}^n w_i^+, \\ \boldsymbol{Q}_\perp &= \sum_{i=1}^n \boldsymbol{q}_{\perp,i}, \quad Q^+ = \sum_{i=1}^n q_i^+. \end{aligned} \tag{5.15}$$

By imposing total momentum conservation in each matrix elements of Eq. (5.13), we have

$$\boldsymbol{Q}_\perp = \boldsymbol{W}_\perp + \boldsymbol{l}_\perp, \quad Q^+ = W^+ = (1-x)p^+. \tag{5.16}$$

Eqs. (5.15) and (5.16) are equivalent to

$$\sum_{i=1}^n \boldsymbol{q}_{\perp,i} = \sum_{i=1}^n \boldsymbol{w}_{\perp,i} + \boldsymbol{l}_\perp, \quad \sum_{i=1}^n \frac{q_i^+}{p^+} = \sum_{i=1}^n \frac{w_i^+}{p^+} = \sum_{i=1}^n x_i = 1 - x. \tag{5.17}$$

Combining the two relations in Eq. (5.17), we find

$$\boldsymbol{q}_{\perp,i} = \boldsymbol{w}_{\perp,i} + \frac{x_i}{1-x}\boldsymbol{l}_\perp. \tag{5.18}$$

As final result, we obtain the expression in Eq. (5.14) for the matrix element of the lensing function from which the conditions 1)–4) follow. By inserting Eq. (5.14) in Eq. (5.13), we have

$$\begin{aligned} \langle k_\perp^i(x)\rangle_{UT} &= \frac{1}{2}\int\{dk_1\}\{dk_2\}\frac{d\boldsymbol{l}_\perp}{(2\pi)^2}\int\frac{dz^-}{2\pi}e^{ixp^+z^-}e^{-i\frac{z^-}{2}(k_1^+ + k_2^+)} \\ &\times \sum_n\sum_\beta\int\prod_{i=1}^m \frac{dw_i^+ d\boldsymbol{w}_{\perp,i}}{(2\pi)^3 2w_i^+}L^i\left(\frac{\boldsymbol{l}_\perp}{1-x}\right) \end{aligned}$$

$$\times \langle p^+, \mathbf{0}_\perp, \boldsymbol{S}_\perp | \phi(k_1)\gamma^+ | \left\{ w_i^+, \boldsymbol{w}_{\perp,i} + \frac{x_i \boldsymbol{l}_\perp}{1-x} \right\}_m \rangle \langle \{w_i^+, \boldsymbol{w}_{\perp,i}\}_m | \psi(k_2) | p^+, \mathbf{0}_\perp, \boldsymbol{S}_\perp \rangle \,. \tag{5.19}$$

We now use the invariance of the matrix elements in Eq. (5.19) under transverse light-front boosts to obtain

$$\begin{aligned}
\langle k_\perp^i(x) \rangle_{UT} &= \frac{1}{2} \int \{dk_1\}\{dk_2\} \frac{d\boldsymbol{l}_\perp}{(2\pi)^2} \int \frac{dz^-}{2\pi} e^{ixp^+z^-} e^{-i\frac{z^-}{2}(k_1^+ + k_2^+)} \\
&\times \sum_n \sum_\beta \int \prod_{i=1}^m \frac{dw_i^+ d\boldsymbol{w}_{\perp,i}}{(2\pi)^3 2w_i^+} \times L^i \left(\frac{\boldsymbol{l}_\perp}{1-x} \right) \\
&\times \langle p^+, -\boldsymbol{l}_\perp, \boldsymbol{S}_\perp | \phi(z_1)\gamma^+ | \{w_i^+, \boldsymbol{w}_{\perp,i}\}_m \rangle \langle \{w_i^+, \boldsymbol{w}_{\perp,i}\}_m | \psi(z_2) | p^+, \mathbf{0}_\perp, \boldsymbol{S}_\perp \rangle \\
&= \frac{1}{2} \int \frac{d\boldsymbol{l}_\perp}{(2\pi)^2} \int \frac{dz^-}{2\pi} e^{ixp^+z^-} L^i \left(\frac{\boldsymbol{l}_\perp}{1-x} \right) \langle p^+, -\boldsymbol{l}_\perp, \boldsymbol{S}_\perp | \phi(k_1)\gamma^+ \psi(k_2) | p^+, \mathbf{0}_\perp, \boldsymbol{S}_\perp \rangle \,.
\end{aligned} \tag{5.20}$$

Eq. (5.20) can be finally Fourier transformed in the impact-parameter space, with the result

$$\begin{aligned}
\langle k_\perp^i(x) \rangle_{UT} &= \frac{1}{2} \int \frac{d\boldsymbol{l}_\perp}{(2\pi)^2} \int \frac{dz^-}{2\pi} e^{ixp^+z^-} \int d\boldsymbol{b}_\perp e^{-i\boldsymbol{b}_\perp \boldsymbol{l}_\perp} L^i \left(\frac{\boldsymbol{l}_\perp}{1-x} \right) \\
&\times \langle p^+, \boldsymbol{R}_\perp = \mathbf{0}_\perp, \boldsymbol{S}_\perp | \phi(z_1)\gamma^+ \psi(z_2) | p^+, \boldsymbol{R}_\perp = \mathbf{0}_\perp, \boldsymbol{S}_\perp \rangle \\
&= \frac{1}{2} \int \frac{dz^-}{2\pi} e^{ixp^+z^-} \int d\boldsymbol{b}_\perp \mathcal{L}^i \left(\frac{\boldsymbol{b}_\perp}{1-x} \right) \\
&\times \langle P^+, \boldsymbol{R}_\perp = \mathbf{0}_\perp, \boldsymbol{S}_\perp | \phi(z_1)\gamma^+ \psi(z_2) | P^+, \boldsymbol{R}_\perp = \mathbf{0}_\perp, \boldsymbol{S}_\perp \rangle \,,
\end{aligned} \tag{5.21}$$

where the convolution of the lensing function $\mathcal{L}(\boldsymbol{b}_\perp/(1-x))$ and the correlator for unpolarized quark in a transversely polarized target, related to the IPD $\mathcal{E}'(x, \boldsymbol{b}_\perp^2)$, can be easily recognized, i.e.

$$\langle k_\perp^i(x) \rangle_{UT} = \int d\boldsymbol{b}_\perp \mathcal{L}^i \left(\frac{\boldsymbol{b}_\perp}{1-x} \right) \frac{\epsilon_\perp^{jk} b_\perp^j S_\perp^k}{M} \mathcal{E}'(x, \boldsymbol{b}_\perp^2). \tag{5.22}$$

For convenience, we are going to discuss the implications of the condition 4) in light-cone gauge with advanced boundary conditions, where the FSIs reduce to the exchange of a transverse gluon at light-cone infinity between the active parton and the spectator system, see Eq. (5.9). One way to obtain a non-vanishing contribution from the FSIs in a model calculation is to assume a perturbative coupling between the Wilson gluon and the spectator system. In this very common scenario the condition 4) can be realized only if the spectator system is modeled as a single constituent, i.e. the hadron target is a two-body bound system. In this peculiar case, through momentum conservation, the light-cone momentum fraction of the spectator is equal to $1-x$ and the constraint on the transverse-momentum transferred by the Wilson gluon to the spectator system follows simply from the conservation of the total momentum

of the hadron target. Otherwise, the condition 4) imposes to share the transverse momentum carried by the Wilson gluon with each spectator parton in a proportion equal to the longitudinal momentum fraction x_i. This can not be realized in systems composed by more than two constituents, under the assumption of an interaction vertex between the gauge boson and a single constituent, i.e. a perturbative interaction at the leading non-vanishing order, We conclude that if, and only if, the above conditions are fulfilled, we can write

$$\begin{aligned}\langle k^i_\perp(x)\rangle_{UT} &= -\int d\boldsymbol{k}_\perp k^i_\perp \frac{\epsilon^{jk}_\perp k^j_\perp S^k_\perp}{M} f^\perp_{1T}(x,\boldsymbol{k}^2_\perp)\\ &= \int d\boldsymbol{b}_\perp \mathscr{L}^i\big(\boldsymbol{b}_\perp/(1-x)\big)\mathcal{F}^{[\gamma^+]}(x,\boldsymbol{b}_\perp,\boldsymbol{S}_\perp)\\ &= \int d\boldsymbol{b}_\perp \mathscr{L}^i\big(\boldsymbol{b}_\perp/(1-x)\big)\frac{\epsilon^{jk}_\perp b^j_\perp S^k_\perp}{M}\mathcal{E}'(x,\boldsymbol{b}^2_\perp),\end{aligned} \tag{5.23}$$

where $\epsilon^{ij}_\perp = \epsilon^{+-ij}$. In the next sections, we will consider explicitly a few model calculations and we will discuss to which extent the conditions 1) – 4) can be satisfied.

In an analogous fashion, we can analyze the average quark transverse momentum of a transversely-polarized quark in an unpolarized target given by

$$\langle k^i_\perp(x)\rangle^j_{TU} = \int d\boldsymbol{k}_\perp k^i_\perp \Phi^{[i\sigma^{j+}\gamma_5]}(x,\boldsymbol{k}_\perp,S). \tag{5.24}$$

With similar steps as before, under the conditions of applicability of the lensing hypothesis, we obtain

$$\begin{aligned}\langle k^i_\perp(x)\rangle^j_{TU} &= -\int d\boldsymbol{k}_\perp k^i_\perp \frac{\epsilon^{kj}_\perp k^k_\perp}{M} h_1^\perp(x,\boldsymbol{k}^2_\perp)\\ &= \int d\boldsymbol{b}_\perp \mathscr{L}^i\big(\boldsymbol{b}_\perp/(1-x)\big)\mathcal{F}^{[i\sigma^{j+}\gamma_5]}(x,\boldsymbol{b}_\perp)\\ &= \int d\boldsymbol{b}_\perp \mathscr{L}^i\big(\boldsymbol{b}_\perp/(1-x)\big)\frac{\epsilon^{kj}_\perp b^k_\perp}{M}\Big(\mathcal{E}'_T(x,\boldsymbol{b}^2_\perp)+2\widetilde{\mathcal{H}}'_T(x,\boldsymbol{b}^2_\perp)\Big).\end{aligned} \tag{5.25}$$

Alternatively, by contracting Eqs. (5.23) and (5.25) with $-\epsilon^{il}_\perp S^l_\perp/(2M)$ and $-\epsilon^{ij}_\perp/(2M)$, respectively, we can write

$$f_{1T}^{\perp(1)}(x) = \int d\boldsymbol{b}_\perp \frac{b^i_\perp}{4}\mathscr{L}^i\big(\boldsymbol{b}_\perp/(1-x)\big)\mathcal{E}^{(1)}(x,\boldsymbol{b}^2_\perp), \tag{5.26}$$

$$h_1^{\perp(1)}(x) = \int d\boldsymbol{b}_\perp \frac{b^i_\perp}{4}\mathscr{L}^i\big(\boldsymbol{b}_\perp/(1-x)\big)\left(\mathcal{E}^{(1)}_T(x,\boldsymbol{b}^2_\perp)+2\widetilde{\mathcal{H}}^{(1)}_T(x,\boldsymbol{b}^2_\perp)\right), \tag{5.27}$$

where we used the following notations

$$f^{(1)}(x,\boldsymbol{k}^2_\perp) = \frac{\boldsymbol{k}^2_\perp}{2M^2} f(x,\boldsymbol{k}^2_\perp), \tag{5.28}$$

$$\mathcal{X}^{(1)}(x,\boldsymbol{b}_\perp^2) = -\frac{2}{M^2}\mathcal{X}'(x,\boldsymbol{b}_\perp^2) = \int \frac{d\boldsymbol{\Delta}_\perp}{(2\pi)^2} e^{-i\boldsymbol{\Delta}_\perp\cdot\boldsymbol{b}_\perp}\frac{\boldsymbol{\Delta}_\perp^2}{2M^2}X(x,\xi=0,-\boldsymbol{\Delta}_\perp^2). \tag{5.29}$$

For spin-zero targets, only Eqs. (5.25) and (5.27) with $\mathcal{E}_T(x,\boldsymbol{b}_\perp^2)=0$ and $2\widetilde{\mathcal{H}}_T \to \widetilde{\mathcal{H}}_T$ survive.

5.3 Lensing relation for the pion

This section will be devoted to the study of how the relation between the Boer-Mulders function and the chiral-odd GPD $\widetilde{\mathcal{H}}_T$ is realized for a spin-zero target described as a quark-antiquark ($q\bar{q}$) bound state. For illustration purposes, we are going to assume that the target hadron is a pion, described in terms of the leading-order Fock-state component. Hence, in the framework of light-front quantization and working in the gauge $A^+=0$, the pion state with momentum p is given by

$$|\pi(p)\rangle = \sum_{\{\lambda_i\}}\sum_{\{q_i\}}\int [Dx]_2\, \Psi_{q\bar{q}}(\beta,r)\,|\lambda_1,q_1,c_1,p_1\rangle\,|\lambda_2,q_2,c_2,p_2\rangle\,. \tag{5.30}$$

In Eq. (5.30), λ_i are the quark light-front helicities (see Sec. 2.2.1), $q_i = q,\bar{q}$ denotes the quark and antiquark flavor, c_i is a color index, and p_i is the parton momentum. The function $\Psi_{q\bar{q}}$ is LFWF of the $q\bar{q}$ state and its arguments are indicated with the collective notation $\beta = (\{\lambda_i\},\{c_i\},\{q_i\})$ and $r = \{x_i,\boldsymbol{k}_{\perp,i}\}$ with the intrinsic transverse momentum $\boldsymbol{k}_{\perp,i}$ of Eq. (2.67). We can make explicit the flavor and helicity structure of the parton composition in Eq. (5.30) in the same way as we did for the proton in Eq. (3.81), to obtain [61]:

$$\begin{aligned}|\pi(p)\rangle = T_\pi \int \frac{dx_1dx_2}{\sqrt{x_1x_2}}\frac{d\boldsymbol{k}_{\perp,1}d\boldsymbol{k}_{\perp,2}}{2(2\pi)^3}\delta(1-x_1-x_2)\,\delta(\boldsymbol{k}_{\perp,2}+\boldsymbol{k}_{\perp,1})\,\frac{\delta_{c_1c_2}}{\sqrt{3}}\\ \times\Big\{\psi^{(1)}(1,2)\left[q_\uparrow^{c_1\dagger}(1)\bar{q}_\downarrow^{c_2\dagger}(2) - q_\downarrow^{c_1\dagger}(1)\bar{q}_\uparrow^{c_2\dagger}(2)\,|0\rangle\right]\\ + \psi^{(2)}(1,2)\left[\boldsymbol{k}_{L,1}q_\uparrow^{c_1\dagger}(1)\bar{q}_\uparrow^{c_2\dagger}(2) + \boldsymbol{k}_{R,1}q_\downarrow^{c_1\dagger}(1)\bar{q}_\downarrow^{c_2\dagger}(2)\,|0\rangle\right]\Big\},\end{aligned} \tag{5.31}$$

where $\boldsymbol{k}_{R(L),i} = k_{x,i} \pm ik_{y,i}$, $q_\lambda^{c_i\dagger}$ and $\bar{q}_\lambda^{c_i\dagger}$ are the creation operators of quark and antiquark with helicity λ and color c_i, respectively, and the arguments i of the LFWAs stand for $(x_i,\boldsymbol{k}_{\perp,i})$. . In Eq. (5.31), T_π is the isospin factor which projects on the different members of the isotriplet of the pion, and is defined as $T_\pi = \sum_{\tau_q,\tau_{\bar{q}}}\langle 1/2\tau_q 1/2\tau_{\bar{q}}|1\tau_\pi\rangle$ with $\tau_{q,\bar{q},\pi}$ the isospin of the quark, antiquark and pion state, respectively. We can recognize the LFWAs $\psi^{(1)}$ and $\psi^{(2)}$ that correspond to quark states with OAM $L_z=0$ and $|L_z|=1$, respectively. We recall that they are scalar functions, and depend on the parton momenta only through scalar products $\boldsymbol{k}_{\perp,i}\cdot\boldsymbol{k}_{\perp,j}$. In the light-cone gauge with advanced boundary conditions for the transverse components of the gauge field,

the LFWAs are complex functions [29, 102, 103]. This will not impact our conclusions. Using the pion state (5.31), we can represent the pion GPD and TMD in terms of overlap of LFWAs in a model-independent way.

The pion chiral-odd GPD is defined as

$$F_{\pi}^{[i\sigma^{j+}\gamma_5]}(x,\Delta^+,\boldsymbol{\Delta}_\perp) = -\frac{i\epsilon_\perp^{kj}\Delta_\perp^k}{M_\pi}\widetilde{H}_{T,\pi}(x,\xi,-\boldsymbol{\Delta}_\perp^2). \tag{5.32}$$

We can introduce the following overlap of LFWAs for the $q\bar{q}$ component of the pion

$$G^k\left(1,1'\right) = F^k\big(x_1,\boldsymbol{k}_{\perp,1};1-x_1,-\boldsymbol{k}_{\perp,1}\big|\big|x_1',\boldsymbol{k}_{\perp,1}';1-x_1',-\boldsymbol{k}_{\perp,1}'\big), \tag{5.33}$$

$$F^k\left(1,2\,||\,1',2'\right) = k_{\perp,1}^k\psi^{(2)}(1,2)\psi^{(1)*}(1',2') - k_{\perp,1}'^k\psi^{(1)}(1,2)\psi^{(2)*}(1',2'), \tag{5.34}$$

where the arguments on the right-hand side of $||$ refer to the momentum dependence of the complex conjugate LFWA of the pion in the final state, and the arguments on the left-hand side give the momentum dependence of the LFWA of the pion in the initial state. Using the definition in Eq. (5.34) one finds at $\xi = 0$

$$\frac{\Delta_\perp^k}{2M_\pi}\widetilde{H}_{T,\pi}(x,0,-\boldsymbol{\Delta}_\perp^2) = \frac{T_\pi^2}{2(2\pi)^3}\int d\boldsymbol{k}_\perp G^k\left(x,\boldsymbol{k}_\perp\,||\,x,\boldsymbol{k}_\perp+(1-x)\boldsymbol{\Delta}_\perp\right). \tag{5.35}$$

We can Fourier transform the integral in Eq. (5.35), with the result

$$\begin{aligned}
&\int d\boldsymbol{k}_\perp G^k\left(x,\boldsymbol{k}_\perp\,||\,x,\boldsymbol{k}_\perp+(1-x)\boldsymbol{\Delta}_\perp\right)\\
&= \int d\boldsymbol{k}_\perp\int d\boldsymbol{A}_\perp d\boldsymbol{B}_\perp e^{-i\boldsymbol{A}_\perp\cdot\boldsymbol{k}_\perp+i\boldsymbol{B}_\perp\cdot(\boldsymbol{k}_\perp+(1-x)\boldsymbol{\Delta}_\perp)}\mathcal{G}^k\left(x,\boldsymbol{A}_\perp\,||\,x,\boldsymbol{B}_\perp\right) &(5.36)\\
&= \int d\boldsymbol{B}_\perp e^{i(1-x)\boldsymbol{B}_\perp\cdot\boldsymbol{\Delta}_\perp}\mathcal{G}^k\left(x,\boldsymbol{B}_\perp\,||\,x,\boldsymbol{B}_\perp\right). &(5.37)
\end{aligned}$$

Using this expression, Eq. (5.35) can easily be transformed into the impact parameter space to obtain the pion chiral-odd IPD

$$\begin{aligned}
\frac{ib_\perp^k}{M_\pi}\widetilde{\mathcal{H}}_{T,\pi}'(x,\boldsymbol{b}_\perp^2) &= \int\frac{d\boldsymbol{\Delta}_\perp}{(2\pi)^2}e^{-i\boldsymbol{b}_\perp\cdot\boldsymbol{\Delta}_\perp}\left(\frac{\Delta_\perp^k}{2M_\pi}H_{T,\pi}(x,0,-\boldsymbol{\Delta}_\perp^2)\right)\\
&= \frac{T_\pi^2}{2(2\pi)^3}\int\frac{d\boldsymbol{\Delta}_\perp}{(2\pi)^2}e^{-i\boldsymbol{b}_\perp\cdot\boldsymbol{\Delta}_\perp}\int d\boldsymbol{B}_\perp e^{i(1-x)\boldsymbol{B}_\perp\cdot\boldsymbol{\Delta}_\perp}\mathcal{G}^k\left(x,\boldsymbol{B}_\perp\,||\,x,\boldsymbol{B}_\perp\right)\\
&= \frac{T_\pi^2}{2(2\pi)^5(1-x)^2}\mathcal{G}^k\left(x,\frac{\boldsymbol{b}_\perp}{1-x}\,||\,x,\frac{\boldsymbol{b}_\perp}{1-x}\right). &(5.38)
\end{aligned}$$

The same Dirac structure giving the GPD $\widetilde{H}_{T,\pi}$ in Eq. (5.35) enters the correlator that defines the Boer-Mulders TMD, i.e.

$$\Phi_\pi^{[i\sigma^{j+}\gamma_5]} = -\frac{\epsilon_\perp^{kj}k_\perp^k}{M_\pi}h_{1,\pi}^\perp(x,\boldsymbol{k}_\perp^2). \tag{5.39}$$

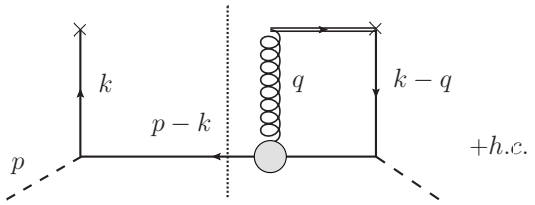

Figure 5.1: Cut diagram contributing to the average transverse momentum of T-odd effects in single-spin asymmetries of a SIDIS process for a pion target. The light-cone gauge is assumed and the target is modeled as a $q\bar{q}$ bound state.

As we already stressed, the tensor structures in Eqs. (5.32) and (5.39) have opposite behavior under time reversal, which reveals the naive T-even and naïve T-odd nature of $\widetilde{H}_{T,\pi}$ and $h_{1,\pi}^{\perp}$, respectively. As outlined in Sec. 5.2, in the calculation of the average transverse momentum of the Boer-Mulders effect the Wilson line reduces to the exchange of one Wilson gluon between the active quark and the spectator system (see Eq. (5.11)). If we describe the pion as a bound $q\bar{q}$ system, the corresponding cut diagram can be represented as in Fig. 5.1, where the blob indicates an effective coupling between the antiquark and the Wilson gluon. We will assume that the coupling is perturbative and consider only the tree-level graph. In this framework, the LFWA overlap representation of the pion Boer-Mulders function has been derived in Ref. [104] and reads

$$k_{\perp}^{k} h_{1,\pi}^{\perp}\left(x, \boldsymbol{k}_{\perp}^{2}\right) = \frac{2\alpha_s}{(2\pi)^4}\frac{4}{3}T_{\pi}^{2} M_{\pi} \int \frac{d\boldsymbol{q}_{\perp}}{\boldsymbol{q}_{\perp}^{2}} G^{k}\left(x, \boldsymbol{k}_{\perp} \,||\, x, \boldsymbol{k}_{\perp} - \boldsymbol{q}_{\perp}\right), \tag{5.40}$$

where $\boldsymbol{q}_{\perp}$ is the transverse momentum of the Wilson gluon (we recall that $q^{+} = 0$ in the eikonal approximation in the light-cone gauge). We note that Eq. (5.40) involves the same overlap of LFWAs as in Eq. (5.35) for the case of the GPD $\widetilde{H}_{T,\pi}$. With the formal identification of

$$-\boldsymbol{q}_{\perp} = (1-x)\boldsymbol{\Delta}_{\perp}, \tag{5.41}$$

the G^{k} functions in Eqs. (5.35) and (5.40) have the same momentum dependence. This is crucial to recover the lensing function relation. Using Eq. (5.40), we can now calculate the average transverse momentum of the Boer-Mulders effect

$$\begin{aligned}
\langle k_{\perp}^{i} \rangle_{TU}^{j} &= -\int d\boldsymbol{k}_{\perp} k_{\perp}^{i} \frac{\epsilon_{\perp}^{kj} k_{\perp}^{k}}{M_{\pi}} h_{1,\pi}^{\perp} \\
&= -\frac{2\alpha_s}{(2\pi)^4}\frac{4}{3}T_{\pi}^{2} \int \frac{d\boldsymbol{q}_{\perp}}{\boldsymbol{q}_{\perp}^{2}} \int d\boldsymbol{k}_{\perp} k_{\perp}^{i} \epsilon_{\perp}^{kj} G^{k}\left(x, \boldsymbol{k}_{\perp} \,||\, x, \boldsymbol{k}_{\perp} - \boldsymbol{q}_{\perp}\right) \\
&= -\frac{2\alpha_s}{(2\pi)^4}\frac{4}{3}T_{\pi}^{2} \int \frac{d\boldsymbol{q}_{\perp}}{\boldsymbol{q}_{\perp}^{2}} \int d\boldsymbol{k}_{\perp} k_{\perp}^{i} \epsilon_{\perp}^{kj} \int d\boldsymbol{A}_{\perp} d\boldsymbol{B}_{\perp} \\
&\times e^{-i\boldsymbol{A}_{\perp}\cdot\boldsymbol{k}_{\perp}} e^{i\boldsymbol{B}_{\perp}\cdot(\boldsymbol{k}_{\perp}-\boldsymbol{q}_{\perp})} \mathcal{G}^{k}\left(x, \boldsymbol{A}_{\perp} \,||\, x, \boldsymbol{B}_{\perp}\right) \\
&= -i\frac{4}{3} 4\pi\alpha_s (1-x)^3 \int d\boldsymbol{B}_{\perp} \int \frac{d\boldsymbol{q}_{\perp}}{\boldsymbol{q}_{\perp}^{2}} \frac{\epsilon_{\perp}^{kj} B_{\perp}^{k}}{M_{\pi}} q_{\perp}^{i}
\end{aligned}$$

$$\times e^{-i\boldsymbol{B}_\perp\cdot\boldsymbol{q}_\perp}\widetilde{\mathcal{H}}'_{T,\pi}(x,\boldsymbol{B}_\perp^2(1-x)^2), \tag{5.42}$$

where we used the following relation

$$\begin{aligned}
&\int d\boldsymbol{k}_\perp k_\perp^i \int d\boldsymbol{A}_\perp d\boldsymbol{B}_\perp e^{-i\boldsymbol{A}_\perp\cdot\boldsymbol{k}_\perp} e^{i\boldsymbol{B}_\perp\cdot(\boldsymbol{k}_\perp-\boldsymbol{q}_\perp)}\mathcal{G}^k(x,\boldsymbol{A}_\perp\,||\,x,\boldsymbol{B}_\perp)\\
&=\frac{q_\perp^i}{2}\int d\boldsymbol{B}_\perp e^{-i\boldsymbol{B}_\perp\cdot\boldsymbol{q}_\perp}\mathcal{G}^k(x,\boldsymbol{B}_\perp||x,\boldsymbol{B}_\perp)\\
&=iq_\perp^i(1-x)^3\frac{(2\pi)^5}{M_\pi T_\pi^2}\int d\boldsymbol{B}_\perp B_\perp^k\ \widetilde{\mathcal{H}}'_{T,\pi}(x,\boldsymbol{B}_\perp^2(1-x)^2))e^{-i\boldsymbol{B}_\perp\cdot\boldsymbol{q}_\perp}.
\end{aligned}$$

Introducing the change of variable $\boldsymbol{B}_\perp\to\boldsymbol{b}_\perp/(1-x)$ in Eq. (5.42), we find [87]

$$\langle k_\perp^i\rangle_{TU}^j=\int d\boldsymbol{b}_\perp\frac{\epsilon_\perp^{kj}b_\perp^k}{M_\pi}\mathcal{L}^i\left(\boldsymbol{b}_\perp/(1-x)\right)\ \widetilde{\mathcal{H}}'_{T,\pi}(x,\boldsymbol{b}_\perp^2), \tag{5.43}$$

where we introduced the lensing function [55]

$$\mathcal{L}^i\left(\boldsymbol{b}_\perp/(1-x)\right)=-i\frac{4}{3}\alpha_s 4\pi\int\frac{d\boldsymbol{q}_\perp}{\boldsymbol{q}_\perp^2}q_\perp^i e^{-i\frac{\boldsymbol{b}_\perp\cdot\boldsymbol{q}_\perp}{(1-x)}}=-\frac{8}{3}\alpha_s 4\pi^2\frac{b_\perp^i}{\boldsymbol{b}_\perp^2}(1-x). \tag{5.44}$$

Before moving on and discussing the proton case, a few comments are in order. The result for the pion relies on the assumption that the coupling between the Wilson gluon and the spectator parton is of perturbative nature, i.e., it is described by the tree-level QCD vertex. The coupling, at leading power of $1/p^+$, conserves the helicity of the spectator parton. Therefore, the helicity flip of the active quark must be compensated by a change of the OAM carried by the partons in the initial and final states. This behavior in the TMD sector is equivalent to the GPD case, where the active and spectator quarks do not experience any helicity flip and the change in the helicity of the target must be compensated by a transfer of OAM between the partons in the initial and final states. In this case, the transfer of parton OAM to the hadron helicity is mediated by the external virtual (or real) photon.

Due to the two-body nature of the problem ($q\bar{q}$ system) the role of the transverse momentum of the gluon $\boldsymbol{q}_\perp$ is the same as the external transverse momentum $\boldsymbol{\Delta}_\perp$ in the GPD case. This can be traced back to the fact that the parton distributions should be invariant by light-front transverse boosts and depend on the intrinsic transverse-momentum coordinates of the partons. In the case of the average transverse-momentum of the Boer-Mulders effect, there is no change of the transverse momentum of the pion between the initial and final state. However, the quark and antiquark have a different intrinsic transverse momentum in the initial and final states due to the gluon exchange. In the GPD case, the momentum transferred to the pion is absorbed by the active quark, while the transverse momentum of the spectator quark does not change in the initial and final states. In terms of the intrinsic transverse-momentum coordinates in the hadron-in and hadron-out frame of the initial and final hadrons, respectively, both the active and spectator quarks experience a transfer

of transverse momentum (see Chapter 6 for a more in-depth discussion about hadron frames in the GPD context). Therefore, one can make the formal identification of Eq. (5.41) in the momentum dependence of the LFWAs describing the contribution of the internal parton dynamics and the effect of the FSIs can be factorized in the lensing function. In the next section, we will see that in the case of a three-body system this correspondence can not be established, and, as a consequence, the lensing-function relation breaks down.

If we do not assume a perturbative coupling between the Wilson gluon and the antiquark spectator, we may model the interaction via an effective vertex that depends on the momenta of the gluon and anti-quark. The coupling with the Wilson gluon may occur with or without flip of the helicity of the antiquark. In the first case, the lensing relation can not hold, as it will be discussed in Sec. 5.4.1. If the helicity flip is not allowed, the lensing relation can still be spoiled by the dependence of the vertex on the momentum of the antiquark. By introducing the general parametrization for the effective vertex $\Lambda\left(\boldsymbol{k}_\perp^2, \boldsymbol{q}_\perp^2, \boldsymbol{k}_\perp \cdot \boldsymbol{q}_\perp\right)\gamma^+$, the average transverse momentum of the Boer-Mulders effect in Eq. (5.42) becomes

$$
\begin{aligned}
&\langle k_\perp^i \rangle_{TU}^j \\
&= -\frac{2\alpha_s}{(2\pi)^4}\frac{4}{3}T_\pi^2 \int d\boldsymbol{k}_\perp k_\perp^i \epsilon_\perp^{kj} \int \frac{d\boldsymbol{q}_\perp}{\boldsymbol{q}_\perp^2} G^k\left(x, \boldsymbol{k}_\perp \,||\, x, \boldsymbol{k}_\perp - \boldsymbol{q}_\perp\right) \Lambda\left(\boldsymbol{k}_\perp^2, \boldsymbol{q}_\perp^2, \boldsymbol{k}_\perp \cdot \boldsymbol{q}_\perp\right) \\
&= -\frac{2\alpha_s}{(2\pi)^4}\frac{4}{3}T_\pi^2 \Bigg\{ \int d\boldsymbol{B}_\perp d\boldsymbol{A}_\perp \int \frac{d\boldsymbol{q}_\perp}{\boldsymbol{q}_\perp^2} e^{-i\boldsymbol{B}_\perp \cdot \boldsymbol{q}_\perp} \frac{q_\perp^i}{2} \\
&\times \epsilon_\perp^{kj} \mathcal{G}^k\left(x, \boldsymbol{B}_\perp - \boldsymbol{A}_\perp \,||\, x, \boldsymbol{B}_\perp\right) \widetilde{\Lambda}\left(\boldsymbol{A}_\perp^2, \boldsymbol{q}_\perp^2, \boldsymbol{A}_\perp \cdot \boldsymbol{q}_\perp\right) + \frac{i}{2} \int d\boldsymbol{B}_\perp d\boldsymbol{A}_\perp \\
&\times \int \frac{d\boldsymbol{q}_\perp}{\boldsymbol{q}_\perp^2} e^{-i(\boldsymbol{B}_\perp + \boldsymbol{A}_\perp)\cdot\frac{\boldsymbol{q}_\perp}{2}} \epsilon_\perp^{kj} \partial_{A_{\perp,i}} \Bigg[\mathcal{G}^k\Big(x, \boldsymbol{A}_\perp \Big|\Big| x, \frac{\boldsymbol{B}_\perp + \boldsymbol{A}_\perp}{2}\Big) \\
&\times \widetilde{\Lambda}\left(\left(\frac{\boldsymbol{B}_\perp - \boldsymbol{A}_\perp}{2}\right)^2, \boldsymbol{q}_\perp^2, \frac{\boldsymbol{B}_\perp \cdot \boldsymbol{q}_\perp - \boldsymbol{A}_\perp \cdot \boldsymbol{q}_\perp}{2}\right) \Bigg] \Bigg\}.
\end{aligned}
\tag{5.45}
$$

It is not possible to manipulate Eq. (5.45) in order to extract a term like $\mathcal{G}\left(x, \boldsymbol{B}_\perp \,||\, x, \boldsymbol{B}_\perp\right)$ and, therefore, recognize the definition of the IPD, as done in Eq. (5.42). However, if the effective vertex is assumed as a function of only $\boldsymbol{q}_\perp$, then the lensing relation (5.43) holds, with the following modified definition of the lensing function

$$
\mathscr{L}^i\left(\boldsymbol{b}_\perp/(1-x)\right) = -i\frac{4}{3}\alpha_s 4\pi \int \frac{d\boldsymbol{q}_\perp}{\boldsymbol{q}_\perp^2} q_\perp^i \Lambda(\boldsymbol{q}_\perp^2) e^{-i\frac{\boldsymbol{b}_\perp \cdot \boldsymbol{q}_\perp}{(1-x)}}. \tag{5.46}
$$

5.4 Lensing relation for the proton

In this section, we discuss the validity of the lensing relations in Eq. (5.3) for the proton system, assumed as the preferential prototype of hadrons with

multiple partons in the remnant. For illustration purposes, we will consider in detail the relation between the Sivers TMD and the IPD $\mathcal{E}$. However, the same arguments can be applied for the relation involving the Boer-Mulders TMD and the combination $\mathcal{E}_T + 2\widetilde{\mathcal{H}}_T$ of chiral-odd IPDs.

We limit ourselves to analyze the general structure of the LFWA overlap representation of the GPDs and the Sivers function, since the explicit dependence on the LFWAs is not relevant for our discussion. We refer to [95, 97] for the full calculation of the LFWA overlap. We introduce the LFWA overlap

$$F_T\left(x_1, \boldsymbol{k}_{\perp,1}; x_2, \boldsymbol{k}_{\perp,2}; x_3, \boldsymbol{k}_{\perp,3} \,||\, x_1', \boldsymbol{k}'_{\perp,1}; x_2', \boldsymbol{k}'_{\perp,2}; x_3', \boldsymbol{k}'_{\perp,3}\right) \tag{5.47}$$

and define the function G_T as

$$\begin{aligned} &G_T\big(x_1, \boldsymbol{k}_{\perp,1}; x_2, \boldsymbol{k}_{\perp,2} \,||\, x_1', \boldsymbol{k}'_{\perp,1}; x_2', \boldsymbol{k}'_{\perp,2}\big) \\ &= F_T\big(x_1, \boldsymbol{k}_{\perp,1}; x_2, \boldsymbol{k}_{\perp,2}; 1-x_1-x_2, -\boldsymbol{k}_{\perp,1} - \boldsymbol{k}_{\perp,2} \\ &\qquad \big|\big| x_1', \boldsymbol{k}'_{\perp,1}; x_2', \boldsymbol{k}'_{\perp,2}; 1-x_1'-x_2', -\boldsymbol{k}'_{\perp,1} - \boldsymbol{k}'_{\perp,2}\big). \end{aligned} \tag{5.48}$$

The GPD E in the limit of $\xi = 0$ is obtained from the quark-quark correlator (3.50) with $\Gamma = \gamma^+$ and transversely polarized proton, as it is illustrated by Eq. (3.52). The incoming and outgoing quark momenta are related by $p_i' = p_i$ $(i \neq j)$ for the spectator quarks and $p_j' = p_j + \Delta$ for the active quark that takes the momentum transferred to the proton. The intrinsic momenta are then obtained via the transverse boost and are related as (see also the $\xi \to 0$ limit of Eqs. (6.49)-(6.50))

$$x_i' = x_i, \qquad \boldsymbol{k}'_{\perp,i} = \boldsymbol{k}_{\perp,i} - x_i \boldsymbol{\Delta}_\perp, \qquad \text{spectator quarks,} \tag{5.49}$$

$$x_j' = x_j, \qquad \boldsymbol{k}'_{\perp,j} = \boldsymbol{k}_{\perp,j} + (1-x_j)\boldsymbol{\Delta}_\perp, \qquad \text{active quark.} \tag{5.50}$$

Using momentum conservation for the intrinsic variables, i.e., $\sum_i x_i = 1$ and $\sum_i \boldsymbol{k}_{\perp,i} = \boldsymbol{0}_\perp = \sum_i \boldsymbol{k}'_{\perp,i}$, one finds the following LFWA overlap representation [97]

$$\begin{aligned} &\frac{i\epsilon_\perp^{ij}\Delta_\perp^j S_T^i}{M} E(x, \xi=0, -\boldsymbol{\Delta}_\perp^2) = \frac{1}{4(2\pi)^6} \\ &\times \int d\boldsymbol{k}_\perp \int_0^x dy \int d\boldsymbol{t}_\perp G_T\left(x, \boldsymbol{k}_\perp; y, \boldsymbol{t}_\perp \,||\, x, \boldsymbol{k}_\perp + (1-x)\boldsymbol{\Delta}_\perp; y, \boldsymbol{t}_\perp - y\boldsymbol{\Delta}_\perp\right). \end{aligned} \tag{5.51}$$

The results for the IPD distribution are then obtained taking the Fourier transform of Eq. (5.51) with respect to $\boldsymbol{b}_\perp$ and expressing G_T in terms of its Fourier integral. One finds

$$\begin{aligned} &-\frac{\epsilon_\perp^{ij} b_\perp^j S_T^i}{M} \mathcal{E}'(x, \xi=0, \boldsymbol{b}_\perp^2) = \frac{1}{4(2\pi)^8} \frac{1}{1-x} \\ &\times \int_0^x dy \int d\boldsymbol{B}_\perp \mathcal{G}_T\left(x, \frac{y\boldsymbol{B}_\perp - \boldsymbol{b}_\perp}{1-x}; y, \boldsymbol{B}_\perp \,||\, x, \frac{y\boldsymbol{B}_\perp - \boldsymbol{b}_\perp}{1-x}; y, \boldsymbol{B}_\perp\right). \end{aligned} \tag{5.52}$$

The LFWA overlap representation of the Sivers function has been derived in Ref. [95], using the three-quark component of the nucleon state and the one-gluon exchange approximation, with a perturbative quark-gluon coupling. It is given by the same function G_T as for the GPD E, but with different arguments, i.e.,

$$\frac{\epsilon_\perp^{ij} k_\perp^j S_T^i}{M} f_{1T}^\perp\left(x, \boldsymbol{k}_\perp^2\right) = -\frac{\alpha_s}{3(2\pi)^7} \times \int \frac{d\boldsymbol{q}_\perp}{\boldsymbol{q}_\perp^2} \int_0^x dy \int d\boldsymbol{t}_\perp G_T\left(x, \boldsymbol{k}_\perp; y, \boldsymbol{t}_\perp \,||\, x, \boldsymbol{k}_\perp - \boldsymbol{q}_\perp; y, \boldsymbol{t}_\perp + \boldsymbol{q}_\perp\right). \tag{5.53}$$

From this expression, one clearly sees that the formal identification in Eq. (5.41) does not apply in the case of Eqs. (5.51) and (5.53), since $(1-x)$ and y are independent variables. As we will see, this is sufficient to break the lensing-function relation in the case of the proton, see Ref. [87].

From Eq. (5.53), one can calculate the average transverse momentum of the Sivers effect as

$$\begin{aligned}
\langle k_\perp^i \rangle_{UT} &= -\int d\boldsymbol{k}_\perp k_\perp^i \frac{\epsilon_\perp^{ij} k_\perp^j S_T^i}{M} f_{1T}^\perp = \alpha_s \frac{M}{3(2\pi)^7} \\
&\times \int d\boldsymbol{k}_\perp k_\perp^i \int \frac{d\boldsymbol{q}_\perp}{\boldsymbol{q}_\perp^2} \int_0^x dy \int d\boldsymbol{t}_\perp G_T\left(x, \boldsymbol{k}_\perp; y, \boldsymbol{t}_\perp \,||\, x, \boldsymbol{k}_\perp - \boldsymbol{q}_\perp; y, \boldsymbol{t}_\perp + \boldsymbol{q}_\perp\right) \\
&= \alpha_s \frac{M}{3(2\pi)^7} \int_0^x dy \int d\boldsymbol{A}_\perp d\boldsymbol{B}_\perp \int \frac{d\boldsymbol{q}_\perp}{\boldsymbol{q}_\perp^2} \\
&\times \frac{q_\perp^i}{2} e^{i\boldsymbol{q}_\perp \cdot \boldsymbol{A}_\perp} \mathcal{G}_T\left(x, \boldsymbol{B}_\perp - \boldsymbol{A}_\perp; y, \boldsymbol{B}_\perp \,||\, x, \boldsymbol{B}_\perp - \boldsymbol{A}_\perp; y, \boldsymbol{B}_\perp\right) \\
&= -i\alpha_s \frac{M}{6(1-x)(2\pi)^6} \int_0^x dy \int d\boldsymbol{b}_\perp d\boldsymbol{B}_\perp \\
&\times \frac{b_\perp^i}{\boldsymbol{b}_\perp^2} \mathcal{G}_T\left(x, \frac{\boldsymbol{B}_\perp - \boldsymbol{b}_\perp}{1-x}; y, \boldsymbol{B}_\perp \,||\, x, \frac{\boldsymbol{B}_\perp - \boldsymbol{b}_\perp}{1-x}; y, \boldsymbol{B}_\perp\right).
\end{aligned} \tag{5.54}$$

Comparing this equation with Eq. (5.52), we immediately notice that the different dependence of the function G_T on $\boldsymbol{B}_\perp$ prevents us to factorize the contribution of the IPD from a lensing function. This can be traced back to the fact that in the LFWF overlap representation of the GPD the transverse momentum $\boldsymbol{\Delta}_\perp$ appears multiplied by both $(1-x)$ and y, since both the two spectator quarks have different intrinsic transverse momentum in the initial and final states. In other words, the transverse boost from a given frame to the hadron frames transforms the transverse-momentum coordinates of the two spectator quarks in a different way, depending on their fraction x_i of longitudinal momentum. Vice versa, in the TMD case the hadron does not change the transverse momentum in the initial and final states, and the gluon interaction occurs between the active quark and a single spectator quark, leaving unchanged the intrinsic momentum of the other spectator quark.

The non-validity of the lensing relation is ultimately related to the, at least, three-body nature of the nucleon together with the assumption of the interac-

tion of the Wilson gluon with a single constituent in the remnant. A multi-particle, non-perturbative coupling between the Wilson gluon and the remnant can be used to restore the lensing relation. The coupling should be constructed in such a way to satisfy the conditions $1) - 4)$ illustrated in Sec. 5.2. If the perturbative vertex is chosen, then the lensing relation is spoiled also for the pion when considering Fock-state components beyond the leading-order $q\bar{q}$ state. For the nucleon, one way in which it might be possible to recover the lensing relation is to consider models in which the nucleon is described as a two-body system. Examples of such models are the quark diquark models, in which the spectator system is described as an on-shell, point-like particle with quantum numbers of a diquark. However, one has to distinguish between different variants of diquark spectator models, depending on the spin structure of the diquark and its coupling with the Wilson gluon, as we will discuss in the following section.

5.4.1 Diquark spectator models for the proton

The basic idea of spectator models is to evaluate the quark-quark correlators entering the definition of the TMDs and of the GPDs by inserting a complete set of intermediate states, assigning an effective vertex for the transition $p \to q + \{X_i\}$. The spectator models which we are going to consider, are collectively known as diquark models, in which the remnant complexity is hidden inside a single particle, the diquark, which is assumed to be on-shell and with the quantum numbers that can be obtained from the combination of the quantum numbers of two quarks. The way in which the diquark is constructed forces it to be either an isospin singlet with spin 0 (scalar diquark) or an isospin triplet with spin 1 (axial-vector diquark). In the last case, the axial nature of the diquark is due to the axial coupling between the proton and the quark-diquark state which ensures the angular momentum conservation. The target is then seen as made of an off-shell quark that participates in the hard reaction of the process and an on-shell diquark. Different spectator diquark models can be obtained by varying the form of the effective vertex with the proton and the vertex form factor that effectively parametrizes the composite nature of the target and by choosing different polarization four-vectors for the axial-vector diquark. The approximation of a diquark spectator spoils part of the richness of the non-perturbative structure of the proton, that is impossible to capture via the vertex form factor alone.

The very first hint on the validity of the lensing relation came from the scalar diquark calculation performed in Ref. [53]. The general arguments which lead to the lensing relations are the same as discussed in Sec. 5.3 for the pion, i.e., the hadron described as a two-body system and the assumption of a perturbative helicity-conserving coupling between the gauge boson and the spectator system. For the axial-vector diquark model (AVDQ), the validity of the lensing-function relations depends entirely on the helicity structure of the diquark. One way to classify AVDQ models is to distinguish between models that allow for the

presence of a longitudinal polarization and models that admit only transverse polarizations for the axial-vector diquark. The latter presents similarities to the quark-target model, in which the diquark is substituted by an on-shell gluon and the proton is assumed to be a single quark. The former AVDQ models do not satisfy the lensing relation, and to illustrate why, we introduce the polarization vectors of the AVDQ (see, e.g., Ref. [92]):

$$\varepsilon_{+1}(l) = \left(0, \frac{-l_R}{\sqrt{2}l^+}, \boldsymbol{\varepsilon}_{+1,\perp}\right), \tag{5.55}$$

$$\varepsilon_{-1}(l) = \left(0, \frac{-l_L}{\sqrt{2}l^+}, \boldsymbol{\varepsilon}_{-1,\perp}\right), \tag{5.56}$$

$$\varepsilon_{0}(l) = \frac{1}{M_a}\left(l^+, \frac{l_\perp^2 - M_a^2}{2l^+}, \boldsymbol{l}_\perp\right), \tag{5.57}$$

where M_a is the AVDQ mass, $l \equiv p - k$, and:

$$\boldsymbol{\varepsilon}_{+1,\perp} = -\left(\boldsymbol{\varepsilon}_{-1,\perp}\right)^* = -\frac{1}{\sqrt{2}}\left(1, i\right). \tag{5.58}$$

Here we do not consider the (unphysical) time-like polarization that is discussed in Ref. [92]. The polarization vectors in Eqs. (5.55)-(5.57) satisfy the following relations: $\varepsilon_{+1}(l)\cdot\varepsilon^*_{-1}(l') = 0$ for any value of l, l', whereas $\varepsilon_{\pm1}(l)\cdot\varepsilon^*_0(l) = 0$ and $\varepsilon_{\pm1}(l)\cdot\varepsilon^*_0(l') \neq 0$ for $l \neq l'$. The interaction between the diquark and the gluon is given by the following coupling tensor

$$\frac{i}{e_c}\Gamma^\rho_{\nu\sigma} = (2l+q)^\rho g_{\nu\sigma} - (l + (1+\kappa_a)q)_\sigma \delta^\rho_\nu - (l - \kappa_a q)_\nu \delta^\rho_\sigma, \tag{5.59}$$

where e_c and κ_a are, respectively, the diquark color charge and the diquark anomalous chromomagnetic moment, which takes into account that the diquark is not a point-like massive axial particle, but is an effective constituent degree of freedom. In the calculation of the T-odd TMDs, the indices of the coupling tensor (5.59) are saturated with the gluon propagator and the AVDQ polarization vector (see Fig. 5.2). The contraction of the coupling tensor with the polarization vectors of the axial-vector diquark gives the following interaction vertex

$$\mathcal{R}^\rho = \sum_{\lambda_1,\lambda_2=\pm1,0} \varepsilon^{\nu*}_{\lambda_1}(l)\varepsilon^\sigma_{\lambda_2}(l+q)\Gamma^\rho_{\nu\sigma}. \tag{5.60}$$

This expression can be compared with the corresponding $\bar{q}gq$ interaction vertex, which enters the calculation of the Boer-Mulders function of the pion, i.e.

$$\mathcal{R}^\rho = \sum_{\lambda_1,\lambda_2=\pm1/2} \bar{v}_{\lambda_1}(l+q)\gamma^\rho v_{\lambda_2}(l). \tag{5.61}$$

In both cases, the vertex function has the following scaling behavior [87]

$$\mathcal{R}^+ \simeq \mathcal{O}(p^+), \qquad \mathcal{R}^i_\perp \simeq \mathcal{O}(1), \qquad \mathcal{R}^- \simeq \mathcal{O}(1/p^+). \tag{5.62}$$

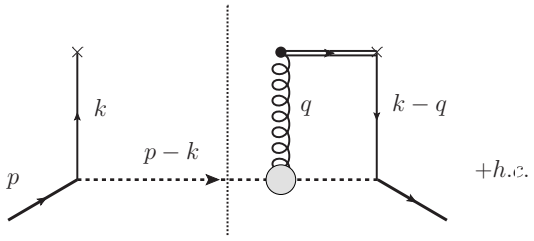

Figure 5.2: Cut diagram contributing to the average transverse-momentum of T-odd effects in single spin asymmetries of a SIDIS process, in the $A^+ = 0$ gauge and for a proton target described in a quark-diquark model.

However, in the case of the pion, the leading-order term $\mathcal{R}^+$ in Eq. (5.61) is helicity conserving, whereas the leading contribution $\mathcal{R}^+$ in Eq. (5.60) for the axial-vector diquark contains terms that flip the helicity of the diquark. As a result, the following transitions are allowed for the AVDQ interacting with the Wilson gluon

$$\lambda_a = \pm 1 \leftrightarrow \lambda_a = 0, \pm 1. \tag{5.63}$$

On the contrary, in the calculations of the GPDs, since the Wilson line in the light-cone gauge reduces to unity, the spectator can not flip the helicity between the initial and final states. We conclude that the LFWA overlap must be different for the average transverse momentum of the T-odd TMD functions and for the GPDs, hence the lensing relation cannot hold. Only if one assumes that the longitudinal polarization for the AVDQ is absent in the proton, the lensing relation can be restored. This situation occurs within the quark target model, where the non-abelian three-gluon vertex enters the computation of the T-odd TMDs and allows only for helicity-conserving transitions.

5.5 Conclusions

Models are a useful resource in theoretical calculations to investigate problems and, by consequence, to learn more about the fundamental theories. However, models rely on simplifying assumptions and may lead to approximate results that do not hold in general. In this Chapter, based on Ref. [87], we stressed this point by investigating the origin of non-trivial relations between transverse distortions in the distribution of quarks in impact-parameter space and analogous distortions in transverse-momentum space. The former can be encoded in non-perturbative objects called impact-parameter distributions (IPDs) and contribute to observable asymmetries in exclusive processes involving hadrons. The latter are expressed in terms of the naive T-odd Sivers and Boer-Mulders transverse-momentum distributions (TMDs), and give rise to observable asymmetries in semi-inclusive processes involving hadrons.

We identified the conditions under which it is possible to express the Sivers and Boer-Mulders functions as convolutions of an IPD and a lensing function,

incorporating the effects of the FSIs between the active parton and the rest of the hadron. These conditions, listed in Sec. 5.2, appear to be very specific and hold in a restricted class of models.

To better illustrate the nature of these conditions, we investigated the emerging of the lensing relation in three distinct cases: (1) the pion, taken as a prototype of hadrons with a two-body valence structure; (2) the proton, described as a bound state of three quarks; (3) the proton described as bound state of a quark and a spectator, using the framework of a particular class of models where the lensing relations have been originally established. The conditions of validity of the lensing relations can be fulfilled in models where the hadron is described as a two-body bound system, as in the model classes (1) and (3). However, they can be violated even in these simple models, as happens in certain versions of (3), e.g., with axial-vector spectator that admits longitudinal polarization. Finally, the conditions are violated in models that belong to class (2) and, in general, the conditions cannot be obtained if the hadron is described by more than two constituents and the interaction vertex of the gauge boson occurs with a single constituent.

In conclusion, it seems that the lensing relation is unlikely to survive in the full complexity of non-perturbative QCD, even approximately. Phenomenological studies of the Sivers and Boer-Mulders function, as well as possible lattice QCD studies, should be able to confirm the violation of the lensing hypothesis.

Chapter 6

A model for the Light-Front Wave Amplitudes

In Secs. 3.4.1 and 3.4.4, we introduced the concept of proton Distribution Amplitudes (DAs) and how they can be linked to the light-front wave amplitudes (LFWAs) of the proton. We claimed that an explicit model for the transverse momentum dependence of the LFWAs is necessary for a full inversion of the relations between DAs and LFWAs. In this Chapter, we are going to illustrate the model that we chose to work with. The model consists in two parts: the first one concerns the transverse-momentum dependence of the LFWAs, which is also necessary to link them to the DAs. The second one concerns the DAs, for which we are going to assume a model inspired from Ref. [105]. The model will be used to obtain explicit predictions for a variety of PDFs, TMDs and GPDs. To obtain results that are as close as possible to the current available knowledge of the partonic structure of the proton, we are going to fit our model to a phenomenoligical parametrization for the up, down and gluon unpolarized PDF $f_1(x)$. Although the model is unable to reproduce the full phenomenological extraction, it proves satisfactory in its simplicity.

6.1 The construction of the model

A rather standard approach to model the transverse-momentum dependence of the LFWAs is to assume a product of N gaussian functions in the transverse-momentum space, where N corresponds to the number of partons of the corresponding Fock state. The transverse momentum of each parton is weighted with the inverse of the corresponding fraction of longitudinal momentum. This construction assumes that eventual hard gluon contributions have been already subtracted from the DAs, leaving the intrinsic soft contributions only. This argument is valid if the scale at which the model is constructed is low enough ($\lesssim 1$ GeV). This construction is shown in Ref. [105] and is known as the Brodsky-Huang-Lepage prescription [106]. We are going to modify the model of Ref. [105] by including the masses of the constituent partons. The masses are treated as

effective masses and are assumed to be generated by non-perturbative dynamical processes that bind the partons inside the nucleon. For the three-quark state we are going to consider only LFWAs with $L_z = 0, \pm 1$, i.e. only LFWAs that can be linked to DAs of twist-3 and twist-4. Since the LFWAs $\psi^{(2)}$ is linked to a twist-5 DA we are not going to consider it. For consistency, the only LFWAs for the three-quark plus one-gluon state that we include are the ones with $L_z = 0$, since they are linked to the four-parton twist-4 DAs. The model for the LFWAs reads (in the first line we have $l = 0, 3, 4, 5$):

$$\psi^{(l)}(\{x_i, \boldsymbol{k}_{\perp,i}\}) = \frac{\phi^{(l)}(x_1, x_2, x_3)}{4\sqrt{6}} \Omega_3(\{x_i, \boldsymbol{k}_{\perp,i}\}, a_l)\ e^{\left(-a_l^2 \sum_{j=1}^{3} \frac{m_j^2}{x_j}\right)}, \tag{6.1}$$

$$\Psi^{\downarrow}(\{x_i, \boldsymbol{k}_{\perp,i}\}) = \frac{\phi^{\downarrow}(x_1, x_2, x_3, x_4)}{\sqrt{2x_4}} \Omega_4(\{x_i, \boldsymbol{k}_{\perp,i}\}, a_{\downarrow})\ e^{\left(-a_{\downarrow}^2 \sum_{j=1}^{4} \frac{m_j^2}{x_j}\right)}, \tag{6.2}$$

$$\Psi^{1,2\uparrow}(\{x_i, \boldsymbol{k}_{\perp,i}\}) = \frac{\phi^{1,2\uparrow}(x_1, x_2, x_3, x_4)}{\sqrt{2x_4}} \Omega_4(\{x_i, \boldsymbol{k}_{\perp,i}\}, a_{1,2\uparrow})\ e^{\left(-a_{1,2\uparrow}^2 \sum_{j=1}^{4} \frac{m_j^2}{x_j}\right)}, \tag{6.3}$$

where

$$\Omega_N(\{x_i, \boldsymbol{k}_{\perp,i}\}, a) = \frac{(4\pi a)^{2(N-1)}}{\prod_{i=1}^{N} x_i}\ e^{\left(-a^2 \sum_{i=1}^{N} \frac{\boldsymbol{k}_{\perp,i}^2}{x_i}\right)}, \tag{6.4}$$

and m_i are the effective parton masses. The normalization of the Gaussian in Eq. (6.4) is chosen in such a way that the following identity holds:

$$\int [d\boldsymbol{k}_{\perp}]_N \Omega_N(\{x_i, \boldsymbol{k}_{\perp,i}\}, a) = 1. \tag{6.5}$$

We introduce only two parton masses: one for the gluon and one for the quarks, independently from their flavor. The explicit representation of the transverse-momentum dependent part of the LFWAs in Eqs. (6.1)-(6.4) is enough to explicitly compute the integrals in Eqs. (3.153)-(3.155) and then invert the relations between the DAs and the LFWAs. As it is clear from Eqs. (3.153)-(3.155), once the system of equations is inverted, one last piece of information is needed in order to obtain explicit results for the LFWAs with $L_z \neq 0$: the integrals of the four-parton DAs, see Eqs. (3.150)-(3.152). Therefore, an analytical expression for the DAs must be fixed. To do so, we follow Ref. [105] and expand the DAs onto a basis of orthogonal polynomials. Each element of the basis is an eigenfunction of the one-loop evolution kernel. We truncate the expansion for the three-parton DAs to the second non-trivial term and the four-parton DAs to the first term (see Refs. [65, 66, 68, 105, 107]):

$$\Phi_3(x_1, x_2, x_3) = 120 f_N x_1 x_2 x_3 \left(1 + f_0^-(x_1 - x_3) + f_0^+(x_1 + x_3 - 2x_2)\right), \tag{6.6}$$

$$\Phi_4(x_1, x_2, x_3) = 24 x_1 x_2 (\phi_4^0 + \phi_4^-(x_1 - x_2) + \phi_4^+(1 - 5x_3)), \tag{6.7}$$

$$\Psi_4(x_1,x_2,x_3) = 24x_1x_3(\psi_4^0 + \psi_4^-(x_1-x_3) + \psi_4^+(1-5x_2)), \tag{6.8}$$

$$\Xi_4(x_1,x_2,x_3) = 24x_2x_3(\xi_4^0 + \xi_4^-(x_2-x_3) + \xi_4^+(1-5x_1)), \tag{6.9}$$

$$\Phi_4^g(x_1,x_2,x_3,x_4) = -\frac{8!}{4}x_1x_2x_3x_4^2\left(\lambda_2^g - \frac{\lambda_3^g}{3}\right), \tag{6.10}$$

$$\Psi_4^g(x_1,x_2,x_3,x_4) = \frac{8!}{4}x_1x_2x_3x_4^2\left(\lambda_2^g + \frac{\lambda_3^g}{3}\right), \tag{6.11}$$

$$\Xi_4^g(x_1,x_2,x_3,x_4) = \frac{8!}{6}x_1x_2x_3x_4^2\lambda_1^g. \tag{6.12}$$

Via Eq. (3.104), we have the following identification:

$$\phi^{(0)}(x_1,x_2,x_3) = \tilde{\Phi}_3(x_1,x_2,x_3)e^{\left(a_0^2\sum_{j=1}^3\frac{m_j^2}{x_j}\right)} = \Phi_3(x_1,x_2,x_3), \tag{6.13}$$

where we assumed that the total twist-3 DA $\tilde{\Phi}_3(x_1,x_2,x_3)$ can be written as the product of Eq. (6.6) and the mass exponential. From Eqs. (3.108)-(3.110) we obtain the similar results for the three-quark plus one-gluon LFWAs:

$$\begin{aligned}\phi^{\downarrow}(x_1,x_2,x_3,x_4) &= e^{\left(a_\downarrow^2\sum_{j=1}^4\frac{m_j^2}{x_j}\right)}\frac{M}{96g_s}\left(2\tilde{\Xi}_4^g(x_1,x_2,x_3,x_4) + \tilde{\Xi}_4^g(x_2,x_1,x_3,x_4)\right)\\ &= \frac{M}{96g_s}\left(2\Xi_4^g(x_1,x_2,x_3,x_4) + \Xi_4^g(x_2,x_1,x_3,x_4)\right),\end{aligned} \tag{6.14}$$

$$\begin{aligned}\phi^{1,\uparrow}(x_1,x_2,x_3,x_4) &= -e^{\left(a_{1,\uparrow}^2\sum_{j=1}^4\frac{m_j^2}{x_j}\right)}\\ &\times\frac{M}{96g_s}\left(2\tilde{\Psi}_4^g(x_2,x_1,x_3,x_4) + \tilde{\Phi}_4^g(x_1,x_2,x_3,x_4)\right)\\ &= -\frac{M}{96g_s}\left(2\Psi_4^g(x_2,x_1,x_3,x_4) + \Phi_4^g(x_1,x_2,x_3,x_4)\right),\end{aligned} \tag{6.15}$$

$$\begin{aligned}\phi^{2,\uparrow}(x_1,x_2,x_3,x_4) &= e^{\left(a_{2,\uparrow}^2\sum_{j=1}^4\frac{m_j^2}{x_j}\right)}\\ &\times\frac{M}{96g_s}\left(2\tilde{\Phi}_4^g(x_1,x_2,x_3,x_4) + \tilde{\Psi}_4^g(x_2,x_1,x_3,x_4)\right)\\ &= \frac{M}{96g_s}\left(2\Phi_4^g(x_1,x_2,x_3,x_4) + \Psi_4^g(x_2,x_1,x_3,x_4)\right),\end{aligned} \tag{6.16}$$

where we assumed that the total twist-4 DAs $\tilde{\Xi}_4$, $\tilde{\Phi}_4$ and $\tilde{\Psi}_4$ can be written as the product of the corresponding expression in Eqs. (6.10)-(6.12) and the mass exponential.

All the parameters in Eqs. (6.6)-(6.12) encapsulate the scale dependence of the DAs. However, since we shall not deal with the problem of evolving the DAs to different scales, we are going to ignore such dependence. A numerical estimate for the parameters can be obtained using both QCD sum-rule techniques [108, 109] and lattice-QCD results [66, 107, 110, 111] for the DA moment at the low-energy scale of $\mu = 1$ GeV.

The inversion of Eqs. (3.153)-(3.155) leads to the following results:

$$\phi^{(3)}(x_1,x_2,x_3) = -Ma_3^2\left(\frac{1-x_2}{x_1}A(x_1,x_2,x_3)+\frac{x_2}{x_1}B(x_1,x_2,x_3)\right), \tag{6.17}$$

$$\phi^{(4)}(x_1,x_2,x_3) = -Ma_4^2\left(A(x_1,x_2,x_3)-B(x_1,x_2,x_3)\right), \tag{6.18}$$

$$\phi^{(5)}(x_1,x_2,x_3) = Ma_5^2\left(\frac{1-x_1}{x_3}C(x_2,x_1,x_3)+\frac{x_1}{x_3}C(x_1,x_2,x_3)\right), \tag{6.19}$$

where we introduced the functions[1]

$$A(x_1,x_2,x_3) = -\Phi_4(x_2,x_1,x_3)+\frac{7!}{6}\left(\lambda_2^g-\frac{\lambda_3^g}{3}\right)x_1x_2x_3^2-\frac{m_q}{Mx_3}\Phi_3(x_1,x_2,x_3), \tag{6.20}$$

$$\begin{aligned}B(x_1,x_2,x_3) = &-\Psi_4(x_1,x_2,x_3)-\frac{7!}{6}\left(\lambda_2^g+\frac{\lambda_3^g}{3}\right)x_1x_2^2x_3\\ &+\frac{m_q}{Mx_2}\left(\Phi_3(x_2,x_3,x_1)+\Phi_3(x_1,x_3,x_2)\right),\end{aligned} \tag{6.21}$$

$$C(x_1,x_2,x_3) = \Xi_4(x_1,x_2,x_3)+\frac{7!\lambda_1^g}{9}x_1^2x_2x_3-\frac{m_q}{Mx_1}\Phi_3(x_2,x_1,x_3). \tag{6.22}$$

The values of the parameters, obtained from the QCD sum rules and lattice results, are given in the second column of Tab. 6.1. The other columns of the table contain the fit results that are going to be discussed in Sec. 6.4. Notice that no information about the transverse-momentum parameters is available. In order to fix the values of these parameters, we chose to perform a fit of the collinear unpolarized parton distribution $f_1(x)$ for the up and down quark, as well as for the gluon. Before presenting the results of the fit, we are going to show in Sec. 6.2 the explicit LFWA overlap representations for the twist-2 T-even TMDs and in Sec. 6.3 the LFWA overlap representation for the twist-2 chiral-even GPDs. The overlap representations depend only on the chosen truncation of the Fock-state expansion, not on the specific Ansätze for the LFWAs. To obtain the PDF $f_1(x)$ is enough to perform an integration over $\boldsymbol{k}_\perp$ of the unpolarized TMD $f_1(x,\boldsymbol{k}_\perp)$. In Sec. 6.4, we are going to illustrate the results of the fit and in Sec. 6.4.2 a discussion on the numerical results for the twist-2 T-even TMDs and chiral-even GPDs is given.

6.2 Light-Front Wave Amplitude overlap representation of TMDs

The twist-2 TMD definitions were given in Sec. 3.3.2 in terms of the trace of the quark-quark correlator contracted with specific Dirac structures. We are going to obtain the LFWA overlap representation for the TMDs, by expanding

[1] We neglect the mass exponentials of Eqs. (6.13)-(6.16), and use the DAs of Eqs. (6.6)-(6.12).

the proton state in terms of the LFWAs defined above. The results of this section depend only on the truncation imposed to the Fock-state expansion (see Eq. (3.59)), but not on the specific model for the LFWAs. In this section, we are going to introduce and present the results for the LFWA overlap representation of the unpolarized and longitudinally polarized gluon TMDs. This is possible since in our model we have an intrinsic gluon contribution to the proton. To lighten the notation, we adopt the following conventions:

$$\delta_i = \delta(x - x_i)\delta(\boldsymbol{k}_\perp - \boldsymbol{k}_{\perp,i}), \tag{6.23}$$

$$\psi_{ijl} = \psi(x_i, \boldsymbol{k}_{\perp,i}, x_j, \boldsymbol{k}_{\perp,j}, x_l, \boldsymbol{k}_{\perp,l}), \quad \text{for } \psi = \psi^{(0)}, \psi^{(3)}, \psi^{(4)}, \psi^{(5)}, \tag{6.24}$$

$$\psi_{ijlm} = \psi(x_i, \boldsymbol{k}_{\perp,i}, x_j, \boldsymbol{k}_{\perp,j}, x_l, \boldsymbol{k}_{\perp,l}, x_m, \boldsymbol{k}_{\perp,m}), \quad \text{for } \psi = \Psi^{\downarrow}, \Psi^{1,\uparrow}, \Psi^{2,\uparrow}, \tag{6.25}$$

$$d\mu_N = \delta\left(1 - \sum_{i=1}^{N} x_i\right) \delta\left(\sum_{i=1}^{N} \boldsymbol{k}_{\perp,i}\right) \frac{1}{\left(2(2\pi)^3\right)^{N-1}} \prod_{i=1}^{N} \left(dx_i d\boldsymbol{k}_{\perp,i}\right). \tag{6.26}$$

In the light-cone gauge with advanced boundary conditions for the transverse components of the gauge field, the gauge-link becomes unity. However, the LFWAs acquire a complex phase that encodes the effects of the final state interactions [29, 102, 103]. For this reason we are going to present the results assuming complex LFWAs, even if we are going to discard the effect of the complex phase in our model.

$$\begin{aligned}
f_1^u/g_1^u(x, \boldsymbol{k}_\perp) = \int d\mu_3 \Bigg\{ & 2\delta_1 \left(\left|\psi^{(0)}_{123}\right|^2 + \psi^{(0)}_{123}\psi^{(0)*}_{321} \right) + (\delta_3 \pm \delta_2) \left|\psi^{(0)}_{123}\right|^2 \\
& \pm 2\delta_2 \left(k_{R,1}\psi^{(3)}_{123} + k_{R,2}\psi^{(4)}_{123}\right) \left(k_{L,1}\psi^{(3)*}_{123} + k_{L,2}\psi^{(4)*}_{123} + k_{L,1}\psi^{(3)}_{132} + k_{L,3}\psi^{(4)*}_{132}\right) \\
& + (\delta_1 \pm \delta_3) \left(k_{R,1}\psi^{(3)}_{123} + k_{R,2}\psi^{(4)}_{123}\right) \left(k_{L,1}\psi^{(3)*}_{123} + k_{L,2}\psi^{(4)*}_{123}\right) \\
& + (\delta_1 + \delta_2) k_{L,2}\psi^{(5)}_{123} \left(k_{R,2}\psi^{(5)*}_{123} + k_{R,1}\psi^{(5)*}_{213}\right) \Bigg\} \\
& + 4 \int d\mu_4 \Bigg\{ (\delta_1 + \delta_2)(2\left|\Psi^{\downarrow}_{1234}\right|^2 - \Psi^{\downarrow *}_{2134}\Psi^{\downarrow}_{1234}) + \delta_1 \Big[\pm 4|\Psi^{1,\uparrow}_{1234}|^2 \pm 4|\Psi^{2,\uparrow}_{1234}|^2 \\
& \pm 2\mathcal{R}e\left(\Psi^{1,\uparrow *}_{1324}\Psi^{2,\uparrow}_{1234} + \Psi^{2,\uparrow *}_{1324}\Psi^{1,\uparrow}_{1234}\right) \mp \Psi^{1,\uparrow *}_{3214}\Psi^{1,\uparrow}_{1234} \mp \Psi^{2,\uparrow *}_{2134}\Psi^{2,\uparrow}_{1234} \mp 2\Psi^{2,\uparrow *}_{3124}\Psi^{1,\uparrow}_{1234} \\
& \mp 2\Psi^{1,\uparrow *}_{2314}\Psi^{2,\uparrow}_{1234} \Big] + \delta_2 \Big[2|\Psi^{1,\uparrow}_{1234}|^2 \pm 2|\Psi^{2,\uparrow}_{1234}|^2 + \Psi^{2,\uparrow *}_{1324}\Psi^{1,\uparrow}_{1234} \mp 2\Psi^{1,\uparrow *}_{2314}\Psi^{2,\uparrow}_{1234} \\
& \pm \Psi^{1,\uparrow *}_{1324}\Psi^{2,\uparrow}_{1234} \mp \Psi^{2,\uparrow *}_{2134}\Psi^{2,\uparrow}_{1234} \Big] + \delta_3 \Big[2|\Psi^{2,\uparrow}_{1234}|^2 \pm 2|\Psi^{1,\uparrow}_{1234}|^2 + \Psi^{1,\uparrow *}_{1324}\Psi^{2,\uparrow}_{1234} \\
& \mp \Psi^{1,\uparrow *}_{3214}\Psi^{1,\uparrow}_{1234} \mp 2\Psi^{2,\uparrow}_{3124}\Psi^{1,\uparrow}_{1234} \pm \Psi^{2,\uparrow *}_{1324}\Psi^{1,\uparrow}_{1234} \Big] \Bigg\},
\end{aligned} \tag{6.27}$$

$$\begin{aligned}
f_1^d/g_1^d(x, \boldsymbol{k}_\perp) = \int d\mu_3 \Bigg\{ & \pm \delta_2 \left(\left|\psi^{(0)}_{123}\right|^2 + \psi^{(0)}_{123}\psi^{(0)*}_{321} \right) + \delta_3 \left|\psi^{(0)}_{123}\right|^2 \\
& + \delta_1 \left(k_{R,1}\psi^{(3)}_{123} + k_{R,2}\psi^{(4)}_{123}\right) \left(k_{L,1}\psi^{(3)*}_{123} + k_{L,2}\psi^{(4)*}_{123} + k_{L,1}\psi^{(3)}_{132} + k_{L,3}\psi^{(4)*}_{132}\right)
\end{aligned}$$

$$
\begin{aligned}
&\pm \delta_3 \left(k_{R,1}\psi^{(3)}_{123} + k_{R,2}\psi^{(4)}_{123}\right)\left(k_{L,1}\psi^{(3)*}_{123} + k_{L,2}\psi^{(4)*}_{123}\right)\\
&+ \delta_3 k_{L,2}\psi^{(5)}_{123}\left(k_{R,2}\psi^{(5)*}_{123} + k_{R,1}\psi^{(5)*}_{213}\right)\Bigg\}\\
&+ 4\int d\mu_4 \Bigg\{ \delta_3 (2\left|\Psi^{\downarrow}_{1234}\right|^2 - \Psi^{\downarrow *}_{2134}\Psi^{\downarrow}_{1234}) + \delta_2\Big[2|\Psi^{1,\uparrow}_{1234}|^2 \pm 2|\Psi^{2,\uparrow}_{1234}|^2 - \Psi^{1,\uparrow *}_{3214}\Psi^{1,\uparrow}_{1234}\\
&+ \Psi^{2,\uparrow *}_{1324}\Psi^{1,\uparrow}_{1234} \pm \Psi^{1,\uparrow *}_{1324}\Psi^{2,\uparrow}_{1234} - 2\Psi^{2,\uparrow *}_{3124}\Psi^{1,\uparrow}_{1234}\Big] + \delta_3\Big[2|\Psi^{2,\uparrow}_{1234}|^2 \pm 2|\Psi^{1,\uparrow}_{1234}|^2\\
&+ \Psi^{1,\uparrow *}_{1324}\Psi^{2,\uparrow}_{1234} \pm \Psi^{2,\uparrow *}_{1324}\Psi^{1,\uparrow}_{1234} - 2\Psi^{1,\uparrow *}_{2314}\Psi^{2,\uparrow}_{1234} - \Psi^{2,\uparrow *}_{2134}\Psi^{2,\uparrow}_{1234}\Big]\Bigg\},
\end{aligned}
\tag{6.28}
$$

$$
\begin{aligned}
h_1^u(x,\boldsymbol{k}_\perp) = 2\int d\mu_3 \Bigg\{ &\delta_3 \psi^{(0)*}_{312}\psi^{(0)}_{123} + \delta_1 \psi^{(0)}_{123}\left(2\psi^{(0)*}_{132} + \psi^{(0)*}_{231}\right)\\
&- 2\delta_1\left(k_{R,2}\psi^{(5)}_{123} + k_{R,1}\psi^{(5)}_{213}\right)\left(k_{L,1}\psi^{(3)*}_{123} + k_{L,2}\psi^{(4)*}_{123}\right)\Bigg\}\\
- 4\int d\mu \Bigg\{ &\delta_2\Big[2\Psi^{\downarrow *}_{1234}\Psi^{1,\uparrow}_{1234} - \Psi^{\downarrow *}_{2134}\Psi^{1,\uparrow}_{1234}\Big] + \delta_3\Big[\Psi^{\downarrow *}_{3124}\Psi^{2,\uparrow}_{1234} + \Psi^{\downarrow *}_{1324}\Psi^{2,\uparrow}_{1234}\Big]\Bigg\},
\end{aligned}
\tag{6.29}
$$

$$
\begin{aligned}
h_1^d(x,\boldsymbol{k}_\perp) = 2\int d\mu_3 \Bigg\{ &\delta_3\left(-\psi^{(0)*}_{213}\psi^{(0)}_{123}\right)\\
&+ 2\delta_3\left(k_{R,2}\psi^{(5)}_{123} + k_{R,1}\psi^{(5)}_{213}\right)\left(k_{L,3}\psi^{(3)*}_{321} + k_{L,2}\psi^{(4)*}_{321}\right)\Bigg\}\\
+ 4\int d\mu_4 \Bigg\{ &\delta_2\left(2\Psi^{\downarrow *}_{1324}\Psi^{1,\uparrow}_{1234} - \Psi^{\downarrow *}_{3124}\Psi^{1,\uparrow}_{1234}\right) + \delta_3\left(\Psi^{\downarrow *}_{1234}\Psi^{2,\uparrow}_{1234} - 2\Psi^{\downarrow *}_{2134}\Psi^{2,\uparrow}_{1234}\right)\Bigg\}.
\end{aligned}
\tag{6.30}
$$

Incidentally, we note that we have a different sign for the gluon part of h_1 compared to the results for the collinear version $h_1(x)$ given in Ref. [68]. This is due to a sign mistake in Ref. [68] for the three-quark plus one-gluon state $|P,\downarrow\rangle$.

The TMDs so far presented are the only ones that survive the collinear limit, leading to the PDFs f_1, g_1 and h_1, respectively. The other TMDs, albeit they can have non-vanishing $\boldsymbol{k}_\perp$ integrals, appear in the quark-quark correlator expansion with pre-factors that contain odd powers of $\boldsymbol{k}_\perp$. This leads to the vanishing contribution of the following TMDs to the collinear parton correlator:

$$
\begin{aligned}
g^u_{1T}(x,\boldsymbol{k}_\perp) = -\frac{2M}{\boldsymbol{k}^2_\perp}\sum_{j=1,2} k^j \int d\mu_3 \Bigg\{ &\delta_1 \psi^{(0)*}_{123}\left(k_2^j\psi^{(3)}_{213} + k_1^j\psi^{(4)}_{213}\right)\\
&- \delta_2\psi^{(0)}_{123}\left(k_2^j\psi^{(3)*}_{213} + k_1^j\psi^{(4)*}_{213}\right)
\end{aligned}
$$

$$+ (\delta_1 + \delta_3)\, \psi^{(0)*}_{123} \left(k_2^j \psi^{(3)}_{213} + k_1^j \psi^{(4)}_{213} + k_2^j \psi^{(3)}_{231} + k_3^j \psi^{(4)}_{231} \right) \Bigg\}, \tag{6.31}$$

$$g^d_{1T}(x, \boldsymbol{k}_\perp) = -\frac{2M}{\boldsymbol{k}_\perp^2} \sum_{j=1,2} k^j \int d\mu_3 \Bigg\{ \delta_3 \psi^{(0)*}_{123} \left(k_2^j \psi^{(3)*}_{213} + k_1^j \psi^{(4)*}_{213} \right)$$

$$- \delta_2 \psi^{(0)}_{123} \left(k_2^j \psi^{(3)*}_{213} + k_1^j \psi^{(4)*}_{213} + k_2^j \psi^{(3)*}_{231} + k_3^j \psi^{(4)*}_{231} \right) \Bigg\}, \tag{6.32}$$

$$h^u_{1L}(x, \boldsymbol{k}_\perp) = \sum_{j=1,2} \frac{2Mk^j}{\Lambda \boldsymbol{k}_\perp^2} \int d\mu_3 \Bigg\{ \delta_1 \psi^{(0)}_{123} \Big(k_3^j \psi^{(3)*}_{321} + k_2^j \psi^{(4)*}_{321} + k_3^j \psi^{(3)*}_{312} + k_1^j \psi^{(4)*}_{312} \Big)$$

$$+ \delta_2 \left(k_1^j \psi^{(3)*}_{123} + k_2^j \psi^{(4)*}_{123} \right) \left(\psi^{(0)}_{132} + \psi^{(0)}_{231} \right) + k_2^j \psi^{(5)*}_{123} \psi^{(0)}_{123} \Bigg\}, \tag{6.33}$$

$$h^d_{1L}(x, \boldsymbol{k}_\perp) = -\sum_{j=1,2} \frac{2Mk^j}{\Lambda \boldsymbol{k}_\perp^2} \int d\mu_3 \Bigg\{ \delta_3 \psi^{(0)}_{123} \left(k_1^j \psi^{(3)*}_{123} + k_2^j \psi^{(4)*}_{123} \right)$$

$$+ \delta_2 \psi^{(0)}_{123} \left(k_3^j \psi^{(5)*}_{132} + k_1^j \psi^{(5)*}_{312} \right) \Bigg\}, \tag{6.34}$$

$$(h^\perp_{1T})^u(x, \boldsymbol{k}_\perp) = \frac{2M^2}{(k^2)^2 - (k^1)^2} \int d\mu_3 2\delta_2 \Bigg\{ \left(k_{R,1} \psi^{(3)}_{123} + k_{R,2} \psi^{(4)}_{123} \right)$$

$$\times \left(k_{R,3} \psi^{(3)*}_{321} + k_{R,2} \psi^{(4)*}_{321} + k_{R,3} \psi^{(3)*}_{312} + k_{R,1} \psi^{(4)*}_{312} \right) \Bigg\}, \tag{6.35}$$

$$(h^\perp_{1T})^d(x, \boldsymbol{k}_\perp) = -\frac{2M^2}{(k^2)^2 - (k^1)^2} \int d\mu_3 \delta_3 \Bigg\{ \left(k_{R,1} \psi^{(3)}_{123} + k_{R,2} \psi^{(4)}_{123} \right)$$

$$\times \left(k_{R,2} \psi^{(3)*}_{213} + k_{R,1} \psi^{(4)*}_{213} \right) \Bigg\}. \tag{6.36}$$

To conclude this section, we are going to give the results for the unpolarized and longitudinally polarized gluon TMDs. They are defined in terms of the gluon-gluon correlator as follows:

$$f_1^g(x, \boldsymbol{k}_\perp) = -g_{\perp,ij} \Phi^{g,ji}(x, \boldsymbol{k}_\perp) = \sum_{a=1}^{8} \sum_{i=1}^{2} \frac{1}{xP^+} \int \frac{d\xi^- d\boldsymbol{\xi}_\perp}{(2\pi)^3} e^{ik\cdot\xi}$$

$$\times \langle P, S | \mathcal{W} \left(\frac{\xi}{2}, -\frac{\xi}{2} \right) F_a^{+i} \left(-\frac{\xi}{2} \right) \mathcal{W} \left(-\frac{\xi}{2}, \frac{\xi}{2} \right) F_a^{+i} \left(\frac{\xi}{2} \right) | P, S \rangle \Big|_{\xi^+ = 0}, \tag{6.37}$$

$$g_1^g(x, \boldsymbol{k}_\perp) = -i\varepsilon_\perp^{ij} \Phi^{g,ji}(x, \boldsymbol{k}_\perp) = \sum_{a=1}^{8} \frac{1}{xP^+} \int \frac{d\xi^- d\boldsymbol{\xi}_\perp}{(2\pi)^3} e^{ik\cdot\xi}\ i\varepsilon_\perp^{ij}$$

$$\times \langle P, S | \mathcal{W} \left(\frac{\xi}{2}, -\frac{\xi}{2} \right) F_a^{+i} \left(-\frac{\xi}{2} \right) \mathcal{W} \left(-\frac{\xi}{2}, \frac{\xi}{2} \right) F_a^{+j} \left(\frac{\xi}{2} \right) | P, S \rangle \Big|_{\xi^+ = 0}, \tag{6.38}$$

where $g_\perp^{ij} = -\delta^{i1}\delta^{j1} - \delta^{i2}\delta^{j2}$, being δ^{ij} the Kronecker symbol.

We notice that the gluon TMDs (and all the gluon distributions in general) are defined with two gauge links in the adjoint representation. Usually three distinct type of gluon distributions are identified, each one associated with a specific combination of paths for the gauge links: both links being SIDIS-like, both links being Drell-Yan-like and one link being Drell-Yan-like and the other one being SIDIS-like (see Fig. 6.1). Which specific gauge link to use is determined by the process in which the gluon TMDs enter. We are going to ignore the gauge-link part, as we did for the quark TMDs. We obtain the following LFWA overlap representation:

$$\begin{aligned} f_1^g/g_1^g(x,\boldsymbol{k}_\perp) = 4\int d\mu_4\delta_4 \;\Big\{ &\pm 2|\Psi^{\downarrow}_{1234}|^2 \mp \Psi^{\downarrow *}_{2134}\Psi^{\downarrow}_{1234} + 4|\Psi^{1,\uparrow}_{1234}|^2 - \Psi^{1,\uparrow *}_{3214}\Psi^{1,\uparrow}_{1234} \\ &+ 4|\Psi^{2,\uparrow}_{1234}|^2 - \Psi^{2,\downarrow *}_{2134}\Psi^{2,\uparrow}_{1234} + 2\Psi^{1,\uparrow *}_{1324}\Psi^{2,\uparrow}_{1234} + 2\Psi^{2,\uparrow *}_{1324}\Psi^{1,\uparrow}_{1234} \\ &- 2\Psi^{1,\uparrow *}_{2314}\Psi^{2,\uparrow}_{1234} - 2\Psi^{2,\uparrow *}_{2314}\Psi^{1,\uparrow}_{1234} \Big\}. \end{aligned} \tag{6.39}$$

All the results shown in this section can prove useful for combined phenomenological analysis of TMDs and PDFs, since all these distributions are obtained by the overlap of the same LFWAs in different kinematical domains. We will give an idea of how this process might work in Sec. 6.4.2, by using the simple polynomial model for the LFWAs illustrated in Sec. 6.1.

6.3 Light-Front Wave Amplitude overlap representation of GPDs

As we did for the TMDs in the previous section, we are going to give explicit results for the LFWA overlap representation of the twist-2 chiral-even GPDs. It will be clear how the GPDs E and $\tilde{E}$ connect LFWAs for Fock states with different values of L_z. The GPD E can be used to extract information on the total angular momentum carried by the quarks [51], see Eq. (3.55). We recall the GPD definitions given in Sec. 3.3.3:

$$\begin{aligned} F_{\Lambda'\Lambda}(x,\xi,t) &= \frac{1}{2}\int \frac{dz^-}{2\pi} e^{iz^- xP^+} \langle p',\Lambda'|\,\bar{\psi}(0)\gamma^+\psi(z)\,|p,\Lambda\rangle\,|_{z^+=\boldsymbol{z}_\perp=0} \\ &= \frac{1}{2P^+}\bar{u}(p',\Lambda')\left(\gamma^+ H(x,\xi,t) + \frac{i\sigma^{+\Delta}}{2M}E(x,\xi,t)\right)u(p,\Lambda), \end{aligned} \tag{6.40}$$

$$\begin{aligned} \tilde{F}_{\Lambda'\Lambda}(x,\xi,t) &= \frac{1}{2}\int \frac{dz^-}{2\pi} e^{iz^- xP^+} \langle p',\Lambda'|\,\bar{\psi}(0)\gamma^+\gamma_5\psi(z)\,|p,\Lambda\rangle\,|_{z^+=\boldsymbol{z}_\perp=0} \\ &= \frac{1}{2P^+}\bar{u}(p',\Lambda')\left(\gamma^+\gamma_5 \tilde{H}(x,\xi,t) + \frac{\Delta^+\gamma_5}{2M}\tilde{E}(x,\xi,t)\right)u(p,\Lambda). \end{aligned} \tag{6.41}$$

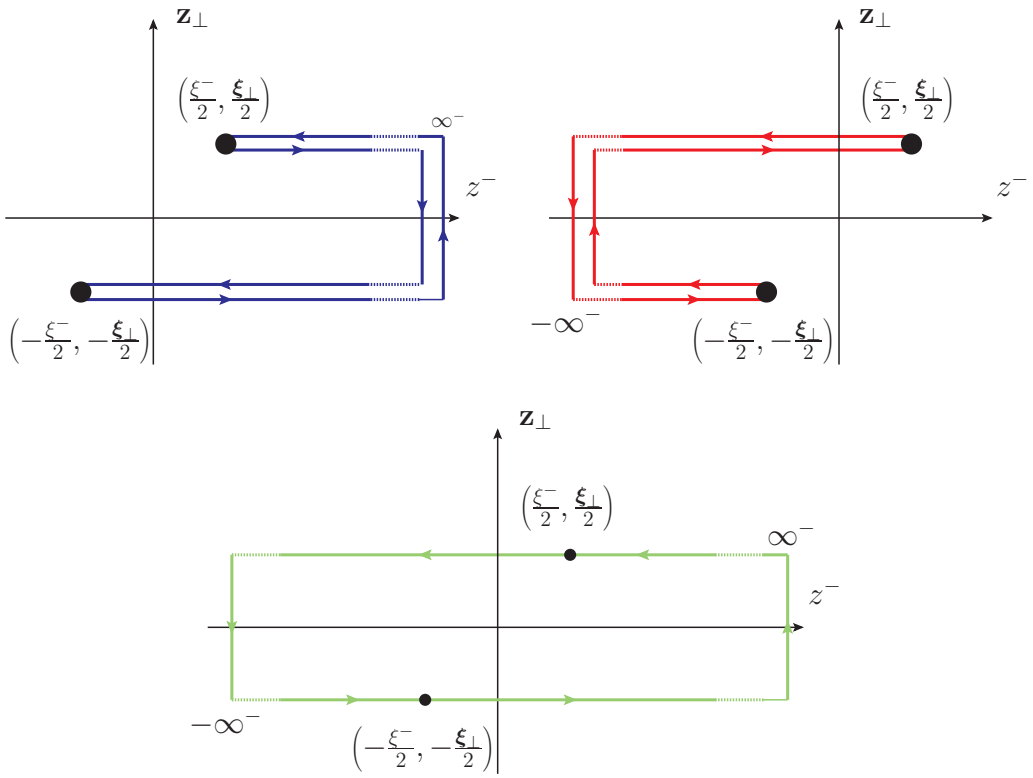

Figure 6.1: Possible gauge-link paths for the gluon TMDs. The double SIDIS-like link is in top left, the double DY-like link is in the top right and the mixed one is at the bottom.

In the following, we will give the LFWA overlap representation of the helicity amplitudes, that appears more simple than in the GPD case. The GPDs can then be obtained from the following combination of helicity amplitudes, see, e.g., Ref. [21]:

$$H(x,\xi,t) = \frac{1}{\sqrt{1-\xi^2}}\left(F_{++}(x,\xi,t) + \frac{2M\xi^2}{\eta\sqrt{t_0-t}\sqrt{1-\xi^2}}F_{-+}(x,\xi,t)\right), \quad (6.42)$$

$$E(x,\xi,t) = \frac{2M}{\eta\sqrt{t_0-t}}F_{-+}(x,\xi,t), \quad (6.43)$$

$$\tilde{H}(x,\xi,t) = \frac{1}{\sqrt{1-\xi^2}}\left(\tilde{F}_{++}(x,\xi,t) + \frac{2M\xi}{\eta\sqrt{t_0-t}\sqrt{1-\xi^2}}\tilde{F}_{-+}(x,\xi,t)\right), \quad (6.44)$$

$$\tilde{E}(x,\xi,t) = \frac{2M}{\eta\xi\sqrt{t_0-t}}\tilde{F}_{-+}(x,\xi,t), \quad (6.45)$$

where we defined:

$$-t_0 = \min_{\boldsymbol{\Delta}_\perp}(-t) = \frac{4\xi^2M^2}{1-\xi^2}, \quad \eta = \frac{\Delta_R}{\sqrt{\boldsymbol{\Delta}_\perp^2}}. \quad (6.46)$$

We notice how each GPD is in one-to-one correspondence with a specific helicity amplitude in the limit of vanishing skewness ($\xi = 0$).

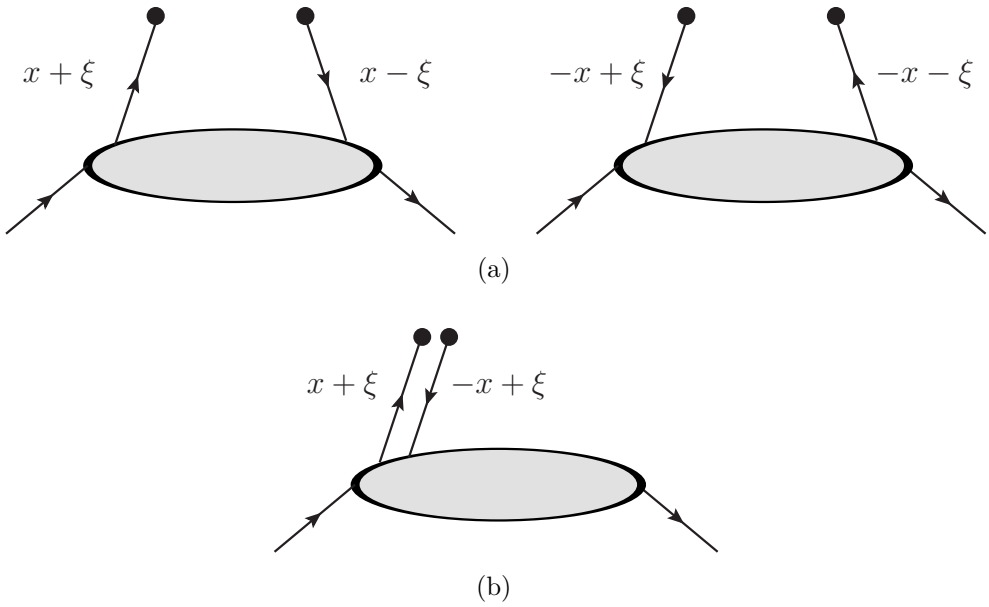

Figure 6.2: Different possible diagrams for the quark GPDs with $\xi > 0$. The diagrams (a) represent the GPDs in the DGLAP region, in which a quark ($x > \xi > 0$) or an antiquark ($x < -\xi < 0$) is emitted from the proton and reabsorbed after the hard scattering (represented with the black dots). The diagram (b) represents the GPDs in the ERBL region, in which a quark-antiquark pair is extracted from the proton ($-\xi < x < \xi$). We refer to the main text for a broader discussion about the two regions.

The helicity amplitudes satisfy the following constraints:

$$F_{++}(x,\xi,t) = F_{--}(x,\xi,t), \quad F_{+-}(x,\xi,t) = -F^*_{-+}(x,\xi,t), \tag{6.47}$$

$$\tilde{F}_{++}(x,\xi,t) = -\tilde{F}_{--}(x,\xi,t), \quad \tilde{F}_{+-}(x,\xi,t) = \tilde{F}^*_{-+}(x,\xi,t). \tag{6.48}$$

Therefore, out of the eight possible helicity amplitudes, only four are independent, consistently with the number of independent GPDs.

General results for the overlap representation of the GPDs in terms of LFWFs are known for a very long time now, see Refs. [21, 97, 98, 112]. It is also a commonly known fact that the skewness variable[2] ξ identifies two distinct regions in x, namely $R_{\rm DGLAP} = \{x \in (-1,1) : |x| > \xi\}$ and $R_{\rm ERBL} = \{x \in (-1,1) : |x| < \xi\}$. The LFWF representation of the GPDs allows us to investigate the differences between the two regions. In the first one, i.e. $R_{\rm DGLAP}$, the GPDs are obtained from the diagrams in Fig. 6.2a. In the region $\xi < x < 1$, the process is described as the emission of a quark with momentum fraction $x+\xi$ from the proton and the absorption of a quark with momentum fraction $x-\xi$. In the region $-1 < x < -\xi$, the process is described as the emission of an antiquark with momentum fraction $-x-\xi$ from the proton and

[2]In all known processes where GPDs may be measured one has $\xi \geq 0$, which we will tacitly assume unless otherwise specified.

the absorption of an antiquark with momentum fraction $-x+\xi$. These regions are named DGLAP, since here the GPDs evolve to different scales through the DGLAP evolution equations. As clear from the description above, in the Fock-state decompositions of the initial and final proton states, we have only terms that have the same parton content, i.e. the GPDs in the DGLAP region are diagonal in the Fock space. In the second region, R_{ERBL}, we extract from the proton a quark-antiquark pair and we annihilate it in the hard-scattering part of the process. The diagram that corresponds to the ERBL region is shown in Fig. 6.2b. In the Fock-state decompositions of the initial and final proton states, we have only terms where the parton content of the initial and final state differs for a quark-antiquark pair. Therefore, the GPDs in the ERBL region are not diagonal in the Fock space. Also for the ERBL region the name derives from the evolution equation that are used to evolve the GPDs to different scales, see Refs. [113, 114]. Some information on the GPDs in the ERBL region can be extracted from the DGLAP region by exploiting the connection between GPDs and double parton distributions, see Refs. [115–117]. We will restrict ourself to the DGLAP region in the remaining of this Chapter, because in our model we do not consider the three-quark plus the quark-antiquark pair state, hence we cannot explicitly compute the ERBL region contribution.

Finally, before being able to obtain explicit results, we must fix a reference frame, i.e. we must fix the convention of how to split the transferred momentum Δ between the initial and final proton states. Two common choices exist: the photon-proton center of mass frame and the symmetric frame, see Ref. [20]. We choose to work with the symmetric frame, in which the initial-state partonic variables read:

$$\begin{aligned} x_i &= \frac{\bar{x}_i+\xi}{1+\xi}, \quad \boldsymbol{k}_{\perp,i} = \boldsymbol{\kappa}_{\perp,i} - \frac{1-\bar{x}_i}{1+\xi}\frac{\boldsymbol{\Delta}_\perp}{2}, \quad \text{active quark}, \\ x_i &= \frac{\bar{x}_i}{1+\xi}, \quad \boldsymbol{k}_{\perp,i} = \boldsymbol{\kappa}_{\perp,i} + \frac{\bar{x}_i}{1+\xi}\frac{\boldsymbol{\Delta}_\perp}{2}, \quad \text{spectator quark}, \end{aligned} \tag{6.49}$$

and the final-state partonic variables are

$$\begin{aligned} \hat{x}_i &= \frac{\bar{x}_i-\xi}{1-\xi}, \quad \hat{\boldsymbol{k}}_{\perp,i} = \boldsymbol{\kappa}_{\perp,i} + \frac{1-\bar{x}_i}{1-\xi}\frac{\boldsymbol{\Delta}_\perp}{2}, \quad \text{active quark}, \\ \hat{x}_i &= \frac{\bar{x}_i}{1-\xi}, \quad \hat{\boldsymbol{k}}_{\perp,i} = \boldsymbol{\kappa}_{\perp,i} - \frac{\bar{x}_i}{1-\xi}\frac{\boldsymbol{\Delta}_\perp}{2}, \quad \text{spectator quark}, \end{aligned} \tag{6.50}$$

where $\bar{x}_i$ and $\boldsymbol{\kappa}_{\perp,i}$ are the average fraction of longitudinal momentum and the average transverse momentum of the partons, respectively[3].

To facilitate the reading, we use the shorthand notations:

$$d\bar{\mu}_N = \delta\left(1-\sum_{i=1}^{N}\bar{x}_i\right)\delta\left(\sum_{i=1}^{N}\boldsymbol{\kappa}_{\perp,i}\right)\frac{1}{(2(2\pi)^3)^{N-1}}\prod_{i=1}^{N}\left(d\bar{x}_i d\boldsymbol{\kappa}_{\perp,i}\right), \tag{6.51}$$

[3]The average fraction longitudinal of momentum is defined as the the average plus momentum of the partons divided by the average plus momentum P^+ of the proton.

and

$$\psi^{(34)}_{123} = k_{1,R}\psi^{(3)}_{123} + k_{2,R}\psi^{(4)}_{123},$$
$$\tilde{\psi}^{(34)}_{123} = k_{1,L}\psi^{(3)}_{123} + k_{2,L}\psi^{(4)}_{123}, \quad \tilde{\psi}^{(5)}_{123} = k_{2,L}\psi^{(5)}_{123}.$$

The results for the quark helicity-conserving amplitudes read:

$$F^u_{++,L=0}\left(\tilde{F}^u_{++,L=0}\right) = \int \frac{d\bar{\mu}_3}{\sqrt{1-\xi^2}}\Bigg\{\delta_1\psi^{(0)}_{123}\left(2\psi^{(0)*}_{\hat{1}\hat{2}\hat{3}} + \psi^{(0)*}_{\hat{3}\hat{2}\hat{1}}\right) + \delta_3\psi^{(0)}_{123}\left(\psi^{(0)*}_{\hat{1}\hat{2}\hat{3}} + \psi^{(0)*}_{\hat{3}\hat{2}\hat{1}}\right) \pm \delta_2\psi^{(0)}_{123}\psi^{(0)*}_{\hat{1}\hat{2}\hat{3}}\Bigg\}, \tag{6.52}$$

$$F^d_{++,L=0}\left(\tilde{F}^d_{++,L=0}\right) = \int \frac{d\bar{\mu}_3}{\sqrt{1-\xi^2}}\Bigg\{\delta_3\psi^{(0)}_{123}\psi^{(0)*}_{\hat{1}\hat{2}\hat{3}} \pm \delta_2\psi^{(0)}_{123}\left(\psi^{(0)*}_{\hat{1}\hat{2}\hat{3}} + \psi^{(0)*}_{\hat{3}\hat{2}\hat{1}}\right)\Bigg\}, \tag{6.53}$$

$$F^u_{++,L=1}\left(\tilde{F}^u_{++,L=1}\right) = \int \frac{d\bar{\mu}_3}{\sqrt{1-\xi^2}}\Bigg\{\left(\delta_1 \pm \delta_2\right)\psi^{(34)}_{123}\psi^{(34)*}_{\hat{1}\hat{2}\hat{3}} \pm \left(\delta_2 + \delta_3\right)\psi^{(34)}_{123}\left(\psi^{(34)*}_{\hat{1}\hat{2}\hat{3}} + \psi^{(34)*}_{\hat{1}\hat{3}\hat{2}}\right)\Bigg\}, \tag{6.54}$$

$$F^d_{++,L=1}\left(\tilde{F}^d_{++,L=1}\right) = \int \frac{d\bar{\mu}_3}{\sqrt{1-\xi^2}}\Bigg\{\left(\delta_1 \pm \delta_3\right)\psi^{(34)}_{123}\psi^{(34)*}_{\hat{1}\hat{2}\hat{3}} + \delta_1\psi^{(34)}_{123}\psi^{(34)*}_{\hat{1}\hat{3}\hat{2}}\Bigg\}, \tag{6.55}$$

$$F^u_{++,L=-1}\left(\tilde{F}^u_{++,L=-1}\right) = \int \frac{d\bar{\mu}_3}{\sqrt{1-\xi^2}}\Bigg\{\left(\delta_1 + \delta_2\right)\tilde{\psi}^{(5)}_{123}\left(\tilde{\psi}^{(5)*}_{\hat{1}\hat{2}\hat{3}} + \tilde{\psi}^{(5)*}_{\hat{2}\hat{1}\hat{3}}\right)\Bigg\}, \tag{6.56}$$

$$F^d_{++,L=-1}\left(\tilde{F}^d_{++,L=-1}\right) = \int \frac{d\bar{\mu}_3}{\sqrt{1-\xi^2}}\Bigg\{\delta_3\tilde{\psi}^{(5)}_{123}\left(\tilde{\psi}^{(5)*}_{\hat{1}\hat{2}\hat{3}} + \tilde{\psi}^{(5)*}_{\hat{2}\hat{1}\hat{3}}\right)\Bigg\}, \tag{6.57}$$

$$F^u_{++,g\downarrow}\left(\tilde{F}^u_{++,g\downarrow}\right) = 4\int \frac{d\bar{\mu}_4}{1-\xi^2}\Bigg\{\left(\delta_1 + \delta_2\right)\Psi^{\downarrow}_{1234}\left(2\Psi^{\downarrow *}_{\hat{1}\hat{2}\hat{3}\hat{4}} - \Psi^{\downarrow *}_{\hat{2}\hat{1}\hat{3}\hat{4}}\right)\Bigg\}, \tag{6.58}$$

$$F^d_{++,g\downarrow}\left(\tilde{F}^d_{++,g\downarrow}\right) = 4\int \frac{d\bar{\mu}_4}{1-\xi^2}\Bigg\{\delta_3\Psi^{\downarrow}_{1234}\left(2\Psi^{\downarrow *}_{\hat{1}\hat{2}\hat{3}\hat{4}} - \Psi^{\downarrow *}_{\hat{2}\hat{1}\hat{3}\hat{4}}\right)\Bigg\}, \tag{6.59}$$

$$\begin{aligned} F^u_{++,g\uparrow}\left(\tilde{F}^u_{++,g\uparrow}\right) = 4\int \frac{d\bar{\mu}_4}{1-\xi^2}\Bigg\{&\delta_1\Big[\pm 4\Psi^{1,\uparrow}_{1234}\Psi^{1,\uparrow *}_{\hat{1}\hat{2}\hat{3}\hat{4}} \\ &\pm 4\Psi^{2,\uparrow}_{1234}\Psi^{2,\uparrow *}_{\hat{1}\hat{2}\hat{3}\hat{4}} \pm 2\mathcal{R}e\left(\Psi^{1,\uparrow *}_{\hat{1}\hat{3}\hat{2}\hat{4}}\Psi^{2,\uparrow}_{1234} + \Psi^{2,\uparrow *}_{\hat{1}\hat{3}\hat{2}\hat{4}}\Psi^{1,\uparrow}_{1234}\right) \\ &\mp \Psi^{1,\uparrow *}_{\hat{3}\hat{2}\hat{1}\hat{4}}\Psi^{1,\uparrow}_{1234} \mp \Psi^{2,\uparrow *}_{\hat{2}\hat{1}\hat{3}\hat{4}}\Psi^{2,\uparrow}_{1234} \mp 2\Psi^{2,\uparrow *}_{\hat{3}\hat{1}\hat{2}\hat{4}}\Psi^{1,\uparrow}_{1234} \mp 2\Psi^{1,\uparrow *}_{\hat{2}\hat{3}\hat{1}\hat{4}}\Psi^{2,\uparrow}_{1234}\Big] \\ &+ \delta_2\Big[2\Psi^{1,\uparrow}_{1234}\Psi^{1,\uparrow *}_{\hat{1}\hat{2}\hat{3}\hat{4}} \pm 2\Psi^{2,\uparrow}_{1234}\Psi^{2,\uparrow *}_{\hat{1}\hat{2}\hat{3}\hat{4}}\end{aligned}$$

$$
\begin{aligned}
&+ \Psi^{2,\uparrow *}_{\hat{1}\hat{3}\hat{2}\hat{4}} \Psi^{1,\uparrow}_{1234} \mp 2\Psi^{1,\uparrow *}_{\hat{2}\hat{3}\hat{1}\hat{4}} \Psi^{2,\uparrow}_{1234} \pm \Psi^{1,\uparrow *}_{\hat{1}\hat{3}\hat{2}\hat{4}} \Psi^{2,\uparrow}_{1234} \mp \Psi^{2,\uparrow *}_{\hat{2}\hat{1}\hat{3}\hat{4}} \Psi^{2,\uparrow}_{1234} \Big] \\
&+ \delta_3 \Big[2\Psi^{2,\uparrow}_{1234} \Psi^{2,\uparrow *}_{\hat{1}\hat{2}\hat{3}\hat{4}} \pm 2\Psi^{1,\uparrow}_{1234} \Psi^{1,\uparrow *}_{\hat{1}\hat{2}\hat{3}\hat{4}} \\
&+ \Psi^{1,\uparrow *}_{\hat{1}\hat{3}\hat{2}\hat{4}} \Psi^{2,\uparrow}_{1234} \mp \Psi^{1,\uparrow *}_{\hat{3}\hat{2}\hat{1}\hat{4}} \Psi^{1,\uparrow}_{1234} \mp 2\Psi^{2,\uparrow}_{\hat{3}\hat{1}\hat{2}\hat{4}} \Psi^{1,\uparrow}_{1234} \pm \Psi^{2,\uparrow *}_{\hat{1}\hat{3}\hat{2}\hat{4}} \Psi^{1,\uparrow}_{1234} \Big] \Bigg\},
\end{aligned}
\tag{6.60}
$$

$$
\begin{aligned}
F^{d}_{++,g\uparrow}\left(\tilde{F}^{d}_{++,g\uparrow}\right) = 4 \int \frac{d\bar{\mu}_4}{1-\xi^2} \Bigg\{ & \delta_2 \Big[2\Psi^{1,\uparrow}_{1234} \Psi^{1,\uparrow *}_{\hat{1}\hat{2}\hat{3}\hat{4}} \pm 2\Psi^{2,\uparrow}_{1234} \Psi^{2,\uparrow *}_{\hat{1}\hat{2}\hat{3}\hat{4}} \\
&- \Psi^{1,\uparrow *}_{\hat{3}\hat{2}\hat{1}\hat{4}} \Psi^{1,\uparrow}_{1234} + \Psi^{2,\uparrow *}_{\hat{1}\hat{3}\hat{2}\hat{4}} \Psi^{1,\uparrow}_{1234} \pm \Psi^{1,\uparrow *}_{\hat{1}\hat{3}\hat{2}\hat{4}} \Psi^{2,\uparrow}_{1234} - 2\Psi^{2,\uparrow *}_{\hat{3}\hat{1}\hat{2}\hat{4}} \Psi^{1,\uparrow}_{1234} \Big] \\
&+ \delta_3 \Big[2\Psi^{2,\uparrow}_{1234} \Psi^{2,\uparrow *}_{\hat{1}\hat{2}\hat{3}\hat{4}} \pm 2\Psi^{1,\uparrow}_{1234} \Psi^{1,\uparrow *}_{\hat{1}\hat{2}\hat{3}\hat{4}} + \Psi^{1,\uparrow *}_{\hat{1}\hat{3}\hat{2}\hat{4}} \Psi^{2,\uparrow}_{1234} \\
&\pm \Psi^{2,\uparrow *}_{\hat{1}\hat{3}\hat{2}\hat{4}} \Psi^{1,\uparrow}_{1234} - 2\Psi^{1,\uparrow *}_{\hat{2}\hat{3}\hat{1}\hat{4}} \Psi^{2,\uparrow}_{1234} - \Psi^{2,\uparrow *}_{\hat{2}\hat{1}\hat{3}\hat{4}} \Psi^{2,\uparrow}_{1234} \Big] \Bigg\}.
\end{aligned}
\tag{6.61}
$$

The results for the quark helicity-flip amplitudes read:

$$
\begin{aligned}
F^{u}_{+-,L=0,L=-1}\left(\tilde{F}^{u}_{+-,L=0,L=-1}\right) = -\int \frac{d\bar{\mu}_3}{\sqrt{1-\xi^2}} \Bigg\{ & \left(\delta_2 \pm \delta_1\right) \tilde{\psi}^{(34)}_{123} \psi^{(0)*}_{\hat{2}\hat{1}\hat{3}} \\
&+ \left(\delta_2 + \delta_3\right) \tilde{\psi}^{(34)}_{123} \left(\psi^{(0)*}_{\hat{2}\hat{1}\hat{3}} + \psi^{(0)*}_{\hat{3}\hat{1}\hat{2}} \right) \Bigg\},
\end{aligned}
\tag{6.62}
$$

$$
\begin{aligned}
F^{d}_{+-,L=0,L=-1}\left(\tilde{F}^{d}_{+-,L=0,L=-1}\right) = -\int \frac{d\bar{\mu}_3}{\sqrt{1-\xi^2}} \Bigg\{ & \left(\delta_3 \pm \delta_1\right) \tilde{\psi}^{(34)}_{123} \psi^{(0)*}_{\hat{2}\hat{1}\hat{3}} \\
&\pm \delta_1 \tilde{\psi}^{(34)}_{123} \psi^{(0)*}_{\hat{3}\hat{1}\hat{2}} \Bigg\},
\end{aligned}
\tag{6.63}
$$

$$
\begin{aligned}
F^{u}_{+-,L=1,L=0}\left(\tilde{F}^{u}_{+-,L=1,L=0}\right) = \int \frac{d\bar{\mu}_3}{\sqrt{1-\xi^2}} \Bigg\{ & \left(\delta_2 \pm \delta_1\right) \psi^{(0)}_{123} \psi^{(34)*}_{\hat{2}\hat{1}\hat{3}} \\
&\pm \left(\delta_1 + \delta_3\right) \psi^{(0)}_{123} \left(\psi^{(34)*}_{\hat{2}\hat{1}\hat{3}} + \psi^{(34)*}_{\hat{2}\hat{3}\hat{1}} \right) \Bigg\},
\end{aligned}
\tag{6.64}
$$

$$
F^{d}_{+-,L=1,L=0}\left(\tilde{F}^{d}_{+-,L=1,L=0}\right) = \int \frac{d\bar{\mu}_3}{\sqrt{1-\xi^2}} \psi^{(0)}_{123} \Bigg\{ \left(\delta_3 \pm \delta_2\right) \psi^{(34)*}_{\hat{2}\hat{1}\hat{3}} + \delta_2 \psi^{(34)*}_{\hat{2}\hat{3}\hat{1}} \Bigg\}.
\tag{6.65}
$$

The pre-factors

$$
\frac{1}{\sqrt{\left(1-\xi^2\right)}^{N-2}}
\tag{6.66}
$$

that appear in front of the integrals in the previous equations are derived from

the following change of variables:

$$\int \frac{[dx]_N[d\hat{x}]_N}{\sqrt{x_1...x_N\hat{x}_1...\hat{x}_N}}\prod_{i=2}^{N} p_i^+\delta(p_i^+-\hat{p}_i^+) = \int \frac{[dx]_N[d\hat{x}]_N}{\sqrt{x_1...x_N\hat{x}_1...\hat{x}_N}}\prod_{i=2}^{N} \bar{x}_i\delta(\bar{x}_i-\bar{\hat{x}}_i)$$
$$= \int (1+\xi)^{1-N/2}\,(1-\xi)^{1-N/2}\,\frac{[d\bar{x}]_N}{\bar{x}_1^2}. \tag{6.67}$$

From the GPDs, by taking the integral over x, we can compute the electromagnetic form factors of the proton, see Fig. 3.3. The integral over x remove the ξ dependence: this follows from the Lorentz invariance, see Eq. (3.55). We have:

$$F_1^q(t) = e_q\int_{-1}^{1} dx F_{++}(x,\xi,t), \quad F_2^q(t) = 2Me_q\frac{\Delta_L}{\boldsymbol{\Delta}_\perp^2}\int_{-1}^{1} dx F_{-+}(x,\xi,t), \tag{6.68}$$

where e_q is the quark electric charge.

The GPDs at non-vanishing t give also an immediate generalization of Eq. (3.55):

$$J^q(t) = \frac{1}{2}\int_{-1}^{1} dx\; x\,(H^q(x,\xi,t)+E^q(x,\xi,t))\,. \tag{6.69}$$

At vanishing momentum transfer $t=0$ and if we sum over all the quark flavors, we must have:

$$\sum_{q=u,d,...} J^q(t=0) = \frac{1}{2} - J^g(t=0), \tag{6.70}$$

where the gluon total angular momentum is defined in a similar fashion as the quark contribution:

$$J^g = \frac{1}{2}\int_{-1}^{1} dx\,(H^g(x,\xi,t)+E^g(x,\xi,t))\,. \tag{6.71}$$

In our model, it is possible to compute only partially the gluon GPDs, since to compute E^g and $\tilde{E}^g$ it is necessary to incorporate the four-parton state with non-vanishing parton OAM. In Chapter 8, we are going to see that the total angular momentum introduced in Eq. (6.69) can be obtained directly from a local matrix element of a suitable operator.

6.4 Fit of the parameters

In this section, we are going to illustrate our fitting strategy. Despite its simplicity, our model (Eqs. (6.6)-(6.12)) is able to reproduce the main features of the parton distributions in the valence region. The model can be further refined to improve the agreement with the phenomenological extractions of the parton distributions. A refined version of the model can be used as a starting point for future combined fits of TMDs and GPDs. As anticipated, our focus will be

on the collinear and unpolarized PDF f_1. We fit the parameters of the model to the phenomenological parametrizations of the collinear parton distributions extracted from available experimental data. The fit of the model to the parametrization allows us to find the best set of parameters that are compatible with the QCD sum rules and lattice estimation. It also provides a way to fix the effective quark and gluon masses (see Eqs. (6.1)-(6.3)) and the widths of the transverse-momentum Gaussians. We chose to not compute the evolution of f_1 with the scale, because a consistent procedure would require to have a non-vanishing sea-quark contribution that is not included in our model. Among the available phenomenological parametrizations, we use the MMHT2014 [118] that provides results at the same scale of our model, i.e. $\mu = 1$ GeV. We chose to use the results of MMHT2014 at NLO. We will perform a simultaneous fit of both the quark and gluon contribution to f_1, using the results of Sec. 6.2.

In historical order, we first included in our model only the contributions that come from the $L_z = 0$ LFWAs (see Ref. [119]). The more recent development of the model allows us to include in the analysis also the LFWAs for the states with $|L_z| = 1$. The new results including the non-vanishing OAM components of the LFWFs will be presented also in a forthcoming manuscript [120].

6.4.1 Fit methodology

A variety of minimization algorithms can be applied to fit the model parameters to the experimental data. One of the most used is the gradient-descendent method. In this approach, the parameter space is explored in the opposite direction with respect to the gradient of a loss function that defines the goodness of the current set of parameters (usually a χ^2-like function). Gradient methods rely on analytical or numerical evaluations of the gradient of the loss function. In general, these types of methods work well enough, however they might fail in some situations. For example, the loss function can be almost flat or, on the opposite, it can have a large number of local minima that differ not very much from the global one (pathological situations, in which the global minima is reached for a divergent value of some parameters, are also possible). Also, gradient methods are not very suited for a problem with a high-dimensional parameter space[4]. Alternatives to the gradient methods are geometrical methods that do not require to compute the derivative of the loss function. The gold standard for geometrical minimization methods is the simplex algorithm. The simplex is a geometrical construction that is the generalization of the triangle to any dimension $d > 2$. The simplex minimization algorithm consists in a set of rules that construct the simplex in the parameter space and collapse it into the global minimum of the loss function. The simplex algorithm has the advantage of avoiding the evaluation of the derivative of the loss function. However, it is quite slow, especially for a high-dimensional parameter space. Last, a large class of Monte-Carlo based methods exists. Monte-Carlo methods are, in general, best suited for problems with high-dimensional parameter

[4] A good gradient method suited for large parameter sets is ADAM, see Ref. [121].

space. For this reason, we chose a simple version of Monte-Carlo methods, in which n parameter-configurations are sampled and the best one is selected. The best parameter configuration is defined as the one that minimizes the following χ^2-like function:

$$\begin{aligned}\chi^2 = &\sum_{i=1}^{N} \frac{\left(x_i f_1^u(x_i) - P(x_i, \text{valence up})\right)^2}{\sigma_{i,u}^2} \\ &+ \frac{\left(x_i f_1^d(x_i) - P(x_i, \text{valence down})\right)^2}{\sigma_{i,d}^2} \\ &+ \theta(x_i - 0.4)\frac{\left(x_i f_1^g(x_i) - P(x_i, \text{gluon})\right)^2}{\sigma_{i,g}^2},\end{aligned} \tag{6.72}$$

where $P(x, \text{parton})$ is the value of the MMHT2014 parametrization at NLO for $x f_1^{parton}(x)$ and σ_i is the associated error. For the points x_i we assumed an equally spaced grid:

$$x_i = \frac{i+1}{N+1}, \tag{6.73}$$

with $N = 100$. In Eq. (6.72), the gluon PDF appears only for values of $x > 0.4$, since in the mid-to-low x range our model is not able to reproduce the phenomenological behavior of the gluon distribution.

To obtain a set for one Monte-Carlo iteration, all the parameters of the DAs in Eqs. (6.6)-(6.12) are assumed to follow a gaussian distribution with mean and standard deviation equal, respectively, to the central value and the error of the QCD sum-rule or lattice evaluations (see the second column of Tab. 6.1). For the widths of the transverse-momentum gaussian functions we chose central values that are consistent with the values in Ref. [105]. The standard deviations were fixed in such a way to ensure a good variability of the parameters. A close inspection reveals that the gaussian-width parameters a_i participate in the total PDF normalization, hence it is possible a relatively narrow range of variation. The masses are sampled uniformly in the whole possible range, i.e. the quark mass is sampled in the interval

$$m_q \in \left[0, \frac{M}{3}\right], \tag{6.74}$$

and the gluon mass is sampled in the interval

$$m_g \in [0, M - 3m_q], \tag{6.75}$$

in such a way that we always ensure that $0 \leq 3m_q + m_g \leq M$. Finally, the gaussian widths a_3 and a_4 for the $L_z = 1$ state are assumed to be equal, and the same is assumed for the widths of the three-quark plus one-gluon state, i.e. we have that:

$$a_3 = a_4, \quad a_\downarrow = a_{1,2\uparrow}. \tag{6.76}$$

We performed two separate fits. First, we ignored the LFWAs for the states $|L_z| = 1$ and performed the fit only with the LFWAs for $L_z = 0$, following the analysis of Ref. [119]. The results are shown in the column labeled "Old Fit" in Tab. 6.1. Instead, in the new fit configuration, we considered also the LFWAs for the three-quark state with $|L_z| = 1$, and the results are given in the last column of Tab. 6.1. From the table, one can appreciate how the parameters that were present in both versions of the fit do not change value drastically: all the parameters in the two configurations are separated by less than one standard deviation, beside λ_3^g which varies about two standard deviations. Overall this indicates that the values of the parameters of the LFWA expansion are quite robust under different truncation of the Fock-space expansion.

Finally, in Figs. 6.3-6.4 we show the results for the fitted PDFs $xf_1(x)$ in both the old and new configuration. In Fig. 6.3 the total results for the PDFs $xf_1(x)$ are compared with the MMHT2014 parametrization. The results for the quark PDFs reproduce fairly the MMHT2014 parametrization at large x ($x \gtrapprox 0.3$), while they have a much faster fall-off for $x \to 0$ than the Regge-motivated behavior of the parametrization. We notice how the inclusion of $L_z \neq 0$ LFWAs slightly improves the behavior for medium-to-low-x, while it makes slightly worse the comparison at large x between the MMHT2014 parametrization and the model results. In Fig. 6.4 the different OAM contributions to $xf_1(x)$ are compared. One can notice how the LFWAs for $L_z \neq 0$ produce a relatively small contribution *per se*, but have a large impact on the $L_z = 0$ contributions.

6.4.2 Fit results

Using the parameters that are obtained from the fit, we can now compute all the parton distributions given in Secs. 6.2 and 6.3. First, let us start with the analysis of the norm of the proton in our model. The results are shown in Tab. 6.2. The total norm, including the states with $|L_z| = 1$, is

$$\mathcal{N} \simeq 0.645. \tag{6.77}$$

The norm gives an indication of the goodness of the approximation introduced by the truncation in the Fock expansion. For comparison, our older results, that did not include the states with non-vanishing OAM, give a norm equal to 0.56. The norm in Eq. (6.77) can be separated into the contributions from the various Fock states, with the results:

$$\begin{aligned} &\mathbb{P}_{3qg\uparrow} + \mathbb{P}_{3qg\downarrow} = 0.502, \\ &\mathbb{P}_{3q,L_z=0} = 0.120, \quad \mathbb{P}_{3q,L_z=1} = 0.004, \quad \mathbb{P}_{3q,L_z=-1} = 0.019. \end{aligned} \tag{6.78}$$

Comparing these results with the old ones from Ref. [119]:

$$\mathbb{P}_{3qg\uparrow} + \mathbb{P}_{3qg\downarrow} = 0.384, \quad \mathbb{P}_{3q,L_z=0} = 0.176, \tag{6.79}$$

we observe that even a relatively small variation in the parameters can produce a sizable effect on the norm of the different Fock-state components. Another

Parameter	Lattice/QCD sum rules	Old Fit	New Fit
f_N (GeV^2)	$5.0 \pm 0.5\ 10^{-3}$	$4.68\ 10^{-3}$	$4.92\ 10^{-3}$
f_0^-	1 ± 0.3	1.14	1.04
f_0^+	4 ± 1.5	0.5	1.87
ϕ_4^0 (GeV^2)	$-1.11 \pm 0.45\ 10^{-2}$	NA	$-1.52\ 10^{-2}$
ϕ_4^- (GeV^2)	$3.50 \pm 2.73\ 10^{-2}$	NA	$1.64\ 10^{-2}$
ϕ_4^+ (GeV^2)	$2.11 \pm 1.51\ 10^{-2}$	NA	$1.98\ 10^{-2}$
ψ_4^0 (GeV^2)	$1.58 \pm 0.45\ 10^{-2}$	NA	$1.18\ 10^{-2}$
ψ_4^- (GeV^2)	$-6.10 \pm 5.25\ 10^{-2}$	NA	$-6.88\ 10^{-2}$
ψ_4^+ (GeV^2)	$1.07 \pm 0.97\ 10^{-2}$	NA	$-0.70\ 10^{-2}$
ξ_4^0 (GeV^2)	$0.85 \pm 0.32\ 10^{-2}$	NA	$1.08\ 10^{-2}$
ξ_4^- (GeV^2)	$2.79 \pm 1.77\ 10^{-2}$	NA	$4.11\ 10^{-2}$
ξ_4^+ (GeV^2)	$0.56 \pm 0.35\ 10^{-2}$	NA	$-0.48\ 10^{-2}$
λ_1^g (GeV^2)	$2.6 \pm 1.2\ 10^{-3}$	$2.79\ 10^{-3}$	$3.11\ 10^{-3}$
λ_2^g (GeV^2)	$2.3 \pm 0.7\ 10^{-3}$	$1.33\ 10^{-3}$	$1.63\ 10^{-3}$
λ_3^g (GeV^2)	$0.54 \pm 0.2\ 10^{-3}$	$0.36\ 10^{-3}$	$0.76\ 10^{-3}$
Parameter	Initial values	Old Fit	New Fit
a_0 (GeV^{-1})	0.73 ± 0.2	0.85	0.61
a_3 (GeV^{-1})	0.5 ± 0.1	NA	0.31
a_4 (GeV^{-1})	0.5 ± 0.1	NA	a_3
a_5 (GeV^{-1})	0.5 ± 0.1	NA	0.47
$a_{1,2\uparrow}$ (GeV^{-1})	0.8 ± 0.1	0.782	0.76
$a_\downarrow$ (GeV^{-1})	0.8 ± 0.1	$a_{1,2\uparrow}$	$a_{1,2\uparrow}$
m_q (GeV)	$\left[0, \frac{M}{3}\right]$	0.161	0.149
m_g (GeV)	$[0, M - 3m_q]$	0.05	0.030

Table 6.1: Parameters of the model illustrated in Eqs. (6.6)-(6.11). The theoretical central values are shown in the top part with the associated errors and the fit results in the old configuration from Ref. [119] (only $L_z = 0$ LFWAs) and in the new configuration of this work (three-quark LFWAs with $L_z = \pm 1$ included). The bottom part of the table contains the initial guess for the parameters, the standard deviation and the fit results in the two configurations. For the masses, the uniform range of sampling is shown. In Ref. [119], $f_0^\mp$ were given as A, B.

interesting aspect to investigate are the momentum fractions carried by quarks and gluons. The average fraction of longitudinal momentum is defined via the

State	Old Fit	New Fit
$\mathbb{P}\left(\lvert 3q, L_z = 0\rangle\right)$	0.176	0.120
$\mathbb{P}\left(\lvert 3q, L_z = +1\rangle\right)$	0	0.002
$\mathbb{P}\left(\lvert 3q, L_z = -1\rangle\right)$	0	0.019
$\mathbb{P}\left(\lvert 3qg, g\uparrow\rangle\right)$	0.103	0.168
$\mathbb{P}\left(\lvert 3qg, g\downarrow\rangle\right)$	0.281	0.334

Table 6.2: Norm of the various Fock components in the old fit configuration from Ref. [119] and in the new fit configuration of the present work.

second Mellin moment of the unpolarized distribution:

$$\langle x \rangle_a = \int_0^1 dx\ x f_1^a(x), \tag{6.80}$$

where a distinguishes between the up quark, the down quark and the gluon. The results for the average longitudinal-momentum fractions are shown in Tab. 6.3 in both fit configurations and for the MMHT2014 parametrization as well. We notice that the results of the new fit are in better agreement with the phenomenological parametrization than the results from the old fit. The prediction for the gluon is still not able to correctly reproduce the phenomenological value: this is due to the fact that the model is not able to capture correctly the gluon dynamic below $x \simeq 0.4$.

	Old Fit	New Fit	valence MMHT2014 (NLO)
$\langle x \rangle_{\text{up}}$	0.305	0.339	0.346 ± 0.008
$\langle x \rangle_{\text{down}}$	0.136	0.148	0.143 ± 0.007
$\langle x \rangle_{\text{gluon}}$	0.119	0.158	0.350 ± 0.033

Table 6.3: Results for the average longitudinal-momentum fraction for the up and down quarks and for the gluon, corresponding to the configuration from Ref. [119] (second column), the new fit configuration of this work (third column) and the MMHT2014 parametrization (last column).

So far we explored mainly the x-dependence of the parton distributions. To gain information on the transverse-momentum part, it is useful to introduce the average transverse-momentum fractions. These quantities allow us to compare the spread in the transverse-momentum space of the different distributions. At variance with Ref. [119], we adopt the following convention, that has the merit

of producing dimensionless numbers:

$$\langle k_\perp \rangle = \int_0^1 dx \int_{\mathbb{R}^2} d\boldsymbol{k}_\perp \, \frac{k_\perp}{M} \mathrm{TMD}(x, \boldsymbol{k}_\perp), \tag{6.81}$$

$$\langle k_\perp^2 \rangle = \int_0^1 dx \int_{\mathbb{R}^2} d\boldsymbol{k}_\perp \, \frac{\boldsymbol{k}_\perp^2}{2M^2} \mathrm{TMD}(x, \boldsymbol{k}_\perp). \tag{6.82}$$

The results for the different distributions are given in Tab. 6.4. We notice how the values for the TMDs that have no collinear counterpart are smaller compared to the ones that have a PDF counterpart. This is due to the fact that g_{1T} and $h_{1L}^\perp$ are given as superposition of LFWAs with different L_z (see Sec. 6.2), and, as can be seen from Fig. 6.3, the contributions of the LFWAs with $|L_z| = 1$ are rather small compared to the contributions of $L_z = 0$.

We can also study the x-dependence of the average transverse momentum for different distributions (see Ref. [16]). We define

$$\langle k_\perp \rangle (x) = \int_{\mathbb{R}^2} d\boldsymbol{k}_\perp \, \frac{k_\perp}{M} \mathrm{TMD}(x, \boldsymbol{k}_\perp), \tag{6.83}$$

$$\langle k_\perp^2 \rangle (x) = \int_{\mathbb{R}^2} d\boldsymbol{k}_\perp \, \frac{\boldsymbol{k}_\perp^2}{2M^2} \mathrm{TMD}(x, \boldsymbol{k}_\perp). \tag{6.84}$$

In Fig. 6.5 are shown the results for the PDFs $f_1(x), g_1(x)$ and $h_1(x)$ and for $\langle k_\perp \rangle (x)$ for the TMDs g_{1T} and $h_{1L}^\perp$. We notice that, due to a factor $k_1^2 - k_2^2$ at the denominator (see Eqs. (6.35)-(6.36)), $h_{1T}^\perp$ presents numerical instabilities and is not shown. Our model, at variance with other models, like the one of Ref. [96], does not assume $SU(6)$ symmetry for the LWFAs. This implies that our model does not comply with the TMD relations discussed in Ref. [89].

Finally, the results for the GPDs at different values of ξ and t as function of x are shown in Figs. 6.6-6.8. In Fig. 6.6, we present the results for $H^u(x, \xi, t)$ and $\tilde{H}^u(x, \xi, t)$ as function of x for three selected values of ξ and t. In particular we choose $\xi = 0$, $t = 0$ GeV^2, $\xi = 0$, $t = -0.2$ GeV^2 and $\xi = 0.2$, $t = -0.34$ GeV^2. The results for the three-quark and the three-quark plus one-gluon states are shown separately as well as the total results. In Fig. 6.7, the same configuration as in Fig. 6.6 is used to show the results for $H^d(x, \xi, t)$ and $\tilde{H}^d(x, \xi, t)$ as function of x. For both the up and down quark we observe how the three-quark plus one-gluon contribution tends to dominate in the mid-to-low x region, whereas the three-quark contribution dominates at high values of x. We also note how increasing the value of ξ tends to decrease the magnitude of the GPDs. We can notice how the three-quark contribution to $\tilde{H}^d$ is the only negative contribution among the GPDs $H^{u,d}$ and $\tilde{H}^{u,d}$. In Fig. 6.8 we present the results for $E^{u,d}(x, \xi, t)$ and $\tilde{E}^{u,d}(x, \xi, t)$ as function of x for three selected values of ξ and t. In particular we choose $\xi = 0.1$, $t = -0.1$ GeV^2, $\xi = 0.1$, $t = -0.2$ GeV^2 and $\xi = 0.2$, $t = -0.34$ GeV^2. The limit $\xi \to 0$ and $t \to 0$ GeV^2, although being finite in the model, presents numerical instabilities and, therefore, it is not shown. The two GPDs $\tilde{H}(x, \xi, t)$ and $E(x, \xi, t)$ have a clear different behavior for the up and down quark. For $\tilde{H}(x, \xi, t)$ this is

especially evident in the three-quark contribution. Comparing our results with the one presented in Ref. [16], we can notice profound differences in $\tilde{H}^d$ and in $E^{u,d}$. These discrepancies are probably due to the very different modeling of the $L_z = \pm 1$ LFWAs in the two models. Within our model we find very poor results for the electromagnetic proton form factors. This can be due to different reasons. We believe that the model can be significantly improved either by increasing the number of polynomials in the expansion of the DAs, since it is known that the convergence in the polynomial expansion is slow. Another approach could be to abandon the polynomial expansion for the DAs, replacing it with a more comprehensive and sophisticated model, like a neural network approach. Work in this direction has been planned and will be pursued in the future. The work presented so far served to provide model-independent relations between the LFWAs and DAs and a unified framework to calculate a variety of parton distributions. This gives us an essential playground for future more refined phenomenological analysis.

TMD	$\langle k_\perp \rangle$	$\langle k_\perp^2 \rangle$
f_1^u	0.493	0.130
f_1^d	0.240	0.061
f_1^g	0.193	0.048
g_1^u	0.322	0.086
g_1^d	0.071	0.018
g_1^g	-0.064	-0.016
h_1^u	0.192	0.050
h_1^d	-0.059	-0.014
g_{1T}^u	-0.006	-0.002
g_{1T}^d	0.001	0.001
$h_{1L}^{\perp,u}$	-0.008	-0.003
$h_{1L}^{\perp,d}$	-0.049	-0.012
$h_{1T}^{\perp,u}$	0.005	0.002
$h_{1T}^{\perp,d}$	0.003	0.001

Table 6.4: Average transverse-momentum (second column) and average squared transverse-momentum (third column) for the leading-twist T-even TMDs as defined in Eqs. (6.81)-(6.82). The $h_{1T}^\perp$ is not showed because it present problems of numerical nature during the integration due to the $k_1^2 - k_2^2$ factor at the denominator, see Eqs. (6.35)-(6.36).

6.5 Conclusions

In this Chapter, we presented our model for the LFWAs of the three-quark and three-quark plus one-gluon states. The model discussed in Sec. 6.1 was constructed in three steps: first, we assumed a gaussian Ansatz for the transverse-momentum dependence of the LFWAs. Second, we inverted the relations between the DAs and the LFWAs (see Sec. 3.4.4) to obtain the LFWAs in terms of the DAs. Third, we assumed a specific polynomial expansion for the DAs based on the conformal expansion of Ref. [66]. This procedure gives the complete model for the LFWAs. In Secs. 6.2 and 6.3, we illustrated the LFWA overlap representation for the leading-twist T-even TMDs and chiral-even GPDs. These expressions are independent from the explicit model for the LFWAs and, therefore, have an importance that transcends the specific of our model. The parametrization we adopted for the DAs has already been discussed in similar form in the literature, see Refs. [65, 66, 68, 105, 107]. These studies provided the values for the parameters of the DAs via QCD sum-rule techniques and lattice-QCD estimation, at the scale $\mu = 1$ GeV. However, we modified the model including the quark and gluon effective masses. The values of the masses along with the parameters of the DAs have been fitted to a phenomenological parametrization of the unpolarized PDF $f_1(x)$. Specifically, we chose the phenomenological extraction MMHT2014 [118], since it provides results at the same scale ($\mu = 1$ GeV) of the QCD sum rules and lattice calculations of the DAs, which represent a benchmark for our model results.

The fit procedure and the fit results have been illustrated in Sec. 6.4 along with a selection of results for the GPDs and TMDs. The possibility of fitting the LFWAs to a sub-set of parton distributions and using the information acquired in such a way to obtain predictions for other parton distributions is one of the main advantages of using LFWAs for phenomenological analysis. Moreover, since the LFWAs can provide a parametrization of different parton distributions, they can be used to fit simultaneously experimental data for different distributions. These features prove valuable in view of the future EIC and upcoming new data from JLab and COMPASS.

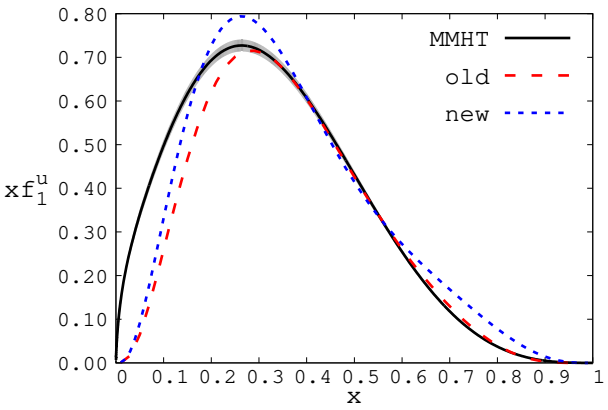

(a)

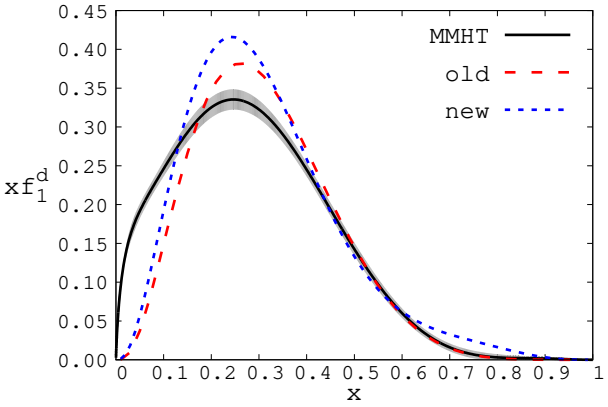

(b)

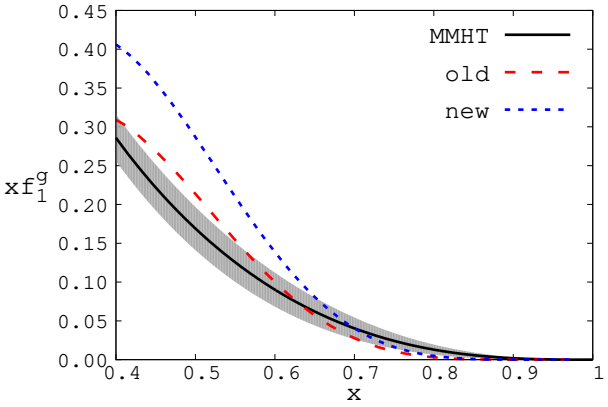

(c)

Figure 6.3: Fit results both in the old configuration from Ref. [119] (only $L_z = 0$ states) and in the new configuration of this work (also $|L_z| = 1$ three-quark states included). In (a), (b) and (c) are shown the comparison between MMHT2014 and the total results for the up, down and gluon contributions, respectively.

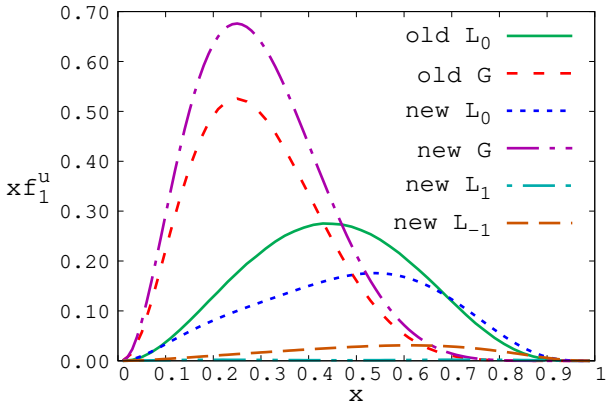

(a)

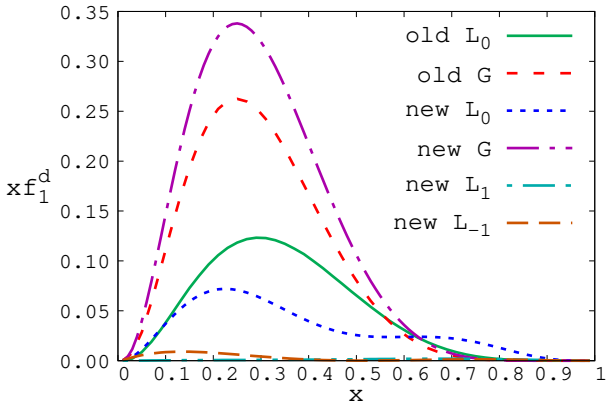

(b)

Figure 6.4: Fit results both in the old configuration from Ref. [119] (only $L_z = 0$ states) and in the new configuration of this work (also $|L_z| = 1$ three-quark states included). In (a) and (b) are shown the comparison of the old and new fit results for the different LFWA contributions to the up and down quark unpolarized PDF.

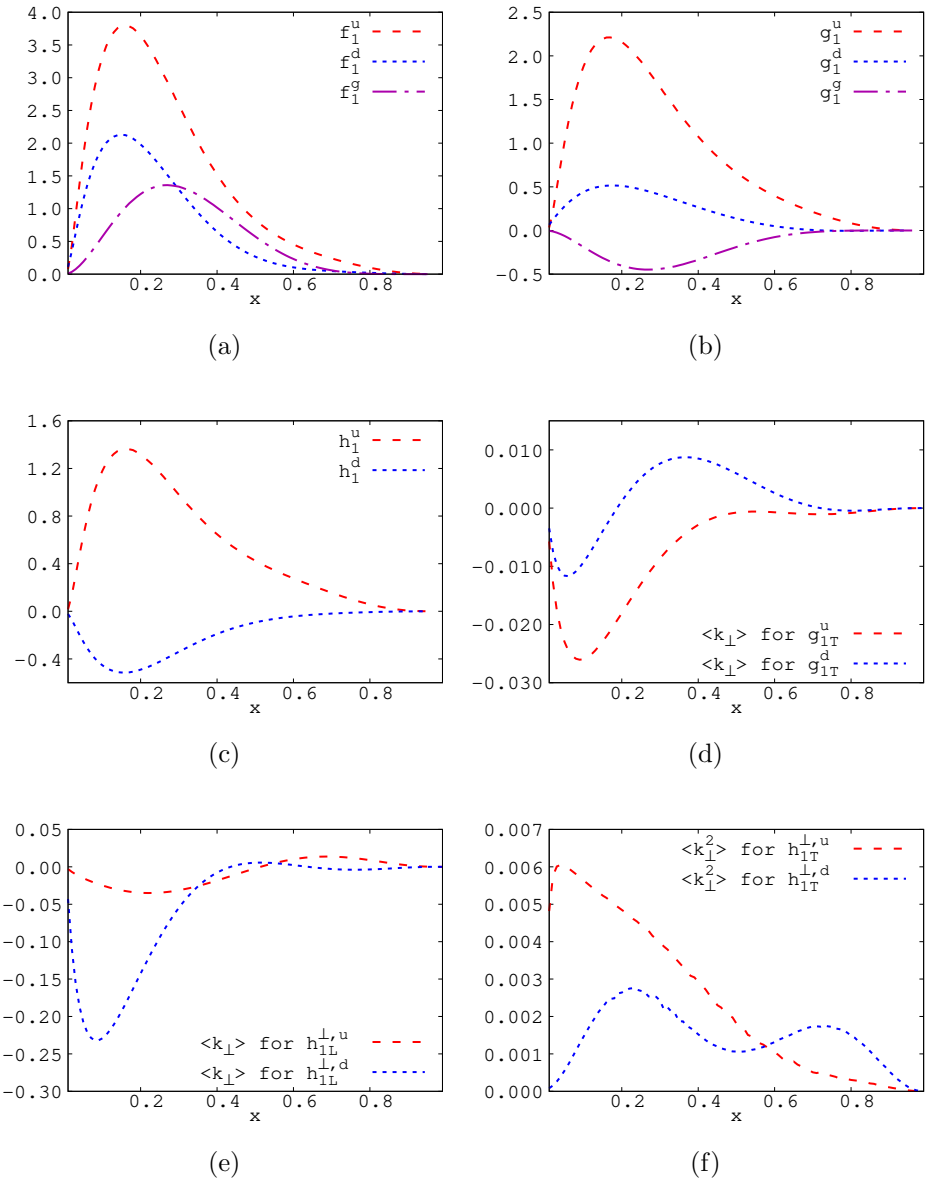

Figure 6.5: Panels (a) and (b) show the PDFs $f_1(x)$ and $g_1(x)$, respectively, for the up and down quark and for the gluon. Panel (c) shows the PDF $h_1(x)$ for the up and down quark. Panels (d) and (e) show the average transverse-momentum as function of x of Eq. (6.83) for the TMDs g_{1T} and $h_{1L}^{\perp}$. Panel (f) shows the average transverse-momentum as function of x of Eq. (6.83) for the TMD $h_{1T}^{\perp}$.

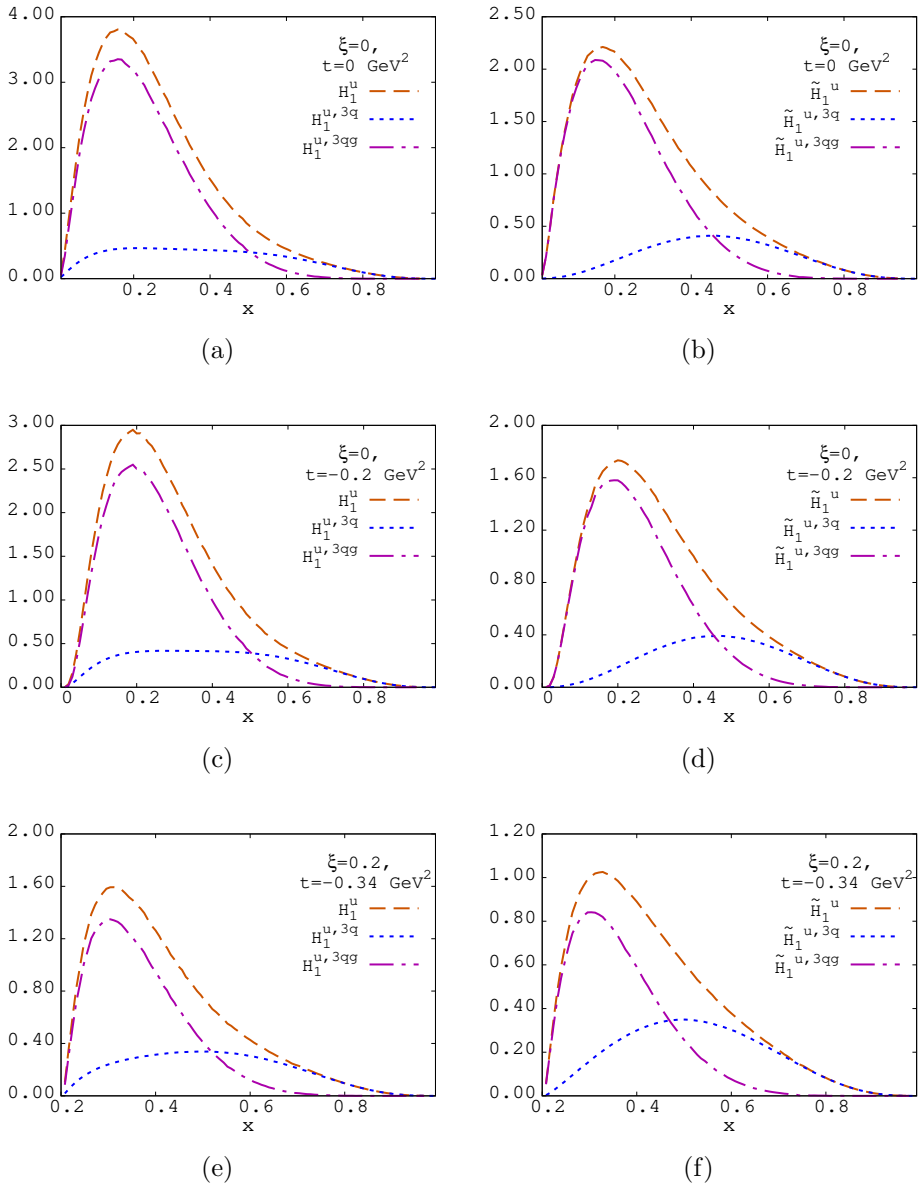

Figure 6.6: Results for the up quark contribution to the GPDs $H^u(x,\xi,t)$ and $\tilde{H}^u(x,\xi,t)$ as function of x at different values of ξ and t: $\xi = 0$ and $t = 0$ in the panels (a) and (b); $\xi = 0, t = -0.2$ GeV^2 in the panels (c) and (d) and $\xi = 0.2, t = -0.34$ GeV^2 in the panels (e) and (f).

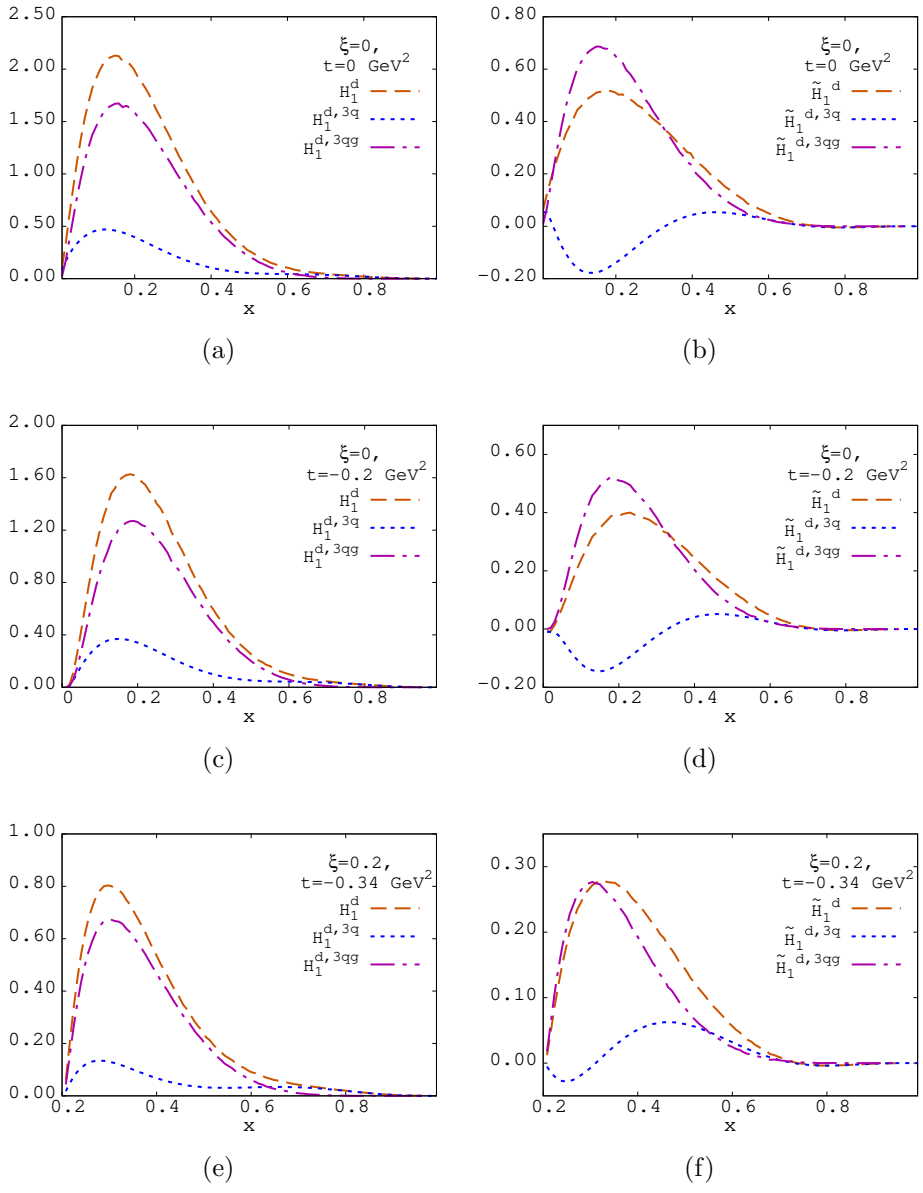

Figure 6.7: Results for the down quark contribution to the GPDs $H^d(x,\xi,t)$ and $\tilde{H}^d(x,\xi,t)$ as function of x at different values of ξ and t: $\xi = 0$ and $t = 0$ in the panels (a) and (b); $\xi = 0, t = -0.2$ GeV^2 in the panels (c) and (d) and $\xi = 0.2, t = -0.34$ GeV^2 in the panels (e) and (f).

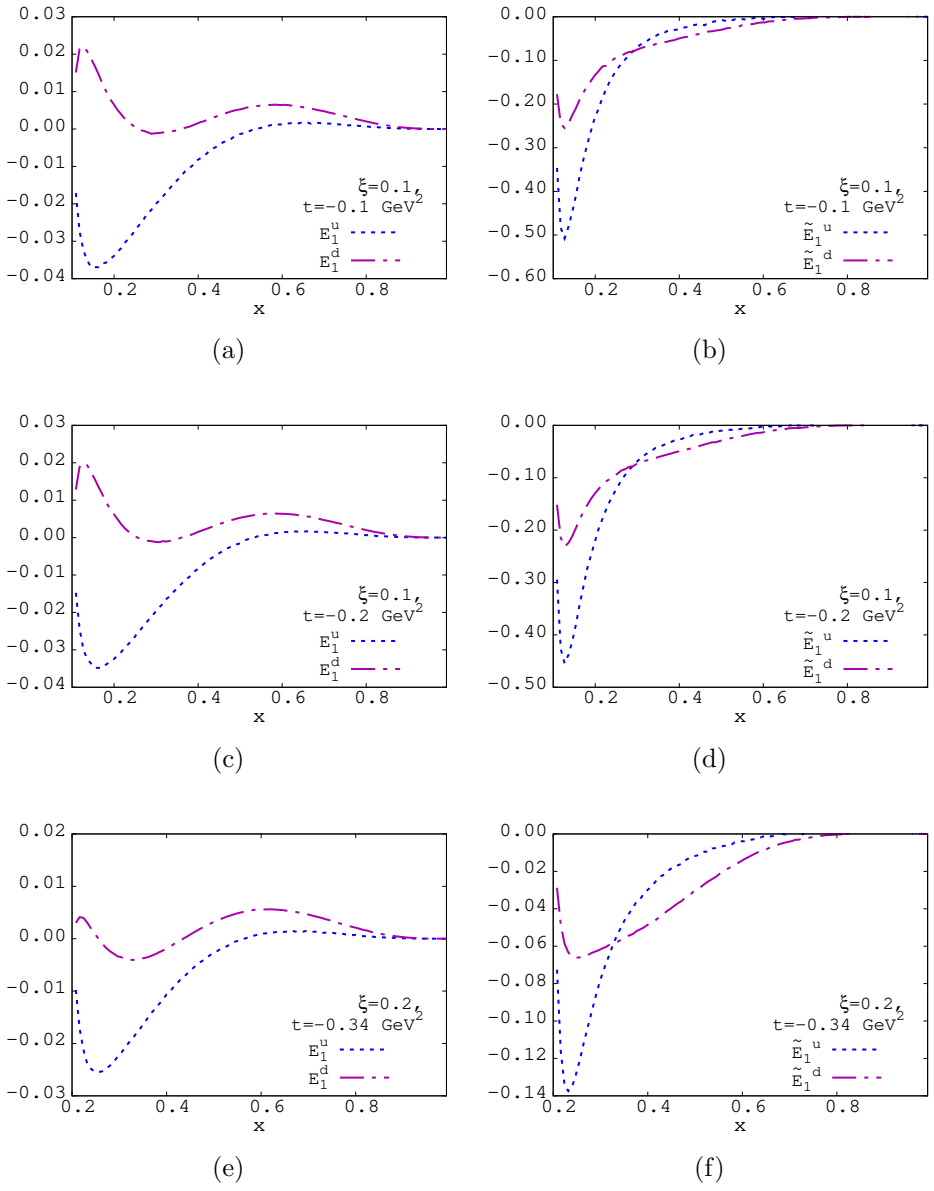

Figure 6.8: Results for the up and down quark contribution to the GPDs $E(x,\xi,t)$ and $\tilde{E}(x,\xi,t)$ as function of x at different values of ξ and t: $\xi = 0.1, t = -0.1$ GeV^2 in the panels (a) and (b); $\xi = 0.1, t = -0.2$ GeV^2 in the panels (c) and (d) and $\xi = 0.2, t = -0.34$ GeV^2 in the panels (e) and (f).

Chapter 7

Twist-3 distributions

7.1 Introduction

In the previous Chapters, we focused our attention on the leading-twist parton distributions (mainly GPDs and TMDs). These distributions have a probabilistic interpretation as parton densities, at variance with the sub-leading twist parton distributions that are going to be the focus of this Chapter. Twist-3 parton distributions, especially when the dependence on the parton transverse momenta is taken into account, give access to a wealth of information about the proton parton structure [17, 47, 122]. They describe multiparton correlations inside the proton, corresponding to the interference between scattering from a coherent quark-gluon pair and from a single quark [123–126]. As such, they help understanding the quark-gluon dynamics inside the hadrons.

Twist-3 TMDs contribute to various observables in SIDIS. Although being suppressed with respect to twist-2 observables, twist-3 structure functions are not negligible in the kinematics of fixed-target experiments. As an example of the importance of twist-3 distributions, one of the priority tasks of the experimental program at JLab12 is the measurement of different twist-3 spin-azimuthal asymmetries in SIDIS [127–129]. The future electron ion collider planned in USA will extend such experimental investigation by accessing different kinematical regions [130, 131].

Historically, model studies have been shown to have important impact for the understanding of sub-leading twist TMDs and the theoretical interpretation of related observables (see, e.g., Ref. [132]). Twist-3 quark PDFs and TMDs can, in general, be decomposed into contributions from leading-twist mass terms, singular terms and pure interaction-dependent ("tilde") terms. The procedure to obtain such decomposition is similar to the case of the distribution amplitudes discussed in Sec. 3.4.1. The approximation of vanishing tilde and singular terms is sometimes referred to as Wandzura-Wilczek approximation [133] and has been often used both as starting point to simplify the description of twist-3 SIDIS observables [134–136], and as a useful numerical approximation [91]. However, there is no real experimental evidence of its valid-

ity, and it misses one of the main motivation to study sub-leading twist, i.e. the intrinsic, non-perturbative physics of quark-gluon correlations encoded in the tilde terms. We note that twist-3 effects can be introduced also by the perturbative exchange of gluons between the active parton and the remnant. This procedure, that must be taken into account for a full twist-3 description of an observable, is spurious, since it does not encapsulate any real non-perturbative information about quark-gluon correlations inside the proton [137, 138].

Twist-3 TMDs have been calculated in various models: the MIT bag model [123, 137, 139, 140], diquark spectator models [141–144], instanton models of QCD vacuum [145, 146], chiral quark soliton models [147–151] and perturbative light-front Hamiltonian approaches with a quark target [152–155]. More recently, in Ref. [69] twist-3 and twist-4 distributions have been computed employing perturbative methods. Moreover, the work in Ref. [156] discusses the possibility of a vanishing singular contribution to $e^q(x, \boldsymbol{k}_\perp)$. We will not treat the twist-3 distributions thoroughly as we did with the leading-twist ones, since a very limited amount of information is available about them and, moreover, most of the twist-3 distributions involve gluon states with non-vanishing OAM, that are not included in our model. We will not discuss GTMDs of higher twist, since for now an extraction of them is unrealistic in the near-to-mid future.

The twist-3, unpolarized, chiral-odd quark TMD $e^q(x, \boldsymbol{k}_\perp)$ [125] is going to be the focus of this Chapter. This distribution can be constructed as the overlap of LFWAs for states with the same L_z, but different parton content. More specifically, the states must differ by one gluon. For this reason, the model presented in Chapter 6 is particularly well suited to study $e^q(x, \boldsymbol{k}_\perp)$.

In Sec. 7.2, we are going to derive the general decomposition of $e^q(x, \boldsymbol{k}_\perp)$ in tilde, mass and singular terms using the EOM. The overall complexity of the calculation is increased compared to the similar procedure utilized in Sec. 3.4.1, due to the presence of a non-unity transverse gauge-link. In Sec. 7.3 we are going to discuss in detail the derivation of the singular contribution to $e^q(x, \boldsymbol{k}_\perp)$, commenting on the results presented in Refs. [69, 156]. Finally, in Sec. 7.4, we are going to use the truncated Fock-state expansion of Eq. (3.67) to derive the LFWA overlap representation for $e^q(x, \boldsymbol{k}_\perp)$. We are going to utilize the explicit model presented in Chapter 6 to obtain predictions for both the TMD $e^q(x, \boldsymbol{k}_\perp)$ and the PDF $e^q(x)$. Conclusions are drawn in Sec. 7.5.

7.2 Twist-3 decomposition

In Sec. 3.3.2, we reviewed the definition of the quark TMDs in terms of the trace of the quark-quark correlator with an appropriate Dirac structure, see Eq. (5.1) and Refs. [17, 39].

For the sake of clearness, we recall here the definition of $e^q(x, \boldsymbol{k}_\perp)$:

$$\frac{M}{p^+}\, e^q(x, \boldsymbol{k}_\perp) = \int \frac{dz^- d\boldsymbol{z}_\perp}{2(2\pi)^3} e^{ik\cdot z}\, \langle p|\overline{\psi}(0)\mathcal{W}(0;z)\mathbb{1}\psi(z)|p\rangle\,|_{z^+=0}. \tag{7.1}$$

To fully specify the TMD, we need to fix the Wilson line $\mathcal{W}(0;z)$. In this case, we choose to work with a SIDIS-like Wilson line [25] (see Fig. 3.5). The generalization to a Drell-Yan-like Wilson line is straightforward, whereas more complicated Wilson line structures would demand a dedicated study.

The bilocal quark operator in Eq. (7.1) can be rewritten as

$$\begin{aligned}\mathcal{O}\left(0;z^-,\boldsymbol{z}_\perp\right) &= \overline{\psi}(0)\mathcal{W}(0;z)\psi(z)|_{z^+=0} \\ &= \overline{\psi}_+(0)\mathcal{W}(0;z)\psi_-(z)|_{z^+=0} + \overline{\psi}_-(0)\mathcal{W}(0;z)\psi_+(z)|_{z^+=0}. \end{aligned} \tag{7.2}$$

If we assume that the plus component k^+ of the quark momentum is strictly positive, we can invert the EOM (3.132) in a straightforward way. Instead, problems arise when we include the contribution from zero modes corresponding to $k^+ = 0$. In this case, as can be easily seen from Eq. (3.120), there appear singularities in the bad components of the field, and one needs a regularization prescription [69, 157, 158]. For this reason, we use the EOM (2.32) to derive the following operator identity

$$\begin{aligned}&\mathcal{W}(0;z)\,\psi_-(z)|_{z^+=0} = \mathcal{W}_1(0^-,\boldsymbol{0}_\perp;0^-,\boldsymbol{z}_\perp)\psi_-(0^+,0^-,\boldsymbol{z}_\perp) \\ &- i\int_{0^-}^{z^-} d\zeta^-\mathcal{W}_1(0^-,\boldsymbol{0}_\perp;\zeta^-,\boldsymbol{z}_\perp)\frac{\gamma^+}{2}\left(i\boldsymbol{\gamma}_\perp\cdot\boldsymbol{D}_\perp + m\right)\psi_+(0^+,\zeta^-,\boldsymbol{z}_\perp), \end{aligned} \tag{7.3}$$

where we defined $\mathcal{W}_1(a^-,\boldsymbol{a}_\perp;b^-,\boldsymbol{b}_\perp) \equiv \mathcal{W}(0^+,a^-,\boldsymbol{a}_\perp;0^+,b^-,\boldsymbol{b}_\perp)$. Note that this approach, that we used in Ref. [119], is different with respect to using the Green function to solve the EOM as presented in Eq. (3.120). With the present approach, we will be able to give a more clear interpretation of the singular term after the integration over $\boldsymbol{k}_\perp$. The derivation using Eq. (3.120) would lead to different-looking, but equivalent, results. Using the expression in Eq. (7.3) for the bad components, Eq. (7.2) can be rewritten as

$$\mathcal{O}\left(0;z^-,\boldsymbol{z}_\perp\right) = \mathcal{O}_s + \mathcal{O}_m + \mathcal{O}_{\text{tw3}}, \tag{7.4}$$

with

$$\mathcal{O}_s = \overline{\psi}(0)\mathcal{W}_1(0^-,\boldsymbol{0}_\perp;0^-,\boldsymbol{z}_\perp)\psi(0^+,0^-,\boldsymbol{z}_\perp), \tag{7.5}$$

$$\mathcal{O}_m = -im\int_0^{z^-} d\zeta^-\overline{\psi}_+(0)\mathcal{W}_1(0^-,\boldsymbol{0}_\perp;\zeta^-,\boldsymbol{z}_\perp)\gamma^+\psi_+(0^+,\zeta^-,\boldsymbol{z}_\perp), \tag{7.6}$$

$$\begin{aligned}\mathcal{O}_{\text{tw3}} = -\frac{i}{2}\int_0^{z^-} d\zeta^-\overline{\psi}_+(0)\sigma^{j+}\Big[&\mathcal{W}_1(0^-,\boldsymbol{0}_\perp;\zeta^-,\boldsymbol{z}_\perp)\overrightarrow{D}_{\perp,j}(\zeta^-,\boldsymbol{z}_\perp) \\ &+ \overleftarrow{D}^\dagger_{\perp,j}(0)\mathcal{W}_1(0^-,\boldsymbol{0}_\perp;\zeta^-,\boldsymbol{z}_\perp)\Big]\psi_+(0^+,\zeta^-,\boldsymbol{z}_\perp), \end{aligned} \tag{7.7}$$

where the index $j = 1,2$ labels the transverse components.

The bad components ψ_- contribute only to $\mathcal{O}_s$ in Eq. (7.5). This operator, when inserted in the matrix element of Eq. (7.1) and integrated over z^-, gives a singular contribution proportional to $\delta(x)$:

$$e_s^q\left(x,\boldsymbol{k}_\perp\right) = \frac{\delta(x)}{2M}\int\frac{d\boldsymbol{z}_\perp}{(2\pi)^2}e^{-i\boldsymbol{z}_\perp\cdot\boldsymbol{k}_\perp}\left\langle P|\overline{\psi}(0)\mathcal{W}_1(0^-,\boldsymbol{0}_\perp;0^-,\boldsymbol{z}_\perp)\psi(0^+,0^-,\boldsymbol{z}_\perp)|P\right\rangle. \tag{7.8}$$

This contribution is well known for the PDF $e^q(x)$, being related to the pion-nucleon sigma term (see, e.g., Ref. [125]).

The contribution to e^q from the operator $\mathcal{O}_m$ can be worked out using the Fourier expansion of the matrix element of the operator (7.6) and the definition of f_1^q in (3.37), as explained in Sec. 7.3, with the result

$$e^q_m = \frac{m}{Mx} f_1^q(x, \boldsymbol{k}_\perp) - \frac{m}{M}\delta(x)\int_{-1}^{1} dy \frac{f_1^q(y, \boldsymbol{k}_\perp)}{y}, \tag{7.9}$$

where the singular term is a natural consequence of the divergences associated with the zero modes ($x = 0$).

Limiting ourselves to the T-even sector and to the target-spin averaged matrix element, the contribution from the operator $\mathcal{O}_{\rm tw3}$ can be rewritten as

$$\begin{aligned} e_{tw3} = &-\frac{P^+}{M}\frac{g_s}{2}\int \frac{dz^- d\boldsymbol{z}_\perp}{2(2\pi)^3} e^{ik^+z^- - \boldsymbol{k}_\perp\cdot\boldsymbol{z}_\perp} \\ &\times \Bigg(\int_{0^-}^{z^-} d\zeta^- \int_{\infty^-}^{\zeta^-} d\eta^- \, \langle P| \overline{\psi}(0) \mathcal{W}_1(0^-, \boldsymbol{0}_\perp; \eta^-, \boldsymbol{z}_\perp) G^+_{\ j}(0^+, \eta^-, \boldsymbol{z}_\perp) \\ &\times \sigma^{j+} \mathcal{W}_1(\eta^-, \boldsymbol{z}_\perp; \zeta^-, \boldsymbol{z}_\perp) \psi(0^+, \zeta^-, \boldsymbol{z}_\perp) \, |P\rangle \\ &+ \int_{0^-}^{z^-} d\zeta^- \int_{0^-}^{\infty^-} d\eta^- \, \langle P| \overline{\psi}(0) \mathcal{W}_1(0^-, \boldsymbol{0}_\perp; \eta^-, \boldsymbol{0}_\perp) G^+_{\ j}(0^+, \eta^-, \boldsymbol{0}_\perp) \\ &\times \sigma^{j+} \mathcal{W}_1(\eta^-, \boldsymbol{0}_\perp; \zeta^-, \boldsymbol{z}_\perp) \psi(0^+, \zeta^-, \boldsymbol{z}_\perp) \, |P\rangle \Bigg), \end{aligned} \tag{7.10}$$

where $G^{\mu\nu}$ is the gluon-field strength tensor. Using the results in Sec. 7.3, Eq. (7.10) can be rewritten in the form

$$e^q_{\rm tw3}(x, \boldsymbol{k}_\perp) = \tilde{e}^q(x, \boldsymbol{k}_\perp) - \delta(x)\int_{-1}^{1} dy\, \tilde{e}^q(y, \boldsymbol{k}_\perp), \tag{7.11}$$

where

$$\tilde{e}^q(x, \boldsymbol{k}_\perp) = -\frac{i}{Mx}\Phi^{[\sigma^{j+}]}_{A,j}(x, \boldsymbol{k}_\perp) \tag{7.12}$$

is a pure twist-3 contribution defined in terms of the quark-gluon-quark correlation function [33]

$$\begin{aligned} \Phi^{[\sigma^{j+}]}_{A,j}(x, \boldsymbol{k}_\perp) = \frac{1}{2}{\rm Tr}\left[\Phi_{A,j}(x, \boldsymbol{k}_\perp)\sigma^{j+}\right] = \frac{g_s}{2}\int \frac{dz^- d\boldsymbol{z}_\perp}{2(2\pi)^3} e^{ik^+z^- - \boldsymbol{k}_\perp\cdot\boldsymbol{z}_\perp} \\ \times \Bigg(\int_{\infty^-}^{\zeta^-} d\eta^- \langle P|\overline{\psi}(0)\mathcal{W}_1(0^-, \boldsymbol{0}_\perp; \eta^-, \boldsymbol{z}_\perp) G^+_{\ j}(0^+, \eta^-, \boldsymbol{z}_\perp) \\ \times \sigma^{j+}\mathcal{W}_1(\eta^-, \boldsymbol{z}_\perp; \zeta^-, \boldsymbol{z}_\perp)\psi(0^+, \zeta^-, \boldsymbol{z}_\perp)|P\rangle \\ + \int_{0^-}^{\infty^-} d\eta^- \langle P|\overline{\psi}(0)\mathcal{W}_1(0^-, \boldsymbol{0}_\perp; \eta^-, \boldsymbol{0}_\perp) G^+_{\ j}(0^+, \eta^-, \boldsymbol{0}_\perp) \end{aligned}$$

$$\times \sigma^{j+} \mathcal{W}_1(\eta^-, \mathbf{0}_\perp; \zeta^-, \boldsymbol{z}_\perp) \psi(0^+, \zeta^-, \boldsymbol{z}_\perp) |P\rangle \Bigg). \tag{7.13}$$

Collecting the results in Eqs. (7.8)-(7.11), we end up with the following decomposition:

$$\begin{aligned} e^q(x, \boldsymbol{k}_\perp) = e_s^q(x, \boldsymbol{k}_\perp) + \tilde{e}^q(x, \boldsymbol{k}_\perp) + \frac{m}{xM} f_1^q(x, \boldsymbol{k}_\perp) \\ - \delta(x) \int_{-1}^{1} dy \left(\frac{m}{My} f_1^q(y, \boldsymbol{k}_\perp) + \tilde{e}^q(y, \boldsymbol{k}_\perp) \right). \end{aligned} \tag{7.14}$$

The singular term beyond the contribution of e_s was usually not discussed in literature before Ref. [119]. Using the Green function approach for the inversion of the EOM, the singular terms of Eq. (7.14) would have been originated from the boundary condition terms of Eq. (3.115).

The decomposition (7.14) is independent on the choice of the gauge. In the light-cone gauge $A^+ = 0$, with advanced boundary conditions for the transverse components of the gauge field, the gauge links in the correlators can be ignored[1] and $\Phi_{A,j}$ in Eq. (7.13) becomes [33, 83]:

$$\begin{aligned} \tilde{\Phi}_{A,j}^{[\sigma^{j+}]}(x, \boldsymbol{k}_\perp) = \frac{g_s}{2} \int \frac{dz^- d\boldsymbol{z}_\perp}{2(2\pi)^3} e^{ik\cdot z} \\ \times \langle P, S | \overline{\psi}(0) \left[A_{\perp,j}(z) - A_{\perp,j}(0) \right] \sigma^{j+} \psi(z) | P, S \rangle_{z^+=0}. \end{aligned} \tag{7.15}$$

Integrating Eq. (7.14) over $\boldsymbol{k}_\perp$, one obtains the corresponding decomposition for the PDF $e^q(x)$

$$e^q(x) = e_s(x) + \tilde{e}^q(x) + \frac{m}{xM} f_1^q(x) - \delta(x) \int_{-1}^{1} dy \left(\frac{m}{My} f_1^q(y) + \tilde{e}^q(y) \right), \tag{7.16}$$

from which one can easily infer well-known relations for the first Mellin moments of $e^q(x)$ [125]. The singular contribution $e_s(x)$ reads:

$$e_s(x) = \frac{\delta(x)}{2M} \langle P | \overline{\psi}(0) \psi(0) | P \rangle = \frac{\delta(x)}{m} \sigma_{\pi N}, \tag{7.17}$$

where $\sigma_{\pi N}$ is the pion-nucleon sigma term.

7.3 Derivation of the singular terms

In this section, we show the derivation of the contributions e_m^q in Eq. (7.9) and e_{tw3}^q in Eq. (7.11).

[1] This argument is strictly related to the choice of a SIDIS-like Wilson line. Different choices of the Wilson line would require different boundary conditions in order to reproduce a similar-looking equation.

We start by considering the matrix elements of the operators $\mathcal{O}_m$ and $\mathcal{O}_{\rm tw3}$ in Eqs. (7.6) and (7.7), respectively, which enter the definition (7.1) of the TMD $e^q(x, \boldsymbol{k}_\perp)$ ($l = m, \text{tw3}$):

$$\int \frac{dz^- d\boldsymbol{z}_\perp}{(2\pi)^3} e^{iz^- xP^+ - i\boldsymbol{z}_\perp \cdot \boldsymbol{k}_\perp} \int_{0^-}^{z^-} d\zeta^- \mathcal{M}_l(\zeta^-, \boldsymbol{z}_\perp), \tag{7.18}$$

with

$$\mathcal{M}_m(\zeta^-, \boldsymbol{z}_\perp) := -\frac{im}{2} \langle P|\overline{\psi}(0)\gamma^+ \mathcal{W}_1\left(0^-, \boldsymbol{0}_\perp; \zeta^-, \boldsymbol{z}_\perp\right) \psi(\zeta^-, \boldsymbol{z}_\perp)|P\rangle\,, \tag{7.19}$$

$$\begin{aligned}\mathcal{M}_{\rm tw3}(\zeta^-, \boldsymbol{z}_\perp) := \frac{g_s}{2}\Big(&\int_{\infty^-}^{\zeta^-} d\eta^- \langle P|\overline{\psi}(0)\mathcal{W}_1\left(0^-, \boldsymbol{0}_\perp; \eta^-, \boldsymbol{z}_\perp\right) G^+{}_j(\eta^-, \boldsymbol{z}_\perp) \\ &\sigma^{j+}\mathcal{W}_1\left(\eta^-, \boldsymbol{z}_\perp; \zeta^-, \boldsymbol{z}_\perp\right) \psi(\zeta^-, \boldsymbol{z}_\perp)|P\rangle \\ &+ \int_{0^-}^{\infty^-} d\eta^- \langle P|\overline{\psi}(0)\mathcal{W}_1\left(0^-, \boldsymbol{0}_\perp; \eta^-, \boldsymbol{0}_\perp\right) G^+{}_j(\eta^-, \boldsymbol{0}_\perp) \\ &\sigma^{j+}\mathcal{W}_1\left(\eta^-, \boldsymbol{0}_\perp; \zeta^-, \boldsymbol{z}_\perp\right) \psi(\zeta^-, \boldsymbol{z}_\perp)|P\rangle\Big),\end{aligned} \tag{7.20}$$

where $z^+ = 0$ is understood in the argument of the fields. By integrating over $\boldsymbol{z}_\perp$ and introducing the Fourier-transform in the variable ζ^- of the matrix element $\mathcal{M}_l$, Eq. (7.18) can be rewritten as

$$\int \frac{dz^-}{2\pi} e^{iz^- xp^+} \int_{0^-}^{z^-} d\zeta^- \int dh^+ e^{-i\zeta^- h^+} \mathcal{M}_l(h^+, \boldsymbol{k}_\perp). \tag{7.21}$$

The integral over ζ^- in Eq. (7.21) can be easily performed, giving

$$i \int \frac{dz^-}{2\pi} e^{iz^- xp^+} \int dh^+ \frac{e^{-iz^- h^+} - 1}{p^+} \mathcal{M}_l(h^+, \boldsymbol{k}_\perp). \tag{7.22}$$

Finally, integrating Eq. (7.22) over z^- and changing the integration variable as $p^+ = yP^+$, we obtain

$$\frac{i}{xp^+}\, \mathcal{M}_l(xp^+, \boldsymbol{k}_\perp) - \frac{i\delta(x)}{p^+} \int \frac{dy}{y}\, \mathcal{M}_l(yp^+, \boldsymbol{k}_\perp). \tag{7.23}$$

The Eq. (7.23), for $l = m$ and with the definition (3.37) for f_1^q, corresponds to the contribution e_m^q in Eq. (7.9). Analogously, Eq. (7.23), for the matrix element with $l = \text{tw3}$ and with the definition (7.12) for $\tilde{e}^q$, gives the contribution $e_{\rm tw3}^q$ in Eq. (7.11).

Two works appeared recently in literature, discussing the singular behaviour of the $e^q(x)$ distributions [69, 156]. In Ref. [156], it is claimed that the decomposition in Eq. (7.14) is actually wrong and no singular term should appear. The authors of Ref. [69] argued that, using Eq. (3.120), the claim of Ref. [156] is valid only in the limit of vanishing zero-mode contributions. We discuss here an alternative argument, with respect to the one provided by Ref. [69], that

explains why the singular terms are not vanishing. In Eq. (7.3), we could have chosen the subtraction point at ∞^- instead of 0^-, as it is done in Ref. [156]. This would have given the following expression instead of Eq. (7.22):

$$i\int\frac{dz^-}{2\pi}e^{iz^-xP^+}\int dp^+\left(\frac{e^{-iz^-p^+}}{p^+}\mathcal{M}_l(p^+,\boldsymbol{k}_\perp)-\lim_{z^-\to\infty^-}\frac{e^{-iz^-p^+}}{p^+}\mathcal{M}_l(p^+,\boldsymbol{k}_\perp)\right). \tag{7.24}$$

The second term is proportional to

$$\mathcal{M}_l(p^+=0^+,\boldsymbol{k}_\perp). \tag{7.25}$$

Since $\mathcal{M}_l(p^+,\boldsymbol{k}_\perp)$ is written exclusively in terms of dynamical field components (good components for the quark fields and transverse components for the gluon field), we have that

$$\mathcal{M}_l(p^+=0^+,\boldsymbol{k}_\perp)=0. \tag{7.26}$$

This entails that the total singular contribution to $e^q(x,\boldsymbol{k}_\perp)$ (see Eq. (7.14))

$$e^q_s(x,\boldsymbol{k}_\perp)-\delta(x)\int_{-1}^{1}dy\left(\frac{m}{My}f_1^q\left(y,\boldsymbol{k}_\perp\right)+\tilde{e}^q\left(y,\boldsymbol{k}_\perp\right)\right) \tag{7.27}$$

can be equivalently written as:

$$\begin{aligned}&\frac{\delta(x)}{2M}\int\frac{d\boldsymbol{z}_\perp}{(2\pi)^2}e^{-i\boldsymbol{z}_\perp\cdot\boldsymbol{k}_\perp}\Big(\langle P|\overline{\psi}_+(0)\mathcal{W}_1(0;\infty^-,\boldsymbol{z}_\perp)\psi_-(0^+,\infty^-,\boldsymbol{z}_\perp)|P\rangle\\&+\langle P|\overline{\psi}_-(0^+,\infty^-,-\boldsymbol{z}_\perp)\mathcal{W}_1(\infty^-,-\boldsymbol{z}_\perp;0)\psi_+(0)|P\rangle\Big).\end{aligned} \tag{7.28}$$

From this it is rather simple seeing how no singular part arises, under the assumption of Ref. [156] of vanishing $\psi_-(\infty^-)$ (see Eq. (17) of Ref. [156], in which $\psi_-(\infty^-)$ is clearly assumed to vanish). However, as we stressed, while it is safe to assume that $\psi_+(\infty^-)=0$ because it is a dynamical field, it is not guaranteed that the same holds for the bad component.

From Eq. (7.8), one can also see why we chose 0^- instead of ∞^- as a subtraction point. Integrating Eq. (7.8) over $\boldsymbol{k}_\perp$, instead of recovering the pion-nucleon sigma term of Eq. (7.17) and the integrals of the PDFs in the last term of Eq. (7.16), one would have obtained:

$$\frac{\delta(x)}{2M}\left\langle P|\overline{\psi}_+(0)\psi_-(0^+,\infty^-,\boldsymbol{0}_\perp)+\overline{\psi}_-(0^+,\infty^-,\boldsymbol{0}_\perp)\psi_+(0)|P\right\rangle. \tag{7.29}$$

The meaning of the singular part, when expressed in this form, is more obscure.

7.4 Model results

7.4.1 Light-Front Wave Amplitude overlap representation

We can use the truncated Fock-space expansion for the proton state in Eq. (3.67) to derive the LFWA overlap representation of $\tilde{e}^q(x,\boldsymbol{k}_\perp)$. Since we are not con-

sidering three-quark plus one-gluon states with $L_z \neq 0$, the overlap representation is given in terms of only $L_z = 0$ LFWAs:

$$\begin{aligned}
\tilde{e}^u(x,k_\perp) = \frac{4g_s}{Mx\sqrt{3}} \int \frac{d\mu_4}{\sqrt{x_4}} \Bigg\{ & -\delta(x-x_4-x_1)\delta(\boldsymbol{k}_\perp - \boldsymbol{k}_{\perp 4} - \boldsymbol{k}_{\perp 1}) \\
& \times \Bigg[\left(4\psi^{(0)*}_{(-2-3)32} + 2\psi^{(0)*}_{23(-2-3)} \right) \Psi^{1,\uparrow}_{1234} \\
& + \left(2\psi^{(0)*}_{(-2-3)23} + \psi^{(0)*}_{32(-2-3)} \right) \Psi^{2,\uparrow}_{1234} - 2\psi^{(0)*}_{2(-2-3)3} \Psi^{\downarrow}_{1234} \Bigg] \\
& + \delta(x-x_4-x_2)\delta(\boldsymbol{k}_\perp - \boldsymbol{k}_{\perp 4} - \boldsymbol{k}_{\perp 2}) \left[2\psi^{(0)*}_{(-1-3)13} \Psi^{2,\uparrow}_{1234} - \psi^{(0)*}_{1(-1-3)3} \Psi^{\downarrow}_{1234} \right] \\
& + \delta(x-x_4-x_3)\delta(\boldsymbol{k}_\perp - \boldsymbol{k}_{\perp 4} - \boldsymbol{k}_{\perp 3})\, \psi^{(0)*}_{(-1-2)12} \Psi^{1,\uparrow}_{1234} \Bigg\},
\end{aligned} \tag{7.30}$$

$$\begin{aligned}
\tilde{e}^d(x,k_\perp) = -\frac{4g_s}{Mx\sqrt{3}} \int \frac{d\mu_4}{\sqrt{x_4}} \Bigg\{ & \delta(x-x_4-x_2)\delta(\boldsymbol{k}_\perp - \boldsymbol{k}_{\perp 4} - \boldsymbol{k}_{\perp 2}) 2\psi^{(0)*}_{31(-1-3)} \Psi^{2,\uparrow}_{1234} \\
& + \delta(x-x_4-x_3)\delta(\boldsymbol{k}_\perp - \boldsymbol{k}_{\perp 4} - \boldsymbol{k}_{\perp 3}) \\
& \times \left[\psi^{(0)*}_{21(-1-2)} \Psi^{1,\uparrow}_{1234} - \left(\psi^{(0)*}(1,-1-2,2) + \psi^{(0)*}_{2(-1-2)1} \right) \Psi^{\downarrow}_{1234} \right] \Bigg\},
\end{aligned} \tag{7.31}$$

where we used the notation of Eqs. (6.23)-(6.26) and we defined

$$\psi^{(0)}_{ij(-i-j)} = \psi^{(0)}\left(x_i, \boldsymbol{k}_{\perp,i}, x_j, \boldsymbol{k}_{\perp,j}, 1-x_i-x_j, -\boldsymbol{k}_{\perp,i} - \boldsymbol{k}_{\perp,j}\right). \tag{7.32}$$

By integrating Eqs. (7.30) and (7.31) over $\boldsymbol{k}_\perp$, the corresponding results for the PDF $\tilde{e}^q(x)$ can be obtained.

7.4.2 Pure twist-3 distribution

By inserting the explicit parametrization for the LFWAs given in Sec. 6.1 into the LFWA overlap representations (7.30)-(7.31), we obtain the results shown in Figs. 7.1. The results are obtained using the parameters in the new fit configuration corresponding to the last column of Tab. 6.1. The dot-dashed curves represent the pure twist-3 contributions, whereas the leading-twist ones are represented by the dashed-double-dot curves. The sum of the two contributions is given by the solid curve. We can appreciate how the pure twist-3 contributions to the total $xe^q(x)$ become sizable for moderate-to-high values of x. This can be intuitively understood because the longitudinal-momentum fraction x is given by the sum of the quark and gluon longitudinal-momentum fractions, hence, low values of x entail low values for both the momentum fraction of the quark and gluon and, in our model, the LFWAs vanish for small values of any longitudinal-momentum fraction. The relative size of twist-2 and pure

twist-3 contributions depends critically on the quark-mass parameter, which enters as proportionality constant that weights the twist-2 term in Eq. (7.16). In our model calculation, the partons masses also appear in the functions Ω_N in Eq. (6.4) and have a direct effect on the shape of the x dependence. In Figs. 7.2 we compare our results with the two sets of parameters given in Tab. 6.1. The oldest set corresponds to the parameters that we used in Ref. [119]. The two sets of parameters have been obtained from the fit of the unpolarized PDFs $f_1^{u,d,g}$. It is evident how the inclusion of LFWAs with non-vanishing OAM does not alter in a significant way the dominant contribution of the $L_z = 0$ LFWAs to the unpolarized distributions. The strong dependence on the mass for the relative size of the leading-twist and twist-3 contributions is always understood.

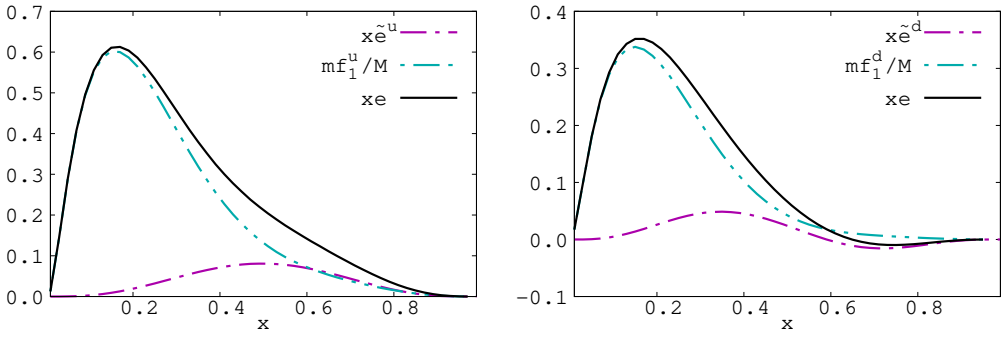

(a) (b)

Figure 7.1: Results for the PDFs $xe^u(x)$ (panel (a)) and $xe^d(x)$ (panel (b)) with the new set of parameters of Tab. 6.1. The dot-dashed light-blue curves are the twist-2 contributions, the dashed-double-dot purple curves are the pure twist-3 contributions and the sum of the two terms, corresponding to the total PDFs $xe^{u,d}(x)$, is given by the solid black curves.

The CLAS collaboration has reported preliminary results of a measurement of the beam asymmetry in di-hadron SIDIS, using a longitudinally polarized 6 GeV electron beam off an unpolarized proton target [129, 159]. These data have been analyzed to extract the following flavor combination of the valence-quark contribution to $e^q(x)$:

$$e^V(x) = \frac{4}{9}e^u(x) - \frac{1}{9}e^d(x). \tag{7.33}$$

In Fig. 7.3, the preliminary CLAS data points at the scale $\mu^2 = 1.5$ GeV^2 are compared with our model predictions at the scale $\mu^2 = 1$ GeV^2 for both the old set of parameters from Ref. [119] and the new set of parameters of the present work. We can appreciate how the new set of parameters goes into the direction of a slightly better agreement with the experimental data. The model results for the separate twist-2 and pure twist 3-terms are also shown.

Our results are in quite good agreement with the experimental extraction at the two higher-x bins, but they are not able to reproduce the observed fast

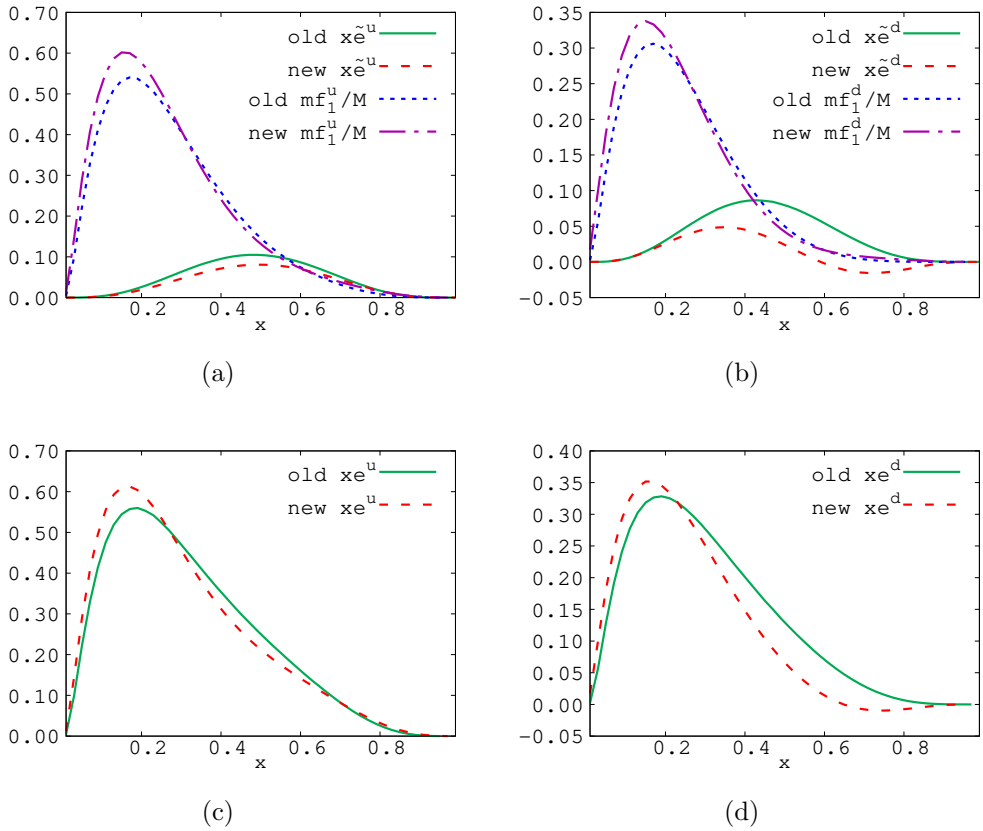

Figure 7.2: Comparison between the results for the PDFs $xe^{u,d}(x)$ in the old and new fit configuration of Tab. 6.1. In panel (a) and (b) are shown the results for the twist-2 and twist-3 contributions for the up quark (panel (a)) and for the down quark (panel (b)). The short-dashed blue curves and the solid green curves represent the twist-2 contributions and the pure twist-3 contributions, respectively, in the old configuration. The dot-dashed purple blue curves and the long-dashed red curves represent the twist-2 contributions and the pure twist-3 contributions, respectively, in the new configuration. In panel (c) and (d) are shown the results for the total PDF $xe^u(x)$ (panel (c)) and $xe^d(x)$ (panel (d)). The solid green curves represent the results in the old configuration, whereas the long-dashed red curves represent the results in the new configuration.

rising at lower x. This is due to a lack of our model, that, according to the fit results for the unpolarized PDF f_1 shown in Fig. 6.3, is unreliable in the mid-to-low x region. We also notice that the pure twist-3 contribution in the considered x-range is very small, supporting the results within the light-front constituent-quark picture that was used in Ref. [137] and shown to be able to reproduce the results of the CLAS data at higher x. However, one should bear in mind that these data are still preliminary and have unestimated systematic uncertainties.

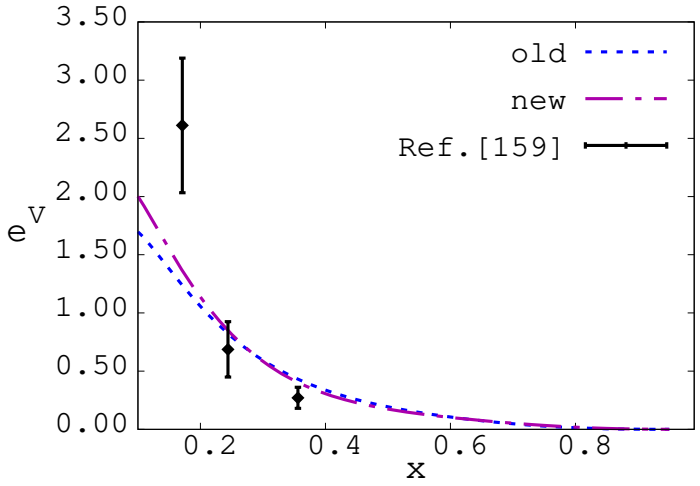

(a)

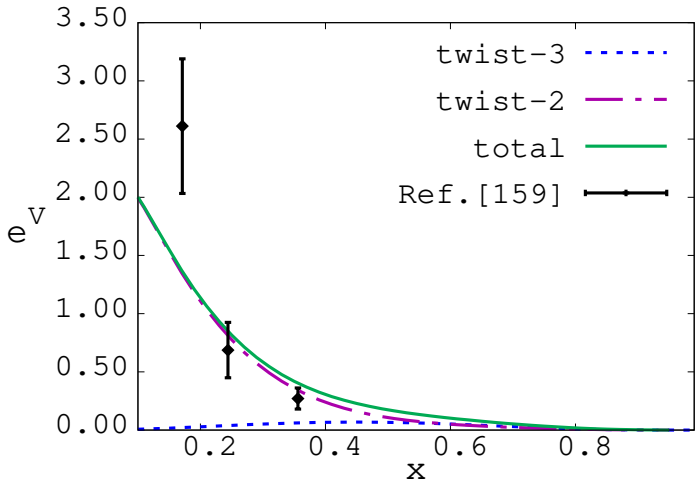

(b)

Figure 7.3: Predictions for the combination $e^V = \frac{4}{9}e^u(x) - \frac{1}{9}e^d(x)$ at the scale $\mu^2 = 1$ GeV^2, in comparison with the extraction of Ref. [159] at the scale $\mu^2 = 1.5$ GeV^2. We can clearly see how the new set of parameters slightly improves the agreement with the extraction.

7.4.3 Transverse momentum dependence

To study the transverse-momentum dependence of $e^q(x, \boldsymbol{k}_\perp)$, we use the definitions given in Eqs. (6.81) and (6.84). These equations allow for a direct comparison between the different contributions to the total distribution $e^q(x, \boldsymbol{k}_\perp)$. The average transverse-momentum densities as function of x are shown in Fig. 7.4. It can be appreciated how, also for the transverse momentum, the twist-2 contributions dominate compared to the pure twist-3 ones. Moreover, the peaks of $\langle k_\perp^2 \rangle (x)$ for the pure twist-3 contributions are shifted to larger values of x

	$\tilde{e}^u$	$\tilde{e}^d$
$\langle k_\perp \rangle$	0.037	0.019
$\langle k_\perp^2 \rangle$	0.011	0.005

Table 7.1: Average transverse momentum for the pure twist-3 contributions. The second and third columns show the results for the up and down quark, respectively.

compared to the twist-2 contributions. It is also interesting to compare the results for the up and down quark distributions, especially for the pure twist-3 terms. The results are shown in Fig. 7.5 for both $\tilde{e}^q(x, \boldsymbol{k}_\perp)$ and $e^q(x, \boldsymbol{k}_\perp)$. We notice how the pure twist-3 distributions are considerably different, whereas the shape, but not the magnitude, of the total distributions is rather similar. This last feature can be traced back to the dominance of the twist-2 contributions to $e^{u,d}$ and to the very similar shape and different magnitude of f_1^u and f_1^d. In Tab. 7.1 are given the results for the total average transverse momentum for the pure twist-3 distribution $\tilde{e}^{u,d}$.

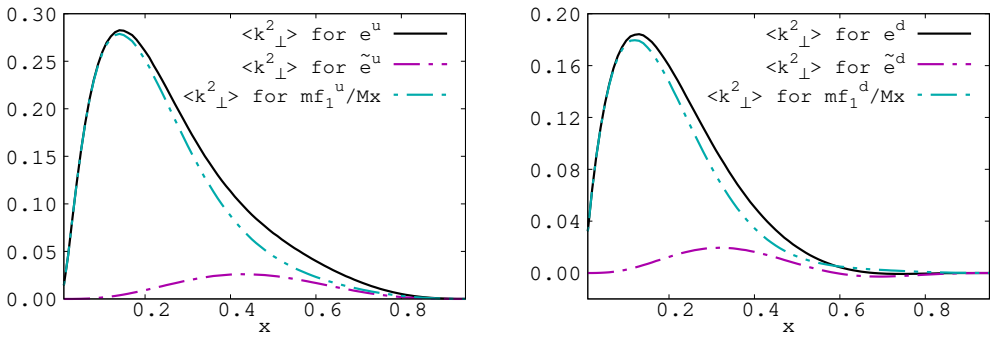

(a) (b)

Figure 7.4: Average transverse momentum of Eq. (6.84) for e^u in panel (a) and for e^d in panel (b) as function of x. The dashed-dot purple curves are the results for the pure twist-3 distribution, the dashed-double-dot light blue curves are the results for the twist-2 contributions and the solid black curves are the total results.

7.5 Conclusions

In this Chapter, the twist-3 distribution $e^q(x, \boldsymbol{k}_\perp)$ has been studied. Subleading-twist distributions are interesting since they encode the physics of quark-gluon correlations inside the proton. A model-independent decomposition of $e^q(x, \boldsymbol{k}_\perp)$ has been presented using the QCD EOM. In particular, the decom-

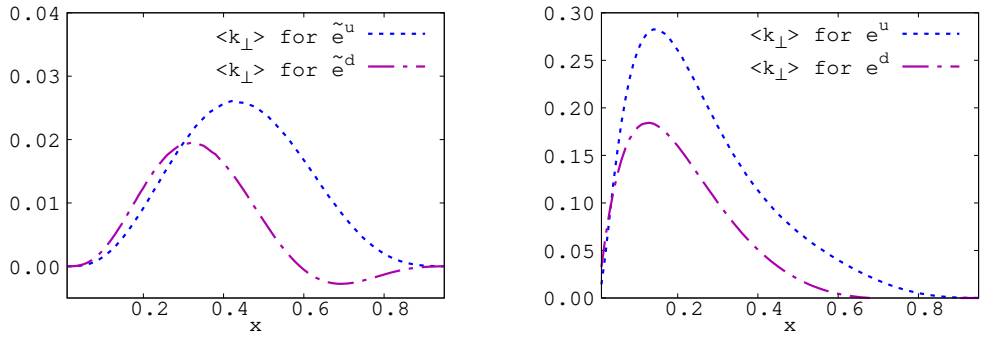

(a) (b)

Figure 7.5: Comparison between the up and down average transverse momentum of Eq. (6.83) for $\tilde{e}$ (panel (a)) and e (panel (b)) as function of x.

position produces a pure twist-3 part, i.e. the "tilde" term encoding the quark-gluon correlations, a pure twist-2 contribution and a singular (δ-like) term. The singular term is in turn given by a well-know contribution that can be related to the pion-nucleon sigma term, and an additional term that is, instead, poorly discussed in literature. We discussed some of the most recent arguments that either point in the direction of a vanishing singular contribution or in the direction of a non-vanishing δ-like term. We tried to clarify how the claim of a vanishing singular contribution derives from incorrect boundary conditions for the bad components of the quark field at light-cone infinity.

The second part of the Chapter has been devoted to study the twist-3 distribution using the LFWA overlap approach. To this aim, we used the model presented in Chapter 6. We constructed the $\tilde{e}$ distribution as an overlap of $L_z = 0$ LFWAs for the three-quark and three-quark plus one-gluon states. The $L_z = \pm 1$ LFWAs for the three-quark state would appear in combination with the $L_z = \pm 1$ LFWAs for the three-quark plus one-gluon state. However, the latter are not present in our model. Using the parameters of the model fitted to the phenomenological parametrization of the leading-twist unpolarized PDF as explained in Sec. 6.4 (see Tab. 6.1), we provided predictions for both $\tilde{e}^q(x)$ and $\tilde{e}^q(x, \boldsymbol{k}_\perp)$, in comparison with the corresponding twist-2 contribution given in terms of f_1^q. We also considered preliminary results from a phenomenological extraction of a particular flavor combination of the valence-quark contribution to $e^q(x)$ [159]. For this quark-flavor combination, our model predictions are almost saturated by the twist-2 contribution to $e^q(x)$, and showed a quite good agreement with the extracted results in the large x-region.

Chapter 8

The Energy-Momentum Tensor

In this final Chapter, we part ourselves from the study of parton distributions and light-front wave functions to approach a different problem. We want to investigate the physics of the Energy-Momentum Tensor, a local operator that encodes the information about the global properties of a particle, such as the mass and the spin. A detailed study of the possible decompositions of the Energy-Momentum tensor in separate contributions (like the quark and gluon contribution to the proton matrix elements of the QCD Energy-Momentum Tensor) could lead to important clues on how the global properties of a particle emerge from the dynamics of its elementary constituents. We will first discuss the electron matrix elements of the QED Energy-Momentum Tensor using perturbation theory. Using this benchmark calculation, we will then tackle the more challenging case in QCD, where a full perturbative treatment is not practicable. We follow the discussion of Refs. [160, 161] for the electron and proton mass decompositions, while the results for the form factors of the electron EMT will be presented in a forthcoming work [162]. Throughout this Chapter, the instant-form quantization is used. This is a non-limiting choice, since the fundamental objects of interest are the EMT form-factors, which are identical in both quantization forms. We chose the instant form over the light-front form to make more direct contact with the pre-existing literature on the proton mass.

8.1 Introduction

Let us suppose to study a generic field theory (quantum or classical) described in terms of the Lagrangian:

$$\mathcal{L}(\phi_s(x), \partial^\mu \phi_s(x)), \tag{8.1}$$

where ϕ_s is a generic field and x the space-time position. The index s has different meaning for different types of fields. For example, it is inessential for a scalar field, it is a Dirac index for a spin 1/2 field, and it plays the role of a Lorentz index for a vector field. Of course spin-1/2 fields are not present in a classical field theory. We aim to specify the Lagrangian to a relativistic field

theory. This can be done by requiring the invariance of the Lagrangian under Poincaré transformations. In the Poincaré group are contained the translations and the (proper and orthochronous) Lorentz transformations, see Chapter 2 for more details on the Poincaré group. From the Noether theorem, it follows that there exists a conserved current for each symmetry in the Lagrangian. The conserved current associated with the translations is the Energy-Momentum Tensor (EMT), and the "canonical" Noether construction leads to the following definition for the EMT:

$$\tilde{T}^{\mu\nu} = \frac{\delta \mathcal{L}}{\delta \left(\partial_\mu \phi_s(x)\right)} \partial^\nu \phi_s(x) - g^{\mu\nu} \mathcal{L}. \tag{8.2}$$

If the Lagrangian describes a gauge invariant theory, such as Electrodynamics (ED), the EMT defined as in Eq. (8.2) can be gauge non-invariant. Because a gauge non-invariant object poses problems when one wants to extract it from experimental data, it is often stated that additional manipulations are needed to construct a gauge-invariant (and therefore physically meaningful) EMT. However, it was shown that also a canonical construction of the Noether current can lead to a gauge invariant EMT. The procedure is quite involuted and it is discussed in detail in Refs. [163–166].

The conserved current associated with the Lorentz transformations is the generalized angular momentum tensor. We are going to focus only on the EMT in the remaining of the Chapter. Some study of the generalized angular momentum tensor could be found in [167]. The continuity equation that characterizes the EMT as a Noether current reads:

$$\partial_\mu \tilde{T}^{\mu\nu} = 0. \tag{8.3}$$

The spatial components of the EMT must decrease fast enough at spatial infinity, in order to have well defined conserved charges:

$$P^\nu = \int d^3x \; \tilde{T}^{0\nu}(x). \tag{8.4}$$

These can be identified with the four-momentum carried by the field (in a quantum theory P^ν obviously become operators, see Chapter 2). Since the charges represent the physical information contained in the EMT, all the redefinitions of the EMT that leave the charges unmodified are equivalent. One example of such redefinitions is the addition of a superpotential $\Phi^{\rho\mu\nu}$

$$T^{\mu\nu} = \tilde{T}^{\mu\nu} + \partial_\rho \Phi^{\rho\mu\nu}, \tag{8.5}$$

where $\Phi^{\rho\mu\nu} = -\Phi^{\mu\rho\nu}$. Furthermore, to preserve Eq. (8.4) we must require that $\partial_\rho \Phi^{\rho 0\nu}$ decrease fast enough at spatial infinity. This redefinition of the EMT is known as the Belinfante-Rosenfeld procedure [168, 169], and it allows one to incorporate specific properties in the EMT, such as the gauge invariance and the symmetry in the Lorentz indexes. In the following section, we are going to specify this procedure to the particular case of QED.

The Chapter is organized as follows: in Sec. 8.2 we are going to review the basic definitions and concepts about the EMT, specifically for the QED case. In Sec. 8.3, we are going to address the problem of renormalizing the individual operators that enter in the EMT definition. Some of the procedures are illustrated, as an example, in the QED case. However, most of the results are general and can be applied also to other gauge theories, like the non-abelian case of QCD. In Sec. 8.4, we are going to extensively study the EMT form factors for an electron in QED both in the off-forward and forward case. In Sec. 8.5, we are going to use the results of the form factors in the forward limit to study a variety of mass decompositions proposed in the literature. We are going to use this section as the foundation for the study of the proton mass decompositions, that is discussed in Sec. 8.6. Finally, in Sec. 8.7 we are going to summarize our results.

8.2 Definitions

Let us start with the definition of the QED Lagrangian:

$$\mathcal{L}_{\text{QED}} = \bar{\psi}\left(\frac{i}{2}\overleftrightarrow{\not{D}} - m\right)\psi - \frac{1}{4}F_{\mu\nu}F^{\mu\nu}. \tag{8.6}$$

Via the canonical construction in Eq. (8.2), we obtain:

$$\tilde{T}^{\mu\nu} = \bar{\psi}\frac{i}{2}\gamma^{\mu}\overleftrightarrow{\partial^{\nu}}\psi - F^{\mu\rho}F^{\nu}{}_{\rho} - F^{\mu\rho}\partial_{\rho}A^{\nu} + \frac{1}{4}g^{\mu\nu}F^{\alpha\beta}F_{\alpha\beta}. \tag{8.7}$$

This is an example in which the standard canonical construction fails to provide a gauge-invariant EMT. We can use now the Belinfante-Rosenfeld procedure to obtain a gauge invariant and, incidentally, symmetric EMT in the photon sector. Note that the superpotential is determined by the gauge sector only. Let us define the superpotential as the following combination

$$\Phi^{\rho\mu\nu} = \frac{1}{2}\left(S^{\rho\mu\nu} + S^{\mu\nu\rho} + S^{\nu\mu\rho}\right) \tag{8.8}$$

with the spin tensor defined as:

$$S^{\rho\mu\nu} = \frac{\delta\mathcal{L}}{\delta\left(\partial_{\rho}A_{\mu}\right)}A^{\nu} - \frac{\delta\mathcal{L}}{\delta\left(\partial_{\rho}A_{\nu}\right)}A^{\mu} = F^{\mu\rho}A^{\nu} - F^{\nu\rho}A^{\mu}. \tag{8.9}$$

A straightforward calculation leads to:

$$\Phi^{\rho\mu\nu} = F^{\mu\rho}A^{\nu}, \tag{8.10}$$

which, with the addition of the equation of motion for the gauge field

$$\partial_{\nu}\frac{\delta\mathcal{L}}{\delta\left(\partial_{\nu}A_{\mu}\right)} = \partial_{\nu}F^{\mu\nu} = \frac{\delta\mathcal{L}}{\delta A_{\mu}} = -e\bar{\psi}\gamma^{\mu}\psi, \tag{8.11}$$

leads to the following redefinition of the EMT:

$$\begin{aligned} T^{\mu\nu} &= \bar{\psi}\frac{i}{2}\gamma^{\mu}\overset{\leftrightarrow}{\partial^{\nu}}\psi - F^{\mu\rho}F^{\nu}{}_{\rho} - F^{\mu\rho}\partial_{\rho}A^{\nu} + \frac{1}{4}g^{\mu\nu}F^{\alpha\beta}F_{\alpha\beta} + \partial_{\rho}\left(F^{\mu\rho}A^{\nu}\right) \\ &= \bar{\psi}\frac{i}{2}\gamma^{\mu}\overset{\leftrightarrow}{\partial^{\nu}}\psi - F^{\mu\rho}F^{\nu}{}_{\rho} + \frac{1}{4}g^{\mu\nu}F^{\alpha\beta}F_{\alpha\beta} - e\bar{\psi}\gamma^{\mu}A^{\nu}\psi \\ &= \bar{\psi}\frac{i}{2}\gamma^{\mu}\overset{\leftrightarrow}{D^{\nu}}\psi - F^{\mu\rho}F^{\nu}{}_{\rho} + \frac{1}{4}g^{\mu\nu}F^{\alpha\beta}F_{\alpha\beta}. \end{aligned} \tag{8.12}$$

Note that, whereas this procedure leads to a symmetric tensor in the photon case, the leptonic sector contains both the symmetric and antisymmetric part. The antisymmetrtic part is related to the spin density of the leptonic field. In a classical theory, where the notion of non-integer spin is absent, it should be eliminated by an additional Belinfante-Rosenfeld superpotential. The Belinfante-Rosenfeld procedure allows one to shuffle some of (or all) the spin contributions into the orbital angular momentum contributions of the EMT. Being the spin of the electron a natural notion in QED, we are not going to modify further the EMT. A challenging problem in quantum field theory is the presence of divergences associated with quantum fluctuations of the fields. These fluctuations in a quantum field theory framework and in the language of Feynman diagrams are commonly known as loops. Each loop can come with a divergent integral. In order to produce predictions from the theory, a regularization and renormalization procedure is needed. The first one deals with the problem of parametrizing the divergences in terms of a suitable parameter called regulator. The divergences appear when an appropriate limit of the regulator is taken. A variety of different regularization procedures exist. We are going to adopt one of the most used, which is dimensional regularization. The idea is to work in a space-time with dimension d different than 4, to ensure the convergence of the problematic integrals. The dimensional regularization has the advantage of preserving the Poincaré invariance (in d dimension) and the gauge invariance of the theory. In dimensional regularization it is also introduced a scale μ to ensure that the coupling constant is dimensionless, see, e.g., Ref. [40]. Once the divergences have been regularized, a renormalization procedure must be implemented in order to consistently eliminate the divergences. The modern way to renormalize a Lagrangian quantum-field theory is to rewrite the fields and the parameters of the Lagrangian as the product of the renormalized quantities (fields and parameters) and constants called counterterms. The counterterms contain a divergent part that exactly cancels, order by order in perturbation theory, the divergent part that comes from the quantum loops. The finite parts of the counterterms are unconstrained and different prescriptions to fix them exist. Later in the Chapter, we will see some examples. We can now write the QED Lagrangian in terms of renormalized quantities and counterterms, using dimensional regularization:

$$\mathcal{L}_{\mathrm{QED}} = Z_2\bar{\psi}\left(\frac{i}{2}\overset{\leftrightarrow}{\not{\partial}}\right)\psi - Z_2 e\mu^{2\varepsilon}\bar{\psi}\not{A}\psi - \frac{Z_3}{4}F_{\mu\nu}F^{\mu\nu} - Z_2 Z_m m\bar{\psi}\psi, \tag{8.13}$$

where ϵ is defined in terms of the space-time dimension d as $\epsilon = 2 - d/2$. All the divergences in the theory are parametrized as poles in ϵ. Note that in Eq. (8.13) we introduced the scale μ to an appropriate power to ensure that the electric charge e remains dimensionless. We also point out that the time dimension is not affected by the dimensional regularization, hence a more precise way to define ϵ is via the equation $d = 1 + (3 - 2\epsilon)$. The time dimension is not changed in order to avoid issues with the definition of the equal-time hypersurfaces used to quantize the fields. At variance with the previous part of the thesis, we are going to use only instant-form quantization throughout this Chapter. For completeness, we notice that in light-front quantization the dimensional regularization is chosen usually in such a way to ensure that the plus and minus dimensions are unmodified. Hence in light-front quantization we have $d = 1 + 1 + (2 - 2\epsilon)$. This is because the metric in light-front parametrization is anti-diagonal in the plus-minus components, and then it is useful to have both with integer dimensions.

In Eq. (8.13), we ignored the presence of a gauge-fixing contribution. However, in the end, we will be interested only in matrix elements of the EMT and the gauge-fixing contribution vanishes on physical states. Whenever is needed for explicit calculations, we are going to use the Feynman gauge [40]. The renormalized EMT reads:

$$T^{\mu\nu} = T^{\mu\nu}_{e,S} + T^{\mu\nu}_{e,A} + T^{\mu\nu}_{\gamma}, \tag{8.14}$$

$$T^{\mu\nu}_{e,S} = Z_2 \; \bar{\psi}\frac{i}{4}\gamma^{\{\mu}\overset{\leftrightarrow}{\partial}{}^{\nu\}}\psi - Z_2\mu^{2\varepsilon} \; e\bar{\psi}\gamma^{\{\mu}A^{\nu\}}\psi, \tag{8.15}$$

$$T^{\mu\nu}_{e,A} = Z_2 \; \bar{\psi}\frac{i}{4}\gamma^{[\mu}\overset{\leftrightarrow}{\partial}{}^{\nu]}\psi - Z_2\mu^{2\varepsilon} \; e\bar{\psi}\gamma^{[\mu}A^{\nu]}\psi, \tag{8.16}$$

$$T^{\mu\nu}_{\gamma} = -Z_3 \; F^{\mu\alpha}F^{\nu}{}_{\alpha} + Z_3 \; \frac{g^{\mu\nu}}{4}F^{\alpha\beta}F_{\alpha\beta}, \tag{8.17}$$

where $a^{\{\mu}b^{\nu\}} = a^{\mu}b^{\nu} + a^{\nu}b^{\mu}$, $a^{[\mu}b^{\nu]} = a^{\mu}b^{\nu} - a^{\nu}b^{\mu}$, and the indexes e and γ refer to the electron and photon contributions, respectively.

The general parametrization of the electron and photon EMT matrix element between electron states is ($i = e, \gamma$):

$$\begin{aligned}
&\langle e\,(p')\,, s'|\, T^{\mu\nu}_{i}\,|e\,(p)\,, s\rangle = \left\langle e\left(P + \frac{\Delta}{2}\right), s'\right| T^{\mu\nu}_{i}\left|e\left(P - \frac{\Delta}{2}\right), s\right\rangle \\
&= \bar{u}'\Bigg(A_i(\Delta^2)\frac{P^{\mu}P^{\nu}}{m} + J_i(\Delta^2)\frac{iP^{\{\mu}\sigma^{\nu\}\rho}\Delta_{\rho}}{2m} \\
&+ D_i(\Delta^2)\frac{\Delta^{\mu}\Delta^{\nu} - g^{\mu\nu}\Delta^2}{4m} + m\bar{C}_i(\Delta^2)g^{\mu\nu} + C_i(\Delta^2)P^{[\mu}\gamma^{\nu]}\Bigg)u,
\end{aligned} \tag{8.18}$$

where, for the electron spinors, we used the shorthand notation

$$\bar{u}' = \bar{u}_{s'}\left(P + \frac{\Delta}{2}\right), \quad u = u_s\left(P - \frac{\Delta}{2}\right), \tag{8.19}$$

with s and s' being the initial and final electron helicities, respectively. The Dirac spinors are normalized as $\bar{u}_s(p)u_s(p) = 2m$, with m the electron mass. In Eq. (8.18), A_i, J_i, D_i, C_i and $\bar{C}_i$ ($i = e, \gamma$) are the EMT form factors (sometimes called gravitational form factors). They depend on the momentum transfer and, even if it is not shown for brevity, on the scale μ. We adopt the covariant normalization for the states, i.e.

$$\langle e(p'), s'|e(p), s\rangle = 2p^0(2\pi)^3\delta_{s,s'}\delta(\boldsymbol{p'} - \boldsymbol{p}), \tag{8.20}$$

where $a^\mu = (a^0, \boldsymbol{a})$ for any four-vector a^μ. In the forward limit $\Delta \to 0$, the EMT matrix element simplifies into:

$$\begin{aligned}\langle e(P)|T_i^{\mu\nu}|e(P)\rangle \equiv \langle e|T_i^{\mu\nu}|e\rangle &= 2P^\mu P^\nu A_i(0) + 2m^2 g^{\mu\nu}\bar{C}_i(0) \\ &= \left(2P^\mu P^\nu - \frac{g^{\mu\nu}}{2}M^2\right)A_i(0) + \frac{g^{\mu\nu}}{2}M^2\left(A_i(0) + 4\bar{C}_i(0)\right).\end{aligned} \tag{8.21}$$

Note that only diagonal matrix elements in the spin space survive in the forward limit, hence the spin dependence in Eq. (8.21) has been suppressed. The electron and photon form factors are not completely independent, since the conservation of the total EMT imposes the following sum rule:

$$\bar{C}_e(0) + \bar{C}_\gamma(0) = 0. \tag{8.22}$$

We also have the constraint:

$$A_e(0) + A_\gamma(0) = 1, \tag{8.23}$$

that follows from the momentum conservation. In addition to these equations, we have also:

$$J_e(0) + J_\gamma(0) = \frac{1}{2}. \tag{8.24}$$

This sum rule encodes the total angular momentum conservation and is equivalent to the sum rule for the A_i form factors when the generalized angular-momentum tensor is considered instead of the EMT, see [167].

We are now interested in the explicit expression of the form factors in Eq. (8.18) in perturbation theory. To obtain such expression, we can compute the Green function with the insertion of the EMT operator, i.e.

$$\langle e(p')|T\left[T_i^{\mu\nu}(0)\exp\left(i\int d^4x\mathcal{L}_I\right)\right]|e(p)\rangle, \quad \text{with } \mathcal{L}_I = -e\bar{\psi}\not{A}\psi, \tag{8.25}$$

where the space-time point at which the EMT is evaluated is fixed to 0. If it was evaluated at an arbitrary point y, translational invariance would have led to a simple overall phase factor $e^{-iy\Delta}$.

In Fig. 8.1 are illustrated the diagrams associated with the expansion of Eq. (8.25) up to order α. We use the common notation of a crossed dot for the counterterm diagrams and a black solid dot to indicate the EMT insertion

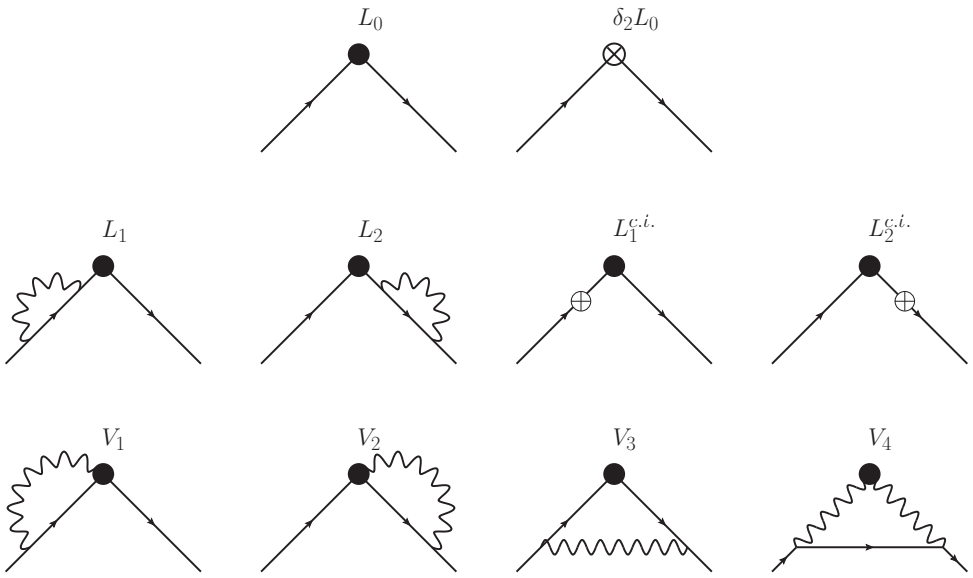

Figure 8.1: Relevant diagrams for the calculation of the electron EMT at $O(\alpha)$. The solid black dot represents the insertion of the EMT into the Green function.

into the Green function. L_0 is the diagram corresponding to the tree-level contribution and $\delta_2 L_0$ is the overall vertex counterterm. Since the total EMT is renormalized with the standard Lagrangian renormalization and we are considering only the matrix elements on the electron state, the vertex counterterm coincides with the electron field counterterm. $L_{1,2}$ are the diagrams with the leg-loop corrections, while $L_{1,2}^{c.t.}$ give the leg counterterms. $V_{1,2}$ are the diagrams associated with the interaction term present in $T_e^{\mu\nu}$, while V_3 is the one-loop electron vertex correction that arises from the the derivative term in $T_e^{\mu\nu}$. V_4 is the one-loop vertex correction with the photon coupled to the external operator.

In this section, we are going to present the results for the electron matrix elements of the EMT, as it turns out from a direct computation of Eq. (8.25). In the calculation of the diagrams in Fig. 8.1, one finds ultraviolet (UV) divergences in the separate electron and photon contributions. Moreover, infrared divergences emerge in the electron contribution. Only $V_1 + V_2$ is infrared safe because of the four-particle vertex where the photon couples directly with the external operator. The infrared divergences are canceled only in the forward limit for the total electron contribution. It is also useful to introduce the following total leg contribution:

$$L_{tot} = (1 + \delta_2)L_0 + L_1 + L_2 + L_1^{c.t.} + L_2^{c.t.}, \tag{8.26}$$

since L_{tot} is independent on the Lagrangian renormalization scheme. We employ the dimensional regularization for both the UV and infrared divergences, indicating with $\epsilon > 0$ and $\epsilon_I > 0$ the corresponding dimension parameters. To obtain the intermediate expressions for the leg contributions, we adopt the on-shell scheme to fix the Lagrangian counterterms. We obtain the following

results:

$$(1+\delta_2)L_0^{\mu\nu} = \left(1+\frac{\alpha}{2\pi}\left(\frac{2}{\varepsilon_I}-1\right)-\mathscr{P}(1+2\varepsilon)\right)L_0^{\mu\nu}, \tag{8.27}$$

where

$$L_0^{\mu\nu} = \left(\frac{P^\mu P^\nu}{m}\bar{u}'u + \bar{u}'\frac{i\sigma^{\{\mu\Delta}P^{\nu\}}}{4m}u - \frac{1}{2}\bar{u}'P^{[\mu}\gamma^{\nu]}u\right), \tag{8.28}$$

and

$$\begin{aligned}\mathscr{P} &= \frac{\alpha\Gamma(\varepsilon)}{4\pi}\left(\frac{4\pi\mu^2}{m^2}\right)^{\varepsilon} = \frac{\alpha}{4\pi}\left(\Delta_{\text{UV}} + \log\left(\frac{\mu^2}{m^2}\right)\right)\\ &= \frac{\alpha}{4\pi}\left(\frac{1}{\varepsilon} - \gamma_E + \log(4\pi) + \log\left(\frac{\mu^2}{m^2}\right)\right).\end{aligned} \tag{8.29}$$

The combination of the leg diagrams evaluates to 0, i.e.

$$L_{o.l.} = L_1 + L_2 + L_1^{c.t.} + L_2^{c.t.} = 0, \tag{8.30}$$

consistently with the on-shell renormalization condition. In fact, one can see that the general expression for $L_{o.l.}$ is as follows:

$$L_{o.l.} = \lim_{\not{p}\to m} 2\bar{u}'\gamma^\mu P^\nu \frac{i(\not{p}+m)}{p^2-m^2}\left(-i\Sigma_R(\not{p})\right)u, \tag{8.31}$$

where

$$\Sigma_R(\not{p}) = \not{p}\left(\Sigma_V(\not{p})+\delta_2\right) - m\left(-\Sigma_S(\not{p})+\delta_2+\delta_m\right). \tag{8.32}$$

The on-shell renormalization condition prescribes that:

$$\lim_{\not{p}\to m}\frac{i(\not{p}+m)}{p^2-m^2}\left(-i\Sigma_R(\not{p})\right) = 0, \tag{8.33}$$

to ensure that the pole of the propagator is at the renormalized electron mass, and the residual is equal to 1.

Therefore we have:

$$L_{tot} = (1+\delta_2)L_0^{\mu\nu} + L_{o.l.} = \left(1+\frac{\alpha}{2\pi}\left(\frac{2}{\varepsilon_I}-1\right)-\mathscr{P}(1+2\varepsilon)\right)L_0^{\mu\nu}. \tag{8.34}$$

As we stated above, this result is scheme independent, and this feature can easily be checked by computing it in other schemes, e.g. the $\overline{\text{MS}}$ scheme[1].

For the sum of the four-particle vertexes, we have:

$$V_1 + V_2 = -2\mathscr{P}(1+3\varepsilon)L_0^{\mu\nu} - m\mathscr{P}(1+\varepsilon)g^{\mu\nu}\bar{u}'u. \tag{8.35}$$

To obtain the explicit expression for the one-loop electron vertex V_3 and the one-loop photon vertex V_4, we have to introduce the Feynman parameters and

[1] Of course, $L_{o.l.}$ is no longer zero in $\overline{\text{MS}}$ and, accordingly, the expression for $(1+\delta_2)L_0^{\mu\nu}$ is different.

perform the corresponding integrals. First, it is useful to isolate the antisymmetric part of $L_0^{\mu\nu}$ by defining:

$$L_0^{\mu\nu} = \tilde{L}_0^{\mu\nu} + A^{\mu\nu}, \quad A^{\mu\nu} = -\frac{1}{2}\bar{u}' P^{[\mu}\gamma^{\nu]} u, \tag{8.36}$$

with $\tilde{L}_0^{\mu\nu} = \tilde{L}_0^{\nu\mu}$, see Eq. (8.28). For the electron vertex, we have:

$$V_3 = \int_0^1 dx \int_0^{1-x} dy N_e^{\mu\nu}, \tag{8.37}$$

having defined

$$\begin{aligned} N_e^{\mu\nu} = \tilde{L}_0^{\mu\nu} \Bigg[& \frac{\alpha}{2\pi \mathcal{M}_e} \left(x(1-x^2-2x) - x d_m^2 (1-z)(1-y) \right) \\ & + \mathcal{U}_e 2x(1-2\varepsilon)\left(1+\frac{\varepsilon}{2}\right) \Bigg] + m g^{\mu\nu} \bar{u}' u (4-2\varepsilon-2x+2\varepsilon x)\left(1+\frac{\varepsilon}{2}\right)\mathcal{U}_e \\ & + \frac{P^\mu P^\nu}{m} \bar{u}' u \frac{\alpha}{\pi \mathcal{M}_e} x^2(-1+x) + \frac{\Delta^\mu \Delta^\nu}{4m} \bar{u}' u \frac{\alpha}{\pi \mathcal{M}_e}(y-z)^2(x-2) \\ & + A^{\mu\nu} \Bigg[\frac{\alpha}{2\pi \mathcal{M}_e} \left(x(1-x^2-2x) - x d_m^2 (1-z)(1-y) \right) \\ & + \mathcal{U}_e \left(2x(1-2\varepsilon) + 4(1-\varepsilon)(1+x) \right)\left(1+\frac{\varepsilon}{2}\right) \Bigg], \end{aligned} \tag{8.38}$$

where

$$\mathcal{M}_e = (1-x)^2 + y(1-x-y)d_m^2, \quad d_m^2 = -\Delta^2/m^2 \geq 0, \tag{8.39}$$

and

$$\mathcal{U}_e = \mathcal{P}\left(1 - \frac{\varepsilon}{2} - \varepsilon \log\left[\mathcal{M}_e\right]\right). \tag{8.40}$$

For the photon coupling to the external operator we have:

$$V_4 = \int_0^1 dx \int_0^{1-x} dy N_\gamma^{\mu\nu}, \tag{8.41}$$

with

$$\begin{aligned} N_\gamma^{\mu\nu} = \tilde{L}_0^{\mu\nu} \Bigg\{ & \frac{\alpha}{\pi \mathcal{M}_\gamma} \left[-x^2 + \frac{\Delta^2}{m^2} y(1-x-y) \right] + 4(1+x)(1-\varepsilon)\left(1+\frac{\varepsilon}{2}\right)\mathcal{U}_\gamma \Bigg\} \\ & + \frac{P^\mu P^\nu}{m} \bar{u}' u \frac{\alpha}{\pi \mathcal{M}_\gamma} x^2(1-x) + \frac{\Delta^\mu \Delta^\nu}{4m} \bar{u}' u \frac{\alpha}{\pi \mathcal{M}_\gamma}(1-x-(1+x)(1-x-2y)^2) \\ & + m g^{\mu\nu} \bar{u}' u \Bigg\{ \frac{\alpha}{8\pi \mathcal{M}_\gamma} \left[2x^3 - 2\frac{\Delta^2}{m^2}(2+x) y(1-x-y) \right] \\ & - \mathcal{U}_\gamma (1+x-2\varepsilon-5x\varepsilon)\left(1+\frac{\varepsilon}{2}\right) \Bigg\}, \end{aligned} \tag{8.42}$$

where

$$\mathcal{M}_\gamma = x^2 + y(1-x-y)d_m^2. \tag{8.43}$$

Since we are using a symmetric definition for the photon EMT, the antisymmetric Lorentz structure is not present in Eq. (8.42).

8.3 Renormalization

The renormalization of the UV divergences is a rather tricky subject, discussed in detail in Refs. [170, 171] for QCD. We retraced the steps of [170, 171] in our works for the QED (see Ref. [160]) and QCD cases (see Ref. [161]). One can introduce the following operators[2]

$$\mathcal{O}_{3,S} = \frac{i}{4}\bar{\psi}\gamma^{\{\mu}\overset{\leftrightarrow}{D}^{\nu\}}\psi, \quad \mathcal{O}_{3,A} = \frac{i}{4}\bar{\psi}\gamma^{[\mu}\overset{\leftrightarrow}{D}^{\nu]}\psi, \quad \mathcal{O}_4 = g^{\mu\nu}m\bar{\psi}\psi, \tag{8.44}$$

$$\mathcal{O}_1 = -F^{\mu\alpha}F^{\nu}{}_{\alpha}, \qquad \mathcal{O}_2 = g^{\mu\nu}F^{\alpha\beta}F_{\alpha\beta}, \tag{8.45}$$

where we suppressed the Lagrangian counterterms to lighten the notation. The full electron operator reads:

$$\mathcal{O}_3 = \mathcal{O}_{3,S} + \mathcal{O}_{3,A}, \tag{8.46}$$

from which we have the full EMT as:

$$T^{\mu\nu} = \mathcal{O}_1 + \frac{\mathcal{O}_2}{4} + \mathcal{O}_3. \tag{8.47}$$

To carry out the renormalization program, we choose to use the $\overline{\text{MS}}$ scheme instead of the MS, that was adopted in Refs. [170, 171]. The transition between the two schemes can be performed via the following substitution (see App. B and Eqs. (B.4)-(B.5) for a more detailed explanation of how to relate the counterterms in the two schemes):

$$\frac{1}{\epsilon} = \frac{1}{\epsilon}S_\epsilon, \tag{8.48}$$

with

$$\begin{aligned} S_\epsilon\big|_{\overline{\text{MS}}_1} &= \frac{(4\pi)^\epsilon}{\Gamma(1-\epsilon)} = 1 + \epsilon\left(\log(4\pi) - \gamma_E\right) \\ &\quad + \epsilon^2\,\frac{6\gamma_E^2 - \pi^2 - 12\gamma_E\log(4\pi) + 6\log^2(4\pi)}{12} + O(\epsilon^3) \\ &\equiv 1 + \epsilon\,\delta_{\text{UV}} + \epsilon^2\,\frac{{\delta_{\text{UV}}}^2}{2} - \epsilon^2\,\frac{\pi^2}{12} + O(\epsilon^3)\,, \end{aligned} \tag{8.49}$$

or

$$S_\epsilon\big|_{\overline{\text{MS}}_2} = (4\pi e^{-\gamma_E})^\epsilon = 1 + \epsilon\,\delta_{\text{UV}} + \epsilon^2\,\frac{{\delta_{\text{UV}}}^2}{2} + O(\epsilon^3)\,, \tag{8.50}$$

where $\delta_{\text{UV}} = \log(4\pi) - \gamma_E$. The definition in Eq. (8.49) is used in Ref. [12] and related works, whereas the definition in Eq. (8.50) seems to be more popular in literature. For the QED case, since we work at $O(\alpha)$, the two definitions of $\overline{\text{MS}}$ coincide. Their difference will be important in Sec. 8.6. Therefore, the transition between MS and either version of $\overline{\text{MS}}$ at $O(\alpha)$ can be simply performed with the replacement $1/\varepsilon \to \Delta_{\text{UV}}$. We will carry out the renormalization for the

[2]To simplify the notation, we omit the tensor indexes in the operator $\mathcal{O}_i$ if not necessary.

operators evaluated between electron states, therefore some of the counterterms associated with the photon contributions are vanishing. Additional work would be required to renormalize the EMT evaluated between photon states. In the following, the Lagrangian renormalization for all the fields is understood (the charge renormalization is not present at order α), and we will deal explicitly with the renormalization of the composite operators $\mathcal{O}_i$, $i = 1, ..., 4$.

We have the following system of equations:

$$\mathcal{O}_1^R = Z_T\mathcal{O}_1 + Z_M\mathcal{O}_2 + Z_L\mathcal{O}_{3,S} + Z_S\mathcal{O}_4, \tag{8.51}$$
$$\mathcal{O}_2^R = Z_F\mathcal{O}_2 + Z_C\mathcal{O}_4, \tag{8.52}$$
$$\mathcal{O}_{3,S}^R = Z_\psi\mathcal{O}_{3,S} + Z_K\mathcal{O}_4 + Z_Q\mathcal{O}_1 + Z_B\mathcal{O}_2, \tag{8.53}$$
$$\mathcal{O}_{3,A}^R = Z_5\mathcal{O}_{3,A}, \tag{8.54}$$
$$\mathcal{O}_4^R = \mathcal{O}_4. \tag{8.55}$$

The counterterms for the trace of the photon EMT (in the $\overline{\text{MS}}$ scheme) are well known in literature from the trace anomaly [172–175]:

$$Z_F = 1 + \frac{\beta(e)}{e}\Delta_{\text{UV}} = 1 + \frac{\alpha}{3\pi}\Delta_{\text{UV}}, \quad Z_C = 2\gamma_m\Delta_{\text{UV}} = \frac{3\alpha}{\pi}\Delta_{\text{UV}}, \tag{8.56}$$

where we used the definitions of the QED β-function and electron anomalous dimension at order α:

$$\frac{\beta(e)}{2e} = -\frac{\alpha\beta_0}{8\pi}, \quad \beta_0 = -\frac{4}{3}, \quad \gamma_m = \frac{3\alpha}{2\pi}. \tag{8.57}$$

To ensure the invariance of the total EMT under renormalization, we have the following constraints on the counterterms:

$$Z_T + Z_Q = 1, \tag{8.58}$$
$$Z_L + Z_\psi = 1, \tag{8.59}$$
$$Z_M + Z_B + \frac{Z_F}{4} = \frac{1}{4}, \tag{8.60}$$
$$Z_S + Z_K + \frac{Z_C}{4} = 0, \tag{8.61}$$
$$Z_5 = 1. \tag{8.62}$$

From Eq. (8.62), we can see that the antisymmetric part does not need any additional renormalization. This happens because there are no gauge-invariant antisymmetric operators with the correct correct dimension to mix with it. The fact that the antisymmetric part is free of divergences can also be checked from the explicit results given in the previous section. From now on in this section we are going to drop the subscript S in the symmetric part of $\mathcal{O}_3$ to lighten the notation.

We can introduce the traceless operators $\widetilde{\mathcal{O}}_i$ for the electron and the photon as:

$$\widetilde{\mathcal{O}}_1^R = \mathcal{O}_1^R + \frac{1}{4}\left(1 - \frac{\beta(e)}{2e} + x\right)\mathcal{O}_2^R + \frac{y - \gamma_m}{4}\mathcal{O}_4^R, \tag{8.63}$$

$$\widetilde{\mathcal{O}}_3^R = \mathcal{O}_3^R - \frac{x}{d}\mathcal{O}_2^R - \frac{1+y}{4}\mathcal{O}_4^R, \tag{8.64}$$

where x, y are finite α-dependent parameters, starting at $O(\alpha)$. We recall from Eq. (8.21) that the traceless operators are directly related to the $A_i(0)$ form factors. Contrary to what is stated in Ref. [170], Eqs. (8.58)-(8.62) do not add new constraints on the values of x, y. For the MS scheme, the correct procedure was described in [171] and it consists in requiring a vanishing finite part for all the counterterms. Depending on the scheme, the procedure to fix x and y is different. Accordingly, the choice of the values for x and y implies to using a specific scheme for the counterterms. We will review the different procedures to fix x and y in MS-like schemes in Sec. 8.6. However, MS-like schemes are not, perhaps, the most physically intuitive because the trace of the renormalized photon operator is written in terms of the combination of the renormalized traces of the photon and electron, as it can be clearly see from Eq. (9) of Ref. [176]:

$$\langle e|\left(T_{e,R}\right)^{\mu}_{\mu}|e\rangle = (1+y)\,\langle e|\left(m\bar{\psi}\psi\right)_R|e\rangle + x\,\langle e|\left(F^{\mu\nu}F_{\mu\nu}\right)_R|e\rangle\,, \tag{8.65}$$

$$\langle e|\left(T_{\gamma,R}\right)^{\mu}_{\mu}|e\rangle = (\gamma_m - y)\,\langle e|\left(m\bar{\psi}\psi\right)_R|e\rangle + \left(\frac{\beta(e)}{2e} - x\right)\langle e|\left(F^{\mu\nu}F_{\mu\nu}\right)_R|e\rangle\,. \tag{8.66}$$

To diagonalize this system of equations, we need to choose a different scheme with respect to MS-like choices. We introduce two schemes, that we call "diagonal" schemes, as follows:

- D_1 scheme (see Ref. [160]): $x = 0$, $y = \gamma_m$. In this scheme, Eqs. (8.65)-(8.66) become diagonal, in the sense that the trace of the renormalized electron EMT is given solely in terms of electron operators.
- D_2 scheme (see Ref. [161]): $x = y = 0$. In this scheme, the entire trace anomaly is attributed to the trace of the renormalized photon part $T_{\gamma,R}$ of the EMT.

The D_2 scheme reflects the fact that, in dimensional regularization, the trace anomaly entirely emerges from the photon sector. Through all the sections dedicated to the QED case, we are going to consider only the D_1 scheme, the D_2 scheme will be used only in Sec. 8.6 when dealing with the proton case.

For the purposes of the one-loop calculation in this section, the value of x is not relevant, since for an electron state the product

$$x\,\langle e|F_R^2|e\rangle \tag{8.67}$$

is of $O(\alpha^2)$. In $\overline{\mathrm{MS}}$ we obtain the same value for x as in the D_1 scheme since we are considering only electron states, but this is a coincidence, not a general feature. We have, therefore:

$$x = 0, \quad y = \begin{cases} \frac{\alpha}{3\pi} & \overline{\mathrm{MS}} \\ \gamma_m = \frac{3\alpha}{2\pi} & \mathrm{D}_1 \end{cases}. \tag{8.68}$$

The counterterms that involve the parameters x and y are $Z_{B,M,K,S}$. They read:

$$Z_M = \frac{Z_T}{d} - \frac{Z_F}{d}\left(1 - \frac{\beta(e)}{2e} + x\right), \tag{8.69}$$

$$Z_S = -\frac{Z_L}{d} - \frac{Z_C}{d}\left(1 - \frac{\beta(e)}{2e} + x\right) - \frac{y - \gamma_m}{d}, \tag{8.70}$$

$$Z_B = \frac{Z_Q}{d} + \frac{x}{d} Z_F, \tag{8.71}$$

$$Z_K = -\frac{Z_\psi}{d} + \frac{x}{d} Z_C + \frac{1+y}{d}. \tag{8.72}$$

The counterterms $Z_{\psi,Q,L,T}$ are fixed from the evolution equations of the form factors $A_i(0)$. Note that $A_i(0)$ is already Lagrangian renormalized, therefore it has a scale dependence that is not acquired during the renormalization procedure of this section. For this reason, the scale dependence of $A_i(0)$ and $A_i^R(0)$ is the same. From our previous results, we can derive immediately:

$$\frac{\partial}{\partial \ln \mu} A_e(0) = -\frac{\partial}{\partial \ln \mu} A_\gamma(0) = -\frac{4\alpha}{3\pi} A_e(0). \tag{8.73}$$

The full evolution equations would require A_e and A_γ also for a photon state. We will not consider them, since we are dealing with an electron state only. However, it is known that the evolution equations of A_i are the second moment of the DGLAP kernel, see Ref. [170] for the explicit expression, with $n_f = 1$, $C_F = 1$ and $C_A = 0$ for the QED case. Following the procedure illustrated in detail in Ref. [171], we obtain in the two schemes:

$$Z_T = 1, \qquad Z_Q = 0, \qquad Z_\psi = 1 + \frac{2\alpha}{3\pi} \Delta_{\rm UV}, \tag{8.74}$$

$$Z_L = -\frac{2\alpha}{3\pi} \Delta_{\rm UV}, \qquad Z_M = -\frac{\alpha}{12\pi} \Delta_{\rm UV}, \quad Z_B = 0, \tag{8.75}$$

$$Z_S = \begin{cases} -\frac{7\alpha}{12\pi} \Delta_{\rm UV}, & \overline{\rm MS} \\ -\frac{7\alpha}{24\pi} - \frac{7\alpha}{12\pi} \Delta_{\rm UV}, & {\rm D}_1 \end{cases}, \qquad Z_K = \begin{cases} -\frac{\alpha}{6\pi} \Delta_{\rm UV}, & \overline{\rm MS} \\ \frac{7\alpha}{24\pi} - \frac{\alpha}{6\pi} \Delta_{\rm UV}, & {\rm D}_1 \end{cases}. \tag{8.76}$$

The difference between the two schemes is a finite part of $O(\alpha)$.

Using the values for the counterterms in Eqs. (8.56) and (8.74)-(8.76), alongside with the tree-level results[3]

$$\langle \mathcal{O}_3 \rangle_{tree} = \tilde{L}_0^{\mu\nu} = L_0^{\mu\nu} + \frac{1}{2} \bar{u}' P^{[\mu} \gamma^{\nu]} u, \quad \langle \mathcal{O}_4 \rangle_{tree} = m g^{\mu\nu} \bar{u}' u, \quad \langle \mathcal{O}_{1,2} \rangle_{tree} = 0, \tag{8.77}$$

we obtain from Eqs. (8.51)-(8.55) in the $\overline{\rm MS}$ scheme

$$\langle \mathcal{O}_3^R \rangle^{\overline{\rm MS}} = \langle \mathcal{O}_3 \rangle + \frac{2\alpha}{3\pi} \Delta_{\rm UV}\, \tilde{L}_0^{\mu\nu} - \frac{\alpha}{6\pi} \Delta_{\rm UV}\, (m g^{\mu\nu} \bar{u}' u), \tag{8.78}$$

[3] We recall that we are considering only the symmetric part of $\mathcal{O}_3$, since the antisymmetric part does not need any additional renormalization, see Eq. (8.62).

$$\langle \mathcal{O}_1^R \rangle^{\overline{\rm MS}} = \langle \mathcal{O}_1 \rangle - \frac{2\alpha}{3\pi} \Delta_{\rm UV}\, \tilde{L}_0^{\mu\nu} - \frac{7\alpha}{12\pi} \Delta_{\rm UV}\, (m g^{\mu\nu} \bar{u}' u), \tag{8.79}$$

$$\langle \mathcal{O}_2^R \rangle^{\overline{\rm MS}} = \langle \mathcal{O}_2 \rangle + \frac{3\alpha}{\pi} \Delta_{\rm UV}\, (m g^{\mu\nu} \bar{u}' u), \tag{8.80}$$

where we introduced the notation

$$\langle \mathcal{O} \rangle = \langle e(p') | \mathcal{O} | e(p) \rangle \,. \tag{8.81}$$

The corresponding results with the counterterms in the $\rm D_1$ scheme are

$$\langle \mathcal{O}_3^R \rangle^{\rm D_1} = \langle \mathcal{O}_3 \rangle + \frac{2\alpha}{3\pi} \Delta_{\rm UV}\, \tilde{L}_0^{\mu\nu} + \left(\frac{7\alpha}{24\pi} - \frac{\alpha}{6\pi} \Delta_{\rm UV} \right) (m g^{\mu\nu} \bar{u}' u), \tag{8.82}$$

$$\langle \mathcal{O}_1^R \rangle^{\rm D_1} = \langle \mathcal{O}_1 \rangle - \frac{2\alpha}{3\pi} \Delta_{\rm UV}\, \tilde{L}_0^{\mu\nu} + \left(-\frac{7\alpha}{24\pi} - \frac{7\alpha}{12\pi} \Delta_{\rm UV} \right) (m g^{\mu\nu} \bar{u}' u), \tag{8.83}$$

$$\langle \mathcal{O}_2^R \rangle^{\rm D_1} = \langle \mathcal{O}_2 \rangle + \frac{3\alpha}{\pi} \Delta_{\rm UV}\, (m g^{\mu\nu} \bar{u}' u). \tag{8.84}$$

As a result, the renormalised contributions read:

$$L_{tot}^R = \left(1 + \frac{\alpha}{\pi\epsilon_I} - \frac{\alpha}{\pi} - \frac{\alpha \mathcal{L}}{4\pi} \right) \tilde{L}_0^{\mu\nu} + \left(1 + \frac{\alpha}{\pi\epsilon_I} - \frac{\alpha}{\pi} \right) A^{\mu\nu}, \tag{8.85}$$

$$(V_1 + V_2)^R = \begin{cases} \left(-\frac{3\alpha}{2\pi} - \frac{\alpha\mathcal{L}}{2\pi} \right) \tilde{L}_0^{\mu\nu} - \frac{3\alpha}{2\pi} A^{\mu\nu} - \left(\frac{\alpha}{4\pi} + \frac{\alpha\mathcal{L}}{4\pi} \right) (m g^{\mu\nu} \bar{u}' u), & \overline{\rm MS} \\ \left(-\frac{3\alpha}{2\pi} - \frac{\alpha\mathcal{L}}{2\pi} \right) \tilde{L}_0^{\mu\nu} - \frac{3\alpha}{2\pi} A^{\mu\nu} - \left(-\frac{\alpha}{24\pi} + \frac{\alpha\mathcal{L}}{4\pi} \right) (m g^{\mu\nu} \bar{u}' u), & \rm D_1 \end{cases}, \tag{8.86}$$

$$\begin{aligned} (N_e^{\mu\nu})^R = {} & \tilde{L}_0^{\mu\nu} \Big[\frac{\alpha}{8\pi \mathcal{M}_e} \left(4x(1 - x^2 - 2x) + 4x \frac{\Delta^2}{m^2} (1 - z)(1 - y) \right) \\ & + \frac{\alpha x}{2\pi} \left(\mathcal{L} - \log(\mathcal{M}_e) - 2 \right) \Big] \\ & + m g^{\mu\nu} \bar{u}' u \frac{\alpha}{2\pi} \left(x - 1 - (2 - x) \left(\log(\mathcal{M}_e) - \mathcal{L} \right) \right) \\ & + \frac{P^\mu P^\nu}{m} \bar{u}' u \frac{\alpha}{\pi \mathcal{M}_e} x^2 (-1 + x) \frac{\Delta^\mu \Delta^\nu}{4m} \bar{u}' u \frac{\alpha}{\pi \mathcal{M}_e} (y - z)^2 (x - 2) \\ & + A^{\mu\nu} \Big[-\frac{\alpha}{2\pi} \left(1 + 3x + x \log(\mathcal{M}_e) \right) \\ & + \frac{\alpha}{2\pi \mathcal{M}_e} \left(x(1 - x^2 - 2x) - x d_m^2 (x + y)(1 - y) \right) \Big], \end{aligned} \tag{8.87}$$

$$\begin{aligned} \left(N_\gamma^{\mu\nu} \right)^R = {} & \tilde{L}_0^{\mu\nu} \Big\{ \frac{\alpha}{\pi \mathcal{M}_\gamma} \left[-x^2 + \frac{\Delta^2}{m^2} y(1 - x - y) \right] \\ & + \frac{\alpha}{\pi} (1 + x) \left(\mathcal{L} - 1 - \log(\mathcal{M}_\gamma) \right) \Big\} + \frac{P^\mu P^\nu}{m} \bar{u}' u \frac{\alpha}{\pi \mathcal{M}_\gamma} x^2 (1 - x) \\ & + \frac{\Delta^\mu \Delta^\nu}{4m} \bar{u}' u \frac{\alpha}{\pi \mathcal{M}_\gamma} (1 - x - (1 + x)(1 - x - 2y)^2) \\ & + m g^{\mu\nu} \bar{u}' u \left(\frac{\alpha}{4\pi \mathcal{M}_\gamma} \left[x^3 + d_m^2 (2 + x) y (1 - x - y) \right] \right) \end{aligned}$$

$$+ mg^{\mu\nu}\bar{u}'u \begin{cases} -\frac{\alpha}{4\pi}\left((1+x)(\mathcal{L}-\log(\mathcal{M}_\gamma))-2-5x\right), & \overline{\text{MS}} \\ -\frac{\alpha}{4\pi}\left((1+x)(\mathcal{L}-\log(\mathcal{M}_\gamma))+\frac{1}{3}-5x\right), & \text{D}_1 \end{cases}, \tag{8.88}$$

where we assigned the finite part of the counterterm of $g^{\mu\nu}$ to $V_1 + V_2$, and defined $\mathcal{L} = \log\left(\frac{\mu^2}{m^2}\right)$.

Note that we used the following relation

$$-\frac{7\alpha}{24\pi} = \frac{\alpha}{4\pi}\int_0^1 dx \int_0^{1-x} dy f(x,y) \tag{8.89}$$

to include the finite part of the counterterm in the photon sector. Imposing $f(x,y) = c$, with c a costant, we find that $c = -7/3$. Of course, one can choose a different function, but it does not matter since we are ultimately interested in the integrated values.

8.4 Form Factors

The integrals over the Feynman parameters can be manipulated to reproduce the total results shown in Ref. [177]. However, they cannot be completely solved using analytic techniques to produce a close form for the results. Only in the forward limit the integrals simplify and lead to the following expressions:

$$L^R_{tot}(\Delta = 0) = 2P^\mu P^\nu \left(1 + \frac{\alpha}{\pi\varepsilon_I} - \frac{\alpha}{\pi} - \frac{\alpha\mathcal{L}}{4\pi}\right), \tag{8.90}$$

$$(V_1+V_2)^R(\Delta = 0) = \begin{cases} 2P^\mu P^\nu\left(-\frac{\alpha\mathcal{L}}{2\pi} - \frac{3\alpha}{2\pi}\right) - 2m^2 g^{\mu\nu}\left(\frac{\alpha\mathcal{L}}{4\pi} + \frac{\alpha}{4\pi}\right), & \overline{\text{MS}} \\ 2P^\mu P^\nu\left(-\frac{\alpha\mathcal{L}}{2\pi} - \frac{3\alpha}{2\pi}\right) - 2m^2 g^{\mu\nu}\left(\frac{\alpha\mathcal{L}}{4\pi} - \frac{\alpha}{24\pi}\right), & \text{D}_1 \end{cases}, \tag{8.91}$$

$$V_3^R(\Delta = 0) = 2P^\mu P^\nu\left(-\frac{\alpha}{\pi\varepsilon_I} + \frac{14\alpha}{9\pi} + \frac{\alpha\mathcal{L}}{12\pi}\right) + 2m^2 g^{\mu\nu}\left(\frac{5\alpha\mathcal{L}}{12} + \frac{7\alpha}{36\pi}\right), \tag{8.92}$$

$$V_4^R(\Delta = 0) = \begin{cases} 2P^\mu P^\nu\left(\frac{2\alpha\mathcal{L}}{3\pi} + \frac{17\alpha}{18\pi}\right) + 2m^2 g^{\mu\nu}\left(-\frac{\alpha\mathcal{L}}{6\pi} + \frac{\alpha}{18\pi}\right), & \overline{\text{MS}} \\ 2P^\mu P^\nu\left(\frac{2\alpha\mathcal{L}}{3\pi} + \frac{17\alpha}{18\pi}\right) + 2m^2 g^{\mu\nu}\left(-\frac{\alpha\mathcal{L}}{6\pi} - \frac{17\alpha}{72\pi}\right), & \text{D}_1 \end{cases}. \tag{8.93}$$

To obtain the form factors in terms of the Feynman-parameter integrals for a generic value of Δ, we can compare Eqs. (8.85)-(8.88) with the general parametrization of the EMT given in Eq. (8.18). We obtain:

$$A_e^R(\Delta^2) = 1 + \frac{\alpha}{\pi}\left(\frac{1}{\epsilon_I} - \frac{3\mathcal{L}}{4} - \frac{5}{2}\right) + \frac{\alpha}{2\pi}\int_0^1 dx \int_0^{1-x} dy \times \left(\frac{x^3 - 4x^2 + x - d_m^2 x(1-y)(x+y)}{\mathcal{M}_e} + x(\mathcal{L} - 2 - \log\mathcal{M}_e)\right), \tag{8.94}$$

$$J_e^R(\Delta^2) = \frac{1}{2} + \frac{\alpha}{2\pi}\left(\frac{1}{\epsilon_I} - \frac{3\mathscr{L}}{4} - \frac{5}{2}\right) + \frac{\alpha}{4\pi}\int_0^1 dx \int_0^{1-x} dy \times \left(\frac{x(1-x^2-2x) - d_m^2 x(1-y)(x+y)}{m_e} + x(\mathscr{L} - 2 - \log m_e)\right), \tag{8.95}$$

$$C_e^R(\Delta^2) = 1 + \frac{\alpha}{\pi}\left(\frac{1}{\epsilon_I} - \frac{5}{2}\right) + \frac{\alpha}{2\pi}\int_0^1 dx \int_0^{1-x} dy \times \left(\frac{x(1-x^2-2x) - d_m^2 x(1-y)(x+y)}{m_e} - 1 - 3x - x\log m_e\right), \tag{8.96}$$

$$D_e^R(\Delta^2) = \frac{\alpha}{\pi}\int_0^1 dx \int_0^{1-x} dy \frac{(x-2)(1-x-2y)^2}{m_e}, \tag{8.97}$$

$$\bar{C}_e^R(\Delta^2) = -\frac{\alpha\mathscr{L}}{4\pi} - \frac{\alpha c_e}{4\pi} + \frac{\alpha}{2\pi}\int_0^1 dx \int_0^{1-x} dy \left(\frac{-d_m^2(x-2)(1-x-2y)^2}{2m_e} + x - 1 - (2-x)\left(\log m_e - \mathscr{L}\right)\right), \tag{8.98}$$

where

$$c_e = \begin{cases} 1, & \overline{\text{MS}} \\ -\frac{1}{6}, & \text{D}_1 \end{cases}, \tag{8.99}$$

$$A_\gamma^R(\Delta^2) = \frac{\alpha}{\pi}\int_0^1 dx \int_0^{1-x} dy \left(\frac{-x^3 - d_m^2 y(1-x-y)}{m_\gamma} + (1+x)(\mathscr{L} - 1 - \log m_\gamma)\right), \tag{8.100}$$

$$J_\gamma^R(\Delta^2) = \frac{\alpha}{2\pi}\int_0^1 dx \int_0^{1-x} dy \left(\frac{-x^2 - d_m^2 y(1-x-y)}{m_\gamma} + (1+x)(\mathscr{L} - 1 - \log m_\gamma)\right), \tag{8.101}$$

$$C_\gamma^R(\Delta^2) = 0, \tag{8.102}$$

$$D_\gamma^R(\Delta^2) = \frac{\alpha}{\pi}\int_0^1 dx \int_0^{1-x} dy \frac{1 - x - (1+x)(1-x-2y)^2}{m_\gamma}, \tag{8.103}$$

$$\bar{C}_\gamma^R(\Delta^2) = \frac{\alpha}{4\pi}\int_0^1 dx \int_0^{1-x} dy \left(-(1+x)(\mathscr{L} - \log m_\gamma) + 5x + 2c_e + \frac{x^3 + d_m^2\left((2+x)y(1-x-y) - 1 + x + (1+x)(1-x-2y)^2\right)}{m_\gamma}\right). \tag{8.104}$$

8.4.1 Feynman-parameter integrals

Although a closed form for the integrals in the previous section is impossible to obtain, we are going to manipulate the integrals to isolate the infrared divergences and then show their cancelation in the forward limit, as well as to obtain a more suitable expression for the numerical implementation. The integrals that we need to analyze can be divided in infrared-safe and infrared-unsafe integrals. The fundamental difference between the electron integrals and the photon integrals (see Eqs. (8.94)-(8.104)) lies in the "mass" function that appears at the denominator and inside the logarithm (see Eqs. (8.39) and (8.43)). We start by introducing the following general integrals:

$$f_\gamma^{(n,m)}(x,y) = x^n y^m \mathcal{M}_\gamma^{-1} = x^n y^m \left(x^2 + y(1-x-y)d_m^2\right)^{-1}, \tag{8.105}$$

$$f_e^{(n,m)}(x,y) = x^n y^m \mathcal{M}_e^{-1} = x^n y^m \left((1-x)^2 + y(1-x-y)d_m^2\right)^{-1}, \tag{8.106}$$

$$I_I^{(n,m)} = \int_0^1 dx \int_0^{1-x} dy \quad f_i^{(n,m)}(x,y). \tag{8.107}$$

We can make use of the following relation:

$$I_I^{(n,m)} = \int_0^1 dx \int_0^{1-x} dy\ f_i^{(n,m)}(x,y) = \int_0^1 dx \int_0^1 dw\ (1-x) f_i^{(n,m)}(x, w(1-x)) \tag{8.108}$$

$$= \frac{-1}{d_m^2} \int_0^1 dx\ (1-x)^{m-1} x^n \int_0^1 dw\ w^m \left(w^2 - w - c_i\right)^{-1}$$

$$= \frac{-1}{d_m^2} \int_0^1 dx\ (1-x)^{m-1} x^n\ J^{(m)}(c_i), \tag{8.109}$$

where

$$c_\gamma = \frac{x^2}{d_m^2(1-x)^2}, \quad c_e = \frac{1}{d_m^2}, \quad c_{\gamma,e} \geq 0\ \forall x \in (0,1). \tag{8.110}$$

The integrals $J^{(m)}$ over w are simple to perform, and here we give some examples:

$$J^{(0)}(c_i) = \frac{2}{\sqrt{1+4c_i}} \log\left(\frac{2c_i}{1+2c_i+\sqrt{1+4c_i}}\right), \tag{8.111}$$

$$J^{(1)}(c_i) = \frac{1}{\sqrt{1+4c_i}} \log\left(\frac{2c_i}{1+2c_i+\sqrt{1+4c_i}}\right), \tag{8.112}$$

$$J^{(2)}(c_i) = 1 - \frac{1+2c_i}{\sqrt{1+4c_i}} \log\left(\frac{1+\sqrt{1+4c_i}}{1-\sqrt{1+4c_i}}\right). \tag{8.113}$$

$$\tag{8.114}$$

With these results in hand, we can classify the infrared behaviour of the integrals easily. We have that:

$$I_e^{(n,0)} = -\infty, \quad \text{the integrand diverges for } x \to 1, \tag{8.115}$$

$$I_\gamma^{(0,m)} = -\infty, \quad \text{the integrand diverges for } x \to 0. \tag{8.116}$$

However, sometimes, the infrared divergent integrals appear in particular combinations, in which the divergences cancel exactly. It is therefore useful to define the following infrared-safe combinations:

$$\begin{aligned} H_e^{(n,m)} &= \int_0^1 dx \int_0^{1-x} dy \ \left(f_e^{(n,m)}(x,y) - f_e^{(n+1,m)}(x,y)\right) \\ &= -\frac{1}{d_m^2}\int_0^1 dx\ (1-x)^m x^n\ J^{(m)}(c_e), \end{aligned} \tag{8.117}$$

$$\begin{aligned} H_\gamma^{(n,m)} &= \int_0^1 dx \int_0^{1-x} dy \ \left(f_\gamma^{(n,m)}(x,y) - f_\gamma^{(n,m+1)}(x,y)\right) \\ &= -\frac{1}{d_m^2}\int_0^1 dx\ (1-x)^{m-1} x^n\ \left(J^{(m)}(c_\gamma) - (1-x)J^{(m+1)}(c_\gamma)\right). \end{aligned} \tag{8.118}$$

The IR-pole in $I_e^{(n,0)}$ is simple to isolate in dimensional regularization. The key equation is:

$$\int_0^1 dx\ x^\sigma \phi(x) = \frac{\phi(0)}{1+\sigma} + \int_0^1 dx\ x^\sigma(\phi(x) - \phi(0)), \tag{8.119}$$

where $\phi(x)$ is some regular function for $x \to 1$. Being $c_e = 1/d_m^2$, we have that:

$$I_e^{(n,0)} = -\frac{1}{d_m^2}\int_0^1 dx \frac{x^n}{1-x} J_e^{(0)}\left(\frac{1}{d_m^2}\right). \tag{8.120}$$

Since J_e is constant in x, we have:

$$\begin{aligned} \int_0^1 dx \frac{x^n}{1-x} &\to \int_0^1 d^d x \frac{(1-x)^n}{x} = \frac{\pi^{\frac{d}{2}}}{\Gamma\left(\frac{d}{2}\right)}\int_0^1 dx \frac{(1-x)^n}{x^{2-d}} \\ &= \frac{\pi^{\frac{d}{2}}}{\Gamma\left(\frac{d}{2}\right)}\left(\frac{1}{1+d-2} + \int_0^1 dx \frac{(1-x)^n - 1}{x}\right) = \left(\frac{1}{\epsilon_I} - \sum_{k=1}^n \frac{1}{k}\right), \end{aligned} \tag{8.121}$$

where $d = 1 + \epsilon_I > 1$. Therefore we have

$$I_e^{(n,0)} = -\frac{1}{d_m^2} J_e^{(0)}\left(\frac{1}{d_m^2}\right)\left(\frac{1}{\epsilon_I} - \sum_{k=1}^n \frac{1}{k}\right). \tag{8.122}$$

The angular-measure prefactor in d dimensions is

$$\frac{2\pi^{\frac{d}{2}}}{\Gamma\left(\frac{d}{2}\right)}. \tag{8.123}$$

However, in Eq. (8.121), the angular measure is half of the total one, since the integral in x is between 0 and 1, i.e. we are integrating over the half-ball in 1D.

With these definitions in hand, we can rewrite the form factors in a more compact form:

$$A_e^R(\Delta^2) = 1 + \frac{\alpha}{\pi}\left(\frac{1}{\epsilon_I} - \frac{2\mathcal{L}}{3} - \frac{8}{3}\right) - \frac{\alpha}{2\pi}\int_0^1 dx \int_0^{1-x} dy\; x \log \mathcal{M}_e + \frac{\alpha}{2\pi}\left(H_e^{(1,0)} - H_e^{(2,0)} - 2I_e^{(2,0)} - d_m^2\left(I_e^{(2,0)} + H_e^{(1,1)} - I_e^{(1,2)}\right)\right), \quad (8.124)$$

$$J_e^R(\Delta^2) = \frac{1}{2} + \frac{\alpha}{2\pi}\left(\frac{1}{\epsilon_I} - \frac{2\mathcal{L}}{3} - \frac{8}{3}\right) - \frac{\alpha}{4\pi}\int_0^1 dx \int_0^{1-x} dy\; x \log \mathcal{M}_e + \frac{\alpha}{4\pi}\left(H_e^{(2,0)} + H_e^{(1,0)} - 2I_e^{(2,0)} - d_m^2\left(I_e^{(2,0)} + H_e^{(1,1)} - I_e^{(1,2)}\right)\right), \quad (8.125)$$

$$C_e^R(\Delta^2) = 1 + \frac{\alpha}{\pi}\left(\frac{1}{\epsilon_I} - 3\right) - \frac{\alpha}{2\pi}\int_0^1 dx \int_0^{1-x} dy\; x \log \mathcal{M}_e + \frac{\alpha}{2\pi}\left(H_e^{(3,0)} + H_e^{(1,0)} - 2I_e^{(2,0)} - d_m^2\left(I_e^{(2,0)} + H_e^{(1,1)} - I_e^{(1,2)}\right)\right), \quad (8.126)$$

$$D_e^R(\Delta^2) = \frac{\alpha}{\pi}\big(-2H_e^{(0,0)} - H_e^{(2,0)} + 3H_e^{(1,0)} - 8I_e^{(0,2)} + 8I_e^{(0,1)} - 12I_e^{(1,1)} + 4I_e^{(1,2)} + 4I_e^{(2,1)}\big), \quad (8.127)$$

$$\bar{C}_e^R(\Delta^2) = \frac{\alpha\mathcal{L}}{6\pi} - \frac{\alpha}{4\pi}\left(c_e + \frac{2}{3}\right) - \frac{\alpha}{2\pi}\int_0^1 dx \int_0^{1-x} dy(2-x) \log \mathcal{M}_e - \frac{d_m^2\alpha}{4\pi}\left(-2H_e^{(0,0)} + 8H_e^{(0,1)} + 3H_e^{(1,0)} - 4H_e^{(0,2)} - 4H_e^{(1,1)} - 4I_e^{(0,2)}\right), \quad (8.128)$$

$$A_\gamma^R(\Delta^2) = -\frac{2\alpha}{3\pi} + \frac{2\alpha\mathcal{L}}{3\pi} - \frac{\alpha}{\pi}\int_0^1 dx \int_0^{1-x} dy(1+x) \log \mathcal{M}_\gamma - \frac{\alpha}{\pi}\left(I_\gamma^{(3,0)} + d_m^2 H_\gamma^{(0,1)} - d_m^2 I_\gamma^{(1,1)}\right), \quad (8.129)$$

$$J_\gamma^R(\Delta^2) = -\frac{\alpha}{3\pi} + \frac{\alpha\mathcal{L}}{3\pi} - \frac{\alpha}{2\pi}\int_0^1 dx \int_0^{1-x} dy(1+x) \log \mathcal{M}_\gamma - \frac{\alpha}{2\pi}\left(I_\gamma^{(2,0)} + d_m^2 H_\gamma^{(0,1)} - d_m^2 I_\gamma^{(1,1)}\right), \quad (8.130)$$

$$C_\gamma^R(\Delta^2) = 0, \quad (8.131)$$

$$D_\gamma^R(\Delta^2) = \frac{\alpha}{\pi}\left(4H_\gamma^{(0,1)} - I_\gamma^{(3,0)} + I_\gamma^{(2,0)} - 4I_\gamma^{(1,2)} - 4I_\gamma^{(2,1)}\right), \quad (8.132)$$

$$\bar{C}_\gamma^R(\Delta^2) = \frac{\alpha}{8\pi}\left(\frac{5}{3} + 2c_e\right) - \frac{\alpha\mathcal{L}}{6\pi} + \frac{\alpha}{4\pi}\int_0^1 dx \int_0^{1-x} dy(1+x) \log \mathcal{M}_\gamma + \frac{\alpha}{4\pi}\left(I_\gamma^{(3,0)} + d_m^2\left(-2H_\gamma^{(0,1)} - I_\gamma^{(1,1)} + I_\gamma^{(3,0)} - I_\gamma^{(2,0)} + 3I_\gamma^{(1,2)} + 3I_\gamma^{(2,1)}\right)\right), \quad (8.133)$$

where c_e is defined in Eq. (8.99).

In Fig. 8.2, the form factors are plotted against the adimensional variable d_m^2, at the scale $\mu^2 = m^2$ and, if present, the infrared divergences are ignored. The red short-dashed curves represent the photon form factors, the blue long-dashed curves show the electron form factors. We can clearly see the different

behavior of the electron and photon, especially for the D_i form factor. We notice that, in the limit of $d_m^2 \to 0$, D_i saturates at very small values in the electron case, whereas it diverges for the photon. We can also investigate the low-Δ behavior of the form factors and compare it to the one given in Ref. [177]. In our notation, the form factors F_i of Ref. [177] are:

$$F_1(d_m^2) = 2J(d_m^2) = 2(J_e^R(d_m^2) + J_\gamma^R(d_m^2)), \tag{8.134}$$

$$F_2(d_m^2) = A(d_m^2) - 2J(d_m^2) = A_e^R(d_m^2) + A_\gamma^R(d_m^2) - 2(J_e^R(d_m^2) + J_\gamma^R(d_m^2)), \tag{8.135}$$

$$F_3(d_m^2) = -\frac{D(d_m^2)}{2} = -\frac{D_e^R(d_m^2) + D_\gamma^R(d_m^2)}{2}. \tag{8.136}$$

From Ref. [177], we have that:

$$F_1(d_m^2 \ll 1) = 1 - \frac{\sqrt{d_m^2}\alpha\pi}{8}, \quad F_2(d_m^2 \ll 1) = -\frac{\sqrt{d_m^2}\alpha\pi}{16}, \quad F_3(d_m^2 \ll 1) = -\frac{\alpha\pi}{8\sqrt{d_m^2}}. \tag{8.137}$$

As it can be appreciated from Fig. 8.3, there is a perfect agreement between the two calculations. We can also see that the divergent behavior of $F_3(d)$ is entirely due to the photon D-term, as can be see from the panels (c) and (d) of Fig. 8.2. Furthermore, one can notice from the panels (a) and (b) of Fig. 8.2 that the electron form factors A_e and J_e tend to have a more flat behavior near $d \simeq 0$ compared to their photon counterparts.

We can now easily compute the form factors in the forward limit $\Delta \to 0$:

$$A_e^R(0) = 1 - \frac{2\alpha\mathcal{L}}{3\pi} - \frac{17}{18}\frac{\alpha}{\pi}, \tag{8.138}$$

$$A_\gamma^R(0) = \frac{2\alpha\mathcal{L}}{3\pi} + \frac{17}{18}\frac{\alpha}{\pi}, \tag{8.139}$$

$$\bar{C}_e^R(0) = \begin{cases} \frac{\alpha\mathcal{L}}{6\pi} - \frac{\alpha}{18\pi}, & \overline{\text{MS}} \\ \frac{\alpha\mathcal{L}}{6\pi} + \frac{17}{72}\frac{\alpha}{\pi}, & \text{D}_1 \end{cases}, \tag{8.140}$$

$$\bar{C}_\gamma^R(0) = \begin{cases} -\frac{\alpha\mathcal{L}}{6\pi} + \frac{\alpha}{18\pi}, & \overline{\text{MS}} \\ -\frac{\alpha\mathcal{L}}{6\pi} - \frac{17}{72}\frac{\alpha}{\pi}, & \text{D}_1 \end{cases}. \tag{8.141}$$

We notice that these results are consistent with the ones derived in Ref. [178] for the dimensional-regularization case.

We can also compute the limit $\Delta \to 0$ for the other form factors, although they do not appear in the decomposition of the forward matrix element (see Eq. (8.18)), since they appear with coefficients that vanish in the limit[4] $\Delta \to 0$. We have:

$$J_\gamma^R(0) = \frac{\alpha}{2\pi}\left(\frac{11}{18} + \frac{2\mathcal{L}}{3\pi}\right), \tag{8.142}$$

[4]We note from Eq. (8.137) that that the photon D-term $1/\Delta$ and the prefactor in Eq. (8.18) vanishes as Δ^2.

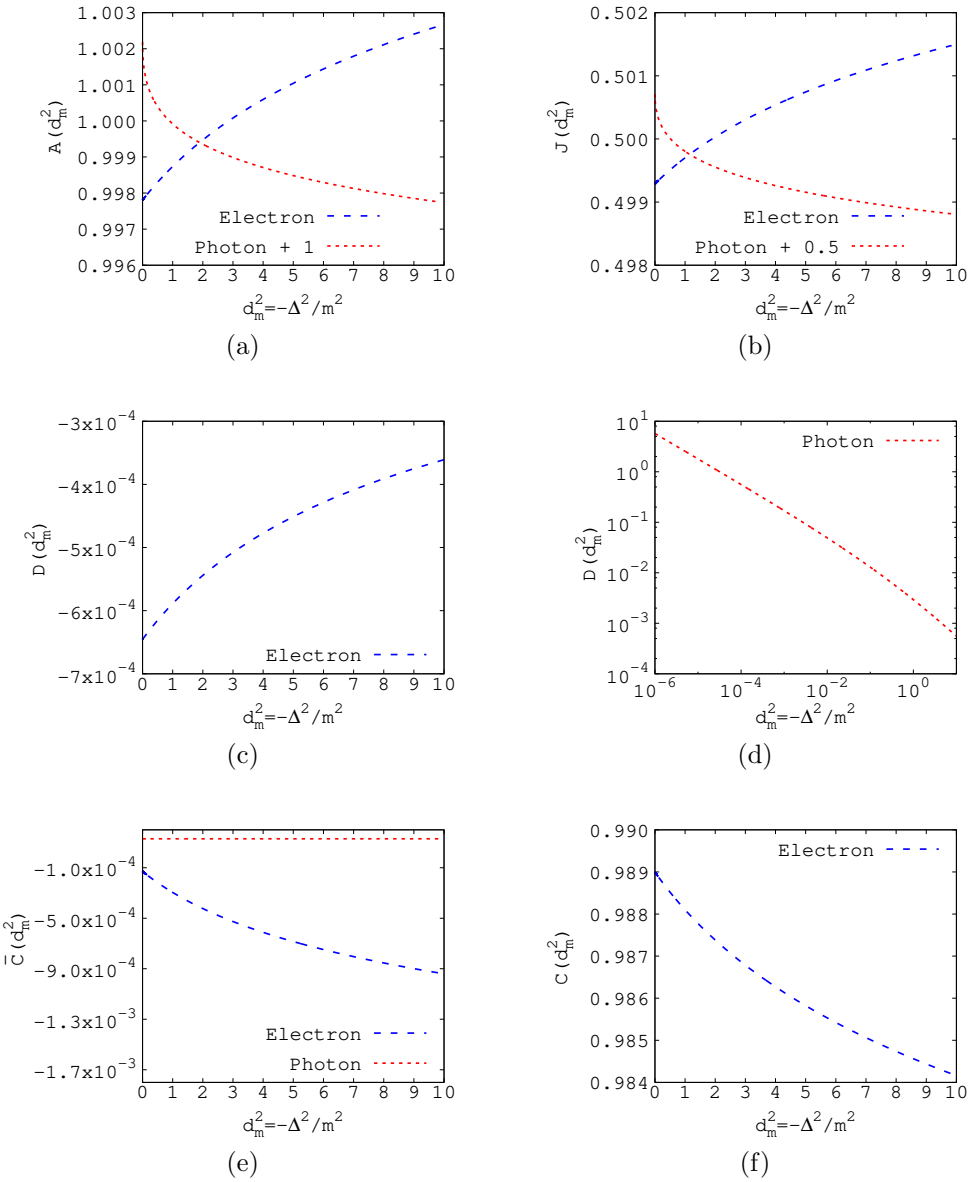

Figure 8.2: The photon and electron contribution to the EMT form factors as function of $d_m^2 = -\Delta^2/m^2$ at the scale $\mu^2 = m^2$. The D form factors are shown in two separate panels ((c) and (d)) because of the huge difference in the absolute values between the photon and the electron contribution. The panel (e) contains the results in $\overline{\text{MS}}$ scheme for the $\bar{C}_i$ form factors. The panel (f) shows the C_e form factor, that is associated with the antisymmetric part of the EMT and it vanishes for the photon, see Eq. (8.131).

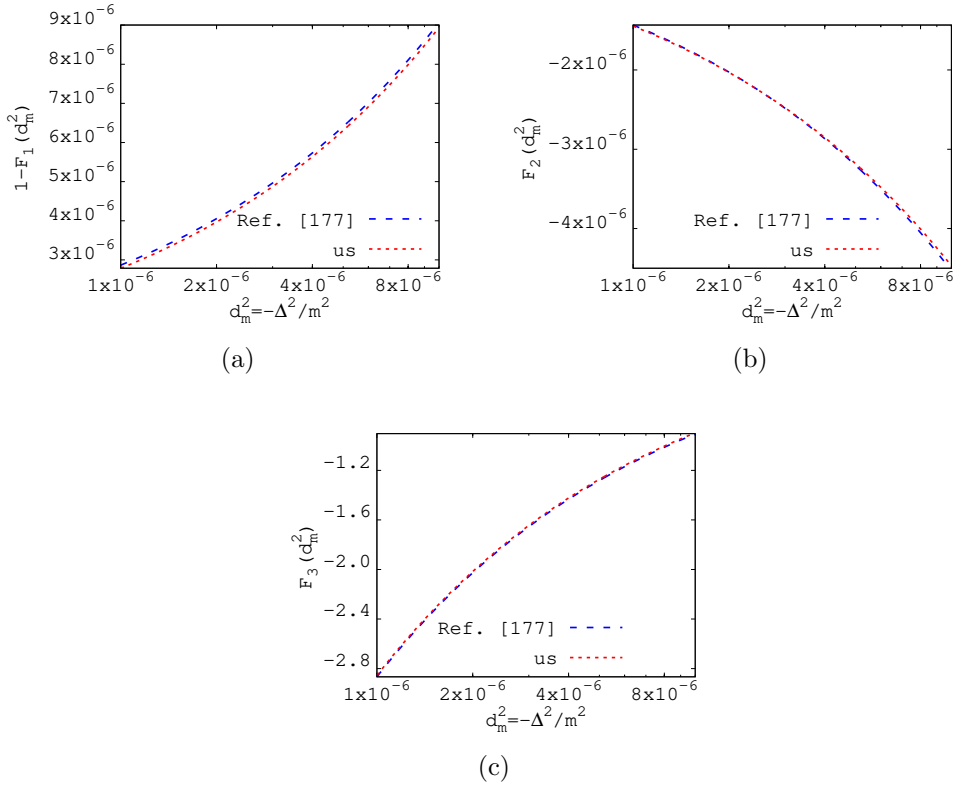

Figure 8.3: Comparison of the low-d_m^2 behavior of the form factors $F_{1,2,3}$ as defined in Eqs. (8.134)-(8.136) between our results (red short-dashed curves) and the calculation of Ref. [177] (blue long-dashed curves).

$$J_e^R(0) = \frac{1}{2} - \frac{\alpha}{2\pi}\left(\frac{11}{18} + \frac{2\mathcal{L}}{3\pi}\right), \tag{8.143}$$

$$D_\gamma^R(0) = +\infty, \quad D_e^R(0) = -\frac{5\alpha}{18\pi}, \quad C_e^R(0) = 1 - \frac{71}{72}\frac{\alpha}{\pi}. \tag{8.144}$$

8.5 Forward limit

Different mass sum rules derived from the EMT exist in the literature: a four-term decomposition proposed by Ji in Ref. [179], a two-term and a four-term decomposition by Lorcé [180], as well as a two-term decomposition of the mass squared by Hatta, Rajan, Tanaka [170]. In the following, we are going to explore the different sum rules for the electron in QED (see Ref. [160]) and for the proton in QCD (see Ref. [161]). All the results at the operator level look identical in QED and QCD (with the obvious difference in the definition of the gauge strength field tensor and an implicit sum over the quark flavors in QCD). For this reason, we are going to discuss in detail the operators in the QED part of the section, whereas in the QCD part we shall focus mainly on the numerics.

8.5.1 Two-term decompositions

We start with the two-term decomposition of m^2 proposed in Ref. [170], which reads

$$m = \left.\frac{\int d^3x \ \left(\langle (T_{e,R}(0))^\mu_\mu \rangle + \langle (T_{\gamma,R}(0))^\mu_\mu \rangle\right)}{\langle e(P)|e(P)\rangle}\right|_{\boldsymbol{P}=\boldsymbol{0}} \equiv \bar{m}_e + \bar{m}_\gamma. \tag{8.145}$$

From Eqs. (8.65)-(8.66), we find:

$$\frac{\bar{m}_e}{m} = A_e^R(0) + 4\bar{C}_e^R(0) = 1 + y - \gamma_m = \begin{cases} 1 - \frac{7\alpha}{6\pi}, & \overline{\text{MS}} \\ 1, & \text{D}_1 \end{cases}, \tag{8.146}$$

$$\frac{\bar{m}_\gamma}{m} = A_\gamma^R(0) + 4\bar{C}_\gamma^R(0) = \gamma_m - y = \begin{cases} \frac{7\alpha}{6\pi}, & \overline{\text{MS}} \\ 0, & \text{D}_1 \end{cases}, \tag{8.147}$$

where we used $\langle (m\bar{\psi}\psi)_R \rangle = 2m^2(1-\gamma_m)$ and neglected $O(\alpha^2)$ terms. We observe that, at $O(\alpha)$ and in the D_1 scheme, the electron mass is exclusively related to the trace of the renormalized electron operator, while the photon contribution vanishes. Once higher-order terms are taken into account, one would find $\bar{m}_\gamma \neq 0$ in the D_1 scheme. However, to any order in perturbation theory, the D_1 scheme ensures that $\bar{m}_e$ is exclusively given by the renormalized fermion operator and $\bar{m}_\gamma$ by the renormalized photon operator. Therefore, the D_1 scheme is perhaps the most natural scheme for the two-term decomposition of m^2 proposed in Ref. [170]. We also point out that one can hardly assign a physical interpretation to both the size and the sign of the $O(\alpha)$ corrections, which may both depend on the scheme.

The two-term sum rule for m of Ref. [170] has the advantage of being a frame-independent decomposition, in the sense that, in a generic frame one has:

$$\frac{\bar{m}_e}{m} = \frac{m}{E}\left(A_e^R(0) + 4\bar{C}_e^R(0)\right), \quad \frac{\bar{m}_\gamma}{m} = \frac{m}{E}\left(A_\gamma^R(0) + 4\bar{C}_\gamma^R(0)\right), \tag{8.148}$$

where E is the electron energy in the moving frame. We can clearly see that the ratio of the two terms remains equal, although they are individually modified.

All the other decompositions that we consider in the following depend on the reference frame, in the sense that the relative contributions change in different frames. We therefore discuss them first in the rest frame of the electron and afterwards comment on the required modifications in a moving frame.

In the two-term decomposition of Ref. [180], the mass of a particle is written as the sum of the energies carried by the constituents and gauge degrees of freedom (electron and photon in our case),

$$m = U_e + U_\gamma. \tag{8.149}$$

The definition of the (partial) energies U_i, in terms of renormalized operators (please note that in Ref. [180] the renormalization was assumed but not discussed in any detail), is

$$U_i = \left.\frac{\int d^3x \ \langle T_{i,R}^{00}(0)\rangle}{\langle e(P)|e(P)\rangle}\right|_{\mathbf{P}=0} = m\left(A_i^R(0) + \bar{C}_i^R(0)\right). \tag{8.150}$$

We can therefore use the results in Eqs. (8.138)–(8.141) to compute the partial energies in the two renormalization schemes,

$$U_e = \begin{cases} m\left(1 - \frac{\alpha\mathscr{L}}{2\pi} - \frac{\alpha}{\pi}\right), & \overline{\rm MS} \\ m\left(1 - \frac{\alpha\mathscr{L}}{2\pi} - \frac{17\alpha}{24\pi}\right), & {\rm D}_1 \end{cases}, \qquad U_\gamma = \begin{cases} m\left(\frac{\alpha\mathscr{L}}{2\pi} + \frac{\alpha}{\pi}\right), & \overline{\rm MS} \\ m\left(\frac{\alpha\mathscr{L}}{2\pi} + \frac{17\alpha}{24\pi}\right), & {\rm D}_1 \end{cases}. \tag{8.151}$$

We repeat that the scheme dependence prevents a clean interpretation of the results. Yet, we find positive values for U_γ in either scheme (unless the renormalization scale μ is extremely low), in agreement with what one would intuitively expect for the contribution due to the photon energy.

We anticipate that the renormalized operators associated with the U_i are[5,6]:

$$T_{e,R}^{00} = g_\mu^0 g_\nu^0 \left(\bar{\psi} i D^\nu \gamma^\mu \psi\right)_R = (m\bar{\psi}\psi)_R + (\psi^\dagger \, i\boldsymbol{D}\cdot\boldsymbol{\alpha}\,\psi)_R\,, \tag{8.152}$$

$$T_{\gamma,R}^{00} = -g_\mu^0 g_\nu^0 \left(F^{\mu\lambda}F^\nu{}_\lambda\right)_R + \frac{1}{4}\left(F^2\right)_R = \frac{1}{2}(E^2 + B^2)_R\,, \tag{8.153}$$

where the first term on the r.h.s. of Eq. (8.152) is the electron-mass contribution to m. The second term in that equation is typically referred to as

[5]We are going to discuss these results in more detail in the next section.

[6]The second equalities in Eqs. (8.152)-(8.153) are valid by assuming that the time dimension is left untouched in the dimensional-regularization procedure. All the results in the present Chapter can be generalized to $d = 4 - 2\epsilon$ dimension by using the first equality in Eqs. (8.152)-(8.153) instead of the second one.

kinetic plus potential energy of the electron [179, 181], while the operator in Eq. (8.153) represents the (total) energy stored in the photon field. Comparing both two-term decompositions in Eqs. (8.145)-(8.149) and the underlying operators (see Eqs. (8.152)-(8.153) and Eqs. (8.65)-(8.66)) we find the relation

$$\begin{aligned}&\left\langle g^0_\mu g^0_\nu \left(\bar\psi i D^\nu \gamma^\mu \psi\right)_R - (m\bar\psi\psi)_R - g^0_\mu g^0_\nu \left(F^{\mu\lambda}F^\nu_{\ \lambda}\right)_R + \frac{1}{4}\left(F^2\right)\right\rangle \\ &= \left\langle (\psi^\dagger\, i\boldsymbol{D}\cdot\boldsymbol{\alpha}\,\psi)_R + \frac{1}{2}(E^2+B^2)_R\right\rangle = \left\langle \gamma_m (m\bar\psi\psi)_R + \frac{\beta(e)}{2e}(F^{\alpha\beta}F_{\alpha\beta})_R\right\rangle,\end{aligned} \tag{8.154}$$

that is, the sum of the electron energy and the photon-field energy coincides with the anomaly contribution to the electron mass.

Note that the same exact results hold for the QCD case and the proton mass.

8.5.2 Four-term decompositions

We now turn to the study of the four-term sum rule proposed in Ref. [179] and studied for the electron for the first time in Ref. [182]. In the latter paper, the individual contributions to the mass decomposition are defined in terms of the bare operators instead of the renormalized composite operators introduced in the previous section. Following Ref. [179], we can decompose the EMT into a trace part and a traceless part according to

$$T^{\mu\nu} = \hat T^{\mu\nu} + \bar T^{\mu\nu}, \tag{8.155}$$

with the trace term given by $\hat T^{\mu\nu} = \frac{1}{4} g^{\mu\nu}\, T^\alpha_\alpha$. As discussed in the initial part of the Chapter, the separation of the two operators in terms of electron and photon contributions depends on the renormalization scheme and, in general, involves mixing of the two contributions under renormalization. Therefore, the procedure of Ref. [179], where the traceless partial operators are obtained by subtracting the trace term from the full EMT separately for the electron and photon, deserves a fresh look. In accordance with Ref. [179], we introduce the QED Hamiltonian H and the Hamiltonian density $\mathcal{H}$ as

$$H = \int d^3x\, T^{00}(0,x) = \int d^3x\, \mathcal{H}(0,x). \tag{8.156}$$

In Ref. [179], the separate electron and photon contributions to the traceless and trace operators were then defined as [7]

$$(\mathcal{H}'_e)_{[179]} = \left[(\bar T^{00}_e)_R\right]_{[179]} = \left(\psi^\dagger\,(i\boldsymbol{D}\cdot\boldsymbol{\alpha})\,\psi\right)_R + \frac{3}{4} m\bar\psi\psi, \tag{8.157}$$

[7] The label indicates that here we are using the definitions of Ref. [179], which will be revised below. Note also the in Ref. [179] the covariant derivative is assumed to be $\boldsymbol{D}_{[179]} = \boldsymbol{\nabla} - ig_s\boldsymbol{A} = -\boldsymbol{\partial} - ig_s\boldsymbol{A} = -\boldsymbol{D}$.

$$(\mathcal{H}'_m)_{[179]} = \left[(\hat{T}_e^{00})_R\right]_{[179]} = \frac{1+\gamma_m}{4} m\bar{\psi}\psi, \tag{8.158}$$

$$(\mathcal{H}'_\gamma)_{[179]} = \left[(\bar{T}_\gamma^{00})_R\right]_{[179]} = \frac{1}{2}\left(E^2+B^2\right)_R, \tag{8.159}$$

$$(\mathcal{H}'_a)_{[179]} = \left[(\hat{T}_\gamma^{00})_R\right]_{[179]} = -\frac{\beta(e)}{4e}\left(E^2-B^2\right)_R. \tag{8.160}$$

In the first and third line we note that the traceless part is erroneously constructed by subtracting the classical trace, and not the full trace. Following Ref. [179], we can define

$$(\mathcal{H}_e)_{[179]} \equiv [(\tilde{T}_e^{00})_R]_{[180]} = (\mathcal{H}'_e)_{[179]} + c_e\,(\mathcal{H}'_m)_{[179]}\,, \tag{8.161}$$

$$(\mathcal{H}_m)_{[179]} \equiv [(\check{T}_e^{00})_R]_{[180]} = (1-c_e)(\mathcal{H}'_m)_{[179]}, \tag{8.162}$$

$$(\mathcal{H}_\gamma)_{[179]} \equiv [(\tilde{T}_\gamma^{00})_R]_{[180]} = (\mathcal{H}'_\gamma)_{[179]} + c_\gamma(\mathcal{H}'_a)_{[179]}, \tag{8.163}$$

$$(\mathcal{H}_a)_{[179]} \equiv [(\check{T}_\gamma^{00})_R]_{[180]} = (1-c_\gamma)(\mathcal{H}'_a)_{[179]}, \tag{8.164}$$

where we give the reference to the corresponding nomenclature from Ref. [180] in terms of the $\tilde{T}_i^{00}$ and $\check{T}_i^{00}$ components of the EMT. Choosing for the constants c_i the values

$$c_e = \frac{-3}{1+\gamma_m}, \quad c_\gamma = 0, \tag{8.165}$$

we then obtain the definitions of Ref. [179], i.e.

$$(\mathcal{H}_e)_{[179]} = \left(\psi^\dagger\left(i\boldsymbol{D}\cdot\boldsymbol{\alpha}\right)\psi\right)_R, \tag{8.166}$$

$$(\mathcal{H}_m)_{[179]} = \frac{4+\gamma_m}{4} m\bar{\psi}\psi, \tag{8.167}$$

$$(\mathcal{H}_\gamma)_{[179]} = (\mathcal{H}'_\gamma)_{[179]}, \tag{8.168}$$

$$(\mathcal{H}_a)_{[179]} = (\mathcal{H}'_a)_{[179]}, \tag{8.169}$$

where $\mathcal{H}_e$ represents the electron kinetic and potential energy, $\mathcal{H}_m$ is the electron mass contribution, $\mathcal{H}_\gamma$ is the photon kinetic and potential energy, and $\mathcal{H}_a$ is the anomaly contribution. We can also introduce the two parameters a and b of Ref. [179] as the matrix elements of the traceless and trace electron contributions, respectively,

$$\frac{3}{2}m^2 a_{[179]} = \left.\frac{\langle(H'_e)_{[179]}\rangle}{e(P)|e(P)}\right|_{\mathbf{P}=0}, \quad 2m^2 b_{[179]} = \left.\frac{\langle(H'_m)_{[179]}\rangle}{e(P)|e(P)}\right|_{\mathbf{P}=0}. \tag{8.170}$$

Using the constraints in Eqs. (8.22) and (8.23), we also obtain the relations

$$\frac{3}{2}m^2(1-a_{[179]}) = \left.\frac{\langle(H'_\gamma)_{[179]}\rangle}{e(P)|e(P)}\right|_{\mathbf{P}=0}, \quad 2m^2(1-b_{[179]}) = \left.\frac{\langle(H'_a)_{[179]}\rangle}{e(P)|e(P)}\right|_{\mathbf{P}=0}. \tag{8.171}$$

So far we have reviewed the main points of the mass sum rule of Ref. [179]. In the following we suggest a modification of the sum rule in order to take into account the correct procedure of the trace subtraction. In Ref. [179], the results for

the traceless photon and electron contributions have been obtained by subtracting from the full EMT the trace part calculated in the classical case, i.e. without the inclusion of the trace anomaly. However, as already discussed in Ref. [171], this manipulation can not be applied when dealing with the renormalized operators $\mathcal{O}_i^R$, since the trace operation and the renormalization do not commute, i.e. $g_{\mu\nu}(F^{\mu\lambda}F^{\nu}_{\lambda})_R \neq (F^{\mu\lambda}F_{\mu\lambda})_R$ and $g_{\mu\nu}(i\bar{\psi}\gamma^{(\mu}\overleftrightarrow{D}^{\ \nu)}\psi)_R \neq (i\bar{\psi}\gamma^{(\lambda}\overleftrightarrow{D}_{\ \lambda)}\psi)_R$. If instead we use the correct renormalized traceless electron and photon operators $\widetilde{\mathcal{O}}_1^R$ and $\widetilde{\mathcal{O}}_3^R$ in Eqs. (8.63)–(8.64), we find that the 00-component of the traceless electron and photon parts are given by

$$\mathcal{H}'_e = (\bar{T}_e^{00})_R = \left(\psi^\dagger\left(i\boldsymbol{D}\cdot\boldsymbol{\alpha}\right)\psi\right)_R + m\bar{\psi}\psi - \frac{1+y}{4}m\bar{\psi}\psi - \frac{x}{4}\left(F^{\mu\nu}F_{\mu\nu}\right)_R, \tag{8.172}$$

$$\mathcal{H}'_\gamma = (\bar{T}_\gamma^{00})_R = \frac{1}{2}\left(E^2+B^2\right)_R + \frac{y-\gamma_m}{4}m\bar{\psi}\psi + \frac{1}{2}\left(\frac{\beta(e)}{2e}-x\right)\left(E^2-B^2\right)_R. \tag{8.173}$$

The matrix element of the revised expression in Eq. (8.172) for the 00-component of the traceless electron operator allows us to identify the parameter a with the renormalized form factor $A_e^R(0)$.

The 00-components of the trace parts also change because of additional mixing, as can be seen from Eqs. (8.65)–(8.66). We find

$$\mathcal{H}'_m = (\hat{T}_e^{00})_R = \frac{1+y}{4}m\bar{\psi}\psi + \frac{x}{4}\left(F^{\mu\nu}F_{\mu\nu}\right)_R, \tag{8.174}$$

$$\mathcal{H}'_a = (\hat{T}_\gamma^{00})_R = \frac{\gamma_m-y}{4}m\bar{\psi}\psi - \frac{1}{2}\left(\frac{\beta(e)}{2e}-x\right)\left(E^2-B^2\right)_R. \tag{8.175}$$

If we take the sum of Eq. (8.172) and (8.174), we obtain the result anticipated in Eq. (8.152), and by taking the sum of Eq. (8.173) and (8.175) we obtain Eq. (8.153). Note that we would have found a non-vanishing (and incorrect) contribution of the trace anomaly to the total 00 EMT component if we would have used Eqs. (8.157)-(8.160). In dimensional regularization, the time dimension, however, is left untouched, which implies that T^{00} is rather special compared to the spatial components of the EMT trace, see, e.g., Refs. [40, 183]. In fact, a careful analysis reveals that the anomaly is entirely contained in the spatial part of the EMT.

To recover the intuitive picture in terms of kinetic and potential energy of the electron and photon, we need to take different combinations of the operators according to

$$\mathcal{H}_e \equiv [(\tilde{T}_e^{00})_R] = \mathcal{H}'_e + c_{em}\mathcal{H}'_m + c_{ea}\mathcal{H}'_a, \tag{8.176}$$

$$\mathcal{H}_m \equiv [(\check{T}_e^{00})_R] = (1-c_{em}-c_{\gamma m})\mathcal{H}'_m + c_{ma}\mathcal{H}'_a, \tag{8.177}$$

$$\mathcal{H}_\gamma \equiv [(\tilde{T}_\gamma^{00})_R] = \mathcal{H}'_\gamma + c_{\gamma m}\mathcal{H}'_m + c_{\gamma a}\mathcal{H}'_a, \tag{8.178}$$

$$\mathcal{H}_a \equiv [(\check{T}_\gamma^{00})_R] = (1-c_{ea}-c_{\gamma a}-c_{ma})\mathcal{H}'_a, \tag{8.179}$$

with the constants

$$c_{em} = \frac{(3-y)\frac{\beta(e)}{2e} - x(3-\gamma_m)}{-(1+y)\frac{\beta(e)}{2e} + x(1+\gamma_m)}, \quad c_{ea} = \frac{4x}{(1+y)\frac{\beta(e)}{2e} - x(1+\gamma_m)}, \tag{8.180}$$

$$c_{\gamma m} = 0, \quad c_{\gamma a} = 1, \quad c_{ma} = -c_{ea}. \tag{8.181}$$

This leads to the definitions

$$\mathcal{H}_e = \left(\psi^\dagger \left(i\boldsymbol{D}\cdot\boldsymbol{\alpha}\right)\psi\right)_R, \quad \mathcal{H}_m = m\bar{\psi}\psi, \quad \mathcal{H}_\gamma = \frac{1}{2}\left(E^2+B^2\right)_R, \quad \mathcal{H}_a = 0. \tag{8.182}$$

We argue that the results in Eq. (8.182) are the appropriate operators for the mass sum rule if one follows the overall logic of Ji's original work, but uses the properly renormalized 00-components of the traceless parts of the EMT for the fermion and the gauge field. It is also noteworthy that the expressions in Eq. (8.182) coincide formally with the classical results, i.e. the results one would obtain from the classical electromagnetic Lagrangian without the inclusion of the trace anomaly. We have arrived at a decomposition with three nontrivial terms only.

We can also work out the revised expressions of the constants a, b, defined as the (correct) traceless and trace electron contributions,

$$\frac{3}{2}m^2 a = \left.\frac{\int d^3x \ \langle\widetilde{\mathcal{O}}^{00}_{3,R}\rangle}{\langle e(P)|e(P)\rangle}\right|_{\mathbf{P}=0}, \tag{8.183}$$

$$2m^2 b = \left.\frac{\int d^3x \ \langle(1+\gamma_m)m\bar{\psi}\psi\rangle}{\langle e(P)|e(P)\rangle}\right|_{\mathbf{P}=0}, \tag{8.184}$$

$$\frac{3}{2}m^2(1-a) = \left.\frac{\int d^3x \ \langle\widetilde{\mathcal{O}}^{00}_{1,R}\rangle}{\langle e(P)|e(P)\rangle}\right|_{\mathbf{P}=0}, \tag{8.185}$$

$$2m^2(1-b) = \left.\frac{\beta(e)}{2e}\frac{\int d^3x \ \langle(F^{\mu\nu}F_{\mu\nu})_R\rangle}{\langle e(P)|e(P)\rangle}\right|_{\mathbf{P}=0}. \tag{8.186}$$

We stress that b is not directly the trace of the renormalized quark operator. Using the above definitions and Eqs. (8.176)-(8.179), we have the following mass decomposition:

$$m_e = \frac{3}{4}ma + \frac{m}{4}\left(x(1-b)\frac{2e}{\beta(e)} + b\frac{y-3}{1+\gamma_m}\right), \tag{8.187}$$

$$m_\gamma = \frac{3}{4}m(1-a) + \frac{m(1-b)}{4}\left(1 - x\frac{2e}{\beta(e)}\right) + mb\frac{\gamma_m - y}{4(1+\gamma_m)}, \tag{8.188}$$

$$m_m = \frac{mb}{1+\gamma_m}, \quad m_a = 0, \tag{8.189}$$

where

$$m_i = \left.\frac{\langle H_i\rangle}{\langle e(P)|e(P)\rangle}\right|_{\mathbf{P}=0}. \tag{8.190}$$

In the two renormalization schemes, the results at $O(\alpha)$ read

$$\frac{m_e}{m} = \begin{cases} \frac{\alpha}{2\pi} - \frac{\alpha\mathscr{L}}{2\pi}, & \overline{\text{MS}} \\ \frac{19\alpha}{24\pi} - \frac{\alpha\mathscr{L}}{2\pi}, & \text{D}_1 \end{cases}, \qquad \frac{m_m}{m} = \begin{cases} 1 - \frac{3\alpha}{2\pi}, & \overline{\text{MS}} \\ 1 - \frac{3\alpha}{2\pi}, & \text{D}_1 \end{cases}, \tag{8.191}$$

$$\frac{m_\gamma}{m} = \begin{cases} \frac{\alpha}{\pi} + \frac{\alpha\mathscr{L}}{2\pi}, & \overline{\text{MS}} \\ \frac{17\alpha}{24\pi} + \frac{\alpha\mathscr{L}}{2\pi}, & \text{D}_1 \end{cases}, \tag{8.192}$$

Equipped with the proper one-loop results for the renormalized operators that appear in Eq. (8.182), one can readily show that at one loop the terms in Eqs. (8.166)–(8.169) do not add up to the mass of the electron. This is just a consequence of the aforementioned issue with the sum rule in Ref. [179].

Before moving on to the second four-term sum rule, we make a brief comparison with the two-term decomposition of Ref. [180]. By means of Eqs. (8.150), (8.172)-(8.175), and (8.182), we find

$$U_e = m_e + m_m, \qquad U_\gamma = m_\gamma. \tag{8.193}$$

Our three-term sum rule above could therefore be considered a refinement of the two-term decomposition of Ref. [180]. The relations in (8.193) also allow one to readily identify the properly renormalized operators for U_e and U_γ, see Eqs. (8.152) and (8.153).

In Ref. [180], another type of four-term decomposition has been discussed, which makes use of the concept of the energy introduced in Eq. (8.150) and of the partial pressure-volume work W_i^j in the directions $j = x, y, z$,

$$W_i^j = g_\mu{}^j g_\nu{}^j \frac{\langle \int d^3x \; T^{\mu\nu}_{i,R}(0) \rangle}{\langle e(P)|e(P)\rangle}\bigg|_{\mathbf{P}=0}. \tag{8.194}$$

While we follow here the general logic of Ref. [180], we (again) pay close attention to the operator renormalization. The partial energies and pressure-volume works can be related to the matrix elements of the operators $(\bar{T}_i^{00})_R$ and $(\hat{T}_i^{00})_R$ according to

$$\frac{\langle (\bar{T}_i^{00})_R \rangle}{\langle e(P)|e(P)\rangle}\bigg|_{\mathbf{P}=0} = \frac{3}{4}(U_i + W_i), \quad \frac{\langle (\hat{T}_i^{00})_R \rangle}{\langle e(P)|e(P)\rangle}\bigg|_{\mathbf{P}=0} = \frac{1}{4}(U_i - 3W_i), \tag{8.195}$$

where $3W_i = W_i^x + W_i^y + W_i^z$. The four-term decomposition of Ref. [180] reads as

$$m = \tilde{U}_e + \tilde{U}_\gamma + \check{U}_e + \check{U}_\gamma, \tag{8.196}$$

where the individual terms correspond to the contributions of the internal energy to the matrix elements of the $\hat{T}_i^{00}$ and $\check{T}_i^{00}$ operators defined in Eqs. (8.161)-(8.164). Using the properly renormalized operators in Eqs. (8.176)–(8.179), we obtain:

$$\tilde{U}_e = \frac{U_e}{4}(3 + c_{em}) + \frac{U_\gamma}{4} c_{ea}, \qquad \check{U}_e = \frac{U_e}{4}(1 - c_{em} - c_{\gamma m}) + \frac{U_\gamma}{4} c_{ma}, \tag{8.197}$$

$$\tilde{U}_\gamma = \frac{U_\gamma}{4}(3 + c_{\gamma a}) + \frac{U_e}{4}c_{\gamma m}, \quad \check{U}_\gamma = \frac{U_\gamma}{4}(1 - c_{ea} - c_{\gamma a} - c_{ma}), \tag{8.198}$$

with the constants c_i defined in Eqs. (8.180) and (8.181). The main difference with respect to Ref. [180] is that we need to mix $(\bar{T}^{00}_e)_R$ with $(\hat{T}^{00}_e)_R$ and $(\hat{T}^{00}_\gamma)_R$, $(\bar{T}^{00}_\gamma)_R$ with $(\hat{T}^{00}_\gamma)_R$ and $(\hat{T}^{00}_e)_R$ with $(\hat{T}^{00}_\gamma)_R$. Using the coefficients in Eqs. (8.180) and (8.181), we find for the photon sector

$$\tilde{U}_\gamma = U_\gamma, \qquad \check{U}_\gamma = 0. \tag{8.199}$$

This means that, once working with properly renormalized operators, the four-term sum rule of Ref. [180] in fact reduces only to three nontrivial contributions. Finally, in the two renormalization schemes we have the following explicit results at $O(\alpha)$

$$\frac{\tilde{U}_e}{m} = \begin{cases} \frac{\alpha}{3\pi}, & \overline{\text{MS}} \\ \frac{3\alpha}{2\pi}, & \text{D}_1 \end{cases}, \qquad \frac{\check{U}_e}{m} = \begin{cases} 1 - \frac{4\alpha}{3\pi} - \frac{\alpha\mathscr{L}}{2\pi}, & \overline{\text{MS}} \\ 1 - \frac{53\alpha}{24\pi} - \frac{\alpha\mathscr{L}}{2\pi}, & \text{D}_1 \end{cases}, \tag{8.200}$$

$$\frac{\tilde{U}_\gamma}{m} = \begin{cases} \frac{\alpha}{\pi} + \frac{\alpha\mathscr{L}}{2\pi}, & \overline{\text{MS}} \\ \frac{17\alpha}{24\pi} + \frac{\alpha\mathscr{L}}{2\pi}, & \text{D}_1 \end{cases}. \tag{8.201}$$

8.5.3 Energy decompositions in a moving frame

Except for the two-term decomposition of Ref. [170], all other mass sum rules only hold in the rest frame. However, one may expect that in a moving frame they still provide meaningful results. In fact they become energy decompositions as we discuss in the following (see Ref. [184] for a more general discussion on the frame dependence of the matrix elements of the EMT). For a moving electron with energy E, the partial energies become

$$U_i = E A_i^R(0) + \frac{m^2}{E}\bar{C}_i^R(0). \tag{8.202}$$

If the electron momentum points along the $\hat{z}$ axis, i.e. $P^\mu = (E, 0, 0, p)$, we find for the partial pressure-volume works

$$W_i^x = W_i^y = -\frac{m^2}{E}\bar{C}_i^R(0), \quad W_i^z = \frac{E^2 - m^2}{E}A_i^R(0) - \frac{m^2}{E}\bar{C}_i^R(0), \tag{8.203}$$

and therefore

$$W_i = \frac{E^2 - m^2}{3E}A_i^R(0) - \frac{m^2}{E}\bar{C}_i^R(0). \tag{8.204}$$

The values of the a, b coefficients are not modified in a moving frame since they are related to the form factors and not to the energy. Recalling the identification $a = A_e^R(0)$, we obtain the following modification of the expectation values of the traceless operators:

$$\frac{\int d^3x\ \langle\widetilde{\mathcal{O}}^{00}_{3,R}\rangle}{\langle e(P)|e(P)\rangle}\Big|_{\mathbf{P}=0} = \frac{3}{4}am \to a\left(E - \frac{m^2}{4E}\right), \tag{8.205}$$

$$\frac{\int d^3x\ \langle\widetilde{\mathcal{O}}^{00}_{1,R}\rangle}{\langle e(P)|e(P)\rangle}\Big|_{\mathbf{P}=0} = \frac{3}{4}(1-a)m \to (1-a)\left(E-\frac{m^2}{4E}\right). \tag{8.206}$$

The trace parts are affected too because of the normalization of the states. We have

$$\frac{\int d^3x\ \langle(1+\gamma_m)m\bar{\psi}\psi\rangle}{\langle e(P)|e(P)\rangle}\Big|_{\mathbf{P}=0} = mb \to b\frac{m^2}{E}, \tag{8.207}$$

$$\frac{\beta(e)}{2e}\frac{\int d^3x\ \langle(F^{\mu\nu}F_{\mu\nu})_R\rangle}{\langle e(P)|e(P)\rangle}\Big|_{\mathbf{P}=0} = m(1-b) \to \frac{m^2}{E}(1-b). \tag{8.208}$$

These results allow us to obtain the counterparts of Eqs. (8.191) and (8.192) for a moving frame:

$$\frac{m_e}{E} = \begin{cases} \frac{E^2-m^2}{E^2}+\frac{\alpha}{\pi}\left(-\frac{17}{18}+\frac{13m^2}{9E^2}-\frac{2\mathscr{L}}{3}+\frac{\mathscr{L}m^2}{6E^2}\right), & \overline{\text{MS}} \\ \frac{E^2-m^2}{E^2}+\frac{\alpha}{\pi}\left(-\frac{17}{18}+\frac{125m^2}{72E^2}-\frac{2\mathscr{L}}{3}+\frac{\mathscr{L}m^2}{6E^2}\right), & \text{D}_1 \end{cases}, \tag{8.209}$$

$$\frac{m_m}{E} = \begin{cases} \frac{m^2}{E^2}\left(1-\frac{3\alpha}{2\pi}\right), & \overline{\text{MS}} \\ \frac{m^2}{E^2}\left(1-\frac{3\alpha}{2\pi}\right), & \text{D}_1 \end{cases},$$

$$\frac{m_\gamma}{E} = \begin{cases} \frac{\alpha}{\pi}\left(\frac{17}{18}+\frac{m^2}{18E^2}+\frac{2\mathscr{L}}{3}-\frac{\mathscr{L}m^2}{6E^2}\right), & \overline{\text{MS}} \\ \frac{\alpha}{\pi}\left(\frac{17}{18}-\frac{17m^2}{72E^2}+\frac{2\mathscr{L}}{3}-\frac{\mathscr{L}m^2}{6E^2}\right), & \text{D}_1 \end{cases}, \tag{8.210}$$

while for the decomposition in Eq. (8.196) we obtain

$$\frac{\tilde{U}_e}{E} = \begin{cases} \frac{\alpha}{3\pi}, & \overline{\text{MS}} \\ \frac{3\alpha}{2\pi}, & \text{D}_1 \end{cases}, \tag{8.211}$$

$$\frac{\check{U}_e}{E} = \begin{cases} 1+\frac{\alpha}{\pi}\left(-\frac{23}{18}-\frac{m^2}{18E^2}-\frac{2\mathscr{L}}{3}+\frac{\mathscr{L}m^2}{6E^2}\right), & \overline{\text{MS}} \\ 1+\frac{\alpha}{\pi}\left(-\frac{22}{9}+\frac{17m^2}{72E^2}-\frac{2\mathscr{L}}{3}+\frac{\mathscr{L}m^2}{6E^2}\right), & \text{D}_1 \end{cases},$$

$$\frac{\tilde{U}_\gamma}{E} = \begin{cases} \frac{\alpha}{\pi}\left(\frac{17}{18}+\frac{m^2}{18E^2}+\frac{2\mathscr{L}}{3}-\frac{\mathscr{L}m^2}{6E^2}\right), & \overline{\text{MS}} \\ \frac{\alpha}{\pi}\left(\frac{17}{18}-\frac{17m^2}{72E^2}+\frac{2\mathscr{L}}{3}-\frac{\mathscr{L}m^2}{6E^2}\right), & \text{D}_1 \end{cases}. \tag{8.212}$$

One can readily verify that the terms in Eq. (8.210) and in Eq. (8.212) add up to E. On the other hand, the individual terms of the energy decompositions cannot be obtained by multiplying the corresponding expressions in the rest frame by a common overall kinematic factor.

8.6 Proton mass decompositions

In this section, we are going to use the general results at the operator level obtained in the QED sector and specify them to the proton in QCD. We are not going to perform a perturbative calculation of the matrix elements, but

rather we are going to make use of the currently available phenomenological and lattice-QCD information to obtain numerical values for the matrix elements. This procedure will also provide us with the opportunity of studying the scheme dependence of the various sum rules.

8.6.1 Numerical results

From the results presented in the previous part of the Chapter, it is evident that two independent numerical inputs suffice to fix all the terms of the different sum rules[8]. One input/constraint comes from the parton momentum fractions a_i in the proton through [179, 181]

$$\frac{3}{2}\,M^2\,a_q = \frac{\int d^3x \langle\, \mathcal{H}'_q \,\rangle}{\langle P|P\rangle}\Big|_{\boldsymbol{P}=\boldsymbol{0}}\,, \qquad \frac{3}{2}\,M^2\,a_g = \frac{\int d^3x \langle\, \mathcal{H}'_g \,\rangle}{\langle P|P\rangle}\Big|_{\boldsymbol{P}=\boldsymbol{0}}\,, \tag{8.213}$$

where a_q is a shorthand notation for the sum of the momentum fractions of all active quark flavors. Note that now the $\langle ...\rangle$ symbol denotes the expectation value between proton states and that $\mathcal{H}'_{q,g}$ are the QCD counterparts to Eqs. (8.172) and (8.173). The sum rule $a_q + a_g = 1$ is satisfied, which is equivalent to the constraint for the form factors $A_i(0)$ in (8.23), and therefore leave us with just one independent input. We take the quark mass term as the second independent input. Specifically, we define a parameter b according to

$$2M^2\,b = \sum_{f=u,d,...}(1+\gamma_m)\,\frac{\int d^3x \langle\, (m\bar{\psi}^{(f)}\psi^{(f)})_R \,\rangle}{\langle P|P\rangle}\,, \tag{8.214}$$

that is the QCD counterpart to Eq. (8.184). Please note that the sum over the flavors will be understood in the remaining of the section.

We make use of Eq. (8.186) to fix the gluon contribution to the trace anomaly from b. We also refer to [185] for a recent attempt to directly compute the gluon contribution to the EMT trace in lattice QCD. With these ingredients, the matrix elements of the QCD counterparts to Eqs. (8.172)-(8.175) can be written as

$$M'_q = \frac{3}{4}\,M\,a_q\,, \tag{8.215}$$

$$M'_m = \frac{1}{4}\,M\left(\frac{(1+y)\,b}{1+\gamma_m} + x(1-b)\frac{2g}{\beta}\right), \tag{8.216}$$

$$M'_g = \frac{3}{4}\,M\,a_g\,, \tag{8.217}$$

$$M'_a = \frac{1}{4}\,M\left(1 - \frac{(1+y)\,b}{1+\gamma_m} - x(1-b)\frac{2g}{\beta}\right), \tag{8.218}$$

which lead to the expressions equivalent to Eqs. (8.187)-(8.189):

$$M_q = \frac{3}{4}\,M\,a_q + \frac{1}{4}\,M\left(\frac{(y-3)\,b}{1+\gamma_m} + x(1-b)\frac{2g}{\beta}\right), \tag{8.219}$$

[8] Only two independent form factors survive in the forward limit of the matrix element of the EMT and they encapsulate all the information on the EMT.

$$M_m = M\,\frac{b}{1+\gamma_m}\,, \tag{8.220}$$

$$M_g = \frac{3}{4}\,M\,a_g + \frac{1}{4}\,M\left[\frac{(\gamma_m - y)\,b}{1+\gamma_m} + \left(1 - x\frac{2g}{\beta}\right)(1-b)\right]. \tag{8.221}$$

Now we have collected all the equations that allow us to evaluate numerically the various sum rules discussed in the Chapter.

Our numerical results are given at the scale $\mu = 2\,\mathrm{GeV}$. We take the parton momentum fractions from the CT18NNLO parameterization [186], which, in the case of four active quark flavors, gives

$$a_q = 0.586 \pm 0.013\,, \qquad a_g = 1 - a_q = 0.414 \pm 0.013\,. \tag{8.222}$$

Other phenomenological fits of parton distributions provide very similar results (see, for instance, Refs. [118, 187–190]). In order to fix the parameter b in Eq. (8.214), we use input for the quark mass term (sigma term), up to and including charm quarks,

$$\sigma_u + \sigma_d = \sigma_{\pi N} = \frac{\langle P|\,\hat{m}\,\left(\bar{u}u + \bar{d}d\right)\,|P\rangle}{2M}\,,$$
$$\sigma_s = \frac{\langle P|\,m_s\,\bar{s}s\,|P\rangle}{2M}\,, \quad \sigma_c = \frac{\langle P|\,m_c\,\bar{c}c\,|P\rangle}{2M}\,, \tag{8.223}$$

with $\hat{m} = (m_u + m_d)/2$, and q=u,d,s, c stands for the field of quark with different flavor. For b we actually consider two cases. In the first one, we take the sigma terms from an analysis in chiral perturbation theory (ChPT) in Refs. [191, 192] for the three lightest quark flavors,

$$\sigma_{\pi N}\big|_{\mathrm{ChPT}} = (59 \pm 7)\,\mathrm{MeV}\,, \qquad \sigma_s\big|_{\mathrm{ChPT}} = (16 \pm 80)\,\mathrm{MeV}\,. \tag{8.224}$$

The independent phenomenological determination in Ref. [193] gives a very similar value for $\sigma_{\pi N}$. In the second scenario, we use results from lattice QCD (LQCD) which also include a sigma term for charm quarks [194],

$$\sigma_{\pi N}\big|_{\mathrm{LQCD}} = (41.6 \pm 3.8)\,\mathrm{MeV}\,, \qquad \sigma_s\big|_{\mathrm{LQCD}} = (39.8 \pm 5.5)\,\mathrm{MeV}\,,$$
$$\sigma_c\big|_{\mathrm{LQCD}} = (107 \pm 22)\,\mathrm{MeV}\,. \tag{8.225}$$

Other LQCD calculations, performed at (nearly) physical quark masses, mostly provide similar results for the sigma terms of the light quarks [195–198]. To the best of our knowledge, Ref. [194] is the only LQCD study which reports a value for the charm sigma term. The numerical values for $\sigma_{\pi N}$ and σ_s are quite different for ChPT and LQCD. However, the difference for the sum $\sigma_{\pi N} + \sigma_s$ is small and irrelevant for our purpose. On the other hand, including or not σ_c has a clear impact on our numerics for the mass sum rules. Moreover, the error on the strange contribution in the phenomenological analysis is very large, leading to large errors in the mass sum rules. To summarize this discussion, we consider numbers for the mass decompositions for the following two scenarios:

	$O(\alpha_s^1)$	$O(\alpha_s^2)$	$O(\alpha_s^3)$
$b\big\vert_{\rm ChPT}$	0.094 ± 0.100	0.101 ± 0.108	0.103 ± 0.110
$b\big\vert_{\rm LQCD}$	0.235 ± 0.029	0.253 ± 0.031	0.258 ± 0.031

Table 8.1: Parameter b for different orders in α_s, obtained from input for the sigma terms from ChPT and LQCD.

		MS	$\overline{\rm MS}_1$	$\overline{\rm MS}_2$	D1	D2
Scenario A	M_q	0.309 ± 0.044	0.194 ± 0.033	0.178 ± 0.032	0.362 ± 0.045	0.357 ± 0.051
	M_m	0.075 ± 0.080	0.075 ± 0.080	0.075 ± 0.080	0.075 ± 0.080	0.075 ± 0.080
	M_g	0.555 ± 0.036	0.669 ± 0.047	0.686 ± 0.048	0.502 ± 0.035	0.507 ± 0.029
Scenario B	M_q	0.234 ± 0.006	0.135 ± 0.003	0.120 ± 0.003	0.286 ± 0.006	0.272 ± 0.008
	M_m	0.187 ± 0.023	0.187 ± 0.023	0.187 ± 0.023	0.187 ± 0.023	0.187 ± 0.023
	M_g	0.517 ± 0.017	0.617 ± 0.020	0.631 ± 0.020	0.465 ± 0.017	0.479 ± 0.015

Table 8.2: Scheme dependence of the (nonzero) terms of the mass sum rule in Eqs. (8.219)-(8.221). All the results are in units of GeV, and for $O(\alpha_s^3)$ accuracy. The definition of the $\overline{\rm MS}_1$ and $\overline{\rm MS}_2$ schemes is given in Eqs. (8.49) and (8.50).

- Scenario A: a_i from (8.222); b from ChPT sigma terms in (8.224).
- Scenario B: a_i from (8.222); b from LQCD sigma terms in (8.225) including charm.

We will show results at 1-loop, 2-loop and 3-loop accuracies. For this we need the QCD beta function and the anomalous dimension of the quark mass through $O(\alpha_s^3)$:

$$\frac{\beta(g)}{2g} = -\frac{\beta_0}{2}\left(\frac{\alpha_s}{4\pi}\right) - \frac{\beta_1}{2}\left(\frac{\alpha_s}{4\pi}\right)^2 - \frac{\beta_2}{2}\left(\frac{\alpha_s}{4\pi}\right)^3 + \dots\,, \tag{8.226}$$

$$\gamma_m(g) = \gamma_{m0}\,\frac{\alpha_s}{4\pi} + \gamma_{m1}\left(\frac{\alpha_s}{4\pi}\right)^2 + \gamma_{m2}\left(\frac{\alpha_s}{4\pi}\right)^3 + \dots\,, \tag{8.227}$$

where the explicit expressions for the coefficients β_i and γ_{mi} are given in Refs. [199, 200]. For the flavor number $n_f = 3$, we find the following values for α_s by using the Mathematica package of Ref. [201]:

$$\alpha_{s,\text{1-loop}} = 0.269\,, \qquad \alpha_{s,\text{2-loop}} = 0.299\,, \qquad \alpha_{s,\text{3-loop}} = 0.302\,. \tag{8.228}$$

In Tab. 8.1, we show the results for the parameter b, based on the sigma terms from ChPT and LQCD. The numbers differ by about 10% between the 1-loop and the 3-loop analysis. The significant difference between the ChPT and LQCD results is caused by the (large) charm sigma term from LQCD.

		$O(\alpha_s^1)$	$O(\alpha_s^2)$	$O(\alpha_s^3)$
Scenario A	$\overline{M}_q$	-0.113 ± 0.102	-0.120 $\pm$0.105	-0.115 ± 0.107
	$\overline{M}_g$	1.051 ± 0.102	1.057 ± 0.105	1.053 ± 0.107
Scenario B	$\overline{M}_q$	0.032 ± 0.030	0.030 ± 0.031	0.035 ± 0.030
	$\overline{M}_g$	0.906 ± 0.030	0.908 ± 0.030	0.903 ± 0.030

Table 8.3: Numerics for the QCD counterpart to the sum rule in Eq. (8.145) for 1-loop, 2-loop and 3-loop analyses with the change of notation $\bar{m}_i \to \bar{M}_i$ for the proton case. All the results are in units of GeV. The errors are obtained by computing the terms for $a_i \pm \Delta a_i$ and $b \pm \Delta b$ and then subtracting the results obtained for a_i and b.

The numerical input for the parameters a_i and b is in the $\overline{\text{MS}}$ scheme.[9] However, as we saw in the previous sections, the numerics for the mass sum rules also depends on the choice (scheme) used for the parameters x and y which, according to Eqs. (8.65) and (8.66), fix the individual contributions to the trace of the EMT. As an example, the scheme dependence of the terms of the mass decomposition in Eqs.(8.219)-(8.221) is shown in Tab. 8.2. The contribution M_m does not depend on x and y, but the quark and gluon energies M_q and M_g do so. In fact, their numerical values change significantly when switching schemes, with the largest discrepancies between the $\overline{\text{MS}}$ scheme(s) and the other three schemes. (As discussed in App. B and in Eqs. (8.48)-(8.50), two commonly used $\overline{\text{MS}}$ subtractions prescription exist. They lead to somewhat different numbers for the proton mass decomposition.)

There is a conceptual difference between the MS scheme and the D-type schemes in the context of our study. In principal, a fully consistent calculation in the MS scheme could be done, since all the numerical input that we use could be obtained in the MS scheme. (Comparing the numerics for the MS scheme and, in particular, the $\overline{\text{MS}}$ scheme(s) should therefore be done with care.) In contrast, the D-type schemes have no meaning beyond fixing x and y, which means that the numbers in these two schemes cannot be "improved." However, according to Tab. 8.2, the numerical values obtained in the MS scheme and the D-type schemes are not very different. All the following results in Tabs. 8.3-8.6 are in the MS scheme, which was used in the previous studies in Refs. [170, 171]. We also point out that obtaining results in the $\overline{\text{MS}}$ scheme(s) is somewhat cumbersome, see App. B for more details.

In Tabs. 8.3-8.6, we present the numerical results for the sum rules for the 1-loop, 2-loop and 3-loop analyses. Generally, the dependence of the numbers on the loop order is very mild. Strictly speaking, our results do not reflect the full dependence on the loop order since in each case we have taken the parton momentum fractions a_i from the 2-loop analysis of Ref. [186]. On the

[9] This statement does not hold for the sigma terms from ChPT though [191, 192].

		$O(\alpha_s^1)$	$O(\alpha_s^2)$	$O(\alpha_s^3)$
Scenario A	U_q	0.384 ± 0.035	0.383 ± 0.036	0.384 ± 0.036
	U_g	0.554 ± 0.035	0.556 ± 0.036	0.555 ± 0.036
Scenario B	U_q	0.420 ± 0.016	0.420 ± 0.017	0.421 ± 0.017
	U_g	0.518 ± 0.016	0.518 ± 0.017	0.517 ± 0.017

Table 8.4: Numerics for the sum rule in Eq. (8.149) for 1-loop, 2-loop and 3-loop analyses. All the results are in units of GeV. (See caption of Tab. 8.3 for more details.)

		$O(\alpha_s^1)$	$O(\alpha_s^2)$	$O(\alpha_s^3)$
Scenario A	M_q	0.311 ± 0.043	0.310 ± 0.043	0.309 ± 0.044
	M_m	0.073 ± 0.080	0.073 ± 0.079	0.074 ± 0.080
	M_g	0.554 ± 0.035	0.556 ± 0.036	0.555 ± 0.036
Scenario B	M_q	0.237 ± 0.006	0.235 ± 0.006	0.234 ± 0.006
	M_m	0.183 ± 0.023	0.184 ± 0.022	0.187 ± 0.023
	M_g	0.518 ± 0.016	0.518 ± 0.017	0.517 ± 0.017

Table 8.5: Numerics for the sum rule in Eqs. (8.219)-(8.221) (with the change of notation $m_i \to M_i$ for the proton case). for 1-loop, 2-loop and 3-loop analyses. All the results are in units of GeV. (See caption of Tab. 8.3 for more details.)

		$O(\alpha_s^1)$	$O(\alpha_s^2)$	$O(\alpha_s^3)$
Scenario A	$\tilde{U}_q$	-0.070 ± 0.008	-0.067 ± 0.009	-0.064 ± 0.009
	$\check{U}_q$	0.455 ± 0.027	0.449 ± 0.026	0.448 ± 0.027
	$\tilde{U}_g$	0.554 ± 0.035	0.556 ± 0.036	0.555 ± 0.036
Scenario B	$\tilde{U}_q$	-0.062 ± 0.004	-0.057 ± 0.004	-0.055 ± 0.004
	$\check{U}_q$	0.482 ± 0.013	0.477 ± 0.012	0.476 ± 0.013
	$\tilde{U}_g$	0.518 ± 0.016	0.518 ± 0.017	0.517 ± 0.017

Table 8.6: Numerics for the sum rule in Eq. (8.196) for 1-loop, 2-loop and 3-loop analyses. All the results are in units of GeV. Recall that $\tilde{U}_g = U_g$ according to the QCD equivalent of Eq. (8.199). (See caption of Tab. 8.3 for more details.)

other hand, we do not expect this point to have a significant impact on the qualitative outcome of a mild sensitivity to the loop order.

The impact of including a sigma term for charm quarks, that is, going from Scenario A to Scenario B, is clearly visible for all the sum rules. In the first place, by definition this switch affects the quark mass term M_m of the sum rule in Eq. (8.220) — see Tab. 8.5 for the corresponding numbers. It is often asked how much of the proton mass can be attributed to the Higgs mechanism. What seems clear is that M_m is entirely due to the Higgs mechanism, as this contribution would vanish if the quark masses were zero. In that case the entire mass of the proton could be associated with either the gluon contribution to the trace anomaly, or the sum of what we have called the quark and gluon energies. In Scenario A, less than 10% of the proton mass are due to the Higgs mechanism, while in Scenario B this number is close to 20%. In view of this discussion, it is important to obtain further independent information about the contribution of heavier quarks to the quark mass term M_m. A direct calculation of, for instance, the expectation value $\langle\, (F^{\alpha\beta}F_{\alpha\beta})_R \,\rangle$ could therefore help to clarify the role played by the Higgs mechanism for the numerics of the proton mass decomposition.

The contribution of the gluon energy M_g to the proton mass is at least 50%. However, we repeat that the precise number depends on the renormalization scheme. We also find some negative contributions to mass sum rules, namely the quark term $\overline{M}_q$ in Tab. 8.3 and $\tilde{U}_g$ in Tab. 8.6. But these terms can become positive when changing the scenario and/or the scheme. We repeat that the quark mass term M_m does not depend on the choice of x and y. It is the only term from the various sum rules showing that feature and, since the operator $(m\bar{\psi}\psi)$ does not get an additional renormalization (respect to the Lagrangian one), this contribution has no renormalization scheme dependence at all.

8.7 Conclusions

In this Chapter, we studied the EMT for both the QED and the QCD case. We reviewed the decomposition of the EMT matrix elements in form factors and we explicitly derived them at $O(\alpha)$ for an electron in QED. We then turned our attention to the forward limit of the EMT matrix elements, studying different mass decompositions proposed in the literature. We reviewed the key ingredient to obtain consistent results, namely the renormalization of multiple local operators. This procedure enlightens the additional dependence on a renormalization scheme [170, 171]. We analyzed in detail both the operator definitions of the different sum rules and their explicit expressions in terms of the forward EMT form factors. We then obtained explicit results at 1-loop order in QED as a proof-of-concept of the renormalization procedure and its application to the different sum rules. In the last section, we applied the same concepts to the proton in QCD, in order to obtain its mass decomposition. We studied different renormalization schemes, and enlightened the strong dependence of the results on the choice of the renormalization scheme. This scheme dependence prevents us to assign a unique physical meaning to the individual terms of the sum rules. Nevertheless, we presented the numerics for the different sum rules,

and we compared the results at different loop orders, finding a very mild dependence on the truncation order of the α_s series. Incidentally, we also found a very strong dependence of the various sum rules on the charm sigma term. It would be interesting to study the effects of even heavier quarks, like the bottom. We also stress that any sum rule for the proton mass one could think of has at most two independent contributions since, for forward kinematics, the EMT has only two form factors.

Chapter 9

Conclusions

The Standard Model of particle physics has proven to be a very accurate model in classifying and describing elementary particles. However, despite the impressive list of achievements, it is still unable to explain some fundamental properties of subatomic particles. This is true, in particular, for what concerns the QCD sector, which describes the strong interactions: the non-Abelian nature of the theory, that results in the auto-interaction of the force mediators and the increasing of the coupling constant at low energies, makes it impossible to apply the ordinary perturbative approaches. This leads to a phenomenon known as confinement. In nature, we never observe free QCD degrees of freedom, that are quarks and gluons, collectively named partons. They always appear in colorless bound states, known as hadrons. One of the unsolved problems in QCD is the explanation of the exact mechanisms that lead to the realization of confinement. The understanding of the confinement has a twofold repercussion on our picture of hadrons. We would be able to resolve the internal dynamics of the hadrons and then to obtain the distributions, along with all the possible correlations, of the partons inside the hadrons at different scales. We tackle the problem in the reverse order: we look for a better description of the structure properties of the hadrons in terms of its constituents to gain insights for an explanation of the dynamics of the confinement.

In this thesis, we investigated different aspects of the partonic structure of the hadrons, with particular emphasis on the proton, as the preferential prototype of hadron. The two main tools that we used to fulfill this study are the parton distribution functions and the Energy-Momentum Tensor (EMT). They offer different and, therefore, complementary descriptions of the partonic structure of the proton. The proton matrix elements of the QCD EMT carry information about global properties of the proton. A detailed study of the possible decompositions of the EMT in the separate contributions from quarks and gluons leads to important clues on how the global properties of the proton emerge from the properties of its elementary constituents. The study of parton distributions has been done within the framework of light-front quantization. Light-front quantization presents many advantages compared to the standard instant-form quantization in the study of parton distributions. It provides the

natural framework to describe processes that give access to the parton distributions, leading to a great simplification of the practical calculation. Furthermore, it provides a relativistic description of bound systems such as the hadrons in terms of quantum-mechanical wave functions and then it allows one to gain a more intuitive physical interpretation of the physical content of the parton distributions. Within light-front quantization it is possible to introduce a well-defined expansion of the proton state in terms of the basis of the Fock space constructed with free quarks and gluon states. This is due to the different vacuum structure between the instant-form and the light-front quantization: in the latter, the vacuum contains only gluons in a very specific kinematic domain, whereas in the former the vacuum is populated by gluons and a quark-antiquark pairs. Each state of the Fock-space basis in light-front quantization enters the expansion of the proton state with a coefficient that represents the probability amplitude of the corresponding state. These coefficients are called Light-Front Wave Functions (LFWFs). Due to the different vacuum structure, the probabilistic interpretation is lost in instant-form quantization, hence the advantage of using the light-front approach. The LFWFs offer one of the most suitable tools for a unified description of the known parton distributions. Moreover, going beyond the leading-twist parton distributions, the LFWFs provide a very intuitive picture of the genuine higher-twist parton distributions in terms of quark-gluon correlations.

Two Chapters deviate from the use of light-front quantization: Chapter 4 and Chapter 8. In Chapter 4, we laid the foundations for the extraction of the Generalized Transverse-Momentum Dependent parton distributions via the study of the cross section for a specific dijet process. In Chapter 8, we investigated the proton mass as emerging property from the underlying parton structure in terms of the EMT, and we used the more natural language, for this context, of instant-form quantization.

9.1 Results

In Chapter 2, we reviewed the basics of different types of quantization, with particular emphasis posed on the light-front quantization. The concepts presented in the Chapter represent the theoretical background on which all the arguments of the thesis are developed.

In Chapter 3, we showed how one can link the LFWFs to the vacuum-to-proton matrix elements of particular combinations of quark and gluon operators. Such matrix elements are parametrizable in terms of distribution amplitudes. We derived the general expressions that allow one to link the LFWFs and the distributions amplitudes when a proton state with non-vanishing parton Orbital Angular Momentum (OAM) is considered. We reviewed how the system of equations for the three-quark LFWFs with non-vanishing OAM involves also the LFWFs for the three-quark plus one gluon state.

We reserved two chapters for studying two general arguments, that are unrelated to the specific model for the LFWFs that we built in this work. In

Chapter 4, we studied the cross-section for exclusive dijet production in lepton-proton collisions. We presented the results for the cross section parametrized in terms of all the possible angular modulations of the detected jets. These results represent the foundations for a possible sensitivity study of the different coefficients of the angular modulations to different types of Generalized Transverse Momentum dependent parton Distributions (GTMDs), extending the studies existing in the literature beyond the small-x approximation.

An application of the language of LFWFs is the investigation of model-induced relations between different types parton distributions. An example of such relation, i.e. the lensing relation, is reviewed in Chapter 5. The lensing relation allows one to write the average transverse momentum of naïve T-odd Transverse Momentum dependent parton Distributions (TMDs) as a convolution of T-even Impact Parameter Distributions and a T-odd lensing function. Using the light-front formalism, we analyzed which features of the models allow the validity of the lensing relation and how, in general, such features are far too restrictive to make them plausible in a full QCD calculation.

In Chapter 6, we exploited the link between distribution amplitudes and LFWFs derived in Chapter 3 to construct a model for the LFWFs based on a parametrization of the distribution amplitudes. We showed the interplay between the three-quark plus one gluon LFWFs and the distribution amplitudes connected to the non-vanishing OAM three-quark states. Estimates for the model parameters have been obtained from QCD sum-rule techniques and lattice QCD. We used these results as starting point for a fit to the unpolarized collinear parton distribution functions $f_1(x)$ for the up and down quark and for the gluon, extracted from a phenomenological analysis. We presented the results for the LFWF overlap representation of the T-even, twist-2 TMDs and of the chiral-even Generalized Parton Distributions. We then discussed the numerical predictions for these distributions, using the parameter set obtained from the fit of the unpolarized collinear parton distribution functions.

We used the LFWFs also to study subleading-twist TMDs. In particular, Chapter 7, is devoted to the study of one particular higher-twist distribution, the $e^q(x, \boldsymbol{k}_\perp)$. Higher-twist distributions are very interesting, since they provide a privileged window to study the quark-gluon correlations inside the proton. We reviewed the general decomposition of higher-twist distributions using the equations of motion for the quark field and discussed some of the recent works on these types of decompositions. Higher-twist parton distributions can be written as spurious lower-twist terms plus a pure higher-twist contribution. The latter can be represented as the overlap of LFWFs for states that differs by one gluon. We exploit our model, in which both the three-quark state and the three-quark plus one gluon state are present, to perform a model-dependent study of the pure higher-twist contribution. We showed within our model that the pure twist-three contribution is indeed small compared to the lower-twist contribution.

Chapter 8 is devoted to a different topic, i.e. the EMT. The EMT offers a different perspective on the partonic structure of hadrons compared to the

parton distributions. In particular, the EMT matrix elements encode information on the global properties of particles, like their mass and their spin. The decomposition of the EMT of a composite system in the individual contributions from its constituents (e.g., quarks and gluons in the the case of hadrons or leptons and photons in the case of leptons) can give insights on how the global properties of the system emerge from the internal dynamics. However, a number of issues must be faced. We first revisited the renormalization of the separate contributions to the EMT from electrons and photons in QED, which is equivalent to the renormalization of the separate contributions of quarks and gluons in QCD. With the correct renormalization procedure at our disposal, we presented the results for the EMT form factors in a one-loop QED calculation for an electron state. The results are then specified to the forward limit, and are used to study the different EMT-based mass decompositions available in the literature. Again, the QED case served as testing ground for the QCD case. For the QCD case, we used the perturbative results for the counterterms and for the QCD beta function at three-loop accuracy. We then used the inputs from phenomenological analysis and lattice QCD to obtain results for the EMT form factors. With these results, we studied the proton-mass decompositions in different renormalization schemes, finding a quite strong scheme dependence of the various terms. Overall, the revised renormalization procedure for the separate lepton and gauge-boson operators allowed us to provide a different interpretation of the renormalized operators and to find a new link between these operators and the trace anomaly at the level of matrix elements.

9.2 Outlooks

Two main perspectives for future works emerge from the thesis.

The first one is related the application of the LFWF formalism to construct models for different types of partonic distributions. Using LFWFs as the underlying theoretical tools, it is possible to fit simultaneously different types of parton distributions. In this way, we can easily transfer the information acquired from the fit of specific parton distributions to others, providing predictions and sensitivity studies that would be valuable for the planning of future phenomenological studies and/or experiments. On a more concrete note, we will work in the direction of improving our model. The link between LFWFs and distribution amplitudes is a powerful tool. However, the resulting model for the LFWFs is as good as the underlying model for the distribution amplitudes. Different proposals to modify the model for the distribution amplitudes are being considered, like a neural-network induced model, and are left for future investigations.

The second point is the detailed analysis of the dijet cross section in terms of GTMDs. A deep study of the cross section in terms of parton distributions could lead to the identification of specific combinations of angular modulations of the cross section suited for the extraction of different GTMDs from experimental data. Moreover, a detailed view in terms of parton distributions could

allow the planning of specific fits and phenomenological analysis. The work in this direction has already been started by a number of authors, which presented studies on an handful of angular modulations of the dijet cross section in the small-x regime. The work that has been pursued in this thesis and its future developments are of great importance in view of the construction of new experimental facilities, such as the Electron-Ion Collider, whose realization at the Brookhaven National Laboratory in the US is under consideration.

The solution of such complicated problems demand an effort that goes beyond the contributions that a single individual or a single group can give. A consistent, prolonged community effort is needed. However, even the tinier contributions are important in order to construct a road that brings us even so little closer to the final goal of understanding the complex world of QCD.

Appendices

Appendix A

Explicit results for the contraction of the leptonic and hadronic tensors

In this appendix, we are going to illustrate a relation that involves the product of two antisymmetric symbols $\varepsilon^{\mu\nu\rho\sigma}$ and the explicit contraction between the unpolarized and symmetric hadronic tensor and the leptonic tensor, see Chapter 4.

The parity matrix introduced in Eq. (4.26), when applied to the totally antisymmetric symbol $\varepsilon^{\mu\nu\rho\sigma}$, satisfies the following identities:

$$L^{\mu}{}_{\alpha} L^{\nu}{}_{\beta} L^{\rho}{}_{\gamma} L^{\sigma}{}_{\delta} \varepsilon^{\alpha\beta\gamma\delta} = -\varepsilon^{\mu\nu\rho\sigma}, \tag{A.1}$$

$$L^{\mu}{}_{\nu} p^{\nu} = \widetilde{p}^{\mu}. \tag{A.2}$$

Others useful identities that have being used to identify the independent Lorentz structures of the hadronic tensor are the following ones:

$$g^{\alpha\beta}\varepsilon^{\mu\nu\rho\sigma} = g^{\alpha\mu}\varepsilon^{\beta\nu\rho\sigma} + g^{\alpha\nu}\varepsilon^{\mu\beta\rho\sigma} + g^{\alpha\rho}\varepsilon^{\mu\nu\beta\sigma} + g^{\alpha\sigma}\varepsilon^{\mu\nu\rho\beta}. \tag{A.3}$$

$$\varepsilon_{i_1,i_2,i_3,i_4}\varepsilon_{k_1,k_2,k_3,k_4} = \det \begin{pmatrix} \delta_{i_1,k_1} & \delta_{i_1,k_2} & \delta_{i_1,k_3} & \delta_{i_1,k_4} \\ \delta_{i_2,k_1} & \delta_{i_2,k_2} & \delta_{i_2,k_3} & \delta_{i_2,k_4} \\ \delta_{i_3,k_1} & \delta_{i_3,k_2} & \delta_{i_3,k_3} & \delta_{i_3,k_4} \\ \delta_{i_4,k_1} & \delta_{i_4,k_2} & \delta_{i_4,k_3} & \delta_{i_4,k_4} \end{pmatrix}. \tag{A.4}$$

Assuming A, B, C, D, j, l, m, n to be generic vectors, Eq. (A.4) explicitly reads:

$$\begin{aligned} \varepsilon_{ABCD}\varepsilon_{jlmn} &\equiv \varepsilon_{\mu\nu\rho\sigma}\varepsilon_{\alpha\beta\gamma\delta} A^{\mu} B^{\nu} C^{\rho} D^{\sigma} j^{\alpha} l^{\beta} m^{\gamma} n^{\delta} \\ &= (Aj)(Bl)(Cm)(Dn) - (Aj)(Bl)(Cn)(Dm) \\ &- (Aj)(Bm)(Cl)(Dn) + (Aj)(Bm)(Cn)(Dl) \\ &+ (Aj)(Bn)(Cl)(Dm) - (Aj)(Bn)(Cm)(Dl) \\ &- (Al)(Bj)(Cm)(Dn) + (Al)(Bj)(Cn)(Dm) \\ &+ (Al)(Bm)(Cj)(Dn) - (Al)(Bm)(Cn)(Dj) \end{aligned}$$

$$
\begin{aligned}
&- (Al)(Bn)(Cj)(Dm) + (Al)(Bn)(Cm)(Dj) \\
&+ (Am)(Bj)(Cl)(Dn) - (Am)(Bj)(Cn)(Dl) \\
&- (Am)(Bl)(Cj)(Dn) + (Am)(Bl)(Cn)(Dj) \\
&+ (Am)(Bn)(Cj)(Dl) - (Am)(Bn)(Cl)(Dj) \\
&- (An)(Bj)(Cl)(Dm) + (An)(Bj)(Cm)(Dl) \\
&+ (An)(Bl)(Cj)(Dm) - (An)(Bl)(Cm)(Dj) \\
&- (An)(Bm)(Cj)(Dl) + (An)(Bm)(Cl)(Dj),
\end{aligned} \tag{A.5}
$$

where we used the notation $(AB) = A \cdot B$ for any four-vector A and B. From Eq. (A.5), one could derive the analogous relations when one index is uncontracted. If we assume that the μ index of the first $\varepsilon^{\mu\nu\rho\sigma}$ is an open index, i.e. is not contracted with A^μ, in the previous equation we just need to perform the substitution:

$$
A \cdot v = (Av) \to v_\mu, \tag{A.6}
$$

with v being any four-vector of the set $\{j, l, m, n\}$.

Finally, we would like to give an example of explicit contraction between the leptonic and hadronic tensor. We will show it only for the symmetric and unpolarized sector, since it is illustrative and not too much complicated:

$$
\left(g^{\mu\nu} - \frac{q^\mu q^\nu}{q^2}\right) \mathcal{R}e\left(L_{\mu\nu}\right) = -Q^2, \tag{A.7}
$$

$$
P_q^{\{\mu} P_q^{\nu\}} \mathcal{R}e\left(L_{\mu\nu}\right) = -\frac{M^2 Q^2 \left(-4 + 4y + y^2\gamma^2\right)}{y^2\gamma^2}, \tag{A.8}
$$

$$
\begin{aligned}
P_q^{\{\mu} j_q^{\nu\}} \mathcal{R}e\left(L_{\mu\nu}\right) &= \frac{-4j^3 M Q^2 \gamma + 4j^3 M Q^2 y\gamma + j^3 M Q^2 y^2\gamma^3}{y^2\gamma^3\sqrt{1+\gamma^2}} \\
&+ \frac{4M(Q^2)^{3/2} z_j \sqrt{1+\gamma^2} - 4M(Q^2)^{3/2} y z_j \sqrt{1+\gamma^2} - M(Q^2)^{3/2} y^2 z_j \gamma^2 \sqrt{1+\gamma^2}}{y^2\gamma^3\sqrt{1+\gamma^2}} \\
&+ \frac{-2j_\perp M Q^2 \gamma^2 \sqrt{4-4y-y^2\gamma^2}\cos\left(\phi_1\right) + j_\perp M Q^2 y\gamma^2 \sqrt{4-4y-y^2\gamma^2}\cos\left(\phi_1\right)}{y^2\gamma^3\sqrt{1+\gamma^2}},
\end{aligned} \tag{A.9}
$$

$$
\begin{aligned}
P_q^{\{\mu} l_q^{\nu\}} \mathcal{R}e\left(L_{\mu\nu}\right) &= \frac{-4l^3 M Q^2 \gamma + 4l^3 M Q^2 y\gamma + l^3 M Q^2 y^2\gamma^3}{y^2\gamma^3\sqrt{1+\gamma^2}} \\
&+ \frac{4M(Q^2)^{3/2} z_l \sqrt{1+\gamma^2} - 4M(Q^2)^{3/2} y z_l \sqrt{1+\gamma^2} - M(Q^2)^{3/2} y^2 z_l \gamma^2 \sqrt{1+\gamma^2}}{y^2\gamma^3\sqrt{1+\gamma^2}} \\
&+ \frac{-2l_\perp M Q^2 \gamma^2 \sqrt{4-4y-y^2\gamma^2}\cos\left(\phi_2\right) + l_\perp M Q^2 y\gamma^2 \sqrt{4-4y-y^2\gamma^2}\cos\left(\phi_2\right)}{y^2\gamma^3\sqrt{1+\gamma^2}},
\end{aligned} \tag{A.10}
$$

$$
j_q^{\{\mu} j_q^{\nu\}} \mathcal{R}e\left(L_{\mu\nu}\right) = \frac{j_\perp^2 Q^2}{1+\gamma^2}\left(\ell^2 - \imath^2\right) + \frac{j_\perp^2 Q^2}{1+\gamma^2}\imath^2\cos\left(2\phi_j\right)
$$

$$
\begin{aligned}
&- \imath^2 \frac{Q^2\left(4j^3 Q z_j \gamma\sqrt{1+\gamma^2} - 2(j^3)^2\gamma^2 - 2Q^2 z_j^2\right)}{\gamma^4\left(1+\gamma^2\right)} \\
&+ \cos\left(\phi_j\right) \frac{2\sqrt{2} j_\perp Q^2\left(Q z_j\sqrt{1+\gamma^2} - j^3\gamma\right)}{\gamma^2\left(1+\gamma^2\right)} \imath\ell, \qquad \text{(A.11)} \\
l_q^{\{\mu} l_q^{\nu\}} \mathcal{R}e\left(L_{\mu\nu}\right) &= \frac{l_\perp^2 Q^2}{1+\gamma^2}\left(\ell^2 - \imath^2\right) + \frac{l_\perp^2 Q^2}{1+\gamma^2}\imath^2\cos\left(2\phi_l\right) \\
&- \imath^2 \frac{Q^2\left(4l^3 Q z_l \gamma\sqrt{1+\gamma^2} - 2(l^3)^2\gamma^2 - 2Q^2 z_l^2\right)}{\gamma^4\left(1+\gamma^2\right)} \\
&+ \cos\left(\phi_l\right) \frac{2\sqrt{2} l_\perp Q^2\left(Q z_l\sqrt{1+\gamma^2} - l^3\gamma\right)}{\gamma^2\left(1+\gamma^2\right)} \imath\ell, \qquad \text{(A.12)}
\end{aligned}
$$

$$
\begin{aligned}
j_q^{\{\mu} l_q^{\nu\}} \mathcal{R}e\left(L_{\mu\nu}\right) &= \cos\left(\phi_j - \phi_l\right)\frac{\ell^2 - \imath^2}{1+\gamma^2} + \cos\left(\phi_j + \phi_l\right)\frac{\imath^2}{1+\gamma^2} \\
&- \imath^2 Q^2 \frac{Q z_l\sqrt{1+\gamma^2}\left(j^3\gamma - Q z_j\sqrt{1+\gamma^2}\right) + l^3\gamma\left(Q z_j\sqrt{1+\gamma^2} - j^3\gamma\right)}{\gamma^4\left(1+\gamma^2\right)} \\
&+ \cos\left(\phi_j\right)\imath\ell \frac{\sqrt{2} j_\perp Q^2\left(Q z_l\sqrt{1+\gamma^2} - l^3\gamma\right)}{\gamma^2\left(1+\gamma^2\right)} \\
&+ \cos\left(\phi_l\right)\imath\ell \frac{\sqrt{2} l_\perp Q^2\left(Q z_j\sqrt{1+\gamma^2} - j^3\gamma\right)}{\gamma^2\left(1+\gamma^2\right)}. \qquad \text{(A.13)}
\end{aligned}
$$

In the last expression, we used the following identity:

$$
\begin{aligned}
&\cos\left(\phi_j - \phi_l\right)\frac{\ell^2 - \imath^2}{1+\gamma^2} + \cos\left(\phi_j + \phi_l\right)\frac{\imath^2}{1+\gamma^2} \\
&= \cos\left(\phi_j\right)\cos\left(\phi_l\right)\ell^2\frac{j_\perp l_\perp Q^2}{1+\gamma^2} + \sin\left(\phi_j\right)\sin\left(\phi_l\right)\frac{j_\perp l_\perp Q^2}{2}.
\end{aligned}
$$

All the complexity of Eqs. (A.7)-(A.13) is hidden inside the coefficients A_i (see Eqs. (4.43)-(4.49)) for the unpolarized and symmetric hadronic tensor. Similar expressions can be obtained for the other contributions to the hadronic tensor.

Appendix B

Counterterms in different renormalization schemes

In this appendix, we discuss the decomposition of the trace of the EMT into individual contributions from quarks and gluons (for the QED case analogous results hold for the electron and photon fields), which requires to fix x and y in Eqs. (8.65) and (8.66). The focus of this appendix is to find x and y in the MS and in the $\overline{\text{MS}}$ schemes. For the MS scheme we just outline the essential steps, since the full procedure can be found in Refs. [170, 171], while we give more details in the case of the $\overline{\text{MS}}$ scheme.

We repeat that, according to Eqs. (8.51)-(8.55), the complete renormalization of the EMT requires to determine ten renormalization constants Z_X, with $X = T,\ M,\ L,\ S,\ F,\ C,\ \psi,\ K,\ Q$ and B. While Z_F and Z_C are associated with the renormalization of the EMT trace, $Z_{T,L,\psi,Q}$ are needed for the renormalization of the traceless part of the EMT. The remaining constants $Z_{M,S,B,K}$ are then constrained through the Eqs. (8.69)–(8.72), which contain x and y. In other words, to fix the finite contributions to $Z_{M,S,B,K}$ requires to fix x and y.

In the MS scheme, the renormalization constants take the form

$$Z_X = \delta_{X,T} + \delta_{X,\psi} + \delta_{X,F} + \frac{a_X}{\epsilon} + \frac{b_X}{\epsilon^2} + \frac{c_X}{\epsilon^3} + \ldots, \tag{B.1}$$

where $\delta_{X,X'}$ denotes the Kronecker symbol, and a_X, b_X, c_X are constants depending on α_s, the number of quark flavors and color factors. In order to fix the values of x and y by means of Eqs. (8.69) and (8.70), we need the results of the four renormalization constants $Z_{T,F,L,C}$ which can be found in Ref. [171] through $O(\alpha_s^3)$. By taking the Laurent expansion of both sides of Eqs. (8.69) and (8.70) about $\epsilon = 0$ and collecting the $O(\epsilon^0)$ terms, we find the relations

$$\begin{aligned}&\frac{1}{32}\Bigg[(8 + 4a_T + 2b_T + c_T + \ldots)\\ &- \left(1 + x - \frac{\beta}{2g}\right)(8 + 4a_F + 2b_F + c_F + \ldots)\Bigg] = 0,\end{aligned} \tag{B.2}$$

$$\frac{1}{32}\Bigg[-(4a_L + 2b_L + c_L + \ldots) \\ -\left(1 + x - \frac{\beta}{2g}\right)(4a_C + 2b_C + c_C + \ldots) + 8(\gamma_m - y)\Bigg] = 0, \tag{B.3}$$

from which follow x and y in the MS scheme. Note that using Eqs. (8.71) and (8.72) (instead of Eqs. (8.69) and (8.70)) provides the same results.

Now we proceed to discuss the process of finding the renormalization constants in the $\overline{\text{MS}}$ scheme when taking results in the MS scheme as starting point. For this purpose, we first write the generic structure of a renormalization constant in the MS scheme as

$$Z\big|_{MS} = (1,0) + \alpha_s \frac{a_1}{\epsilon} + \alpha_s^2\left(\frac{b_2}{\epsilon^2} + \frac{b_1}{\epsilon}\right) + \alpha_s^3\left(\frac{c_3}{\epsilon^3} + \frac{c_2}{\epsilon^2} + \frac{c_1}{\epsilon}\right). \tag{B.4}$$

The corresponding formula in the $\overline{\text{MS}}$ scheme reads

$$Z\big|_{\overline{\text{MS}}} = (1,0) + \alpha_s \frac{\bar{a}_1}{\epsilon} S_\epsilon + \alpha_s^2\left(\frac{\bar{b}_2}{\epsilon^2} + \frac{\bar{b}_1}{\epsilon}\right) S_\epsilon^2 + \alpha_s^3\left(\frac{\bar{c}_3}{\epsilon^3} + \frac{\bar{c}_2}{\epsilon^2} + \frac{\bar{c}_1}{\epsilon}\right) S_\epsilon^3, \tag{B.5}$$

where different conventions for the quantity S_ϵ can be found in the literature. The most popular ones are given in Eqs. (8.49) and (8.50). The comparison between Eqs. (8.49) and (8.50) shows that the two schemes differ at $O(\epsilon^2)$ (and higher), which causes numerical differences for the present study of the proton mass decomposition, see the results for the $\overline{\text{MS}}_1$ and $\overline{\text{MS}}_2$ schemes in Tab. 8.2, but leads to the same result for our QED study. In the following, we present the main steps that are needed to get x and y in a $\overline{\text{MS}}$ scheme, by showing the relevant equations for just the $\overline{\text{MS}}_1$ scheme. In general, using as starting point the results for the renormalization constants in the MS scheme from Ref. [171], it is easier to find x and y in the MS scheme than in a $\overline{\text{MS}}$ scheme.

We first note that the divergent terms on the r.h.s. of Eqs. (B.4) and (B.5) must be identical, which implies

$$\begin{aligned} &\bar{a}_1 = a_1, \qquad \bar{b}_1 = b_1 - 2b_2\delta_{\text{UV}}, \qquad \bar{b}_2 = b_2, \\ &\bar{c}_1 = c_1 - 3c_2\delta_{\text{UV}} + \frac{c_3}{4}(18{\delta_{\text{UV}}}^2 + \pi^2), \qquad \bar{c}_2 = c_2 - 3c_3\delta_{\text{UV}}, \qquad \bar{c}_3 = c_3. \end{aligned} \tag{B.6}$$

The parameters x and y appear in the constant term of renormalization constants, which in the $\overline{\text{MS}}_1$ scheme take the general form

$$\begin{aligned} C\big|_{\overline{\text{MS}}_1} = {} & \alpha_s \bar{a}_1 \delta_{\text{UV}} + \alpha_s^2\left(2\bar{b}_1\delta_{\text{UV}} + 2\bar{b}_2{\delta_{\text{UV}}}^2 + \frac{\pi^2}{6}\bar{b}_2\right) \\ & + \alpha_s^3\left(3\bar{c}_1\delta_{\text{UV}} + \frac{9}{2}\bar{c}_2{\delta_{\text{UV}}}^2 + \frac{9}{2}\bar{c}_3{\delta_{\text{UV}}}^3 - \frac{\pi^2}{4}\bar{c}_2 - \frac{3\pi^2}{4}\bar{c}_3\delta_{\text{UV}} + \frac{1}{2}\bar{c}_3\psi^{(2)}(1)\right), \end{aligned} \tag{B.7}$$

with the polygamma function $\psi^{(n)}(z) = \frac{d^{n+1}}{dz^{n+1}} \log\Gamma(z)$. Using the relations in (B.6), we can express the constant term in Eq. (B.7) through the coefficients

of the renormalization constants in the MS scheme, i.e.

$$C|_{\overline{\rm MS}_1} = \alpha_s a_1 \delta_{\rm UV} + \alpha_s^2 \Big(2b_1\delta_{\rm UV} - 2b_2 {\delta_{\rm UV}}^2 - \frac{\pi^2}{6} b_2 \Big) + \alpha_s^3 \Big(3c_1\delta_{\rm UV} - \frac{9}{2} c_2 {\delta_{\rm UV}}^2 + \frac{9}{2} c_3 {\delta_{\rm UV}}^3 - \frac{\pi^2}{4} c_2 + \frac{3\pi^2}{4} c_3 \delta_{\rm UV} + \frac{1}{2} c_3 \psi^{(2)}(1) \Big). \tag{B.8}$$

The renormalization constants $Z_{M,S,B,K}$ in Eqs. (8.69)–(8.72) do not right away appear in the form of Eq. (B.8) if they are computed by combining the finite terms on the r.h.s. of these equations. Here we pick one example to illustrate this point. For the parameter x we use the perturbative expansion

$$x = \alpha_s x_1 + \alpha_s^2 x_2 + \alpha_s^3 x_3, \tag{B.9}$$

and consider the constant Z_B. We find

$$\begin{aligned}
O(\alpha_s) &: \frac{1}{8}\Big(\bar{a}_{1,Q} + 2\bar{a}_{1,Q}\delta_{\rm UV} + 2x_1 \Big), \\
O(\alpha_s^2) &: \frac{1}{48}\Big(6\bar{b}_{1,Q}(1+4\delta_{\rm UV}) + \bar{b}_{2,Q}(3 + 12\delta_{\rm UV} + 24{\delta_{\rm UV}}^2 - 2\pi^2) \\
&\quad + 6\big(\bar{a}_{1,F}\delta_{\rm UV} x_1 (1+2\delta_{\rm UV}) + 2x_2 \big) \Big), \\
O(\alpha_s^3) &: \frac{1}{32}\Big(\bar{c}_{3,Q} + 6\bar{c}_{3,Q}\delta_{\rm UV} + 18\bar{c}_{3,Q}{\delta_{\rm UV}}^2 + 36\bar{c}_{3,Q}{\delta_{\rm UV}}^3 + 4\bar{c}_{1,Q}(1+6\delta_{\rm UV}) \\
&\quad - \bar{c}_{3,Q}\pi^2 - 6\bar{c}_{3,Q}\delta_{\rm UV}\pi^2 + 2\bar{c}_{2,Q}(1 + 6\delta_{\rm UV} + 18{\delta_{\rm UV}}^2 - \pi^2) + 4\bar{b}_{1,F}x_1 \\
&\quad + 2\bar{b}_{2,F}x_1 + 16\bar{b}_{1,F}\delta_{\rm UV}x_1 + 8\bar{b}_{2,F}\delta_{\rm UV}x_1 + 16\bar{b}_{2,F}{\delta_{\rm UV}}^2 x_1 - \frac{4}{3}\bar{b}_{2,F}\pi^2 x_1 \\
&\quad + 4\bar{a}_{1,F}x_2 + 8\bar{a}_{1,F}\delta_{\rm UV}x_2 + 8x_3 + 4\bar{c}_{3,Q}\psi^{(2)}(1) \Big),
\end{aligned} \tag{B.10}$$

instead of

$$\begin{aligned}
O(\alpha_s) &: \frac{1}{4}\bar{a}_{1,Q}\delta_{\rm UV}, \\
O(\alpha_s^2) &: \frac{1}{24}\Big(12\bar{b}_{1,Q}\delta_{\rm UV} + \bar{b}_{2,Q}(6\delta_{\rm UV} + 12{\delta_{\rm UV}}^2 - \pi^2) + 12\bar{a}_{1,F}\delta_{\rm UV}x_1 \Big) \\
O(\alpha_s^3) &: \frac{1}{32}\Big(24\bar{c}_{1,Q}\delta_{\rm UV} + 6\bar{c}_{3,Q}\delta_{\rm UV} + 18\bar{c}_{3,Q}{\delta_{\rm UV}}^2 + 36\bar{c}_{3,Q}{\delta_{\rm UV}}^3 - \bar{c}_{3,Q}\pi^2 \\
&\quad - 6\bar{c}_{3,Q}\delta_{\rm UV}\pi^2 + 2\bar{c}_{2,Q}(6\delta_{\rm UV} + 18{\delta_{\rm UV}}^2 - \pi^2) + 24\bar{b}_{1,F}\delta_{\rm UV}x_1 + 12\bar{b}_{2,F}\delta_{\rm UV}x_1 \\
&\quad + 12\bar{b}_{2,F}{\delta_{\rm UV}}^2 x_1 - 2\bar{b}_{2,F}\pi^2 x_1 + 24\bar{a}_{1,F}\delta_{\rm UV}x_2 + 4\bar{c}_{3,Q}\psi^{(2)}(1) \Big).
\end{aligned} \tag{B.11}$$

By equating the terms for a given order in α_s for the expressions in Eqs. (B.10)-(B.11), we obtain a system of equations that fix the x_i in Eq. (B.9). Applying the same procedure for Z_K, we obtain the values for the corresponding expansion coefficients for y. Using the same method, one can compute x and y from $Z_{M,S}$ instead of $Z_{B,K}$, obtaining identical results.

Bibliography

[1] S. J. Brodsky, H.-C. Pauli and S. S. Pinsky, "Quantum chromodynamics and other field theories on the light cone", *Phys. Rept.* **301** (1998) 299 [hep-ph/9705477].

[2] D. Soper, "Infinite-momentum helicity states", *Phys. Rev. D* **5** (1972) 1956.

[3] J. B. Kogut and D. E. Soper, "Quantum Electrodynamics in the Infinite Momentum Frame", *Phys. Rev. D* **1** (1970) 2901.

[4] G. Leibbrandt, *Noncovariant gauges: Quantization of Yang-Mills and Chern-Simons theory in axial type gauges*. World Scientific Publishing Co Pte Ltd, 1994.

[5] A. Bassetto, G. Nardelli and R. Soldati, *Yang-Mills theories in algebraic noncovariant gauges: Canonical quantization and renormalization*. World Scientific, 1991.

[6] M. Gell-Mann, "Symmetries of baryons and mesons", *Phys. Rev.* **125** (1962) 1067.

[7] J. Collins, "The non-triviality of the vacuum in light-front quantization: An elementary treatment", 1801.03960.

[8] P. D. Mannheim, P. Lowdon and S. J. Brodsky, "Structure of light front vacuum sector diagrams", *Phys. Lett.* **B797** (2019) 134916 [1904.05253].

[9] L. Mantovani, B. Pasquini, X. Xiong and A. Bacchetta, "Revisiting the equivalence of light-front and covariant QED in the light-cone gauge", *Phys. Rev.* **D94** (2016) 116005 [1609.00746].

[10] D. Mustaki, S. Pinsky, J. Shigemitsu and K. Wilson, "Perturbative renormalization of null plane QED", *Phys. Rev.* **D43** (1991) 3411.

[11] A. Bacchetta, L. Mantovani and B. Pasquini, "Electron in three-dimensional momentum space", *Phys. Rev.* **D93** (2016) 013005 [1508.06964].

[12] J. Collins, *Foundations of perturbative QCD*, vol. 32. Cambridge University Press, 11, 2013.

[13] S. Meissner, A. Metz and M. Schlegel, "Generalized parton correlation functions for a spin-1/2 hadron", *J. High Energy Phys.* **08** (2009) 056 [0906.5323].

[14] S. Meissner, A. Metz, M. Schlegel and K. Goeke, "Generalized parton correlation functions for a spin-0 hadron", *J. High Energy Phys.* **08** (2008) 038 [0805.3165].

[15] M. Diehl, "Introduction to GPDs and TMDs", *Eur. Phys. J.* **A52** (2016) 149 [1512.01328].

[16] C. Lorcé, B. Pasquini and M. Vanderhaeghen, "Unified framework for generalized and transverse-momentum dependent parton distributions within a 3Q light-cone picture of the nucleon", *J. High Energy Phys.* **05** (2011) 041 [1102.4704].

[17] K. Goeke, A. Metz and M. Schlegel, "Parameterization of the quark-quark correlator of a spin-1/2 hadron", *Phys. Lett.* **B618** (2005) 90 [hep-ph/0504130].

[18] S. Boffi and B. Pasquini, "Generalized parton distributions and the structure of the nucleon", *Riv. Nuovo Cim.* **30** (2007) 387 [0711.2625].

[19] M. Diehl, "Generalized parton distributions", *Phys.Rep.* **388** (2003) 41 [hep-ph/0307382].

[20] M. Diehl, T. Feldmann, R. Jakob and P. Kroll, "Linking parton distributions to form-factors and Compton scattering", *Eur. Phys. J.* **C8** (1999) 409 [hep-ph/9811253].

[21] M. Diehl, T. Feldmann, R. Jakob and P. Kroll, "The overlap representation of skewed quark and gluon distributions", *Nucl. Phys.* **B596** (2001) 33 [hep-ph/0009255].

[22] J. C. Collins and A. Freund, "Proof of factorization for deeply virtual Compton scattering in QCD", *Phys. Rev.* **D59** (1999) 074009 [hep-ph/9801262].

[23] M. Diehl and S. Sapeta, "On the analysis of lepton scattering on longitudinally or transversely polarized protons", *Eur. Phys. J.* **C41** (2005) 515 [hep-ph/0503023].

[24] J. C. Collins and D. E. Soper, "Parton Distribution and Decay Functions", *Nucl. Phys.* **B194** (1982) 445.

[25] C. J. Bomhof, P. J. Mulders and F. Pijlman, "Gauge link structure in quark-quark correlators in hard processes", *Phys. Lett.* **B596** (2004) 277 [hep-ph/0406099].

[26] C. Bomhof, P. Mulders and F. Pijlman, "The Construction of gauge-links in arbitrary hard processes", *Eur. Phys. J. C* **47** (2006) 147 [hep-ph/0601171].

[27] K. G. Wilson, "Confinement of Quarks", *Phys. Rev.* **D10** (1974) 2445.

[28] C. Lorcé, "Wilson lines and orbital angular momentum", *Phys. Lett. B* **719** (2013) 185 [1210.2581].

[29] A. V. Belitsky, X. Ji and F. Yuan, "Final state interactions and gauge invariant parton distributions", *Nucl. Phys.* **B656** (2003) 165 [hep-ph/0208038].

[30] I. Cherednikov and N. Stefanis, "Wilson lines and transverse-momentum dependent parton distribution functions: A Renormalization-group analysis", *Nucl. Phys. B* **802** (2008) 146 [0802.2821].

[31] I. Cherednikov, A. Karanikas and N. Stefanis, "Wilson lines in transverse-momentum dependent parton distribution functions with spin degrees of freedom", *Nucl. Phys. B* **840** (2010) 379 [1004.3697].

[32] I. Cherednikov, "Layout of Wilson lines and light-cone peculiarities of transverse-momentum dependent PDFs", *PoS* **QNP2012** (2012) 061 [1206.4212].

[33] D. Boer, P. J. Mulders and F. Pijlman, "Universality of T odd effects in single spin and azimuthal asymmetries", *Nucl. Phys.* **B667** (2003) 201 [hep-ph/0303034].

[34] C. Lorcé and B. Pasquini, "Quark Wigner Distributions and Orbital Angular Momentum", *Phys. Rev.* **D84** (2011) 014015 [1106.0139].

[35] C. Lorcé and B. Pasquini, "Structure analysis of the generalized correlator of quark and gluon for a spin-1/2 target", *J. High Energy Phys.* **09** (2013) 138 [1307.4497].

[36] C. Lorcé and B. Pasquini, "Multipole decomposition of the nucleon transverse phase space", *Phys. Rev.* **D93** (2016) 034040 [1512.06744].

[37] M. Burkardt, "Impact parameter space interpretation for generalized parton distributions", *Int. J. Mod. Phys.* **A18** (2003) 173 [hep-ph/0207047].

[38] M. Diehl, "Generalized parton distributions in impact parameter space", *Eur. Phys. J.* **C25** (2002) 223 [hep-ph/0205208].

[39] R. L. Jaffe, "Spin, twist and hadron structure in deep inelastic processes", in *The spin structure of the nucleon. Proceedings, International School of Nucleon Structure, 1st Course, Erice, Italy, August 3-10, 1995*, pp. 42–129, 1996, hep-ph/9602236.

[40] M. E. Peskin and D. V. Schroeder, *An Introduction to quantum field theory*. Addison-Wesley, Reading, USA, 1995.

[41] C. Lorcé, B. Pasquini, X. Xiong and F. Yuan, "The quark orbital angular momentum from Wigner distributions and light-cone wave functions", *Phys. Rev.* **D85** (2012) 114006 [1111.4827].

[42] Y. Hatta, "Notes on the orbital angular momentum of quarks in the nucleon", *Phys. Lett.* **B708** (2012) 186 [1111.3547].

[43] M. Burkardt, "Parton Orbital Angular Momentum and Final State Interactions", *Phys. Rev.* **D88** (2013) 014014 [1205.2916].

[44] J. C. Collins and D. E. Soper, "Back-To-Back Jets in QCD", *Nucl. Phys.* **B193** (1981) 381.

[45] D. W. Sivers, "Single Spin Production Asymmetries from the Hard Scattering of Point-Like Constituents", *Phys. Rev.* **D41** (1990) 83.

[46] A. Kotzinian, "New quark distributions and semiinclusive electroproduction on the polarized nucleons", *Nucl. Phys.* **B441** (1995) 234 [hep-ph/9412283].

[47] P. J. Mulders and R. D. Tangerman, "The Complete tree level result up to order 1/Q for polarized deep inelastic leptoproduction", *Nucl. Phys.* **B461** (1996) 197 [hep-ph/9510301].

[48] D. Boer and P. J. Mulders, "Time reversal odd distribution functions in leptoproduction", *Phys. Rev.* **D57** (1998) 5780 [hep-ph/9711485].

[49] S. Meissner, A. Metz and K. Goeke, "Relations between generalized and transverse momentum dependent parton distributions", *Phys. Rev.* **D76** (2007) 034002 [hep-ph/0703176].

[50] M. Diehl and P. Hagler, "Spin densities in the transverse plane and generalized transversity distributions", *Eur. Phys. J.* **C44** (2005) 87 [hep-ph/0504175].

[51] X.-D. Ji, "Gauge-Invariant Decomposition of Nucleon Spin", *Phys. Rev. Lett.* **78** (1997) 610 [hep-ph/9603249].

[52] M. Burkardt, "Impact parameter dependent parton distributions and off forward parton distributions for zeta —> 0", *Phys. Rev.* **D62** (2000) 071503 [hep-ph/0005108].

[53] M. Burkardt, "Chromodynamic lensing and transverse single spin asymmetries", *Nucl. Phys.* **A735** (2004) 185 [hep-ph/0302144].

[54] M. Burkardt, "Quark correlations and single spin asymmetries", *Phys. Rev.* **D69** (2004) 057501 [hep-ph/0311013].

[55] M. Burkardt and D. S. Hwang, "Sivers asymmetry and generalized parton distributions in impact parameter space", *Phys. Rev.* **D69** (2004) 074032 [hep-ph/0309072].

[56] M. Burkardt, "Impact parameter dependent parton distributions and transverse single spin asymmetries", *Phys. Rev.* **D66** (2002) 114005 [hep-ph/0209179].

[57] M. Burkardt, "Transverse deformation of parton distributions and transversity decomposition of angular momentum", *Phys. Rev.* **D72** (2005) 094020 [hep-ph/0505189].

[58] M. Burkardt and B. Hannafious, "Are all Boer-Mulders functions alike?", *Phys. Lett.* **B658** (2008) 130 [0705.1573].

[59] M. Burkardt and B. Pasquini, "Modelling the nucleon structure", *Eur. Phys. J.* **A52** (2016) 161 [1510.02567].

[60] X.-d. Ji, J.-P. Ma and F. Yuan, "Generalized counting rule for hard exclusive processes", *Phys. Rev. Lett.* **90** (2003) 241601 [hep-ph/0301141].

[61] X.-d. Ji, J.-P. Ma and F. Yuan, "Classification and asymptotic scaling of hadrons' light cone wave function amplitudes", *Eur. Phys. J.* **C33** (2004) 75 [hep-ph/0304107].

[62] C. E. Carlson and C.-R. Ji, "Angular conditions, relations between Breit and light front frames, and subleading power corrections", *Phys. Rev.* **D67** (2003) 116002 [hep-ph/0301213].

[63] C. Mezrag, J. Segovia, L. Chang and C. D. Roberts, "Parton distribution amplitudes: Revealing correlations within the proton and Roper", *Phys. Lett.* **B783** (2018) 263 [1711.09101].

[64] RQCD collaboration, G. S. Bali et al., "Light-cone distribution amplitudes of octet baryons from lattice QCD", *Eur. Phys. J.* **A55** (2019) 116 [1903.12590].

[65] Braun, V.M. and Collins, S. and Gläßle, B. and Göckeler, M. and Schäfer, A. and Schiel, R.W. and Söldner, W. and Sternbeck, A. and Wein, P., "Light-cone Distribution Amplitudes of the Nucleon and Negative Parity Nucleon Resonances from Lattice QCD", *Phys. Rev.* **D89** (2014) 094511 [1403.4189].

[66] QCDSF collaboration, V. M. Braun et al., "Nucleon distribution amplitudes and proton decay matrix elements on the lattice", *Phys. Rev.* **D79** (2009) 034504 [0811.2712].

[67] V. Braun, R. Fries, N. Mahnke and E. Stein, "Higher twist distribution amplitudes of the nucleon in QCD", *Nucl. Phys.* **B589** (2000) 381 [hep-ph/0007279].

[68] V. M. Braun, T. Lautenschlager, A. N. Manashov and B. Pirnay, "Higher twist parton distributions from light-cone wave functions", *Phys. Rev.* **D83** (2011) 094023 [1103.1269].

[69] Y. Hatta and Y. Zhao, "Parton distribution function for the gluon condensate", *Phys. Rev.* **D102** (2020) 034004 [2006.02798].

[70] S. Bhattacharya, A. Metz and J. Zhou, "Generalized TMDs and the exclusive double Drell–Yan process", *Phys. Lett.* **B771** (2017) 396 [1702.04387].

[71] S. Bhattacharya, A. Metz, V. K. Ojha, J.-Y. Tsai and J. Zhou, "Exclusive double quarkonium production and generalized TMDs of gluons", 1802.10550.

[72] T. Altinoluk, N. Armesto, G. Beuf and A. H. Rezaeian, "Diffractive Dijet Production in Deep Inelastic Scattering and Photon-Hadron Collisions in the Color Glass Condensate", *Phys. Lett.* **B758** (2016) 373 [1511.07452].

[73] V. Braun and D. Ivanov, "Exclusive diffractive electroproduction of dijets in collinear factorization", *Phys. Rev.* **D72** (2005) 034016 [hep-ph/0505263].

[74] J. Bartels, H. Lotter and M. Wüsthoff, "Quark-antiquark production in DIS diffractive dissociation", *Phys. Lett.* **B379** (1996) 239 [hep-ph/9602363].

[75] J. Bartels, C. Ewerz, H. Lotter and M. Wusthoff, "Azimuthal distribution of quark - antiquark jets in DIS diffractive dissociation", *Phys. Lett.* **B386** (1996) 389 [hep-ph/9605356].

[76] M. Diehl, "Diffractive production of dijets at HERA", *Z. Phys.* **C66** (1995) 181 [hep-ph/9407399].

[77] A. Dumitru, G. Kapilevich and V. Skokov, "The small-x gluon distribution in centrality biased pA and pp collisions", *Nucl. Phys.* **A974** (2018) 106 [1802.06111].

[78] C. Marquet, C. Roiesnel and P. Taels, "Linearly polarized small-x gluons in forward heavy-quark pair production", *Phys. Rev.* **D97** (2018) 014004 [1710.05698].

[79] S. Benić and Y. Hatta, "Single spin asymmetries in ultra-peripheral $p^{\uparrow}A$ collisions", *Phys. Rev.* **D98** (2018) 094025 [1806.10901].

[80] Y. Hatta, Y. Nakagawa, F. Yuan, Y. Zhao and B. Xiao, "Gluon orbital angular momentum at small-x", *Phys. Rev.* **D95** (2017) 114032 [1612.02445].

[81] H. Mäntysaari, N. Mueller and B. Schenke, "Diffractive Dijet Production and Wigner Distributions from the Color Glass Condensate", *Phys. Rev.* **D99** (2019) 074004 [1902.05087].

[82] X. Ji, F. Yuan and Y. Zhao, "Hunting the Gluon Orbital Angular Momentum at the Electron-Ion Collider", *Phys. Rev. Lett.* **118** (2017) 192004 [1612.02438].

[83] A. Bacchetta, M. Diehl, K. Goeke, A. Metz, P. J. Mulders and M. Schlegel, "Semi-inclusive deep inelastic scattering at small transverse momentum", *J. High Energy Phys.* **02** (2007) 093 [hep-ph/0611265].

[84] S. Gliske, A. Bacchetta and M. Radici, "Production of two hadrons in semi-inclusive deep inelastic scattering", *Phys. Rev.* **D90** (2014) 114027 [1408.5721].

[85] S. Arnold, A. Metz and M. Schlegel, "Dilepton production from polarized hadron hadron collisions", *Phys. Rev.* **D79** (2009) 034005 [0809.2262].

[86] A. Bacchetta, "Transverse Momentum Distributions", //www2.pv.infn.it/~bacchett/teaching/Bacchetta_Trento2012.pdf.

[87] B. Pasquini, S. Rodini and A. Bacchetta, "Revisiting model relations between T-odd transverse-momentum dependent parton distributions and generalized parton distributions", *Phys. Rev. D* **100** (2019) 054039 [1907.06960].

[88] L. Gamberg and M. Schlegel, "Final state interactions and the Sivers function", *AIP Conf. Proc.* **1374** (2011) 309 [1012.3395].

[89] C. Lorcé and B. Pasquini, "On the Origin of Model Relations among Transverse-Momentum Dependent Parton Distributions", *Phys. Rev.* **D84** (2011) 034039 [1104.5651].

[90] J. She, J. Zhu and B.-Q. Ma, "Pretzelosity $h_{1T}^{\perp}$ and quark orbital angular momentum", *Phys. Rev.* **D79** (2009) 054008 [0902.3718].

[91] H. Avakian, A. V. Efremov, K. Goeke, A. Metz, P. Schweitzer and T. Teckentrup, "Are there approximate relations among transverse momentum dependent distribution functions?", *Phys. Rev.* **D77** (2008) 014023 [0709.3253].

[92] A. Bacchetta, F. Conti and M. Radici, "Transverse-momentum distributions in a diquark spectator model", *Phys. Rev.* **D78** (2008) 074010 [0807.0323].

[93] A. Bacchetta and M. Radici, "Constraining quark angular momentum through semi-inclusive measurements", *Phys. Rev. Lett.* **107** (2011) 212001 [1107.5755].

[94] L. Gamberg and M. Schlegel, "Final state interactions and the transverse structure of the pion using non-perturbative eikonal methods", *Phys. Lett.* **B685** (2010) 95 [0911.1964].

[95] B. Pasquini and F. Yuan, "Sivers and Boer-Mulders functions in Light-Cone Quark Models", *Phys. Rev.* **D81** (2010) 114013 [1001.5398].

[96] B. Pasquini, S. Cazzaniga and S. Boffi, "Transverse momentum dependent parton distributions in a light-cone quark model", *Phys. Rev.* **D78** (2008) 034025 [0806.2298].

[97] S. Boffi, B. Pasquini and M. Traini, "Linking generalized parton distributions to constituent quark models", *Nucl. Phys.* **B649** (2003) 243 [hep-ph/0207340].

[98] B. Pasquini, M. Pincetti and S. Boffi, "Chiral-odd generalized parton distributions in constituent quark models", *Phys. Rev.* **D72** (2005) 094029 [hep-ph/0510376].

[99] B. Pasquini and S. Boffi, "Nucleon spin densities in a light-front constituent quark model", *Phys. Lett.* **B653** (2007) 23 [0705.4345].

[100] D. W. Sivers, "Hard scattering scaling laws for single spin production asymmetries", *Phys. Rev.* **D43** (1991) 261.

[101] D. E. Soper, "The Parton Model and the Bethe-Salpeter Wave Function", *Phys. Rev.* **D15** (1977) 1141.

[102] X.-D. Ji and F. Yuan, "Parton distributions in light cone gauge: Where are the final state interactions?", *Phys. Lett.* **B543** (2002) 66 [hep-ph/0206057].

[103] S. J. Brodsky, B. Pasquini, B.-W. Xiao and F. Yuan, "Phases of Augmented Hadronic Light-Front Wave Functions", *Phys. Lett.* **B687** (2010) 327 [1001.1163].

[104] B. Pasquini and P. Schweitzer, "Pion transverse momentum dependent parton distributions in a light-front constituent approach, and the Boer-Mulders effect in the pion-induced Drell-Yan process", *Phys. Rev.* **D90** (2014) 014050 [1406.2056].

[105] V. Braun, A. Manashov and J. Rohrwild, "Baryon Operators of Higher Twist in QCD and Nucleon Distribution Amplitudes", *Nucl. Phys.* **B807** (2009) 89 [0806.2531].

[106] S. J. Brodsky, T. Huang and P. Lepage, *in Particle and Fields*. Capri, A.Z. and Kamal, A.N. (Plenum, New York), 1983.

[107] QCDSF collaboration, V. M. Braun et al., "Nucleon and $N^*(1535)$ Distribution Amplitudes", *PoS* **LATTICE2010** (2010) 158 [1011.1092].

[108] E. Stein, P. Gornicki, L. Mankiewicz, A. Schafer and W. Greiner, "QCD sum rule calculation of twist - three contributions to polarized nucleon structure functions", *Phys. Lett.* **B343** (1995) 369 [hep-ph/9409212].

[109] H. Koibuchi, "Crumpling phase transition of random surfaces with extrinsic curvature", *Phys. Lett.* **B242** (1990) 371.

[110] M. Gockeler, R. Horsley, W. Kurzinger, H. Oelrich, D. Pleiter, P. E. Rakow et al., "A Lattice calculation of the nucleon's spin dependent structure function g_2 revisited", *Phys. Rev.* **D63** (2001) 074506 [hep-lat/0011091].

[111] H.-W. Lin et al., "Parton distributions and lattice QCD calculations: a community white paper", *Prog. Part. Nucl. Phys.* **100** (2018) 107 [1711.07916].

[112] S. Boffi, B. Pasquini and M. Traini, "Helicity dependent generalized parton distributions in constituent quark models", *Nucl. Phys.* **B680** (2004) 147 [hep-ph/0311016].

[113] A. Efremov and A. Radyushkin, "Factorization and Asymptotical Behavior of Pion Form-Factor in QCD", *Phys. Lett.* **B94** (1980) 245.

[114] G. Lepage and S. J. Brodsky, "Exclusive Processes in Quantum Chromodynamics: Evolution Equations for Hadronic Wave Functions and the Form-Factors of Mesons", *Phys. Lett.* **B87** (1979) 359.

[115] M. V. Polyakov and C. Weiss, "Skewed and double distributions in pion and nucleon", *Phys. Rev.* **D60** (1999) 114017 [hep-ph/9902451].

[116] I. Musatov and A. Radyushkin, "Evolution and models for skewed parton distributions", *Phys. Rev.* **D61** (2000) 074027 [hep-ph/9905376].

[117] M. Diehl and D. Ivanov, "Dispersion representations for hard exclusive processes: beyond the Born approximation", *Eur. Phys. J.* **C52** (2007) 919 [0707.0351].

[118] L. A. Harland-Lang, A. D. Martin, P. Motylinski and R. S. Thorne, "Parton distributions in the LHC era: MMHT 2014 PDFs", *Eur. Phys. J.* **C75** (2015) 204 [1412.3989].

[119] B. Pasquini and S. Rodini, "The twist-three distribution $e^q(x, k_\perp)$ in a light-front model", *Phys. Lett.* **B788** (2019) 414 [1806.10932].

[120] B. Pasquini and S. Rodini, "Model independent parametrisation of the nucleon light-front wave functions from distribution amplitudes", in preparation.

[121] D. P. Kingma and J. Ba, "Adam: A Method for Stochastic Optimization", 1412.6980.

[122] R. L. Jaffe, "Parton Distribution Functions for Twist Four", *Nucl. Phys.* **B229** (1983) 205.

[123] R. L. Jaffe and X.-D. Ji, "Chiral odd parton distributions and Drell-Yan processes", *Nucl. Phys.* **B375** (1992) 527.

[124] R. L. Jaffe and X.-D. Ji, "Chiral odd parton distributions and polarized Drell-Yan", *Phys. Rev. Lett.* **67** (1991) 552.

[125] A. V. Efremov and P. Schweitzer, "The Chirally odd twist 3 distribution $e^a(x)$", *J. High Energy Phys.* **08** (2003) 006 [hep-ph/0212044].

[126] M. Burkardt, "Transverse force on quarks in deep-inelastic scattering", *Phys. Rev.* **D88** (2013) 114502 [0810.3589].

[127] H. Avakian et al., "Transverse spin effects in SIDIS at 12 GeV with transversely polarized target", *JLab Experiment E12-06-015* (2008) .

[128] H. Avakian et al., "Probing the Proton's Quark Dynamics in SIDIS at 12 GeV", *JLab Experiment E12-06-112* (2006) .

[129] S. Pisano et al., "Higher-twist collinear structure of the nucleon through di-hadron SIDIS on unpolarized hydrogen and deuterium", *JLab Experiment E12-06-112B/E12-09-008B* (2014) .

[130] D. Boer et al., "Gluons and the quark sea at high energies: Distributions, polarization, tomography", 1108.1713.

[131] A. Accardi et al., "Electron Ion Collider: The Next QCD Frontier", *Eur. Phys. J.* **A52** (2016) 268 [1212.1701].

[132] A. Metz and M. Schlegel, "Recent progress in the understanding of single spin asymmetries", *Annalen Phys.* **13** (2004) 699 [hep-ph/0411118].

[133] S. Wandzura and F. Wilczek, "Sum rules for spin dependent electroproduction: test of relativistic constituent quarks", *Phys. Lett.* **B72** (1977) 195.

[134] A. V. Efremov, K. Goeke and P. Schweitzer, "Azimuthal asymmetries at CLAS: extraction of $e^a(x)$ and prediction of A_{UL}", *Phys. Rev.* **D67** (2003) 114014 [hep-ph/0208124].

[135] A. V. Efremov, K. Goeke and P. Schweitzer, "Azimuthal asymmetry in electroproduction of neutral pions in semiinclusive DIS", *Phys. Lett.* **B522** (2001) 37 [hep-ph/0108213].

[136] E. De Sanctis, W. D. Nowak and K. A. Oganesian, "Single spin azimuthal asymmetries in the 'Reduced twist - three approximation'", *Phys. Lett.* **B483** (2000) 69 [hep-ph/0002091].

[137] C. Lorcé, B. Pasquini and P. Schweitzer, "Unpolarized transverse momentum dependent parton distribution functions beyond leading twist in quark models", *J. High Energy Phys.* **01** (2015) 103 [1411.2550].

[138] C. Lorcé, B. Pasquini and P. Schweitzer, "Transverse pion structure beyond leading twist in constituent models", *Eur. Phys. J.* **C76** (2016) 415 [1605.00815].

[139] A. I. Signal, "Calculations of higher twist distribution functions in the MIT bag model", *Nucl. Phys.* **B497** (1997) 415 [hep-ph/9610480].

[140] H. Avakian, A. V. Efremov, P. Schweitzer and F. Yuan, "The transverse momentum dependent distribution functions in the bag model", *Phys. Rev.* **D81** (2010) 074035 [1001.5467].

[141] R. Jakob, P. J. Mulders and J. Rodrigues, "Modeling quark distribution and fragmentation functions", *Nucl. Phys.* **A626** (1997) 937 [hep-ph/9704335].

[142] Z. Lu and I. Schmidt, "T-odd quark-gluon-quark correlation function in the diquark model", *Phys. Lett.* **B712** (2012) 451 [1202.0700].

[143] W. Mao and Z. Lu, "Beam spin asymmetries of charged and neutral pion production in semi-inclusive DIS", *Eur. Phys. J.* **C73** (2013) 2557 [1306.1004].

[144] W. Mao, Z. Lu and B.-Q. Ma, "Transverse single-spin asymmetries of pion production in semi-inclusive DIS at subleading twist", *Phys. Rev.* **D90** (2014) 014048 [1405.3876].

[145] J. Balla, M. V. Polyakov and C. Weiss, "Nucleon matrix elements of higher twist operators from the instanton vacuum", *Nucl. Phys.* **B510** (1998) 327 [hep-ph/9707515].

[146] B. Dressler and M. V. Polyakov, "On the twist - three contribution to h(L) in the instanton vacuum", *Phys. Rev.* **D61** (2000) 097501 [hep-ph/9912376].

[147] P. Schweitzer, "The Chirally odd twist three distribution function $e^{\alpha}(x)$ in the chiral quark soliton model", *Phys. Rev.* **D67** (2003) 114010 [hep-ph/0303011].

[148] M. Wakamatsu, "Comparative analysis of the transversities and the longitudinally polarized distribution functions of the nucleon", *Phys. Lett.* **B653** (2007) 398 [0705.2917].

[149] M. Wakamatsu and Y. Ohnishi, "The Nonperturbative origin of delta function singularity in the chirally odd twist three distribution function e(x)", *Phys. Rev.* **D67** (2003) 114011 [hep-ph/0303007].

[150] Y. Ohnishi and M. Wakamatsu, "pi N sigma term and chiral odd twist three distribution function e(x) of the nucleon in the chiral quark soliton model", *Phys. Rev.* **D69** (2004) 114002 [hep-ph/0312044].

[151] C. Cebulla, J. Ossmann, P. Schweitzer and D. Urbano, "The Twist-3 parton distribution function $e^a(x)$ in large-N(c) chiral theory", *Acta Phys. Polon.* **B39** (2008) 609 [0710.3103].

[152] M. Burkardt and Y. Koike, "Violation of sum rules for twist three parton distributions in QCD", *Nucl. Phys.* **B632** (2002) 311 [hep-ph/0111343].

[153] R. Kundu and A. Metz, "Higher twist and transverse momentum dependent parton distributions: A Light front Hamiltonian approach", *Phys. Rev.* **D65** (2002) 014009 [hep-ph/0107073].

[154] A. Mukherjee, "Twist Three Distribution e(x): Sum Rules and Equation of Motion Relations", *Phys. Lett.* **B687** (2010) 180 [0912.1446].

[155] A. Accardi, A. Bacchetta, W. Melnitchouk and M. Schlegel, "What can break the Wandzura-Wilczek relation?", *J. High Energy Phys.* **11** (2009) 093 [0907.2942].

[156] J. Ma and G. Zhang, "On the singular behavior of the chirality-odd twist-3 parton distribution $e(x)$", 2003.13920.

[157] W.-M. Zhang and A. Harindranath, "Role of longitudinal boundary integrals in light front QCD", *Phys. Rev.* **D48** (1993) 4868 [hep-th/9302119].

[158] W.-M. Zhang and A. Harindranath, "Light front QCD. 2: Two component theory", *Phys. Rev.* **D48** (1993) 4881.

[159] A. Courtoy, "Insights into the higher-twist distribution $e(x)$ at CLAS", *arXiV:1405.7659* (2014) .

[160] S. Rodini, A. Metz and B. Pasquini, "Mass sum rules of the electron in quantum electrodynamics", *J. High Energy Phys.* **9** (2020) 067 [2004.03704].

[161] A. Metz, B. Pasquini and S. Rodini, "Revisiting the proton mass decomposition", *Phys. Rev. D* **102** (2021) 114042 [2006.11171].

[162] A. Metz, B. Pasquini and S. Rodini, "The form factors of the electron energy-momentum tensor", `in preparation`.

[163] M. Montesinos and E. Flores, "Symmetric energy-momentum tensor in Maxwell, Yang-Mills, and proca theories obtained using only Noether's theorem", *Rev. Mex. Fis.* **52** (2006) 29 [`hep-th/0602190`].

[164] E. Eriksen and J. M. Leinaas, "Gauge invariance and the transformation properties of the electromagnetic four potential", *Phys. Scripta* **22** (1980) 199.

[165] Y. Takahashi, "Energy momentum tensors in relativistic and nonrelativistic classical field theory", *Fortsch. Phys.* **34** (1986) 323.

[166] G. Munoz, "Lagrangian field theories and energy-momentum tensors", *Am. J. Phys.* **64** (1996) 1153.

[167] C. Lorcé, L. Mantovani and B. Pasquini, "Spatial distribution of angular momentum inside the nucleon", *Phys. Lett.* **B776** (2018) 38 [`1704.08557`].

[168] F. J. Belinfante, "On the spin angular momentum of mesons", *Physica* **6** (1939) 887.

[169] F. J. Belinfante, "On the current and the density of the electric charge, the energy, the linear momentum and the angular momentum of arbitrary fields", *Physica* **7** (1940) 449.

[170] Y. Hatta, A. Rajan and K. Tanaka, "Quark and gluon contributions to the QCD trace anomaly", *J. High Energy Phys.* **12** (2018) 008 [`1810.05116`].

[171] K. Tanaka, "Three-loop formula for quark and gluon contributions to the QCD trace anomaly", *J. High Energy Phys.* **01** (2019) 120 [`1811.07879`].

[172] S. L. Adler, J. C. Collins and A. Duncan, "Energy-Momentum-Tensor Trace Anomaly in Spin 1/2 Quantum Electrodynamics", *Phys. Rev.* **D15** (1977) 1712.

[173] S. L. Adler, "Anomalies to all orders", in *50 years of Yang-Mills theory* (G. 't Hooft, ed.), pp. 187–228. World Scientific, 2005. `hep-th/0405040`.

[174] N. K. Nielsen, "The Energy Momentum Tensor in a Nonabelian Quark Gluon Theory", *Nucl. Phys.* **B120** (1977) 212.

[175] R. Tarrach, "The renormalization of FF", *Nucl. Phys.* **B196** (1982) 45.

[176] Y. Hatta, A. Rajan and D.-L. Yang, "Near threshold J/ψ and Υ photoproduction at JLab and RHIC", *Phys. Rev.* **D100** (2019) 014032 [`1906.00894`].

[177] F. A. Berends and R. Gastmans, "Quantum Electrodynamical Corrections to Graviton-Matter Vertices", *Annals Phys.* **98** (1976) 225.

[178] X. Ji, A. Schäfer, F. Yuan, J.-H. Zhang and Y. Zhao, "Spin decomposition of the electron in QED", *Phys. Rev.* **D93** (2016) 054013 [1511.08817].

[179] X.-D. Ji, "Breakup of hadron masses and energy - momentum tensor of QCD", *Phys. Rev.* **D52** (1995) 271 [hep-ph/9502213].

[180] C. Lorcé, "On the hadron mass decomposition", *Eur. Phys. J.* **C78** (2018) 120 [1706.05853].

[181] X.-D. Ji, "A QCD analysis of the mass structure of the nucleon", *Phys. Rev. Lett.* **74** (1995) 1071 [hep-ph/9410274].

[182] X.-D. Ji and W. Lu, "A Modern anatomy of electron mass", *Submitted to: Phys. Rev.* ***D*** (1998) [hep-ph/9802437].

[183] J. Polchinski, *String theory. Vol. 2: Superstring theory and beyond*, Cambridge Monographs on Mathematical Physics. Cambridge University Press, 12, 2007, 10.1017/CBO9780511618123.

[184] C. Lorcé, H. Moutarde and A. P. Trawiński, "Revisiting the mechanical properties of the nucleon", *Eur. Phys. J.* **C79** (2019) 89 [1810.09837].

[185] Y.-B. Yang, J. Liang, Z. Liu and P. Sun, "Trace anomaly and dynamical quark mass", in *37th International Symposium on Lattice Field Theory*, 3, 2020, 2003.12914.

[186] T.-J. Hou et al., "Progress in the CTEQ-TEA NNLO global QCD analysis", 1908.11394.

[187] H1, ZEUS collaboration, H. Abramowicz et al., "Combination of measurements of inclusive deep inelastic $e^{\pm}p$ scattering cross sections and QCD analysis of HERA data", *Eur. Phys. J.* **C75** (2015) 580 [1506.06042].

[188] A. Accardi, L. Brady, W. Melnitchouk, J. Owens and N. Sato, "Constraints on large-x parton distributions from new weak boson production and deep-inelastic scattering data", *Phys. Rev.* **D93** (2016) 114017 [1602.03154].

[189] S. Alekhin, J. Blümlein, S. Moch and R. Placakyte, "Parton distribution functions, α_s, and heavy-quark masses for LHC Run II", *Phys. Rev.* **D96** (2017) 014011 [1701.05838].

[190] NNPDF collaboration, R. D. Ball et al., "Parton distributions from high-precision collider data", *Eur. Phys. J.* **C77** (2017) 663 [1706.00428].

[191] J. Alarcon, J. Martin Camalich and J. Oller, "The chiral representation of the πN scattering amplitude and the pion-nucleon sigma term", *Phys. Rev.* **D85** (2012) 051503 [1110.3797].

[192] J. Alarcon, L. Geng, J. Martin Camalich and J. Oller, "The strangeness content of the nucleon from effective field theory and phenomenology", *Phys. Lett.* **B730** (2014) 342 [1209.2870].

[193] M. Hoferichter, J. Ruiz de Elvira, B. Kubis and U.-G. Meissner, "High-Precision Determination of the Pion-Nucleon σ Term from Roy-Steiner Equations", *Phys. Rev. Lett.* **115** (2015) 092301 [1506.04142].

[194] C. Alexandrou, S. Bacchio, M. Constantinou, J. Finkenrath, K. Hadjiyiannakou, K. Jansen et al., "The nucleon axial, tensor and scalar charges and σ-terms in lattice QCD", 1909.00485.

[195] S. Durr et al., "Lattice computation of the nucleon scalar quark contents at the physical point", *Phys. Rev. Lett.* **116** (2016) 172001 [1510.08013].

[196] xQCD collaboration, Y.-B. Yang, A. Alexandru, T. Draper, J. Liang and K.-F. Liu, "πN and strangeness sigma terms at the physical point with chiral fermions", *Phys. Rev.* **D94** (2016) 054503 [1511.09089].

[197] ETM collaboration, A. Abdel-Rehim, C. Alexandrou, M. Constantinou, K. Hadjiyiannakou, K. Jansen, C. Kallidonis et al., "Direct Evaluation of the Quark Content of Nucleons from Lattice QCD at the Physical Point", *Phys. Rev. Lett.* **116** (2016) 252001 [1601.01624].

[198] RQCD collaboration, G. S. Bali, S. Collins, D. Richtmann, A. Schäfer, W. Söldner and A. Sternbeck, "Direct determinations of the nucleon and pion σ terms at nearly physical quark masses", *Phys. Rev.* **D93** (2016) 094504 [1603.00827].

[199] K. Chetyrkin, "Quark mass anomalous dimension to $O(\alpha_s^4)$", *Phys. Lett.* **B404** (1997) 161 [hep-ph/9703278].

[200] J. Vermaseren, S. Larin and T. van Ritbergen, "The four loop quark mass anomalous dimension and the invariant quark mass", *Phys. Lett.* **B405** (1997) 327 [hep-ph/9703284].

[201] K. Chetyrkin, J. H. Kuhn and M. Steinhauser, "RunDec: A Mathematica package for running and decoupling of the strong coupling and quark masses", *Comput. Phys. Commun.* **133** (2000) 43 [hep-ph/0004189].